ISBN 978-82-326-7944-7 (printed ver.)
ISBN 978-82-326-7943-0 (electronic ver.)
ISSN 1503-8181 (printed ver.)
ISSN 2703-8084 (electronic ver.)

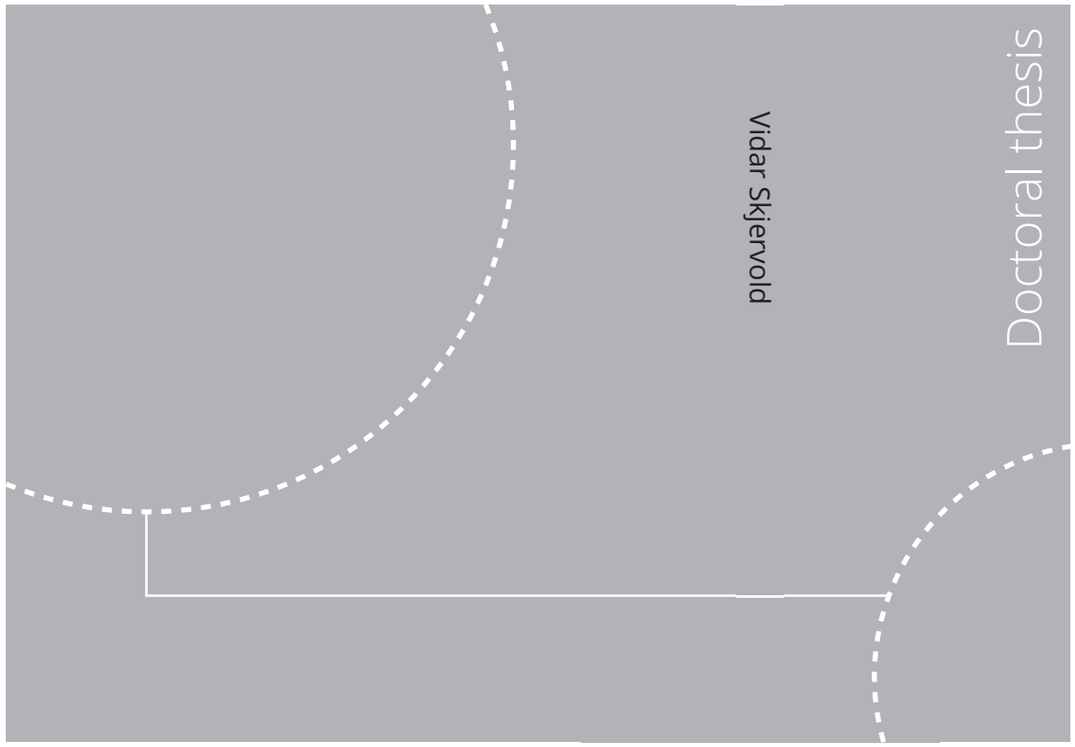

Doctoral theses at NTNU, 2024:176

Vidar Skjervold

Flexible Operation of Thermal Power Plants with Moving Bed Temperature Swing Adsorption Post-Combustion CO_2 Capture

Doctoral theses at NTNU, 2024:176

Vidar Skjervold

NTNU
Norwegian University of Science and Technology

NTNU
Norwegian University of Science and Technology
Thesis for the degree of Philosophiae Doctor
Faculty of Engineering
Department of Energy and Process Engineering

NTNU
Norwegian University of Science and Technology

Vidar Skjervold

Flexible Operation of Thermal Power Plants with Moving Bed Temperature Swing Adsorption Post-Combustion CO_2 Capture

Thesis for the degree of Philosophiae Doctor

Trondheim, May 2024

Norwegian University of Science and Technology
Faculty of Engineering
Department of Energy and Process Engineering

NTNU
Norwegian University of
Science and Technology

NTNU
Norwegian University of Science and Technology

Thesis for the degree of Philosophiae Doctor

Faculty of Engineering
Department of Energy and Process Engineering

ISBN 978-82-326-7944-7 (printed ver.)
ISBN 978-82-326-7943-0 (electronic ver.)
ISSN 1503-8181 (printed ver.)
ISSN 2703-8084 (electronic ver.)

Doctoral theses at NTNU, 2024:176

PRINTED IN NORWAY
NO - 1598

NORDIC SWAN ECOLABEL
Printed matter
2041 0731

Printed by Skipnes Kommunikasjon AS

Preface

This thesis is submitted in partial fulfillment of the requirements for the degree of philosophiae doctor (Ph.D) at the Norwegian University of Science and Technology (NTNU). The work was carried out from January 2021 to December 2023 at the Department of Energy and Process Engineering at the Faculty of Engineering. Professor Lars O. Nord was the main supervisor and Dr. Luca Riboldi (SINTEF Energy Research) and Dr. Marcin Pilarczyk (Aker Solutions) were co-supervisors of the work. The research was performed as part of the InnCapPlant project, funded by the Norway Grants/POLNOR-CCS program (Grant NOR/POLNORCCS/0015/2019-00). The project consortium consisted of NTNU, Cracow University of Technology and SINTEF Industry.

Abstract

To meet our climate targets, global CO_2 emissions must be significantly reduced in the coming decades. The power sector is still dominated by fossil fuel-based thermal power plants and stands for around 42% of anthropogenic CO_2 emissions. This sector will therefore play an important role in the upcoming transition. One solution for decarbonizing the power sector is carbon capture and storage, which in the form of post-combustion CO_2 capture can be retrofitted to existing plants without influencing the core process. Due to increasing shares of intermittent renewable energy sources in the electricity mix, the flexible operation of thermal power plants is expected to be necessary at least in the short to medium term to help balance supply and demand. As a result, the variable operation of thermal power plants with post-combustion carbon capture might play a role in the future energy system.

The moving bed temperature-swing adsorption (MBTSA) technology is currently under development and has shown promise for several post-combustion CO_2 capture applications. However, the dynamic operation of the entire MBTSA process had not been investigated in the literature prior to this Ph.D project. To address this knowledge gap, the main goal of this work was to study the flexible operation of coal-fired power plants with MBTSA post-combustion CO_2 capture. Two main flexibility methods were studied in this project. Firstly, control strategies with the goal of maintaining the performance of the MBTSA process during changes in the power plant operation were developed and evaluated. Secondly, the integration of a steam accumulator thermal energy storage unit into the power plant – carbon capture process was considered. Increasing the maximum load of the power plant and enabling it to rapidly change its load were the primary flexibility modes studied in this work. Two adsorbent materials, activated carbon and Zeolite 13X, and two different power plant scales were investigated.

The first main contribution of this thesis was the development and implementation of a control framework for the MBTSA process. The framework consisted of five controlled and manipulated variable pairs in a decentralized structure that was divided into a regulatory and higher-level layer. The regulatory layer included a controller keeping the fraction of heating and cooling delivered by the internal heat recovery loop stable, a controller for the sorbent temperature leaving the cooling section and a controller for the gas velocity at the top of the precooling section. In the higher-level layer, the sorbent flow rate was used to control the CO_2 recovery and the heating fluid flow to the desorption section was used to control either the CO_2 product purity or the regenerated sorbent temperature. The control framework was added to a mathematical model of the MBTSA process and both the open and closed-loop dynamic responses were studied. A range of scenarios were simulated, including step changes in the incoming flue gas flow rate, ramps in power plant load, setpoint changes for higher-level control variables, variations in flue gas feed CO_2 concentration and variations in the external heat source temperature. The simulations showed that the

developed control framework was able to maintain the performance of the MBTSA process for power plant-driven flexibility scenarios and changes in the operation of the PCC process.

The second main contribution of this thesis was the comparison of several different alternatives for higher-level control of the MBTSA process. Initially, four different control strategies were investigated: a baseline structure with proportional-integral control of both the CO_2 recovery and purity, an option with proportional-integral control of CO_2 purity and feedforward control of the sorbent flow rate, a structure with feedforward control of both the sorbent flow rate and heating fluid velocity to the desorption section, and a case with regular proportional-integral control of the CO_2 recovery and a cascade controller for the CO_2 purity. Due to imperfect ratio adjustment in the feedforward controllers with system load, steady-state offsets from the control variable setpoints were observed. Furthermore, aggressive tuning of the feedback controllers caused oscillations when the power plant load was reduced. To address these limitations and improve the controller performance, two enhanced single-loop control structures were implemented. By adaptively adjusting the controller tuning parameters (gain and integral time) with the system load, no oscillations were observed and tighter control of the CO_2 recovery compared to the standard control structure was achieved. A proportional-integral controller was combined with the feedforward control structure to adjust the ratio based on the control error instead of a parametric relation. This eliminated the steady-state offsets and lead to closer control of the CO_2 recovery rate. When testing the enhanced single-loop control structures, the effect of measurement delays were included. Such delays were found to have a large effect on the relative performance of the investigated control strategies.

The third main contribution of this Ph.D project was a study of how the integration of a steam accumulator thermal energy storage unit could increase the flexibility of the power plant – carbon capture system. A dynamic process model of the steam accumulator was implemented and validated with both experimental and simulation data from the literature. Combined with a steady-state power plant model, simulations were carried out to quantify how charging and discharging the thermal energy storage affected the net electrical power output of the power plant. Charging the accumulator with reheat steam from the power plant could reduce the net power output by up to 1.4 % for around 200 minutes. Two alternatives for discharging of the thermal energy storage were considered, namely covering the regeneration duty of the MBTSA process and meeting the demand of two feedwater heaters. Discharging was found to give relative power plant load increases between 1.7 and 11.2% for up to 37.5 minutes, which exceeds the requirement for primary reserve. Sending steam from the accumulator directly to the MBTSA process could increase the net electrical power output by almost 67 MW for a period of 3.2 minutes. An advantage of using a thermal energy storage system to provide flexibility is that the resulting load changes take place without modifying the boiler load or reducing the CO_2 recovery rate.

Acknowledgements

First and foremost I would like to express my gratitude to my main supervisor Lars O. Nord. Thank you for giving me the opportunity to pursue a Ph.D and for providing helpful advice along the way. I appreciate the freedom you gave me to make decisions and follow my research interests, helping me grow as an independent researcher. I would also like to thank my two co-supervisors, Marcin Pilarczyk and Luca Riboldi. Thank you Marcin for all the help, especially in the first part of my project, and for the conversations during our time as office mates. Thank you Luca for always taking the time to answer my questions. I admire your broad technical understanding and look forward to continue working together as colleagues in SINTEF.

Thank you to the wonderful team at Cracow University of Technology for hosting me during my visit and for our collaboration and discussions in the InnCapPlant project. A special mention to Ewa, Monika and Adam who took the time to show me around Cracow and made me feel welcome. I wish you all the best and hope we can continue working together in the future.

I had the pleasure of sharing an office with many kind and interesting people during these three years. Thank you Ali, Gaurav, Marcin, Valentin, Lasse and Benjamin for the technical discussions, conversations, lunches, coffee breaks and social gatherings.

I would also like to thank my family for always being supportive and showing an interest in my work. Thank you Caroline for always making me laugh and helping me enjoy the small moments in life. This thesis would not have been possible without your encouragement and advice.

Vidar T. Skjervold
Trondheim, 22nd January 2024

Contents

List of Tables

List of Figures

Nomenclature

Latin symbols

a'	Particle specific area	m^2/m^3
A_i	First single-component Virial coefficients	kg/mol
A_{ij}	First multi-component Virial coefficients	kg/mol
$A_{0,i}$	Fitting constants of the first Virial coefficients	kg/mol
$A_{1,i}$	Fitting constants of the first Virial coefficients	K kg/mol
B	Controller bias	-
B_i	Second single-component Virial coefficients	kg^2/mol^2
B_{ijk}	Second multi-component Virial coefficients	kg^2/mol^2
$B_{0,i}$	Fitting constants of the second Virial coefficients	kg^2/mol^2
$B_{1,i}$	Fitting constants of the second Virial coefficients	K kg^2/mol^2
Bi_i	Biot number of the adsorbent particles for component i	-
$c_{p,\mathrm{f}}$	Specific heat capacity of the heating/cooling fluid	J/kg K
$c_{p,\mathrm{g}}$	Specific heat capacity of the gas mixture	J/kg K
$c_{p,\mathrm{pk}}$	Specific heat capacity of packing material	J/kg K
$c_{p,\mathrm{s}}$	Specific heat capacity of the adsorbent	J/kg K
$c_{p,\mathrm{t}}$	Specific heat capacity of the heat exchanger tubes	J/kg K
$\hat{c}_p$	Molar heat capacity of the gas mixture at constant pressure	J/mol K
$\hat{c}_v$	Molar heat capacity of the gas mixture at constant volume	J/mol K
C_i	Molar concentration of component i in the gas phase	mol/m^3
$C_{\mathrm{p},i}$	Molar concentration of component i in the macropores	mol/m^3
C_{T}	Total molar concentration of the gas phase	mol/m^3
d	Disturbance	-
d_{p}	Particle diameter	m
D_{c}^0	Micropore limiting diffusivity at infinite temperature	m^2/s
D_{ij}	Binary molecular diffusivity of components (i, j)	m^2/s
$D_{\mathrm{Kn},i}$	Knudsen diffusivity of component i	m^2/s
$D_{\mathrm{m},i}$	Molecular diffusivity of component i	m^2/s
$D_{\mathrm{p},i}$	Macropore diffusivity of component i	m^2/s
$D_{z,i}$	Axial dispersion coefficient of component i	m^2/s
$E_{\mathrm{a},i}$	Activation energy of micropore diffusion of component i	J/mol
e	Controller error	-
g	Transfer function	-
h_1	Liquid specific enthalpy	J/kg
h_2	Steam specific enthalpy	J/kg
h'	Saturated water specific enthalpy	J/kg
h''	Saturated steam specific enthalpy	J/kg
h_{gs}	Heat transfer coefficient between gas and solid	W/m^2 K

h_{ft}	Heat transfer coefficient between fluid and tube walls	W/m^2 K
h_{gt}	Heat transfer coefficient between gas and tube walls	W/m^2 K
$(ha)_{21}$	Heat transfer parameter	J/(K s m^3)
I	Controller integral term	-
k	Process gain	-
$k_{\mathrm{f,i}}$	Film mass transfer coefficient of component i	m/s
K_{c}	Controller gain	-
$K_{\mathrm{H},i}$	Henry's law constant of component i	mol/kg Pa
$K^{\infty}_{\mathrm{H},i}$	Henry's law constant at infinite temperature	mol/kg Pa
L_{x}	Tube length along flow direction	m
L_{z}	Section length along vertical axis	m
$\dot{m}$	Mass flow rate	kg/s
$\dot{m}_{1,\mathrm{in}}$	Incoming liquid mass flow rate to steam accumulator	kg/s
$\dot{m}_{2,\mathrm{in}}$	Incoming steam mass flow rate to steam accumulator	kg/s
$\dot{m}_{1,\mathrm{out}}$	Outgoing liquid mass flow rate from steam accumulator	kg/s
$\dot{m}_{2,\mathrm{out}}$	Outgoing steam mass flow rate from steam accumulator	kg/s
$\dot{m}_{\mathrm{c}}$	Condensation mass flow rate	kg/s
$\dot{m}_{\mathrm{e}}$	Evaporation mass flow rate	kg/s
M_1	Liquid mass inventory	kg
M_2	Steam mass inventory	kg
M_{w}	Molecular weight	kg/mol
$\dot{n}$	Molar flow rate	mol/s
Nu	Nusselt number	-
P	Total pressure of the gas mixture	Pa
	Controller proportional term	-
P_i	Partial pressure of component i	Pa
Pr	Prandtl number	-
q_i	Adsorbed concentration of component i	mol/kg
q_i^*	Adsorbed concentration of component i at equilibrium	mol/kg
$\dot{Q}$	Heat flow rate	W
r	Latent heat of vaporization	J/kg
r_{c}	Micropore radius	m
r_{p}	Particle radius	m
r_{pore}	Macropore radius	m
R	Ideal gas constant	J/K mol
Re	Reynolds number	-
s	Laplace variable	1/s
Sc_i	Schmidt number of component i	-
Sh_i	Sherwood number of component i	-
t	Time	s
T	Temperature of gas	K
T_1	Temperature of liquid	K

T_2	Temperature of steam	K
T_f	Temperature of the heating/cooling fluid	K
T_s	Temperature of the sorbent particles	K
T_t	Temperature of the heat exchanger tubes wall	K
u	Superficial velocity of the gas	m/s
u'	Ratio used in feedforward control	-
u_calc	Calculated value of manipulated variable	-
u_max	Maximum value of manipulated variable	-
u_min	Minimum value of manipulated variable	-
u_f	Velocity of the heating/cooling fluid	m/s
V_1	Volume of liquid	m^3
V_2	Volume of steam	m^3
V_tank	Tank volume	m^3
v_1	Specific volume of liquid	m^3/kg
v_2	Specific volume of steam	m^3/kg
v_s	Velocity of the adsorbent	m/s
y	Controlled variable	-
y_max	Maximum value of controlled variable	-
y_min	Minimum value of controlled variable	-
y_SP	Controlled variable setpoint	-
Y_i	Molar fraction of component i	-
z	Coordinate along the section height	m

Greek symbols

α	Isobaric expansivity	1/K
α_gt	Ratio of external surface area of tubes to gas-solid volume	$\mathrm{m}^2/\mathrm{m}^3$
$\alpha_\mathrm{t,ext}$	Ratio of external surface area of tubes to fluid volume	$\mathrm{m}^2/\mathrm{m}^3$
$\alpha_\mathrm{t,int}$	Ratio of internal surface area of tubes to fluid volume	$\mathrm{m}^2/\mathrm{m}^3$
ΔH_i	Heat of adsorption of component i	J/mol
ε_c	Column void fraction	-
ε_p	Particle porosity	-
θ	Effective delay	s
λ_g	Axial heat dispersion coefficient of the gas mixture	W/m K
λ_pk	Axial heat dispersion coefficient of the packing	W/m K
κ	Isothermal compressibility	1/Pa
μ_g	Dynamic viscosity of the gas mixture	Pa s
ξ	Packing porosity factor	-
ρ_f	Density of the heating/cooling fluid	kg/m^3
ρ_g	Density of the gas mixture	kg/m^3
ρ_p	Density of the adsorbent particles	kg/m^3
ρ_pk	Density of the packing	kg/m^3

ρ_{t}	Density of the heat exchanger tubes	kg/m^3
ρ_{w}	Density of water	kg/m^3
σ_{ij}	Lennard-Jones parameter of binary diffusivity	m
τ	Time constant	s
τ_{e}	Evaporation relaxation time	s
τ_{c}	Closed-loop time constant	s
	Condensation relaxation time	s
τ_{I}	Controller integral time	s
τ_{p}	Particle tortuosity	-
φ	Flue gas feed flow rate divided by nominal value	-
$\Omega_{D_{ij}}$	Dimensionless collision integral of binary diffusivity	-

Abbreviations

CCS	Carbon Capture and Storage
CFPP	Coal Fired Power Plant
CI	Composition Indicator
CV	Controlled Variable
EMPC	Economic Model Predictive Control
FF	Feedforward
FI	Flow Indicator
FWH	Feedwater Heater
HPT	High Pressure Turbine
IAE	Integral Absolute Error
IEA	International Energy Agency
IPCC	Intergovernmental Panel on Climate Change
IPT	Intermediate Pressure Turbine
LDF	Linear Driving Force
LMPC	Linear Model Predictive Control
LPT	Low Pressure Turbine
MBTSA	Moving Bed Temperature Swing Adsorption
MEA	Monoethanolamine
MPC	Model Predictive Control
MV	Manipulated Variable
NARX	Nonlinear autoregressive with exogeneous input
NGCC	Natural Gas Combined Cycle
NMPC	Nonlinear Model Predictive Control
PCC	Post-Combustion Capture
PCM	Phase Change Material
PI	Proportional-Integral
PID	Proportional-Integral-Derivative
PZ	Piperazine

RC	Recovery Controller
RES	Renewable Energy Sources
SISO	Single Input, Single Output
TES	Thermal Energy Storage
TC	Temperature Controller
TI	Temperature Indicator
VC	Velocity Controller
VI	Velocity Indicator

Chapter 1

Introduction

1.1 Background and motivation

Anthropogenic greenhouse gas emissions since the start of the industrial era have unequivocally led to global warming, with the global surface temperature recently reaching 1.1 °C above values from the period 1850-1900 (IPCC, 2023). This is already causing weather and climate extremes across the globe, disproportionately affecting countries that have contributed little to the overall emissions. Limiting the extent of human-caused global warming requires net zero CO_2 emissions and the European Union aims at achieving this goal by 2050 (European Commission, 2019). Despite these goals, global annual CO_2 emissions from energy and industrial processes reached an all-time high of 36.8 Gt in 2022 (IEA, 2023). This trend must be quickly reversed and then upheld in order to utilize the closing window of opportunity to meet our climate targets (IPCC, 2023). The power sector will be central in this transition since over 60% of global electricity generation comes from fossil fuel-based thermal power plants (Ritchie and Rosado, 2023), causing approximately 42% of global CO_2 emissions (IEA, 2023). One solution for decarbonization of this sector is carbon capture and storage (CCS). The Intergovernmental Panel on Climate Change estimates wide deployment of CCS on both natural gas and coal-fired power plants in scenarios that limit the global temperature increase compared to pre-industrial levels to 1.5 °C (IPCC, 2018). As of September 2022 there were 30 operational CCS facilities worldwide with a combined CO_2 capture capacity of 42.5 Mt per year (Global CCS Institute, 2022).

For large stationary sources like thermal power plants, there are three main methods for capturing CO_2, classified by where the capture takes place relative to the combustion stage (Kazemifar, 2022). The three alternatives are pre-combustion, oxy-combustion and post-combustion capture (PCC). An advantage of PCC is the possibility of fairly simple retrofit to existing plants without influencing its core process (Nord and Bolland, 2022). PCC from power plants with amine solvents is a commercially proven technology. However, other technologies such as membranes, low-temperature separation and adsorption are becoming

more mature and could provide benefits compared to the state-of-the-art (Dziejarski et al., 2023).

Adsorption-based processes have the potential for lower regeneration duties than amine-based absorption (Nie et al., 2018), partly due to the absence of large amounts of water (Samanta et al., 2012). Several types of adsorption-based CO_2 capture exist, depending on the reactor configuration used for gas/solid contact, the mode of regeneration and the adsorbent material (Raganati et al., 2021). The reactor type considered in this work is the moving bed configuration. The most important advantage of the moving bed over the fixed bed configuration is the possibility of operating continuously, avoiding the complexity of multiple beds and switching between operation modes (Dhoke et al., 2021). Compared to fluidized beds, moving beds have the benefit of avoiding the thermodynamic limitations caused by the very efficient heat and mass transfer between the gas and solid particles (Raganati et al., 2021). In the case of post-combustion capture from a thermal power plant, regeneration via temperature swings is a good option due to two main reasons. Firstly, low-grade thermal energy that can be delivered to the PCC process is potentially available in large quantities. Secondly, applying a pressure or vacuum swing to the large flow rates of near-atmospheric flue gas will require significant amounts of electrical power (Zhao et al., 2019).

The moving bed temperature-swing adsorption (MBTSA) process has been shown to deliver high CO_2 recovery rates and purity of the captured CO_2 in the case of PCC from a natural gas combined cycle power plant (Mondino et al., 2019), coal-fired power plant (Mondino et al., 2017) and waste-to-energy plant (Mondino et al., 2022). The moving bed technology has also been found to be more cost-effective than monoethanolamine (MEA)-based PCC for a coal-fired power plant (Jung and Lee, 2022). MBTSA has been demonstrated experimentally at the pilot plant scale (5-40 tons of captured CO_2 per day) through testing of the KCC process developed by Kawasaki Heavy Industries (Okumura et al., 2017, 2018).

The MBTSA configuration used in this work is shown in Figure 1.1. The process is continuous and operated in a cyclic manner. The CO_2-lean adsorbent material enters at the top of the adsorption section, where it moves counter-currently to the flue gas coming from the power plant due to gravity. The CO_2-rich adsorbent then passes through the preheating and desorption sections, which are operated as indirect-contact heat exchangers. The increase in sorbent temperature causes desorption of the CO_2 from the solid phase. The released CO_2 is withdrawn from the desorption section in a high-purity stream. The hot sorbent is then cooled by indirect heat exchangers in the precooling and cooling sections before being transported back to the adsorption section. This closes the cycle and continuous operation is maintained. A fraction of the CO_2-lean flue gas is used as a purge stream in the cooling and precooling sections to avoid re-adsorption of CO_2 in the macropores of the adsorbent as the temperature decreases. The process includes an internal heat recovery loop connecting the preheating and precooling sections, following the approach of Mondino et al. (2022) and Kim et al. (2013). This reduces the need for externally supplied heat and is critical to the performance of the MBTSA process (Morales-Ospino et al., 2021). An alternative to the indirect heaters used in this work is heating the adsorbent by direct contact with steam. This alternative has the advantage of high heat transfer rates due to

efficient mixing between the adsorbent and heating fluid, but makes internal heat recovery difficult. Furthermore, the direct heating option requires adsorbents that are insensitive to water, drying of the regenerated adsorbent and separation of water from the purified CO_2-stream to avoid corrosion in downstream equipment (Dhoke et al., 2021).

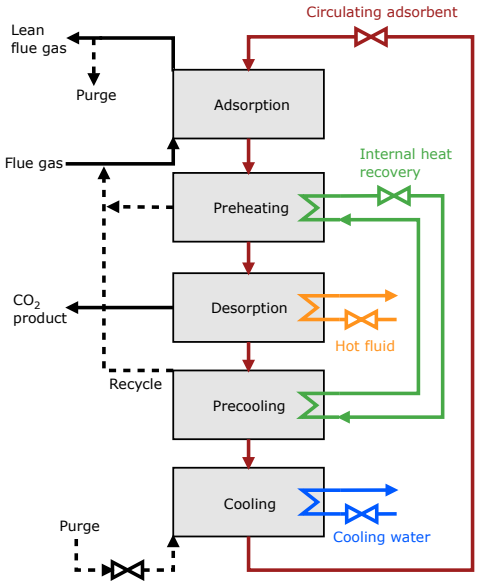

Figure 1.1: The MBTSA post-combustion CO_2 capture process. Figure taken from Publication II.

In the transition to a low-carbon society it is expected that the electricity mix will change significantly, most importantly through increased deployment of renewable energy sources (RES). The International Energy Agency estimates that RES will make up 43% of global electricity generation in 2030 and 65% in 2050 (IEA, 2022). The intermittency of RES represents a challenge, since other means of electricity supply must be used to cover the residual load, i.e. the demand curve after subtracting the power generation from renewable sources (Richter et al., 2015). In the future, grid-scale energy storage systems can mitigate this problem, but the current capacity is quite limited (Kebede et al., 2022). At least in the short to medium term, flexible operation of thermal power plants is expected to be necessary to meet the residual load (Gonzalez-Salazar et al., 2018). This will require several modes of flexibility, including rapid load changes, more frequent start-ups and shutdowns, reduced minimum loads and increased maximum loads (Chalmers et al., 2009).

The MBTSA technology is currently under development and will reach higher maturity levels in the coming years. It is therefore important to evaluate the technology for scenarios relevant for future power plant operation. Despite developing dynamic simulation tools for MBTSA, both Mondino et al. (2022) and Morales-Ospino et al. (2021) consider only steady-state simulations of the process. In the work of Kim et al. (2016), the response of the regeneration step of the moving bed process to typical power plant disturbances was studied. However, since only a part of the process was considered, a complete picture of

the dynamic behavior of the system is not obtained. To the author's knowledge, the flexible (dynamic) operation of the complete MBTSA process has not previously been investigated in the literature. This is the main knowledge gap addressed by this Ph.D project.

1.2 Objectives and scope

The main goal of this Ph.D project was to study flexible operation of coal-fired power plants with MBTSA post-combustion CO_2 capture. This is a broad goal covering several research topics, and five sub-tasks were identified to achieve the overall objective:

- Develop a baseline control framework for the MBTSA process and investigate its controllability.
- Identify and implement scenarios for power plant and PCC-driven modes of flexible operation.
- Compare advanced and standard control structures for the MBTSA process for flexible operation and controller test scenarios.
- Choose a suitable thermal energy storage technology and develop a modeling tool for this process.
- Investigate how thermal energy storage integration can increase the operational flexibility of the power plant – CO_2 capture system.

The MBTSA process model used in this work was based on the model developed in a previous Ph.D project (Mondino, 2022). Modifying the fundamental modeling approach and applied correlations were considered to be outside the scope of this thesis, but changes were made to allow for the comparison of different control structures and the study of dynamic scenarios. Since the focus of the project was on variable operation, the design and working principle of the moving bed process was fixed throughout the thesis. A screening of adsorbent materials was not performed and no experimental work was part of the project. The developed models were validated against experimental data when possible.

1.3 Contributions

The main contributions from this Ph.D project are summarized below:

- MBTSA modelling tool was extended to include multiple process control structures.
- Simulations provided increased knowledge of the dynamic behavior of MBTSA with activated carbon and Zeolite 13X adsorbents at two different system scales.
- A control framework for the MBTSA process was developed, consisting of a regulatory layer for ensuring process stability and a higher-level control layer for process performance. Using this framework, the controllability of the MBTSA system was demonstrated.

- A series of control structures were evaluated and compared, including simple feedback and feedforward structures, cascade control, adaptively tuned controllers and a combined feedback – feedforward scheme.
- The investigated control structures were tested for a range of scenarios, including step changes in incoming flue gas flow, ramps in power plant load, setpoint changes for CO_2 recovery, CO_2 purity and regenerated sorbent temperature, variations in flue gas feed CO_2 concentration and variations in external heat source temperature. Measurement delays for higher-level control variables were also studied.
- A dynamic model of a steam accumulator thermal energy storage unit was implemented in MATLAB and validated.
- An evaluation of how integration of a steam accumulator can increase the flexibility of a power plant with MBTSA-based CO_2 capture was performed.

1.4 Thesis structure

This thesis is structured as a collection of scientific articles preceded by a series of chapters summarizing the work and explaining how the articles are interrelated. In Chapter 1, the background and motivation for the Ph.D project is explained, followed by an overview of the objectives and scope of the work, the main scientific contributions and the publications generated during the project. In Chapter 2, a literature review covering the key topics of the work is presented. The goal of this chapter is to provide context to the research and reasoning for the choice of objectives and methodology. The methodology is explained in Chapter 3, covering the process models and control strategies utilized in the work, investigated scenarios and performance evaluation criteria. In Chapter 4, selected results from the journal articles are presented and discussed. Conclusions and thoughts on future work are given in Chapter 5. The journal articles subject to evaluation in this Ph.D thesis are presented in Appendix A.

1.5 Publications and scientific dissemination

1.5.1 Journal articles

The research carried out during the Ph.D project resulted in three publications in international peer-reviewed journals. They are included in this thesis and subject to evaluation. Vidar Skjervold was the main contributor to these articles, carrying out the majority of the research work and writing the original manuscript drafts. Further details on the individual author contributions are given in the CRediT statement included in each article.

Publication I
V.T. Skjervold, G. Mondino, L. Riboldi and L.O. Nord (2023). Investigation of control strategies for adsorption-based CO_2 capture from a thermal power plant under variable load operation. *Energy*, 268, 126728.

Publication II
V.T. Skjervold and L.O. Nord (2023). Enhanced single-loop control of a moving bed temperature swing adsorption CO_2 capture process. *Computers & Chemical Engineering*, 178, 108387.

Publication III
V.T. Skjervold and L.O. Nord (2024). Thermal energy storage integration for increased flexibility of a power plant with post-combustion CO_2 capture. *Applied Thermal Engineering*, 246, 122907.

1.5.2 Conference articles

In addition to the journal articles listed above, the work resulted in three publications related to participation in international scientific conferences. These papers are not included in the thesis because they either overlap with the content in the journal articles or are outside the scope of the thesis.

Publication IV
V.T. Skjervold, G. Mondino, M. Pilarczyk, R. Blom, L.O. Nord, S. Gradziel, W. Zima, A. Cebula, E. Kozak-Jagiela and M. Rerak (2021). InnCapPlant (part 2): adsorption-based CO_2 capture from a thermal power plant under variable load operation. *Proceedings of the 24th Conference on Process Integration for Energy Saving and Pollution Reduction – PRES'21, Brno, Czech Republic, October 31 – November 3, 2021*.

Vidar Skjervold performed the majority of the research work, including adding a process control framework to the MBTSA process model, defining scenarios, carrying out dynamic simulations and writing the original draft of the manuscript.

Publication V
V. Formont, V.T. Skjervold and L.O. Nord (2022). Data-driven approaches for modelling of sub-critical coal-fired boiler. *Proceedings of the 63rd International Conference of Scandinavian Simulation Society, SIMS 2022, Trondheim, Norway, September 20-21, 2022*.

Vidar Skjervold contributed to conceptualization, literature review, data interpretation and writing of parts of the original manuscript.

Publication VI
V.T. Skjervold and L.O. Nord (2022). Increased flexibility of coal-fired power plant with moving bed temperature-swing adsorption CO_2 capture by use of thermal energy storage. *Proceedings of the 16th Greenhouse Gas Control Technologies Conference (GHGT-16), Lyon, France, October 23-27, 2022*.

Vidar Skjervold was the main contributor to the work, including conceptualization, MBTSA process design, thermal storage simulation model development, performing simulations and writing the original draft of the manuscript.

Chapter 2

Literature review

This chapter presents a literature review covering the key topics of the Ph.D project. The goal of the chapter is not to provide an exhaustive list, but to give context to the research presented in this thesis and provide reasoning for the choice of objectives and applied methods.

2.1 Flexibility definitions, modes and methods

Several definitions of flexibility are used in the literature, depending on which part of the energy system is in focus and what type of study is being performed (Lund et al., 2015). The International Energy Agency defines flexibility as ”the extent to which an electricity system can adapt the pattern of electricity generation and consumption in order to balance supply and demand” (IEA, 2015). As indicated by this definition, flexibility can be achieved through both supply and demand-side measures. This Ph.D project focuses on supply-side flexibility modes that are relevant for coal-fired power plants with post-combustion carbon capture. According to Huber et al. (2014), three main metrics can be used to characterize flexibility requirements for power plants, namely the response time, magnitude and frequency of the load change. In addition, the required duration of the load change is important to consider.

As mentioned in Section 1.1, numerous types of flexibility are relevant for operation of power plants with PCC. The ability to operate at low minimum loads will be important, since this reduces the number of plant shutdowns during periods of low demand (Avagianos et al., 2020). The ability to quickly increase the power plant load, both in the form of start-ups and load ramps for a running plant, will also be beneficial. As pointed out by Gonzalez-Salazar et al. (2018), higher ramp rates and more frequent major power cycles will be required to allow thermal power plants to complement renewables in the future. When there is a high demand for electricity, being able to temporarily operate above the

normal maximum load allows the power plant to participate in grid balancing or increase revenues (Chalmers et al., 2009).

In the literature, multiple methods for achieving power plant flexibility have been investigated. A popular topic has been the development of control strategies for the PCC process with the goal of maintaining its performance during flexible operation. Primarily, flexibility driven by modification of the boiler load is considered in this context. Both classical and advanced control structures have been widely studied (Wu et al., 2020c).

Flexibility by altering the operation of the PCC process has also received attention in the literature. For capture technologies that utilize temperature swings for regeneration, large amounts of thermal energy are required. This leads to a significant reduction in the electricity output of the power plant, but also represents a flexibility mode that can be used to rapidly change the power plant load at the expense of reduced CO_2 recovery rates (Abdilahi et al., 2018). One alternative is to reduce the capture level of the PCC process, which can be achieved by adjusting the amount of solvent being regenerated (Zaman and Lee, 2015; Moioli and Pellegrini, 2020) or lowering the regeneration temperature (Seo et al., 2023). A similar effect would be achieved by partial bypass of the capture unit. Another method is reducing the flow rate of steam going from the power plant to the PCC process, which has been studied for grid balancing and for achieving faster load ramps (Wellner et al., 2016; Tait et al., 2018; Wu et al., 2020b; Akram et al., 2021). A third option is the addition of a solvent storage system to the PCC process, which involves storing the CO_2 rich solvent and selectively performing regeneration at a suitable time (Moioli and Pellegrini, 2019; Cheng et al., 2022). This method has the disadvantage of additional capital costs associated with solvent inventory and storage tanks (Abdilahi et al., 2018).

The final key method for power plant flexibilization is the integration of an energy storage system. An energy storage unit can be charged when the demand is low and discharged during periods of high demand, which contributes to decoupling of the boiler and turbines (Zhang et al., 2022). The advantage of this approach over modifying the operation of the PCC process is that the CO_2 recovery rate can be kept at a high level while increasing the electricity output of the power plant. This was recently demonstrated by Chen et al. (2023), where thermal energy storage (TES), battery energy storage and solvent storage were compared for a coal-fired power plant with MEA-based PCC. For power plants without CO_2 capture, thermal energy storage integration for providing flexibility has been extensively studied.

In Figure 2.1, the main flexibility modes and methods mentioned in the literature for thermal power plants with PCC are summarized. A color-coding scheme is used to show which topics have been investigated as part of this Ph.D project. Green indicates a core topic and yellow symbolizes a topic that was studied in less detail.

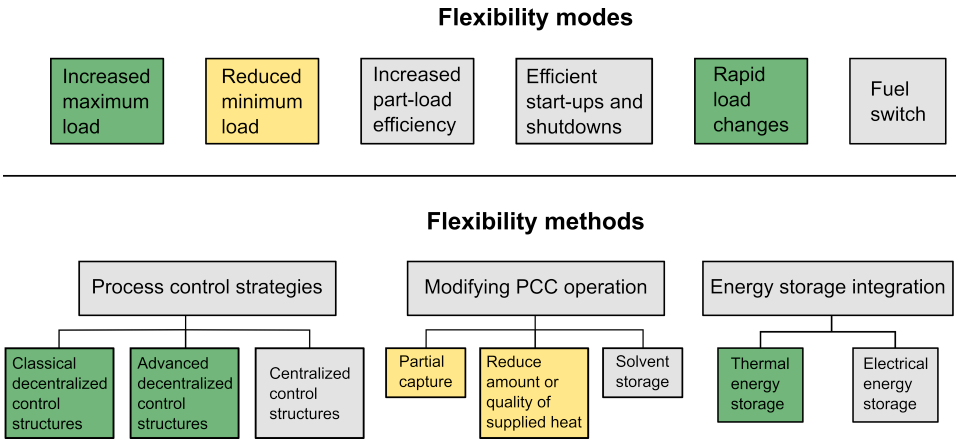

Figure 2.1: Overview of flexibility modes and methods mentioned in the literature for thermal power plants with post-combustion CO_2 capture. Green shading indicates that the topic was a central part of the Ph.D project and yellow shading represents a topic studied in less detail.

In the remaining parts of this chapter, a literature review is presented on process control of PCC processes and TES integration, which are the two main flexibility-related topics considered in this Ph.D project.

2.2 Process control of post-combustion CO_2 capture

Well-functioning control systems for the CO_2 capture process are necessary for flexible operation of power plants, since they ensure safety and robustness under various uncertainties and disturbances (Hasan et al., 2022). Despite its importance, process control of MBTSA for carbon capture had not been studied before this Ph.D project. The focus of this part of the literature review is therefore mostly on solvent-based PCC. Solvent-based processes share some key characteristics with the MBTSA process, including the use of temperature swings for regeneration and a heat exchanger for internal heat recovery. Therefore, such studies can provide relevant inputs for control of the MBTSA system.

2.2.1 Control objectives and pairing of variables

The first discussions in the literature regarding dynamic operation and control of the PCC process emerged in the late 2000s. In Kvamsdal et al. (2009), a dynamic model of a stand-alone absorber unit was presented. The model was used to simulate a part-load scenario where the upstream power plant load was reduced from 100% to 50%, giving a significant decrease in the flue gas flow rate entering the column. The work included a general discussion of control strategies for the capture process, but no controllers were implemented. Among the suggestions was manipulating the solvent flow rate to control the CO_2 recovery rate of the absorber. A similar dynamic model was developed by Lawal et al.

(2009), where the same part-load scenario was used to investigate the dynamic behavior of the absorber column. In this work, adjusting the lean solvent loading by manipulating the reboiler duty or adding fresh solvent were discussed as potential variable pairings. In Ziaii et al. (2009), a stand-alone dynamic model of the desorber was presented. An operation strategy where the reboiler steam flow rate was reduced during periods of high electricity prices was studied, leading to variable CO_2 recovery rates over time.

To the author's knowledge, the article of Lawal et al. (2010) was the first study to consider dynamic modeling and process control of a complete PCC process consisting of an absorber, desorber and rich/lean solvent heat exchanger. A control system consisting of five manipulated variables (MVs) and controlled variables (CVs) connected in single input – single output (SISO) loops was presented. Three of these loops can be viewed as regulatory controllers with the primary goal of stabilizing the operation of the process, namely controlling the condenser temperature by varying its heat duty, controlling the reboiler level by adjusting the bottom outgoing flow rate and controlling the lean solvent composition by manipulating the water makeup flow. The remaining two SISO loops are responsible for controlling the performance of the system. In this layer, the reboiler temperature (which is closely linked to the lean solvent loading) is controlled by varying the reboiler heat duty and the CO_2 recovery rate in the absorber is controlled by changing the lean solvent flow rate. Variations of this general control structure have been used by numerous subsequent studies (Gardarsdottir et al., 2017; Sharifzadeh and Shah, 2019; Wu et al., 2020c). The reverse pairing has also been considered for the performance layer (Panahi and Skogestad, 2012; Nittaya et al., 2014). The two most important higher-level CV – MV pairings mentioned in the literature can be summarized as follows:

1. CO_2 recovery – solvent flow rate and reboiler temperature – reboiler heat duty.
2. CO_2 recovery – reboiler heat duty and reboiler temperature – solvent flow rate.

The process control strategies investigated as part of this Ph.D project follow the first approach, meaning that the circulating sorbent flow rate is used to control the CO_2 recovery rate and the heat flow to the desorption section is used to control variables related to the purity of the CO_2 product.

2.2.2 Classical control structures

Control structures consisting of SISO loops with simple controllers such as proportional-integral (PI) and proportional-integral-derivative (PID) feedback control have been the dominant control techniques for many decades (Seborg et al., 2016). The general term classical control structures is commonly used for such controllers, and they have been widely studied for post-combustion CO_2 capture. As shown in the following paragraphs, several different classical control structures have been discussed in the literature. To evaluate the controller performance, two main types of dynamic scenarios have typically been used. The first type of scenario is meant to emulate flexible power plant operation. If a stand-alone PCC process is considered, they are implemented in the form of an external disturbance to the capture plant. If a coupled model of the power plant and PCC process is used, the variations in e.g. flue gas flow rate and extracted steam flow rate are automatically transferred to the PCC process. The second type of scenario aims at testing

the robustness of the controllers by introducing other types of disturbances and setpoint changes that are not directly caused by flexible power plant operation.

The simplest approach is to focus on modeling and control of only the PCC process. Using this approach, Gaspar et al. (2016) compared the use of MEA and piperazine (PZ) solvents for a gas stream representative of flue gas from a coal-fired power plant (CFPP). Based on the open-loop dynamic behavior of the process and relative gain array analysis, pairing alternative 1 was chosen for MEA and alternative 2 was applied for PZ. In this work, the lean solvent loading was used as CV instead of the reboiler temperature and PI controllers were used for each control loop. The controller performance of the MEA and PZ-based system was compared for multiple ramps in flue gas flow rate (positive and negative), an actuator failure related to the lean solvent valve and a shortage of steam supply.

In Lin et al. (2011), an MEA-based process using the same control structure as Gaspar et al. was studied. No details were given on the type of feedback controllers used in the study. The control system was tested for positive and negative step changes in the water makeup flow rate, incoming flue gas flow rate, CO_2 recovery setpoint, flue gas CO_2 concentration and flue gas water content. Based on heuristics, Mechleri et al. (2014) arrived at the same control structure for an MEA-based process designed for a natural gas combined cycle (NGCC) power plant. The closed-loop dynamic response of the system to a positive and negative step on the flue gas flow rate was studied.

In Gardarsdottir et al. (2015), a comparison of several different control strategies for an MEA-based process designed for CFPP flue gas was presented. In the baseline control structure of this work, pairing alternative 1 was employed to control the CO_2 recovery and lean solvent loading. Using a negative load ramp from full to 60% load, the baseline control structure performance was compared to a case where the CO_2 recovery control was disregarded and a case where the liquid-to-gas ratio in the absorber was controlled instead of the recovery rate. A negative step change in the steam available to the reboiler was also considered. Using the solvent flow to control the ratio between two streams was also considered by Cristea et al. (2020). In this case, the molar ratio between the lean solvent flow rate and the CO_2 molar flow rate in the incoming flue gas was controlled. The CO_2 recovery rate was controlled by the reboiler duty (pairing alternative 2). A solvent buffer tank was also added to the process to reduce interactions within the system. The control structures were tested for disturbances in the flue gas flow rate and inlet CO_2 concentration as well as CV setpoint changes.

Using a coupled model of the power plant and PCC process has been less common than studying the stand-alone capture process, but a few studies have developed such integrated models. Mechleri et al. (2017) studied the coupling of PCC with both a CFPP and NGCC power plant, also including the CO_2 compression in the models. Feedback controllers using pairing alternative 2 were implemented, and a case with dynamic switching between controller modes was also studied. A supercritical CFPP with MEA-based CO_2 capture was studied in Gardarsdottir et al. (2017) and used to compare several different control structures. Both pairing alternative 1 and 2 were considered, in addition to replacing the CO_2 recovery with the liquid-to-gas ratio in the absorber as the CV. These control strategies were also studied in Montañés et al. (2017) for an MEA-based PCC process coupled with

an NGCC power plant. In addition, feedforward control of the solvent and reboiler steam flow was included in the comparison. A model of a subcritical CFPP with amine-based PCC was developed by Lawal et al. (2012). The same controllers as in Lawal et al. (2010) were used for the PCC process.

2.2.3 Advanced control structures

In the case of advanced control, added complexity is introduced in the control structure with the goal of improving its performance. As indicated in Figure 2.1, advanced control structures can be divided into two sub-categories, namely advanced decentralized control and centralized control (Seborg et al., 2016).

Advanced decentralized control for PCC has not received much attention in the literature. An exception is the work of Montañés et al. (2018), where a cascade controller was evaluated for CO_2 recovery control. An outer feedback loop with CO_2 recovery as the CV was used to determine the setpoint for a fast inner loop where the rich solvent mass flow rate was controlled by manipulating the pump speed. In this work, the possibility of using a combined feedforward and feedback algorithm for the PCC process was also discussed. This approach could help avoid the steady-state offsets that have been identified as a drawback of stand-alone feedforward control (Posch and Haider, 2013).

Centralized control of PCC processes has received significant attention in the literature in recent years through studies on model predictive control (MPC). In MPC, an optimization problem is solved at every time step to determine the optimal control action for a specified predictive horizon (Wu et al., 2020c). The advantage of MPC over classical control structures is the improved handling of coupled control loops and the ability to handle constraints (Akinola et al., 2020). A predictive model of the PCC process is required by the MPC algorithm. Such a model should be computationally efficient and able to predict the future values of CVs based on the current state and future values of the MVs with reasonable accuracy. Different types of MPC exist, depending on the type of predictive model. If the model is linear, the control method is called linear MPC (LMPC) and if the predictive model is non-linear, the method is called non-linear MPC (NMPC). The objective function used in the optimization algorithm usually contains terms penalizing setpoint deviations and abrupt changes in MV values (Wu et al., 2020a).

Many studies have investigated LMPC for stand-alone PCC processes. An example is the work of Jung et al. (2020), where LMPC of a typical amine-based PCC process was studied. The predictive model was developed by linearizing a first-principle model validated with data from a pilot plant. To identify the optimal reference point for linearization, gap metric analysis was applied. The same group studied LMPC based on a state-space model for control of PCC with an advanced flash stripper (Jung et al., 2021). Li et al. (2021) investigated LMPC of an MEA-based process with CO_2 recovery as the only controlled variable. System identification applied to simulation data from a first-principle model was used to develop the predictive model. Since the control algorithm only involved one CV and MV, the optimization could be solved analytically. Sultan et al. (2022) investigated the option of ”fast model predictive control” by solving the LMPC optimization problem in smaller fragments, reporting shorter settling times and smaller setpoint deviations

compared to using the standard approach.

Numerous articles have evaluated LMPC using coupled models of the power plant and PCC process. Rúa et al. (2021) investigated the dynamic behavior and control of an NGCC-PCC system using a method where the predictive model consisted of several linear models combined in a local model network. Wu et al. (2019) studied a CFPP-PCC system with a similar control approach. The power plant and capture process were both included in the centralized control structure and state-space predictive models were used for both sub-processes. Tang and Wu (2023) also studied a CFPP-PCC system, where dynamic matrix controllers were developed for both the power plant and capture process. They also implemented a neural network-based feedforward controller for the allocation of reboiler steam between power generation and solvent regeneration. Liao et al. (2023) evaluated a control system based on state-space models and an extended state observer for a similar integrated process.

If the controllers should be applicable in a wide range of operation, NMPC might be necessary in order to capture the non-linear dynamics of the PCC process (Wu et al., 2020c). Akinola et al. (2020) investigated NMPC for the PCC process based on a nonlinear autoregressive with exogeneous input (NARX) predictive model. The NMPC approach was found to outperform LMPC for variations in flue gas flow rate and CV setpoint changes. Mejdell et al. (2022) tested the commercial NMPC software CENIT at the Tiller pilot plant in Norway. The control system was found to handle both setpoint changes and disturbance rejection. Patron and Ricardez-Sandoval (2020) studied a robust NMPC method for the absorber unit of a PCC process, meaning that uncertainties in the parameters of the predictive model were accounted for when determining the optimal control action. For an integrated CFPP-PCC system, Liao et al. (2020) applied a neural network-based algorithm to predict MV values from CV setpoints instead of the process state. A PID compensator was also added to eliminate steady-state offset.

Another advantage of MPC is that additional terms can be included in the objective function, allowing factors not directly associated with the controller performance to influence the control action. The most common example of this in the literature is economic MPC (EMPC), where terms related to process economics are included in the optimization problem. Chan and Chen (2018) studied the effect of including the cost of solvent and utilities in the objective function. In the work of Ma et al. (2021), the carbon emissions costs were included in the EMPC. Yu and Biegler (2018) studied a bubbling fluidized-bed solid-sorbent PCC process, applying EMPC where costs related to cooling water and purge gas were included in the optimization. In Patrón and Ricardez-Sandoval (2022), the EMPC formulation included costs related to energy, chemicals, utilities and emitting CO_2 as well as income from selling captured CO_2.

2.3 Thermal energy storage integration

As stated in Section 2.1, different types of energy storage can be used to provide flexibility. Advantages of thermal energy storage technologies compared to battery-based systems are longer lifetimes and lower levelized cost of electricity (Sayed et al., 2023), meaning TES

could be the preferred option for storage systems with capacities exceeding a few MW (Kebede et al., 2022). In addition, some TES technologies can utilize existing infrastructure in a power plant, leading to lower investment costs.

2.3.1 Coupling of thermal energy storage and CO_2 capture plants

The coupling of TES and PCC processes has mostly been studied in connection with the use of solar thermal energy to reduce the power plant efficiency penalty associated with PCC integration (Saghafifar and Gabra, 2020). Due to the intermittency of this renewable energy source, an energy storage system is needed if a stable supply of heat to the PCC process is desired. The first solution of this type was presented by Wibberley (2007), where energy storage in the form of additional solvent regeneration during periods of abundant solar energy was suggested. A similar concept based on thermochemical storage of calcined sorbent was studied by Tregambi et al. (2015) for a calcium looping PCC process. In recent years, many studies focusing on thermal energy storage have been published. As summarized by Parvareh et al. (2014), there are two main options for coupling TES with the PCC process, namely the direct and indirect option. In the direct option, heat from the TES system is sent directly to the regeneration step of the PCC process. In the indirect option, the TES is discharged to cover a heat demand somewhere in the power plant, which makes more steam available for PCC regeneration.

Cohen et al. (2010) studied a two-tank TES system using a molten nitrate salt as the storage medium for heat delivery to an MEA-based PCC process. The TES system was designed to cover the regeneration duty of the PCC process for six hours. A similar molten-salt TES system was studied in Ordorica-Garcia et al. (2011) for carbon capture from an NGCC power plant. In their suggested process, the TES system was used to generate steam for solvent regeneration. Wang et al. (2021) compared MEA and NH_3-based PCC where a phase change material (PCM) TES was installed between the solar collectors and carbon capture process. The same PCM material (Erythritol) was considered by Li et al. (2012) for MEA-based PCC, and the thermal storage was designed to cover the regeneration duty for a few hours. Mokhtar et al. (2012) investigated the use of a solid sensible TES system for heat delivery to an MEA-based capture process.

Although these articles provide useful information on the coupling of TES and PCC processes, their primary focus is not on using energy storage for enabling flexible power plant operation. To the author's knowledge, the previously mentioned study of Chen et al. (2023) is the only article on TES for this purpose in the literature. However, for power plants without CO_2 capture the topic has been extensively studied and TES solutions have been applied in practice. For example, steam storage tanks for peak demand and balancing purposes were in operation already in 1929 at the Berlin-Charlottenburg power plant in Germany (IEA-ECES, 2018). Since the integration of a TES system with a power plant is similar to coupling with a PCC process, such studies are relevant for this work. A summary of relevant articles is given in the following sub-section.

2.3.2 Thermal energy storage for power plant flexibility

Several studies have focused on TES based on molten salts for power plant integration. In Kosman and Rusin (2020), a molten salt system with the purpose of producing steam for a subcritical turbine during periods of high electricity prices was studied. The TES system was charged either by electrical heating or with steam extracted from a continuously operating supercritical turbine during periods of low demand. In Zhang et al. (2022), a combination of flue gas and live steam from a coal-fired boiler was used for TES charging. Heat from the molten salt was used to cover feedwater heating demands, replacing some of the high and intermediate pressure steam extracted from the power plant. This increases the steam flow rate passing through the turbine train, giving an increase in the electrical power production. Garbrecht et al. (2017) studied a high-temperature and a low-temperature molten salt loop designed to cover different demands in the power plant during discharging. The high-temperature loop was used to cover the additional reheat demand and the low-temperature loop was used for heating of high-pressure feedwater, allowing the closing of a high-pressure steam extraction valve. TES charging was performed by extracting additional steam from the turbine train. Molten salt-based TES has the advantage of delivering heat at a high temperature, but requires several additional heat exchangers and significant modifications of the steam cycle.

Li and Wang (2018) investigated power plant load balancing and frequency control through the use of a PCM-based TES consisting of five different materials in series. The TES was charged with either intermediate or low-pressure steam from the turbine train. Two discharging strategies were compared, i.e. the generation of additional steam sent directly to the low-pressure turbine or covering feedwater heating demands. Based on an evaluation of several TES – power plant integration options, Krüger et al. (2020) identified a combined PCM – steam accumulator concept, molten salt system and solid media thermal storage as the most promising solutions. For the latter, charging takes place by redirecting parts of the evaporator flue gas flow and during discharging an additional air mass flow is heated up before being fed to the boiler. In Cao et al. (2020), an additional supercritical Rankine cycle was retrofitted to a CFPP for covering peak electrical power demands. This additional cycle is fed with steam generated by a high temperature TES system that is charged by an electric boiler when the electricity price is low.

An advantage of using water or steam as the TES medium is that the thermal storage can interact directly with the water/steam cycle of the thermal power plant (Zhang et al., 2022). This avoids exergy losses associated with intermediate heat transfer loops, thus increasing efficiency. The use of pressurized hot water tanks for efficient start-ups and widening of the power plant load range was investigated by Trojan et al. (2019). A steam accumulator system was studied by Richter et al. (2019) for minimum load reduction and increased maximum electricity production. Charging of the accumulator takes place by extracting cold reheat steam at full load and live steam from the coal-fired boiler at lower loads. To increase the net electrical power output of the CFPP, discharged steam is used to cover the demand of one of the high-pressure feedwater heaters. Stevanovic et al. (2020) studied a similar type of TES, where discharged steam was instead used to provide heat to two of the low-pressure condensate heaters in the CFPP.

2.4 Knowledge gaps

Along with the literature discussed in Section 1.1, the literature review presented in this chapter revealed several knowledge gaps that were used to define the objectives and scope of this work. The main knowledge gaps addressed by this Ph.D project are listed below:

1. The dynamic behavior of the complete MBTSA process under disturbances related to flexible power plant operation had not been studied prior to this work.
2. Process control of MBTSA for post-combustion CO_2 capture had not been investigated before this project.
3. Using a thermal energy storage system to deliver heat to the MBTSA process had not previously been considered in the literature.
4. The integration of a thermal energy storage system into a power plant with MBTSA-based PCC with the aim of enabling flexible power plant operation had not been studied prior to this project.

Chapter 3

Methodology

3.1 MBTSA process model

As mentioned in Section 1.2, the MBTSA process model used in this Ph.D project was based on the model developed by Mondino (2022). Although the model is dynamic, it had only been used for steady-state simulations prior to this work. The changes made to the model as part of this project were therefore focused on facilitating dynamic simulations, primarily through the addition of a control framework.

3.1.1 Definitions and assumptions

In this project, two main indicators of the MBTSA process performance are used, namely the CO_2 recovery rate and CO_2 product purity. The recovery rate, often referred to as the CO_2 capture rate, is defined as the ratio between the mass flow of CO_2 leaving via the CO_2-rich stream out of the system and the mass flow of CO_2 entering via the flue gas:

$$\text{CO}_2 \text{ recovery} = \frac{\dot{m}_{\text{CO}_2,\text{out}}}{\dot{m}_{\text{CO}_2,\text{in}}}. \tag{3.1}$$

The CO_2 purity is defined as the molar fraction of CO_2 in the CO_2-rich stream leaving the system:

$$\text{CO}_2 \text{ purity} = \frac{\dot{n}_{\text{CO}_2,\text{out}}}{\dot{n}_{\text{tot, out}}}. \tag{3.2}$$

Where $\dot{n}$ denotes a molar flow rate.

Throughout the project, it has been assumed that the flue gas has been dried and cooled before entering the MBTSA unit. This means that additional energy requirements associated with drying and cooling are not accounted for. Furthermore, it has been assumed that the flue gas consists of a binary mixture of carbon dioxide and nitrogen. This inherently

assumes that O_2 and Ar exhibit similar behavior as N_2 (Mondino et al., 2019). For adsorbents such as Zeolite 13X where nitrogen has a stronger affinity towards the adsorbent than oxygen and argon, dry flue gas is well approximated by this binary mixture (Park et al., 2006; Merel et al., 2008). Correlations for particle fluidization are not included in the MBTSA model, but for the large sorbent flow rates and particle sizes considered in this work this is not expected to be an issue. Mondino (2022) lists the following assumptions that were made in the model development: negligible gradients in the radial direction, constant cross-sectional area, constant sorbent velocity, uniform and constant void fraction and ideal gas behavior in the bulk gas phase.

In Figure 3.1, the MBTSA process with the baseline control structure considered in this work (explained in Section 3.3.1) is shown.

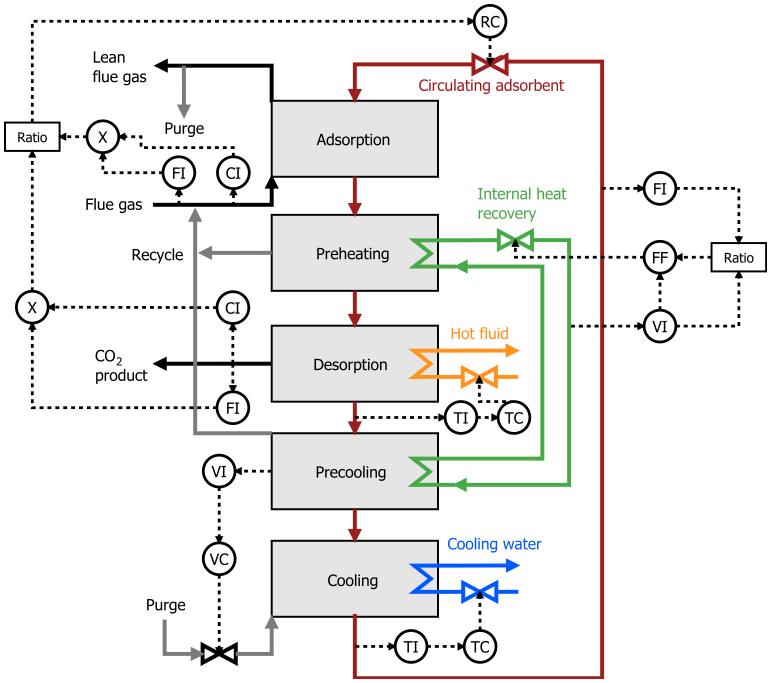

Figure 3.1: Overview of MBTSA process with the baseline control structure. CI, FI, TI and VI indicate composition, flow, temperature and velocity measurements. RC, TC and VC indicate recovery, temperature and velocity controllers. FF indicates a feedforward controller.

3.1.2 Model equations and implementation

The model of the MBTSA process consists of a set of partial differential equations with time and the axial coordinate as independent variables. They account for the mass, energy and momentum balances of each part of the process (i.e. the adsorption, preheating, desorption, precooling and cooling section). Three different phases are considered: the gas phase, solid phase and the gas within the macropores of the adsorbent material. The

underlying set of equations is the same for each section, but design parameter values and operating conditions vary. In this subsection, the equations and correlations used in the model are described.

Mass balance in the gas phase

The species gas phase concentration is governed by convection, axial dispersion and mass transport between the gas and macropores of the adsorbent. The linear driving force (LDF) approximation is used to calculate the interfacial mass transfer. The axial gas phase concentration profile for component i is given by:

$$\varepsilon_{\mathrm{c}}\frac{\partial C_i}{\partial t}+\frac{\partial(uC_i)}{\partial z}=\varepsilon_{\mathrm{c}}\frac{\partial}{\partial z}\left(D_{z,i}C_{\mathrm{T}}\frac{\partial Y_i}{\partial z}\right)-\frac{(1-\varepsilon_{\mathrm{c}}-\xi)\,a'k_{\mathrm{f},i}}{\mathrm{Bi}_i/5+1}(C_i-C_{\mathrm{p},i}), \tag{3.3}$$

where t is the time and z is the axial coordinate. C_i, $C_{\mathrm{p},i}$ and Y_i is the bulk gas concentration, macropore gas concentration and bulk gas molar fraction, respectively. ε_{c} is the column void fraction, ξ is the volume fraction occupied by structured packing, $D_{z,i}$ is the axial dispersion coefficient, u is the superficial gas velocity, a' is the specific area of the adsorbent particles, $k_{\mathrm{f},i}$ is the mass transfer coefficient in the film surrounding the adsorbent particles, Bi_i is the Biot number and C_T is the total bulk gas concentration. The ideal gas equation of state is applied for the bulk gas phase:

$$C_{\mathrm{T}}=\sum_i C_i=\frac{P}{RT}, \tag{3.4}$$

where P and T are the gas pressure and temperature and R is the universal gas constant.

Mass balance in the macropores

The gas concentration of each specie in the macropores depends on both the mass transfer from the bulk phase and the mass transfer to the solid adsorbent phase. The LDF approximation is used to model the mass transfer between the macropores and solid phase, giving the following mass balance:

$$\varepsilon_{\mathrm{p}}\frac{\partial C_{\mathrm{p},i}}{\partial t}+v_{\mathrm{s}}\frac{\partial C_{\mathrm{p},i}}{\partial z}=\varepsilon_{\mathrm{p}}\frac{15D_{\mathrm{p},i}}{r_{\mathrm{p}}^2}\frac{\mathrm{Bi}_i}{5+\mathrm{Bi}_i}\left(C_i-C_{\mathrm{p},i}\right)-\rho_{\mathrm{p}}\frac{15D_{\mathrm{c},i}}{r_c^2}\left(q_i^*-q_i\right), \tag{3.5}$$

where ε_{p} is the particle porosity, r_{p} is the particle radius, $D_{\mathrm{p},i}$ is the macropore diffusivity, ρ_{p} is the particle density, q_i is the adsorbed concentration of component i, q_i^* is the adsorbed concentration at equilibrium with the local macropore gas concentration and v_s is the velocity of the adsorbent in the moving bed. The term $15D_{\mathrm{c},i}/r_{\mathrm{c}}^2$ is treated as a single parameter representing the adsorption rate of component i.

Mass balance in the solid phase

The mass balance for the solid phase is used to determine the adsorbent loading profiles. It is given by:

$$\frac{\partial q_i}{\partial t}+v_{\mathrm{s}}\frac{\partial q_i}{\partial z}=\frac{15D_{\mathrm{c},i}}{r_{\mathrm{c}}^2}\left(q_i^*-q_i\right). \tag{3.6}$$

Adsorption equilibrium

The adsorption equilibrium is determined by the extended Virial isotherm model for multicomponent gas mixtures, taking into account the competitive adsorption of the different species in the mixture:

$$P_i = \frac{q_i^*}{K_{\mathrm{H},i}} \exp\left[\sum_{j=1}^{N} A_{ij} q_j^* + \sum_{j=1}^{N}\sum_{k=1}^{N} B_{ijk} q_j^* q_k^*\right]. \tag{3.7}$$

The mixing Virial coefficients A_{ij} and B_{ijk} are calculated from the pure-component adsorption isotherm parameters by using the following relations:

$$A_{ij} = \frac{A_i + A_j}{2}, \quad \text{and} \quad B_{ijk} = \frac{B_i + B_j + B_k}{3}. \tag{3.8}$$

To find the pure-component isotherm parameters, experimental data is fitted to the pure-component Virial equation, which is given by:

$$P_i = \frac{q_i^*}{K_{\mathrm{H},i}} \exp(A_i q_i^* + B_i q_i^{*2}). \tag{3.9}$$

Here, P_i is the partial pressure and $K_{\mathrm{H},i}$ is the Henry's law constant. The temperature dependence of the pure-component Virial coefficients is given by:

$$A_i = A_{0,i} + \frac{A_{1,i}}{T_\mathrm{s}} \quad \text{and} \quad B_i = B_{0,i} + \frac{B_{1,i}}{T_\mathrm{s}}, \tag{3.10}$$

where T_s is the adsorbent temperature. The temperature dependence of the Henry's law constant is calculated from the Van't Hoff equation:

$$K_{\mathrm{H},i} = K_{\mathrm{H},i}^{\infty} \exp\left(\frac{-\Delta H_i}{R T_\mathrm{s}}\right), \tag{3.11}$$

where $K_{\mathrm{H},i}^{\infty}$ is the adsorption constant at infinite temperature and ΔH_i is the heat of adsorption at zero coverage.

Momentum balances

The bulk gas phase pressure gradient in the axial direction is given by the Ergun equation for all sections except the adsorption section. It can be written as:

$$-\frac{\partial P}{\partial z} = \frac{150\mu_\mathrm{g}(1-\varepsilon_\mathrm{c})^2}{\varepsilon_\mathrm{c}^3 d_\mathrm{p}^2} u + \frac{1.75(1-\varepsilon_\mathrm{c})\rho_\mathrm{g}}{\varepsilon_\mathrm{c}^3 d_\mathrm{p}} u|u|, \tag{3.12}$$

where d_p is the particle diameter, μ_g is the gas viscosity and ρ_g is the gas density. In the adsorption section, the void fraction is higher than in the other sections. Therefore, a simplified momentum balance was used:

$$-\frac{\partial P}{\partial z} = (1 - \varepsilon - \xi)\, a' \,(\rho_\mathrm{p} - \rho_\mathrm{g})\,. \tag{3.13}$$

Energy balances

It is assumed that the gas in the macropores is in thermal equilibrium with the solid material, meaning that no energy balance is required for this phase. The gas temperature is influenced by heat convection, axial heat dispersion, heat transfer between the gas and solid material and heat transfer between the gas and tube wall for sections operated as indirect-contact heat exchangers. The adsorption section is assumed to be operated adiabatically. The gas phase energy balance can be written as:

$$\begin{aligned}\varepsilon_{\mathrm{c}} C_{\mathrm{T}} \hat{c}_v \frac{\partial T}{\partial t} + u C_{\mathrm{T}} \hat{c}_p \frac{\partial T}{\partial z} = \frac{\partial}{\partial z}\left(\lambda_{\mathrm{g}} \frac{\partial T}{\partial z}\right) + \varepsilon_{\mathrm{c}} R T \sum_i \frac{\partial C_i}{\partial t} - \\ (1-\varepsilon_{\mathrm{c}} - \xi)\, a' h_{\mathrm{gs}} \left(T - T_{\mathrm{s}}\right) - \alpha_{\mathrm{gt}} h_{\mathrm{gt}} \left(T - T_{\mathrm{t}}\right),\end{aligned} \tag{3.14}$$

where h_{gs} is the film heat transfer coefficient between the gas and the solid, h_{gt} is the convective heat transfer coefficient between the gas and the wall of the tubes, α_{gt} is heat transfer area per unit volume, T_{t} is the tube wall temperature, $\hat{c}_v$ is the gas molar heat capacity at constant volume, $\hat{c}_p$ is the gas molar heat capacity at constant pressure and λ_{g} is the axial heat dispersion coefficient of the gas.

The energy balance for the solid material is given by:

$$\begin{aligned}[(1-\varepsilon_{\mathrm{c}}-\xi)\rho_{\mathrm{p}} c_{p,\mathrm{s}} + \xi \rho_{\mathrm{pk}} c_{p,\mathrm{pk}}]\left(\frac{\partial T_{\mathrm{s}}}{\partial t} + v_{\mathrm{s}} \frac{\partial T_{\mathrm{s}}}{\partial z}\right) = \xi \frac{\partial}{\partial z}\left(\lambda_{\mathrm{pk}} \frac{\partial T_{\mathrm{s}}}{\partial z}\right) + \\ (1-\varepsilon_{\mathrm{c}}-\xi) a' h_{\mathrm{gs}} (T - T_{\mathrm{s}}) + (1-\varepsilon_{\mathrm{c}}-\xi)\rho_{\mathrm{p}} \sum_i \left(-\Delta H_i \left[\frac{\partial q_i}{\partial t} + v_{\mathrm{s}} \frac{\partial q_i}{\partial z}\right]\right) + \\ (1-\varepsilon_{\mathrm{c}}-\xi)\varepsilon_{\mathrm{p}} R T_{\mathrm{s}} \sum_i \left[\frac{\partial C_{\mathrm{p},i}}{\partial t} + v_{\mathrm{s}} \frac{\partial C_{\mathrm{p},i}}{\partial z}\right],\end{aligned} \tag{3.15}$$

where ΔH_i is the heat of adsorption of component i, $c_{p,s}$ is the specific heat capacity of the adsorbent, $c_{p,\mathrm{pk}}$ is the specific heat capacity of the packing and ρ_{pk} is the density of the packing.

For the sections with embedded heat exchanger tubes, additional equations are needed to calculate the temperature of the tube wall and heat exchanger fluid (T_{f}):

$$\rho_{\mathrm{t}} c_{p,\mathrm{t}} \frac{\partial T_{\mathrm{t}}}{\partial t} = \alpha_{\mathrm{t,ext}} h_{\mathrm{gt}} (T - T_{\mathrm{t}}) - \alpha_{\mathrm{t,int}} h_{\mathrm{ft}} (T_{\mathrm{t}} - T_{\mathrm{f}}) \quad \text{and} \tag{3.16}$$

$$\rho_{\mathrm{f}} c_{p,\mathrm{f}} \frac{\partial T_{\mathrm{f}}}{\partial t} + u_{\mathrm{f}} \rho_{\mathrm{f}} c_{p,\mathrm{f}} \frac{L_z}{L_x} \frac{\partial T_{\mathrm{f}}}{\partial z} = -\alpha_{\mathrm{t,int}} h_{\mathrm{ft}} (T_{\mathrm{f}} - T_{\mathrm{t}}). \tag{3.17}$$

Here, the subscript t refers to the tube wall and the subscript f refers to the heat exchanger fluid. In addition, $\alpha_{\mathrm{t,ext}}$ is the external heat transfer area per unit of fluid volume, $\alpha_{\mathrm{t,int}}$ is the internal heat transfer area per fluid volume, h_{ft} is the convective heat transfer coefficient between the heat exchanger fluid and the tubes and the ratio L_x/L_z is the distance travelled by the heat exchanger fluid per unit of height.

Correlations and dimensionless numbers

The correlations used in the MBTSA process model are summarized in Table 3.1.

Table 3.1: Correlations used in the MBTSA process model.

Description	Equation
Binary diffusivity	$D_{ij} = \frac{0.01883\ T^{3/2}}{P\ \sigma_{ij}^2\ \Omega_{D_{ij}}} \sqrt{\frac{1}{M_{\mathrm{w},i}} + \frac{1}{M_{\mathrm{w},j}}}$
Molecular diffusivity	$D_{\mathrm{m},i} = \frac{1-Y_i}{\sum_{j\neq i}^{n} \frac{Y_i}{D_{ij}}}$
Knudsen diffusivity	$D_{\mathrm{Kn},i} = 97 r_{\mathrm{p}} \sqrt{\frac{T}{M_{\mathrm{w},i}}}$
Macropore diffusivity	$\frac{1}{D_{\mathrm{p},i}} = \tau_{\mathrm{p}} \left(\frac{1}{D_{\mathrm{Kn},i}} + \frac{1}{D_{\mathrm{m},i}}, \right)$
Axial dispersion coefficient	$D_{z,i} = \frac{D_{\mathrm{m},i}}{\varepsilon_{\mathrm{c}}} (20 + 0.5\ \mathrm{Sc}_i\ \mathrm{Re})$
Adsorption rate in micropores	$\frac{15 D_{\mathrm{c},i}}{r_{\mathrm{c}}^2} = \frac{15 D_{\mathrm{c},i}^0}{r_{\mathrm{c}}^2} \exp\left(\frac{-E_{\mathrm{a},i}}{RT}\right)$
Axial thermal conductivity of gas	$\lambda_{\mathrm{g}} = k_{\mathrm{g}} (7 + 0.5\ \mathrm{Pr}\,\mathrm{Re})$
Sherwood number correlation	$\mathrm{Sh} = 2.0 + 1.1 \mathrm{Re}^{0.6} \mathrm{Sc}^{1/3}$
Nusselt number correlation	$\mathrm{Nu} = 2.0 + 1.1 \mathrm{Re}^{0.6} \mathrm{Pr}^{1/3}$

The dimensionless numbers used in the model are defined in Table 3.2.

Table 3.2: Definition of the dimensionless numbers used in the MBTSA process model.

Description	Equation
Biot number	$\mathrm{Bi}_i = \frac{r_{\mathrm{p}} k_{\mathrm{f},i}}{\varepsilon_{\mathrm{p}} D_{\mathrm{p},i}}$
Nusselt number	$\mathrm{Nu} = \frac{h_{\mathrm{gs}} d_{\mathrm{p}}}{k_{\mathrm{g}}}$
Prandtl number	$\mathrm{Pr} = \frac{c_{p,\mathrm{g}} \mu_{\mathrm{g}}}{k_{\mathrm{g}}}$
Reynolds number	$\mathrm{Re} = \frac{\rho_{\mathrm{g}} u\, d_{\mathrm{p}}}{\mu_{\mathrm{g}}}$
Schmidt number	$\mathrm{Sc}_i = \frac{\mu_{\mathrm{g}} \rho_{\mathrm{g}}}{D_{\mathrm{m},i}}$
Sherwood number	$\mathrm{Sh}_i = \frac{k_{\mathrm{f},i} d_{\mathrm{p}}}{D_{\mathrm{m},i}}$

Model implementation

The model equations were implemented in gPROMS ModelBuilder version 7.1.1. To link the individual sections of the model, the composite modeling capabilities of gPROMS were used. When adding the control framework to the model, connectors from the built-in PMLControl library were used to transfer measurements and control signals between model entities. The differential equations were discretized in the axial domain by a central finite difference method. The solvers SRADAU and MA28 were used for differential-algebraic equations and linear algebra, respectively.

3.1.3 Design procedure

The MBTSA process has several geometrical and operational parameters that can be adjusted to influence the design and performance of the process. To maximize the process performance, it is likely that an optimization-based design algorithm will be necessary. However, since the focus of this project was to study the flexible operation of the MBTSA process, the development of such advanced design methods was considered to be outside of the scope of the work. When scaling up the process to a larger flue gas flow rate with a potentially different CO_2 concentration, a manual design approach based on the design at smaller scale was used. The approach can be summarized as follows:

1. From the flue gas flow rate and composition, determine the molar flow of CO_2 in the scaled-up case.
2. Based on the desired CO_2 recovery rate, calculate the molar flow rate of CO_2 that should be captured.
3. Based on the working capacity of the adsorbent from the previous design, estimate the required adsorbent flow rate in the scaled up case.
4. Adjust the geometry of the adsorption, preheating, desorption, precooling and cooling section so that the adsorbent residence time in each section is the same as in the previous design.
5. Based on the superficial gas velocity in the adsorption section of the scaled-up design, verify that fluidization does not occur.
6. If necessary, the operational parameters of each section can be adjusted until the desired process performance is achieved.

3.1.4 Adsorbent materials, system scales and performance targets

The adsorbent materials, system scales and performance targets used in this work were chosen in collaboration with the partners in the InnCapPlant project. Following a selection process within the project, activated carbon and Zeolite 13X were chosen as adsorbent materials. Although the activated carbon has a significantly lower CO_2 adsorption capacity and selectivity than Zeolite 13X, its spherical shape, mechanical properties and particle size makes it interesting to consider for the MBTSA process. Among the goals of the InnCapPlant project was to evaluate the MBTSA technology for two different coal-fired

power plant types, namely a smaller subcritical unit and a larger supercritical power plant. The InnCapPlant project had a target of 85% CO_2 recovery and 95% CO_2 purity.

Within InnCapPlant, operational data from a subcritical power plant in Poland was available from the beginning of the project. It was therefore decided to use this type of CFPP for the first part of the work (Publication I). The subcritical unit had a nominal flue gas mass flow rate of 58 kg/s. To evaluate whether it could meet the recovery and purity targets for this application, activated carbon was chosen as the adsorbent material in this article. From the results in Section 4.1 and 4.2 it is seen that the process was able to meet the purity requirement. However, a nominal CO_2 recovery rate of around 82% was achieved, which is below the target value. The energy requirement of the process was also high. It was therefore decided to use Zeolite 13X as the adsorbent material in Publication II and III, which considered CO_2 capture from the supercritical power plant type. Due to the higher CO_2 adsorption capacity and selectivity, both the purity and recovery targets were achieved when using Zeolite 13X. For these publications, the CO_2 recovery target was increased to 90%, since this is a typical value used in the literature for post-combustion CO_2 capture. The total flue gas mass flow rate from the supercritical CFPP was 804 kg/s. Due to the large amount of gas being processed, it was decided to employ two parallel MBTSA units to avoid unrealistically large column sizes.

3.2 Coal-fired power plant model

In Publication I, the boundary conditions to the MBTSA process were based only on data from the subcritical power plant, meaning that no power plant model was required. For Publication II and II, a power plant design based on the supercritical pulverized coal-fired reference plant from NETL (2019) was used. The steam turbine train consists of one high-pressure turbine, two intermediate-pressure turbines and two low-pressure turbines. A single reheat stage between the high-pressure and intermediate-pressure turbine is included. The net electrical power output of the plant is 598 MW after integration with the CO_2 capture process. Steam for MBTSA regeneration is extracted from the intermediate-pressure turbine and returned to the deaerator. Before being sent to the PCC process, the flue gas from the boiler passes through an electrostatic precipitator, a wet flue gas desulfurization unit and a cooling and drying step. A flow diagram of the power plant is shown in Figure 3.2.

A steady-state model of the power plant was built in version 30 of the STEAM PRO and STEAM MASTER programs from Thermoflow (Thermoflow, 2023). The design of the power plant was done in STEAM PRO and steady-state off-design simulations were performed in STEAM MASTER after fixing the design of the process. In Publication III, the main focus is on flexibility introduced by the opening and closing of valves in the water/steam cycle at constant boiler firing rates. Since such changes will influence the power plant production without significant delays, using a steady-state model is assumed to be sufficient.

When considering ramps in the power plant load through changes in the boiler operation, a dynamic power plant model would give the most accurate results. In this project, a

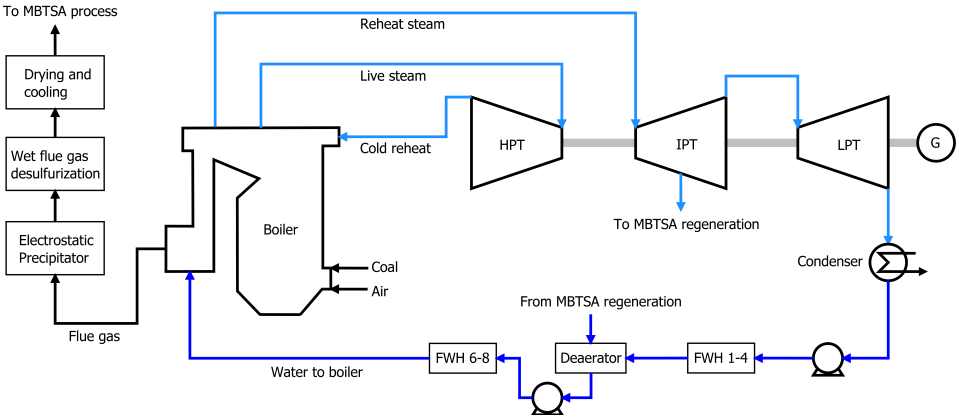

Figure 3.2: Process flow diagram of the supercritical coal-fired power plant configuration used in this work.

simplification was made by assuming a constant ramp rate over a given period of time. For the smaller scale CFPP, a ramp rate of 4% of the nominal load per minute was used. For the supercritical CFPP, the ramp rate was 5% of the nominal power plant load over a period of 30 seconds, which follows the requirement for newly built power plants in Poland (Zima et al., 2023). In Publication I, the flue gas flow rate was assumed to vary linearly with the load. In Publication II, the ramps were made more accurate by performing steady-state off-design simulations to determine the relationship between the flue gas flow rate and power plant load.

3.3 Process control

3.3.1 Investigated control structures

In total, five different types of control structures were studied as part of the Ph.D project. In Publication I, the focus was on simple, decentralized control strategies. Since control of the MBTSA process for PCC had not been investigated prior to the project, this approach was a natural starting point that established a baseline for comparison with more advanced strategies. In Publication II, enhanced single-loop control structures were compared to this baseline. Enhanced single-loop control is a collective term for advanced, decentralized strategies that aim at improving performance beyond what can be achieved with SISO PID loops without the complexity of MPC (Seborg et al., 2016). As shown in the literature review in Chapter 2, MPC is often preferred over decentralized control. However, some studies have concluded that MPC does not provide a large enough performance improvement to justify the increase in complexity (Panahi and Skogestad, 2012; Cormos et al., 2015).

The types of control structures investigated in this Ph.D project are listed below:

1. PI feedback control (baseline structure shown in Figure 3.1)

2. Ratio-based feedforward control
3. Cascade control
4. Combined feedforward and feedback control
5. Adaptively tuned PI control

The strategies listed above were all applied to the performance control layer of the MBTSA process, i.e. involving the control of the CO_2 recovery or purity. As discussed in Section 2.2, there are two main alternatives regarding the variable pairings for this layer. In this project, the CO_2 recovery was controlled by manipulating the sorbent flow rate and the purity or regenerated sorbent temperature was controlled by varying the heating fluid flow to the desorption section. The opposite pairing would also be possible. In addition to the performance layer, a regulatory layer was developed to control additional variables needed for stable operation of the process. This layer was identical in all cases considered in this work. The different control loops and variable pairings are summarized in Table 3.3.

Table 3.3: Summary of the control loops and variable pairings used for the MBTSA process.

No.	Layer	Controlled variable	Manipulated variable
1	Performance	CO_2 recovery	Sorbent mass flow rate
2	Performance	CO_2 purity or regenerated sorbent temperature	Velocity of heating fluid in desorption section
3	Regulatory	Ratio between sorbent flow rate and working fluid velocity in internal heat recovery loop	Velocity of working fluid in internal heat recovery loop
4	Regulatory	Sorbent temperature at the cooling section outlet	Velocity of cooling water
5	Regulatory	Gas velocity at the top of the precooling section	Purge gas mass flow rate

Controller number 4 and 5 in the regulatory layer are PI controllers. Controller 3 is a feedforward controller with the aim of keeping the fraction of heating/cooling delivered by the internal loop stable during operation.

The PI controllers were implemented in the MBTSA model by using the PID controller block available in gPROMS ModelBuilder. For these controllers, the value of the manipulated variable (u_{calc}) is calculated from the following equation:

$$u_{\text{calc}} = K_{\text{c}} \left(P + I\right) \left(u_{\text{max}} - u_{\text{min}}\right) + B \tag{3.18}$$

Where K_{c} is the controller gain, P is the proportional term, I is the integral term, u_{max} is the upper limit of the MV, u_{min} is the lower limit of the MV and B is the controller bias.

The controller error, e, is calculated as the normalized difference between the value of the controlled variable (y) and its setpoint (y_{SP}):

$$e = \frac{y_{\mathrm{SP}} - y}{y_{\max} - y_{\min}} \tag{3.19}$$

In the case of standard PI control, the setpoint is specified by the user. For a cascade controller, the setpoint of the inner loop is the MV of the outer loop, calculated by Eq. 3.18. The proportional and integral contributions are determined based on the error:

$$P = e \tag{3.20}$$

$$\tau_{\mathrm{I}} \frac{\mathrm{d}I}{\mathrm{d}t} = e \tag{3.21}$$

In a ratio-based feedforward structure, the control action is determined directly from a disturbance (d) instead of taking the error into account. The equation for calculation of the MV is therefore simpler than for PI control:

$$u_{\mathrm{calc}} = u' d \tag{3.22}$$

Since it only relies on a measurement of the disturbance, the MV value is quickly calculated. However, the absence of a feedback loop means that the ratio u' must be specified with high accuracy to avoid a steady-state offset between the CV and its desired value. This drawback is addressed in the combined feedforward and feedback control structure. In this case, u' is not specified by the user but calculated by a PI controller, resulting in a special form of cascade control. The integral action of the feedback controller ensures that the ratio over time is adjusted to eliminate the steady-state offset. This control structure is shown in Figure 3.3.

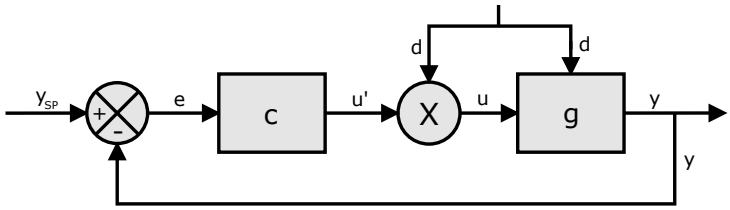

Figure 3.3: Overview of the combined feedforward and feedback control structure. From Publication II.

To allow a power plant to operate flexibly, the control structure for the PCC process must be able to handle a wide range of loads. When the dynamic behavior of the PCC process varies with load, it is necessary to update the controller tuning parameters to maintain controller performance. This is done in the adaptively tuned PI control cases, where the equation for u_{calc} is a modified version of Eq. 3.18:

$$u_{\mathrm{calc}} = K_{\mathrm{c}}(\varphi)\,[P + I(\varphi)]\,(u_{\max} - u_{\min}) + B \tag{3.23}$$

Similarly, the equation for the integral contribution becomes:

$$\tau_{\mathrm{I}}(\varphi)\frac{\mathrm{d}I}{\mathrm{d}t} = e \tag{3.24}$$

In these equations, φ represents the incoming flue gas feed mass flow rate normalized by its value at full load. For flexible operation driven by modification of the boiler load, this variable is a suitable indicator of how far from the nominal point the MBTSA process is operating. The working principle of the adaptively tuned control case is shown in Figure 3.4.

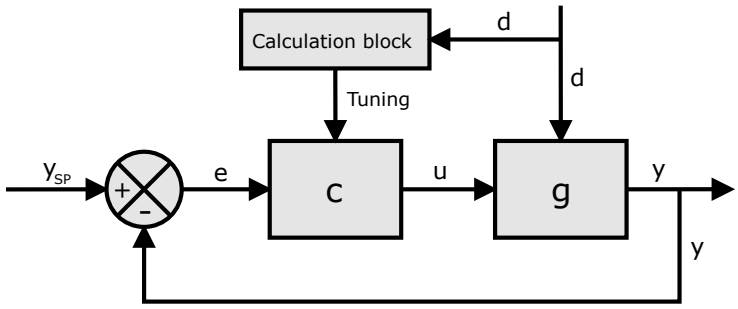

Figure 3.4: Overview of the feedback control structure with adaptive tuning of controller parameters. From Publication II.

3.3.2 Controller tuning

For PI controllers, controller tuning involves determining the controller gain K_{c} and the integral time τ_{I}. In this work, the simplified internal model control (SIMC) rules (Skogestad, 2003) were applied. The SIMC rules use the first-order transfer function with effective delay between the MV and CV as basis for the tuning. This transfer function g can be written as:

$$g(s) = \frac{ke^{-\theta s}}{\tau s + 1} \tag{3.25}$$

Where k is the process gain, θ is the effective delay and τ is the time constant. Two different methods were applied to obtain the transfer function. If the open-loop response of the CV to a step in the MV exhibited first-order behavior, the values of each parameter in the transfer function were found by graphical inspection. The gain was found as the difference between the final and initial value of the CV. The effective delay is the time it takes after the MV step before the CV starts continuously changing in the same direction as the gain, meaning that any inverse initial responses are included in θ. The time constant was taken as the time it took the CV to reach 63% of its final value. For cases where the open-loop step response could not be approximated as first-order, the setpoint overshoot method presented by Shamsuzzoha and Skogestad (2010) was used. In this method, the

transfer function is found by performing a closed-loop simulation with only P-control activated.

In addition to the transfer function parameters, the SIMC rules require the user-specified closed-loop time constant (τ_c). This is an adjustable parameter used to influence the response time of the controller. The equations are as follows:

$$K_c = \frac{1}{k}\frac{\tau}{\tau_c + \theta} \tag{3.26}$$

$$\tau_I = \min\left[\tau, 4\left(\tau_c + \theta\right)\right]. \tag{3.27}$$

In the case of ratio-type feedforward control, tuning involves determining the ratio u'. In some cases, u' was fixed at the ratio between the value of the considered input and disturbance at nominal load. In other cases, a linear regression was used to adjust the ratio based on the load φ.

3.3.3 Quantitative evaluation of controller performance

In addition to graphical comparison of dynamic closed-loop trajectories, three different quantitative metrics have been applied in this work for controller performance evaluation. They are summarized below:

1. Steady-state offset relative to CV setpoint (for controllers without feedback).
2. 99% settling time, defined as the time it takes for the CV to reach and stay within $\pm$ 1% of the final steady-state value.
3. The integral absolute error (IAE).

The following definition for the IAE was used:

$$\text{IAE} = \int_0^t |y_{SP}(t) - y(t)| \mathrm{d}t \tag{3.28}$$

3.4 Steam accumulator thermal energy storage

The main motivation for using a TES system in this work was to achieve rapid changes in the electrical power output of the CFPP that could be maintained for limited periods of time. This requires a TES technology that can deliver high charging/discharging rates. Since water is used both as the storage medium and working fluid in a steam accumulator, rapid charging and discharging is possible. This was the main motivation for using a steam accumulator in this work. As summarized in Section 2.3, several other storage technologies could have been chosen, including phase change materials, molten salt-based systems and solid media thermal storage. Phase change materials can offer high energy storage densities compared to steam accumulators, but the technology is still under development and could suffer from low heat-transfer rates (Beck et al., 2021). Solid media thermal storage can be a cost-efficient alternative, but they are limited by low charging/discharging

rates and therefore not suitable for the intended application (Beck et al., 2021). Molten-salt TES systems also have higher energy storage densities than steam accumulators and are suitable for high-temperature applications. Drawbacks of this technology include high storage media costs and freezing of the working fluid during operation (Haider and Werner, 2013).

3.4.1 Working principle

Steam accumulators utilize the high specific heat capacity of liquid water to store large amounts of sensible heat in a pressurized liquid phase (Steinmann and Eck, 2006). The capacity is decided by the volume of the pressurized tank. The steam accumulator considered in this work operates in a sliding-pressure mode. During charging, superheated steam is fed to the tank, which increases the pressure in the vessel. The temperature of the liquid water will also increase due to condensation of superheated steam. During discharging, the pressure reduction in the vessel leads to superheating and subsequent evaporation of the liquid phase. The generated steam leaves the tank and can be used to cover heat demands in the CFPP-PCC system.

A simplified overview of the steam accumulator is shown in Figure 3.5. The liquid water (phase 1) and steam (phase 2) are modeled separately. A dynamic mathematical model accounting for non-equilibrium thermodynamic effects is used to simulate the steam accumulator. It is based on the approach presented by Stevanovic et al. (2012). For the derivation of the equations, the reader is referred to the original article.

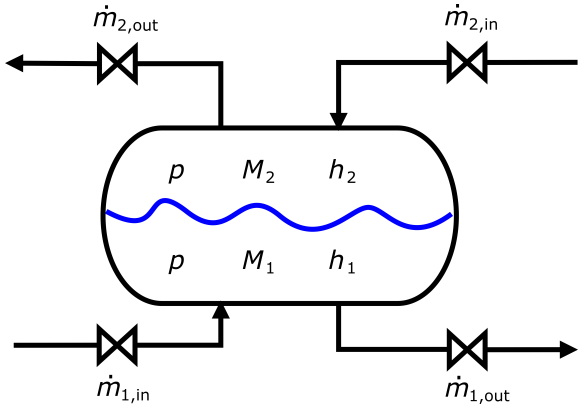

Figure 3.5: Simplified overview of the steam accumulator.

3.4.2 Model equations and implementation

The mass of each phase in the accumulator depends on the inlet and outlet flows as well as the internal mass transfer between the phases due to evaporation or condensation. The

mass balances are given by:

$$\frac{\mathrm{d}M_1}{\mathrm{d}t} = \dot{m}_{1,\text{in}} - \dot{m}_{1,\text{out}} + \dot{m}_\text{c} - \dot{m}_\text{e} \tag{3.29}$$

$$\frac{\mathrm{d}M_2}{\mathrm{d}t} = \dot{m}_{2,\text{in}} - \dot{m}_{2,\text{out}} + \dot{m}_\text{e} - \dot{m}_\text{c} \tag{3.30}$$

The evaporation mass flow rate ($\dot{m}_\text{e}$) and condensation mass flow rate ($\dot{m}_\text{c}$) are calculated based on the difference between the liquid enthalpy h_1 and the saturated liquid enthalpy h'. Evaporation takes place if the water is superheated ($h_1 > h'$), and the mass flow rate is calculated as:

$$\dot{m}_\text{e} = \frac{\rho_1 V_1 \left(h_1 - h'\right)}{\tau_\text{e} r} \tag{3.31}$$

Where r is the latent heat of vaporization. The condensation rate is set to zero in the case of evaporation. If the water is subcooled ($h_1 < h'$), condensation will take place and the evaporation rate is set to zero. The condensation rate is given by:

$$\dot{m}_\text{c} = \frac{\rho_1 V_1 \left(h' - h_1\right)}{\tau_\text{c} r} \tag{3.32}$$

The relaxation time for evaporation (τ_e) and condensation (τ_c) are input parameters specified by the user. The mass-specific enthalpy balances for liquid and steam are given by:

$$\frac{\mathrm{d}h_1}{\mathrm{d}t} = \frac{1}{M_1}\left[\left(\dot{m}h\right)_\text{1B} + \left(\dot{m}_\text{c} - \dot{m}_\text{e}\right)h'' + \dot{Q}_{21} + M_1 v_1 \frac{\mathrm{d}p}{\mathrm{d}t} - h_1 \frac{\mathrm{d}M_1}{\mathrm{d}t}\right] \tag{3.33}$$

$$\frac{\mathrm{d}h_2}{\mathrm{d}t} = \frac{1}{M_2}\left[\left(\dot{m}h\right)_\text{2B} + \left(\dot{m}_\text{e} - \dot{m}_\text{c}\right)h'' - \dot{Q}_{21} + M_2 v_2 \frac{\mathrm{d}p}{\mathrm{d}t} - h_2 \frac{\mathrm{d}M_2}{\mathrm{d}t}\right] \tag{3.34}$$

Where $\left(\dot{m}h\right)_\text{1B} = \dot{m}_{1,\text{in}} h_{1,\text{in}} - \dot{m}_{1,\text{out}} h_1$ and $\left(\dot{m}h\right)_\text{2B} = \dot{m}_{2,\text{in}} h_{2,\text{in}} - \dot{m}_{2,\text{out}} h_2$ account for the balance between incoming and outgoing enthalpy flows of each phase. The heat transfer rate from the steam to the liquid water depends on the temperature difference between the phases:

$$\dot{Q}_{21} = \left(ha\right)_{21}\left(T_2 - T_1\right)V_1 \tag{3.35}$$

If the water is superheated, $\dot{Q}_{21} = 0$. This will be the case for example during discharging of the tank. In this equation, $(ha)_{21}$ is the product of the heat transfer coefficient between superheated steam and liquid and the steam-water interface area concentration. Like the relaxation times, it is an input parameter specified by the user. As the enthalpy balances indicate, the accumulator is assumed to be perfectly insulated so that no heat is lost to the surroundings. Such heat losses were found to be negligible in the work of Richter et al. (2019).

Two different modeling approaches for charging and discharging were used to calculate the pressure in the accumulator. In the case of discharging, the differential equation presented

by Stevanovic et al. (2012) was used. It is derived based on the volume balance of the tank ($V_{\text{tank}} = V_1 + V_2$) and can be written as:

$$\frac{\mathrm{d}p}{\mathrm{d}t} = \frac{\left(h_1 \left.\frac{\partial v_1}{\partial h}\right|_p - v_1\right) \frac{\mathrm{d}M_1}{\mathrm{d}t} + \left(h_2 \left.\frac{\partial v_2}{\partial h}\right|_p - v_2\right) \frac{\mathrm{d}M_2}{\mathrm{d}t} - \left(\dot{m}_{\mathrm{c}} - \dot{m}_{\mathrm{e}}\right) h'' \left.\frac{\partial v_1}{\partial h}\right|_p}{\left(\left.\frac{\partial v_1}{\partial p}\right|_h + v_1 \left.\frac{\partial v_1}{\partial h}\right|_p\right) M_1 + \left(\left.\frac{\partial v_2}{\partial p}\right|_h + v_2 \left.\frac{\partial v_2}{\partial h}\right|_p\right) M_2} - \frac{\left[-\dot{m}_{2,\text{out}} h_2 + \left(\dot{m}_{\mathrm{e}} - \dot{m}_{\mathrm{c}}\right) h''\right] \left.\frac{\partial v_2}{\partial h}\right|_p}{\left(\left.\frac{\partial v_1}{\partial p}\right|_h + v_1 \left.\frac{\partial v_1}{\partial h}\right|_p\right) M_1 + \left(\left.\frac{\partial v_2}{\partial p}\right|_h + v_2 \left.\frac{\partial v_2}{\partial h}\right|_p\right) M_2} \tag{3.36}$$

The partial derivatives of the liquid and water specific volume were calculated from the relations given by Zhu et al. (2019):

$$\left.\frac{\partial v_1}{\partial h}\right|_p = \frac{v_1 \alpha_1}{c_{\mathrm{p},1}} \tag{3.37}$$

$$\left.\frac{\partial v_2}{\partial h}\right|_p = \frac{v_2 \alpha_2}{c_{\mathrm{p},2}} \tag{3.38}$$

$$\left.\frac{\partial v_2}{\partial p}\right|_h = -v_2 \kappa_2 - \frac{v_2^2 \alpha_2}{c_{\mathrm{p},2}} \left(1 - T_2 \alpha_2\right) \tag{3.39}$$

The IAPWS-95 equation of state (Wagner and Pruß, 2002) was used for all thermodynamic properties needed in the model. To calculate the density and temperature of each phase, calls with specific enthalpy and pressure as the input variables were used. Calls with pressure as the only input variable were used to calculate saturated enthalpies, the latent heat of vaporization and single-phase properties such as the isobaric expansivity, specific heat capacities and isothermal compressibility. The partial derivative of liquid water specific volume with regard to pressure was estimated numerically by using first-order differences.

In the case of tank charging, using Eq. 3.36 lead to errors in the volume conservation of the accumulator. Therefore, an alternative method for calculating the tank pressure was applied. In this approach, the volume of the tank was included in the calculation of the steam specific volume to force volume conservation: $v_2 = \left(V_{\text{tank}} - V_1\right) / M_2$. The tank pressure was calculated from a call to the equation of state based on the steam phase properties, i.e. $p = p\left(v_2, h_2\right)$. Using this type of method for calculating the pressure leads to a differential-algebraic equation (DAE) system.

The model was implemented in MATLAB version R2022b and REFPROP version 10 was used for thermodynamic calculations. More information on REFPROP is given in Huber et al. (2022). A Python interface was used to make REFPROP callable directly from MATLAB. To solve the discharging model, the stiff ordinary differential equation solver ode15s was applied. The charging model was solved by the implicit ode15i solver, which can handle DAE systems. The model was validated against both experimental and simulation data from the literature for two different tanks sizes.

3.4.3 Integration into power plant with CO_2 capture

In Figure 3.6, the process flow diagram of the supercritical CFPP with integrated MBTSA PCC and steam accumulator thermal energy storage is shown. The figure shows how the thermal storage system has been integrated into the power plant in this work. Charging of the TES takes place by extracting reheated steam from the intermediate-pressure turbine inlet.

Two alternatives for discharging of the TES are considered. Firstly, steam from the accumulator can be used to cover the regeneration duty of the MBTSA process. As summarized in the knowledge gaps in Section 2.4, using a TES system to deliver heat to the MBTSA process had not previously been studied in the literature and this alternative was therefore interesting to investigate. Due to the large steam flow rate required for sorbent regeneration, this integration option has the potential to significantly affect the net power output of the CFPP. The second investigated discharging option was using the TES to cover feedwater heating demands in the power plant. This option has previously been shown to work well in the studies by Richter et al. (2019) and Stevanovic et al. (2020). Sending steam from the TES directly to the turbine train was also considered, but integration with feedwater heaters was considered to be more realistic for practical implementation due to the sliding-pressure operation of the steam accumulator.

The two integration options for discharging are compared in Publication III. To model the integrated system, a soft-linking of the individual models explained in this chapter was performed. This means that the models were not collected in a single modeling environment. Due to the limited number of simulations required by each model for each case, the additional time required to transfer data between models and sequentially start simulations was acceptable. Transferring the TES model and building a power plant model in gPROMS would likely be significantly more time-consuming than the soft-linking approach, without increasing the accuracy of the results.

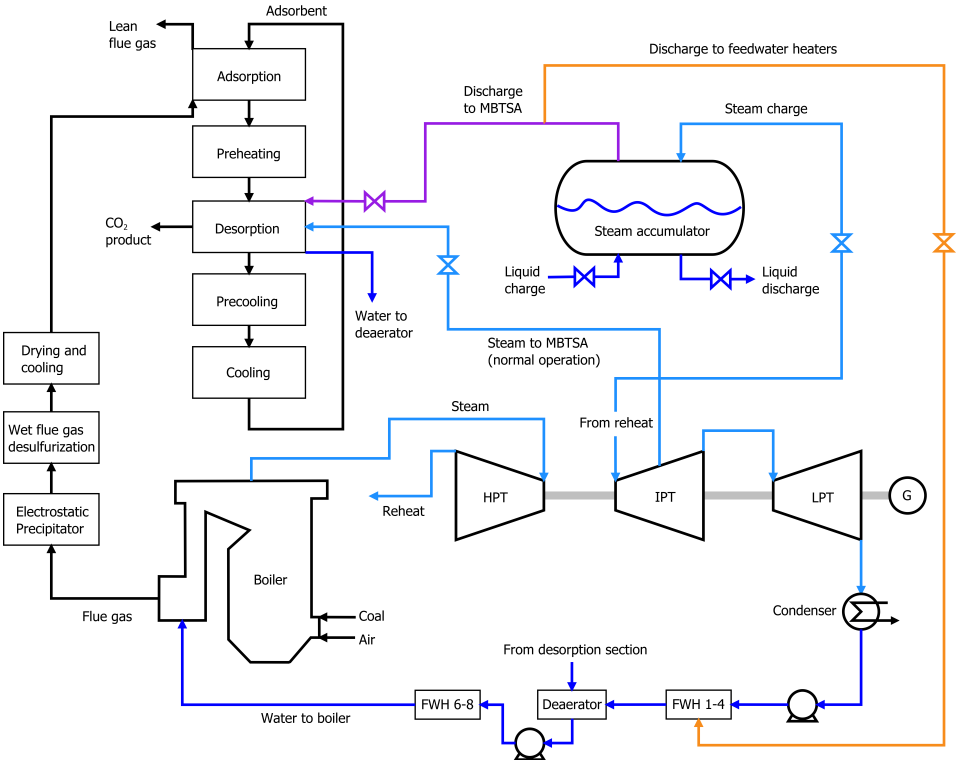

Figure 3.6: Process flow diagram of supercritical coal-fired power plant with integrated MBTSA post-combustion CO_2 capture and steam accumulator thermal energy storage.

Chapter 4

Results and discussions

In this section, selected results from the Ph.D project are presented and discussed, with the goal of demonstrating how the project objectives have been achieved. For a complete overview of the results, the reader is referred to the publications in Appendix A.

4.1 PCC responses to changes in power plant operation

Modifying the power plant operation will influence the PCC process in two main ways. Firstly, the flow rate of the flue gas entering the PCC process will vary when the boiler load is changed. Secondly, changing the power plant operation can influence the available amount and quality of the steam delivered to the PCC process. For the smaller scale CFPP studied in Publication I, ramps between 100-80-100% of the nominal flue gas mass flow rate were used to simulate the closed-loop response of the MBTSA process to changes in boiler operation. The flue gas feed mass flow rate profile is shown in Figure 4.1 and the closed-loop response of the PCC process is shown in Figure 4.2.

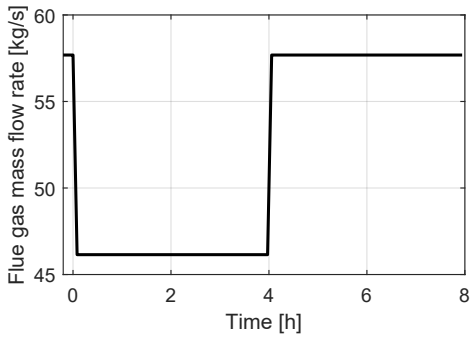

Figure 4.1: Flue gas mass flow rate profile from 100-80-100% ramp simulations.

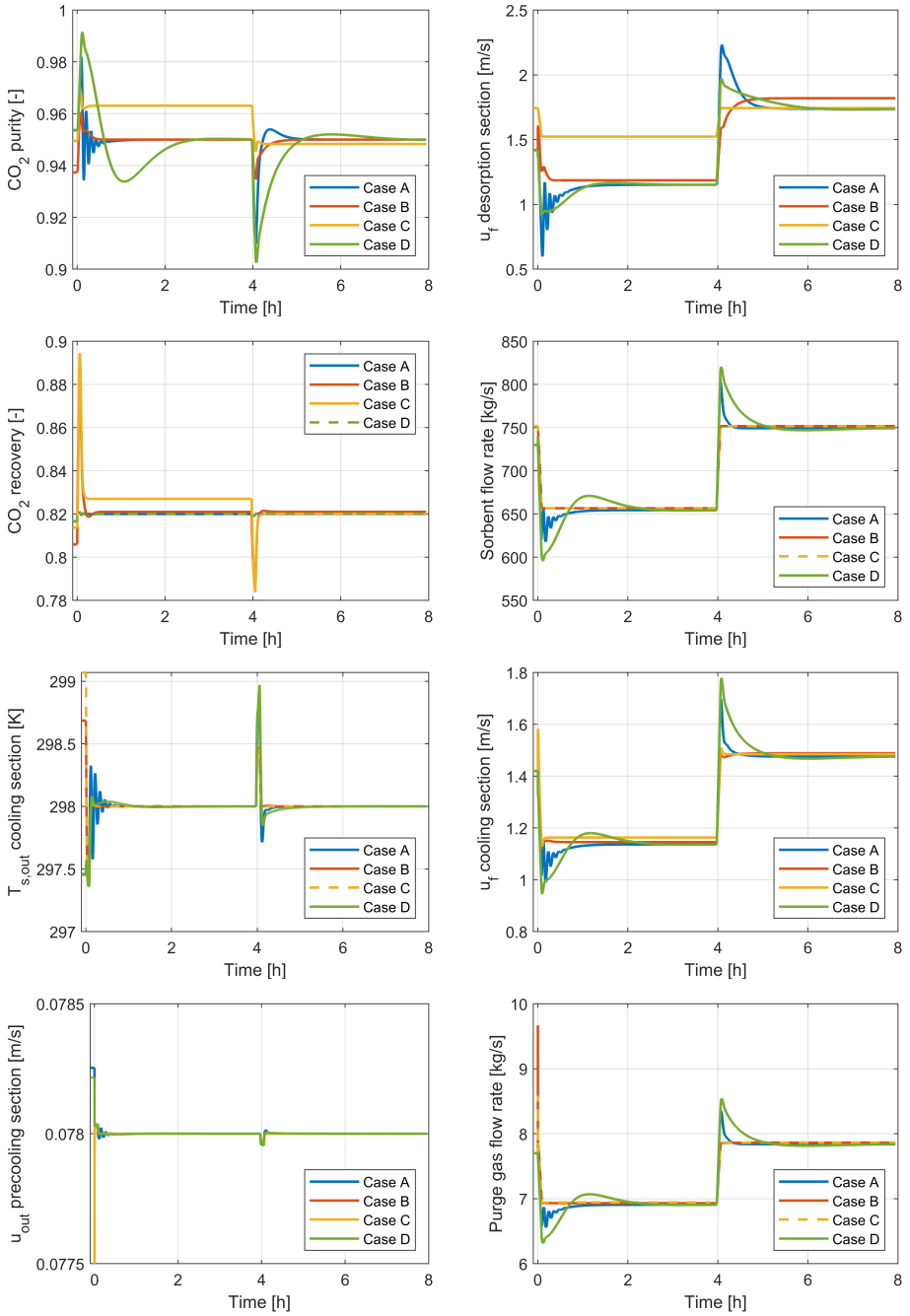

Figure 4.2: Closed-loop response of CVs (left) and MVs (right) to 100-80-100% flue gas feed flow ramp starting at $t = 0$. From Publication I.

In Figure 4.2, four different control strategies are compared. Case A represents the baseline control structure with PI control of both CO_2 recovery and purity, Case B uses PI control of CO_2 purity and ratio control of the sorbent flow rate, Case C uses ratio control of both the sorbent flow rate and desorption section hot fluid and Case D is a PI control structure with cascade control of CO_2 purity.

In these simulations, it was assumed that all measurements are instantly available and that there is no delay between a control action and its implementation in the MBTSA process. Due to these assumptions, the feedforward and cascade controllers do not give a significant improvement in the controller speed compared to the baseline PI structure. Furthermore, due to the imperfect adjustment of the ratio in the feedforward controllers with system load, a clear steady-state offset is observed for the purity and recovery at 80% load. A drawback of the baseline control structure in this case is the oscillations observed during the load reduction ramp. This is an indication of overly aggressive controller tuning and is further addressed in Section 4.3. For both positive and negative ramps, the regulatory control of the cold adsorbent temperature and precooling section gas velocity is fast.

In Publication II, simulations with ramps in power plant load were performed for the large-scale CFPP using Zeolite 13X as the adsorbent material. In this case, positive load ramps between 40 and 100% load were used to represent the gradual ramping up of the power plant load after a period of low demand. The flue gas mass flow rate profile and the closed-loop responses of CVs and MVs are shown in Figure 4.3. Similarly to the ramp simulation shown above, all investigated control structures show similar behavior due to the assumption of instantly available measurements and control actions. The effects of introducing measurement delays are shown in Section 4.3. The enhanced single-loop controllers applied in this case eliminate the steady-state offsets of the feedforward controllers and the oscillations observed in Figure 4.2.

To summarize, the ramp simulations demonstrate that the MBTSA process can be controlled for variations in the boiler load for both small and large scales and different adsorbent materials.

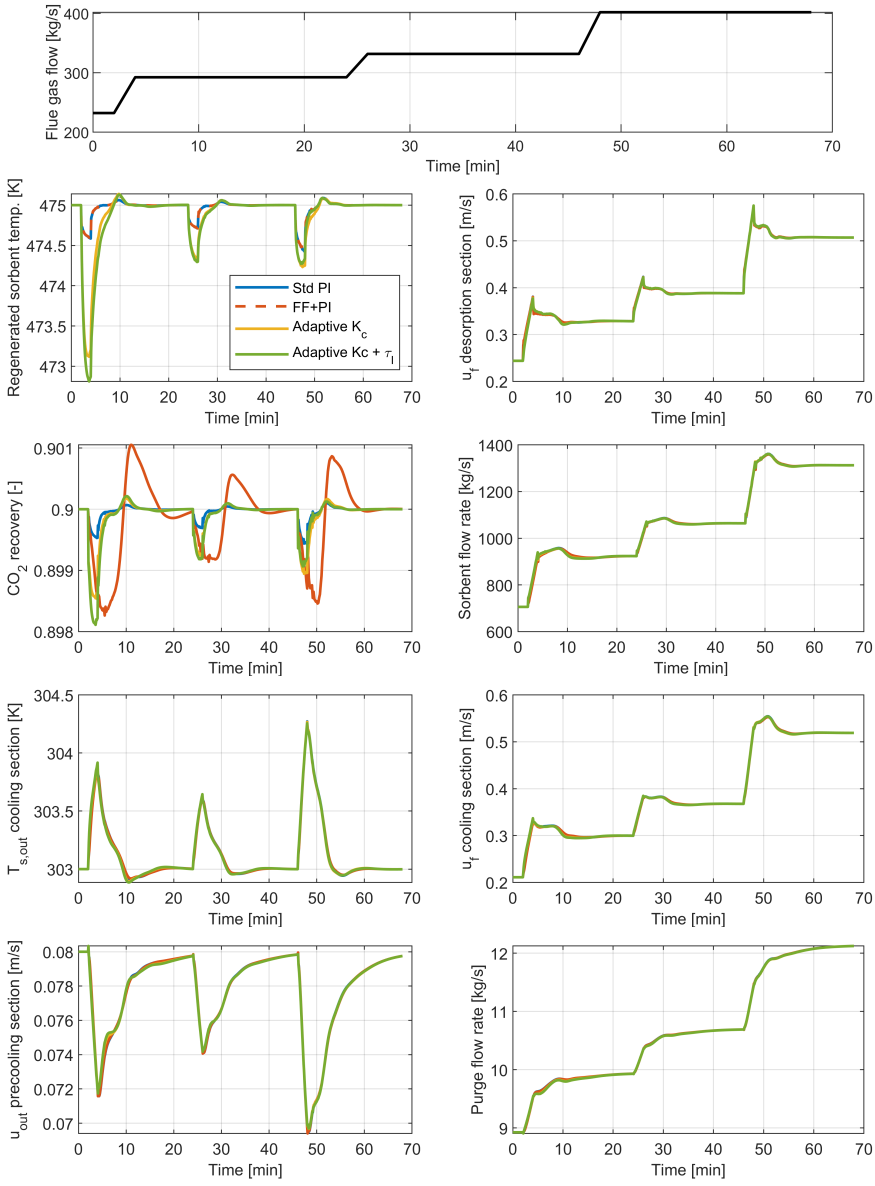

Figure 4.3: Closed-loop response of CVs (left) and MVs (right) to power plant load ramps between 40 and 100%. The top graph shows the variation in flue gas flow rate during the simulation. From Publication II.

In Figure 4.4, the closed-loop response of higher-level CVs and MVs to a 20 K reduction in the hot fluid temperature at full load is shown. This represents a scenario where the power plant operation is changed in a way that leads to a reduction of the temperature of the extracted steam sent to the CO_2 capture process. Alternatively, it can be viewed as a scenario where steam of lower quality is sent to the PCC unit to alter the electrical power output. To maintain similar driving forces for heat transfer as in the nominal case, the setpoint for the regenerated sorbent temperature is also reduced by 20 K.

The results demonstrate that the CO_2 recovery rate target of 90% can be met even though the incoming steam temperature is reduced. To compensate for the reduced working capacity of the adsorbent caused by the lower regeneration temperature, a significant increase in the sorbent mass flow rate is osberved.

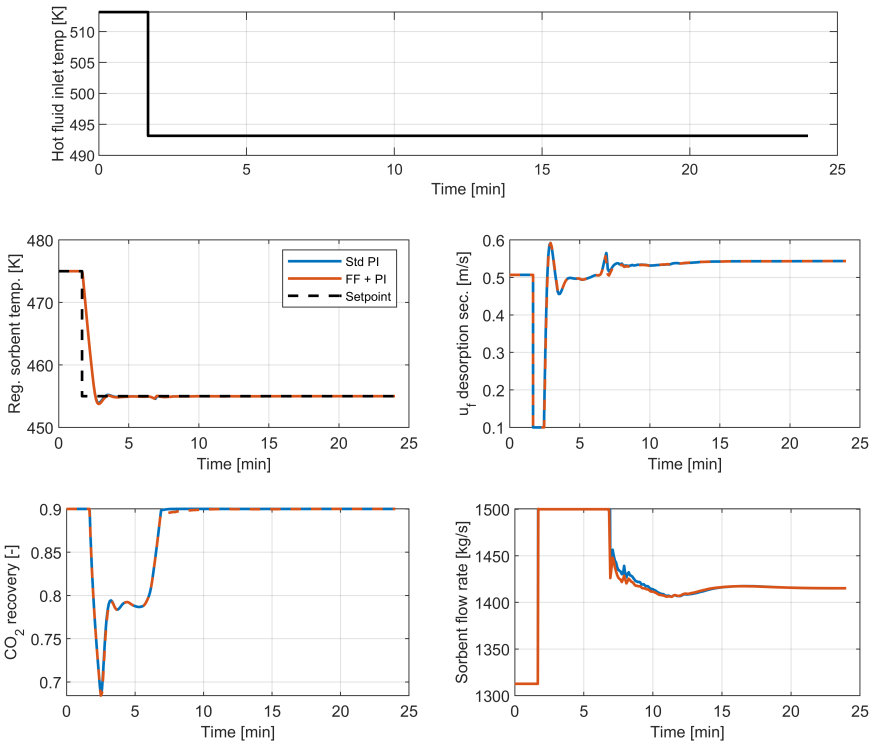

Figure 4.4: The response of higher-level CVs and MVs to a simultaneous change in the hot fluid temperature and regenerated sorbent temperature setpoint at 100% load. The top graph shows the step change in the hot fluid temperature introduced at $t = 1.67$ min. From Publication II.

4.2 Closed-loop responses to changes in PCC operation

As pointed out in Chapter 2, the operation of the PCC process can be modified to provide flexibility to the power plant. Such modifications might also be necessary due to downstream requirements in the CCS chain (e.g. regarding the CO_2 purity) or a change in market conditions (e.g. the cost of emitting CO_2). Furthermore, introducing changes in the PCC operation is a common method for testing the robustness of implemented control structures.

In Figure 4.5, the closed-loop response of higher-level CVs and MVs to a CO_2 recovery setpoint step change is shown. If the PCC process has been operating at reduced recovery rates for a period of time, such a step change represents a return to normal operation. During periods where it is beneficial to capture additional CO_2, a step change of this type would be used to increase the setpoint above the nominal value.

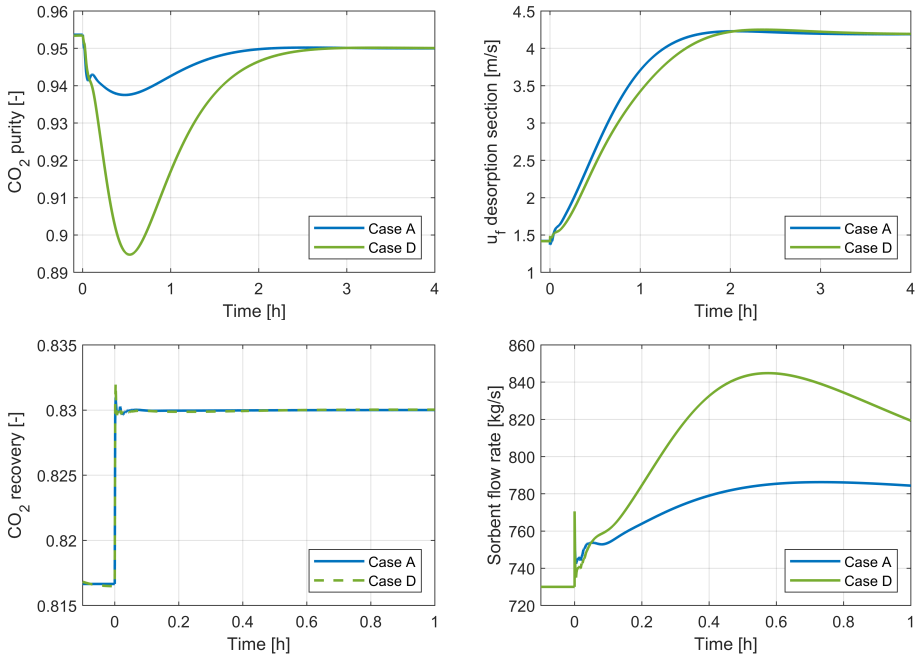

Figure 4.5: Closed-loop response of higher-level CVs (left) and MVs (right) to a CO_2 recovery setpoint step change introduced at $t = 0$. From Publication I.

As the figure shows, the control system is able to closely track the CO_2 recovery setpoint by increasing the sorbent mass flow rate. The CO_2 purity also stabilizes at its setpoint after a period of around 2 h. A significant increase in the heating fluid velocity in the desorption section is observed, which means that a larger amount of extracted steam from the power plant is required. This will lead to a reduction of its electrical power output, demonstrating that modifying the recovery setpoint can provide power generation flexibility. If stricter

limits were imposed on the heating fluid velocity, the control system would compensate by increasing the sorbent mass flow rate to a larger value than what is observed in this simulation.

In Figure 4.6, the closed-loop response of the MBTSA process to a CO_2 purity setpoint step change is shown. Apart from the ratio-based feedforward controller (Case B), the CO_2 recovery is closely controlled also in this case. With the standard PI control structure (Case A), the purity stabilizes at the new setpoint after around 1 hour. Both the heating fluid velocity and sorbent mass flow rate are increased to be able to deliver CO_2 at a higher purity.

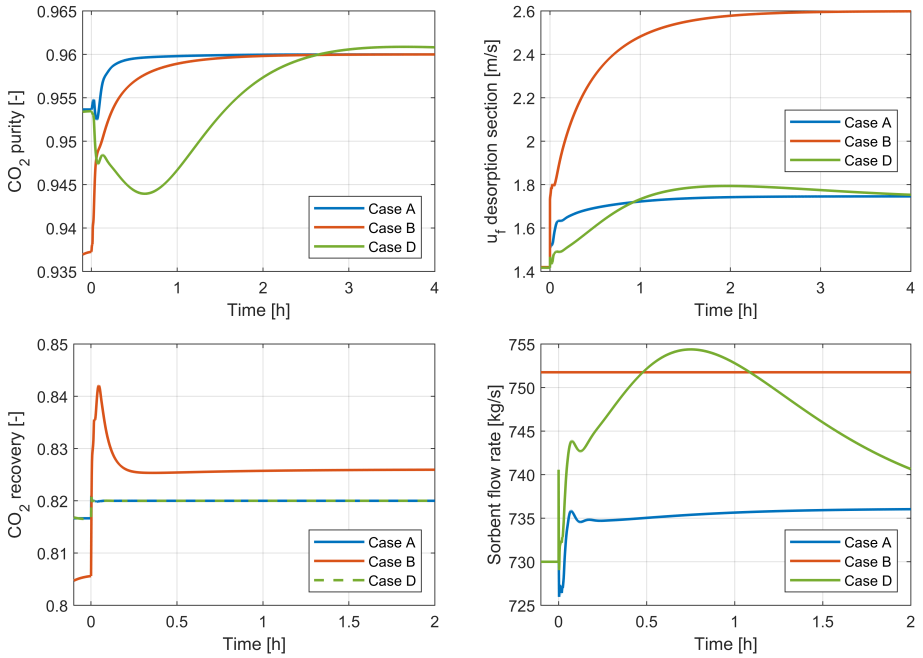

Figure 4.6: Response of higher-level CVs (left) and MVs (right) to a CO_2 purity setpoint step change introduced at $t = 0$. From Publication I.

4.3 Comparison of enhanced single-loop and standard control structures

The ramp results in Figure 4.2 show that the control structures studied in Publication I had several limitations. The standard PI control structure (Case A) showed signs of oscillations when going from 100 to 80% load. The controller tuning was performed based on the open-loop behavior at full load, which leads to overly aggressive controller behavior as the load is decreased. In Figure 4.7, the effect of reducing the controller gain on the closed-loop behavior of the CO_2 purity and its associated MV is shown. By reducing the

gain to one third of the value obtained by tuning at full load, a significantly smoother profile is observed. This demonstrates that adaptive tuning of the controllers based on the system load can be beneficial.

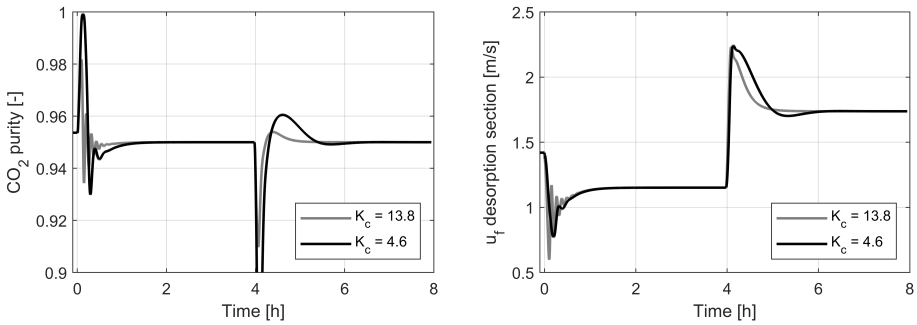

Figure 4.7: Response of CO_2 purity and heating fluid velocity using the standard PI control structure to a 100-80-100% flue gas feed flow ramp for nominal and reduced values of the controller gain. From Publication I.

Another limitation of the cases presented in Section 4.1 is the assumption of instantly available measurements, which is not achievable in practice. To make the simulations more representative of practical operation, measurement delays of 15 seconds for CO_2 recovery and 5 seconds for the regenerated sorbent temperature were introduced. The closed-loop response of the system to a ramp between 60 and 80% power plant load when considering these delays is shown in Figure 4.8.

Since all the enhanced single-loop control structures have a feedback element, the measurement delays have a significant effect on the controller settling times and lead to larger differences between the different control strategies than in the previously presented ramp simulations. In the feedforward part of the FF + PI controller, the sorbent flow rate is increased independently of the CO_2 recovery measurement. This controller is therefore able to keep the recovery rate closer to its setpoint than the other control structures at the start of the ramp. The feedback part of the FF + PI controller eliminates the previously discussed steady-state offset.

The simulation results also show the benefit of adaptive tuning of the controller parameters. Since they can handle more aggressive tuning, the adaptive cases demonstrate a tighter control of the CO_2 recovery than the standard PI case. No clear difference is observed between only adjusting the controller gain and adjusting both the controller gain and integral time. This indicates that the controller gain is the most important parameter to adjust.

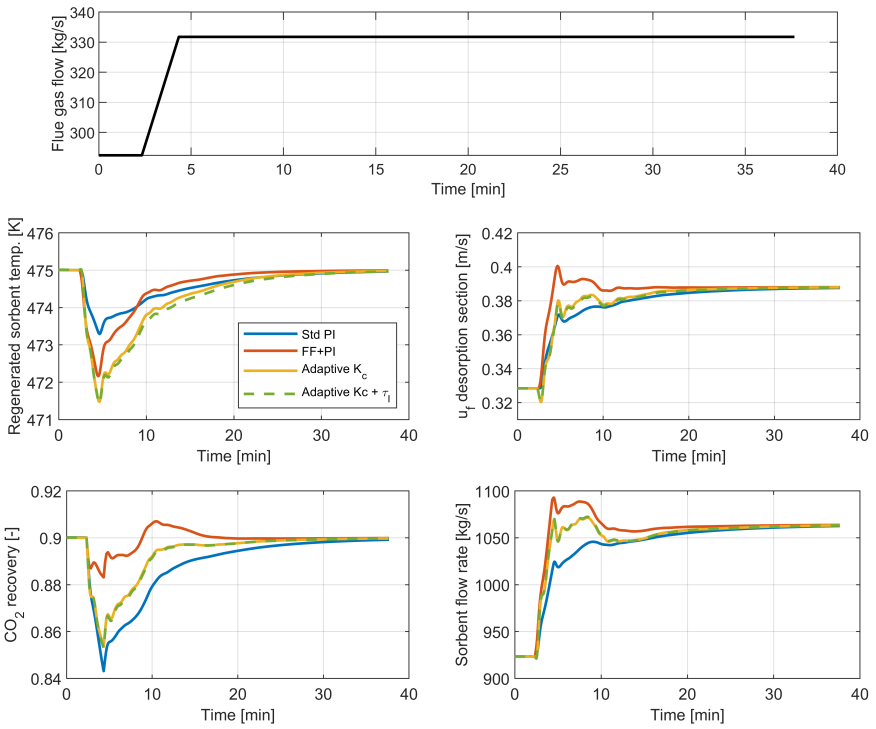

Figure 4.8: The closed-loop response of higher-level CVs and MVs to a 60-80% power plant load ramp with a 15 s delay in the CO_2 recovery measurement and a 5 s delay in the regenerated sorbent temperature measurement. From Publication II.

4.4 Thermal storage integration effect on flexibility

The main motivation for application of a TES system in this project was to contribute to positive and negative reserve for the power plant without modifying the boiler load or reducing the CO_2 recovery rate.

Achieving a reduction in the net electrical power output is particularly useful at the minimum load, since additional startups and shutdowns during periods of very low electricity prices can be avoided. However, due to the large amounts of extracted steam needed for sorbent regeneration, it is not possible to simultaneously charge the TES and maintain a high CO_2 recovery rate at the minimum load. Therefore, simulations at 60% load were performed to quantify the effect of TES charging at reduced power plant loads. The net and relative electrical power output profile when charging with an extracted reheat steam mass flow rate of 5 kg/s at 60% load is shown in Figure 4.9. It takes around 139 minutes before the pressure in the steam accumulator equals the reheat steam pressure and the charging process is stopped. In this case, the final tank pressure was 27.7 bar. The net electrical power output is reduced by 5.6 MW, leading to a 13.0 MWh reduction in electrical energy production.

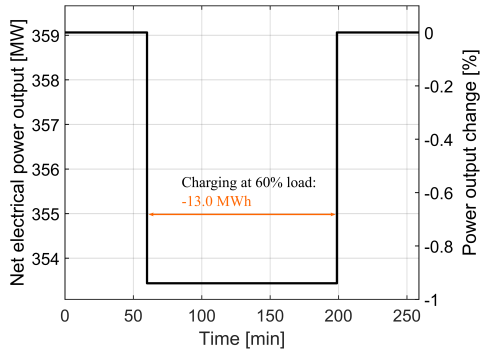

Figure 4.9: Profiles of the net electrical power output and relative power output change during TES charging at 60% load with a steam flow rate of 5 kg/s. From Publication III.

A disadvantage of charging at reduced loads is that the extracted steam is at a significantly lower pressure than at full load, leading to a lower final pressure in the steam accumulator. In Figure 4.10, the results of a charging simulation at full load with a steam flow rate of 5 kg/s are shown. In this case, the charging process takes around 200 minutes, giving a final tank pressure of 46.7 bar. The net power output is reduced by 8.2 MW, giving a reduction in the electrical energy output of 27.3 MWh.

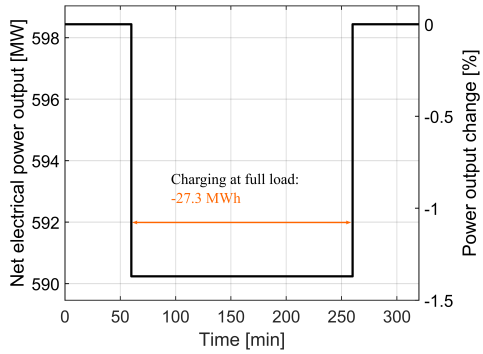

Figure 4.10: Profiles of the net electrical power output and relative power output change during TES charging at 100% load with a steam flow rate of 5 kg/s. From Publication III.

As described in Section 3.4, two alternatives for discharging of the steam accumulator were considered in this project. All discharging simulations were carried out at full load with an initial tank pressure of 46.7 bar. In Figure 4.11, the net electrical power output and relative power output profile for the case where the TES is used to cover the heat demands of FWH4 and FWH3 in the power plant are shown. During the initial part of the discharging process, the pressure in the accumulator is high enough to cover both feedwater heaters. This gives a net electrical power output increase of 20.5 MW for around 23 minutes. After this period, the pressure of the TES is only sufficient to deliver steam

to FWH3. This part of the discharging process lasts for around 13 minutes, giving a net electrical power output increase of 10.2 MW.

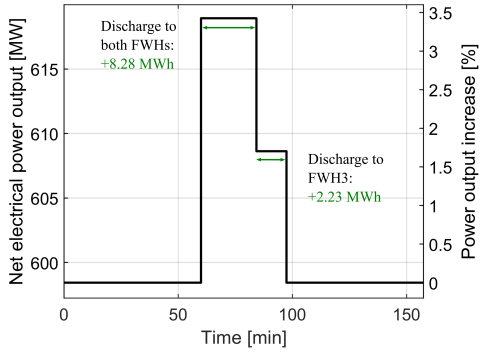

Figure 4.11: Net electrical power output profile and relative power output change when thermal storage is used to cover FWH3 and FWH4 heat demand at full power plant load. From Publication III.

In Figure 4.12, the results from a simulation with the second discharging option are shown. In this case, the TES is first used to cover the regeneration duty of the MBTSA process. Due to the large steam flow rates required, this integration option gives a significant net electrical power output increase of nearly 67 MW. However, the tank pressure reaches the threshold value after only 3.2 minutes. After this point, steam is sent to FWH4 and FWH3 for around 15 minutes and to only FWH3 for 13 minutes.

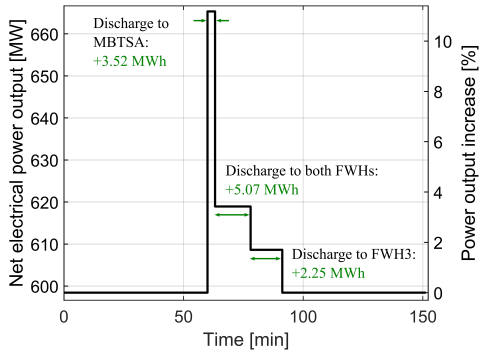

Figure 4.12: Net electrical power output profile and relative power output change when thermal storage is used to cover MBTSA regeneration duty and then feedwater heating demand at full power plant load. From Publication III.

Both discharging options give an increase in the electrical energy production between 10.5 and 11.0 MWh. The FWH discharge case has a duration of 37.5 minutes, which is approximately 6 minutes longer than the MBTSA + FWH case. Both options exceed the requirement for primary reserve from Palizban and Kauhaniemi (2016), where it is stated

that primary reserve should have a duration between 15 and 30 minutes. An advantage of discharging to the MBTSA process is the large increase in net electrical power output.

4.5 Uncertainty of results

The main source of uncertainty in the results presented in this Ph.D project is that the MBTSA process model can not be fully validated due to a lack of openly available experimental data. The parameters in the extended Virial isotherm model used to describe the adsorption equilibrium are fitted to experimental data, but other aspects of the MBTSA process such as the pressure drop and the heat and mass transfer within the different sections are not possible to validate. As a consequence, the performance and dynamic behavior predicted by the model are uncertain. Determining the heat transfer coefficient between the heat exchanger tubes and the gas/solid phase on the sorbent side is particularly important, since this is the dominating thermal resistance in the system (Mondino, 2022). This coefficient influences both the steady-state and dynamic behavior of the MBTSA process.

In the simulations presented in Publication I and II, the closed-loop profiles of different control structures are compared against each other. Although the absolute values predicted by the model are uncertain, comparing the relative performance of different controllers can still provide useful insights, assuming that the prediction error does not vary significantly between the different control strategies. Furthermore, it can be argued that the control framework presented in this project would be suitable for controlling the MBTSA process even if the model predictions were different. Since model-based tuning methods based on the open-loop behavior of the system are applied, a change in the underlying model would be accounted for in the form of updated controller tuning parameters.

Errors in the MBTSA model predictions would also influence the results presented in Publication III, primarily through an incorrect estimate of the amount of heat required for regeneration of the PCC process. This directly affects the amount of steam that is sent from the power plant to the MBTSA process and will also influence the charging of the steam accumulator. As an example, extracting more steam from the power plant to cover the MBTSA regeneration duty will lead to a lower final tank pressure after charging. In addition, an error in the regeneration duty estimate will affect the estimate of the net electrical power output increase achieved by discharging the steam accumulator to the MBTSA process. It is expected that comparing the relative performance of different integration strategies will be more reliable than considering the absolute value of individual predictions.

Chapter 5

Conclusions and future work

5.1 Conclusions

The main goal of this Ph.D project was to study the flexible operation of coal-fired power plants with moving bed temperature-swing adsorption post-combustion CO_2 capture. Two main flexibility methods were studied in this project. Firstly, control strategies with the goal of maintaining the performance of the capture process during changes in the power plant operation were developed and evaluated. Secondly, the integration of a steam accumulator thermal energy storage unit into the coal-fired power plant – carbon capture process was considered. Increasing the maximum load of the power plant and enabling it to rapidly change its load were the primary flexibility modes studied in this work. Two adsorbent materials (activated carbon and Zeolite 13X) and two different power plant scales were investigated.

The first main contribution of this thesis was the development and implementation of a control framework for the MBTSA process. The framework consisted of five controlled and manipulated variable pairs in a decentralized structure that was divided into a regulatory and higher-level layer. The regulatory layer included a controller keeping the fraction of heating and cooling delivered by the internal heat recovery loop stable, a controller for the sorbent temperature leaving the cooling section and a controller for the gas velocity at the top of the precooling section. In the higher-level layer, the sorbent flow rate was used to control the CO_2 recovery and the heating fluid flow to the desorption section was used to control either the CO_2 product purity or the regenerated sorbent temperature. The control framework was added to a gPROMS model of the MBTSA process and both the open and closed-loop dynamic responses were studied. A range of scenarios were simulated, including step changes in the incoming flue gas flow, ramps in power plant load, setpoint changes for higher-level control variables, variations in flue gas feed CO_2 concentration and variations in the external heat source temperature. The simulations showed that the developed control framework was able to maintain the performance of the MBTSA process for power

plant-driven flexibility scenarios and changes in the operation of the post-combustion capture process.

The second main contribution of this thesis was the comparison of several different alternatives for higher-level control of the MBTSA process. In Publication I, four different control strategies were investigated, namely a baseline structure with PI control of both the CO_2 recovery and purity, an option with PI control of CO_2 purity and feedforward control of the sorbent flow rate, a structure with feedforward control of both the sorbent flow rate and heating fluid velocity to the desorption section and a case with regular PI control of the CO_2 recovery and a cascade controller for the CO_2 purity. Due to imperfect ratio adjustment in the feedforward controllers with system load, steady-state offsets from the CV setpoints were observed. Furthermore, aggressive tuning of the PI controllers caused oscillations when the power plant load was reduced. To address these limitations and improve the controller performance, two enhanced single-loop control structures were studied in Publication II. By adaptively adjusting the controller tuning parameters (gain and integral time) with the system load, no oscillations were observed and tighter control of the CO_2 recovery compared to the standard PI control structure was achieved. A PI controller was combined with the feedforward control structure to adjust the ratio based on the control error instead of a parametric relation. This eliminated the steady-state offsets and lead to closer control of the CO_2 recovery rate. When testing the enhanced single-loop control structures, the effect of measurement delays were included. Such delays were found to have a large effect on the relative performance of the investigated control strategies.

The third main contribution of this Ph.D project was a study of how the integration of a steam accumulator thermal energy storage unit could increase the flexibility of the power plant – CO_2 capture system. A dynamic model of the steam accumulator was implemented in MATLAB and validated with both experimental and simulation data from the literature. Combined with a steady-state power plant model, simulations were carried out to quantify how charging and discharging the thermal energy storage affected the net electrical power output of the power plant. Charging the accumulator with reheat steam from the power plant could reduce the net power output by up to 1.4 % for around 200 minutes. Two alternatives for discharging of the thermal energy storage were considered, namely covering the regeneration duty of the MBTSA process and meeting the demand of two feedwater heaters. Discharging was found to give relative power plant load increases between 1.7 and 11.2% for up to 37.5 minutes, which exceeds the requirement for primary reserve. Sending steam from the accumulator directly to the MBTSA process could increase the net electrical power output by almost 67 MW for a period of 3.2 minutes. An advantage of using a thermal energy storage system to provide flexibility is that the resulting load changes take place without modifying the boiler load or reducing the CO_2 recovery rate.

5.2 Future work

There are several opportunities for future work on the design and modeling of the MBTSA process. This includes the development of optimization-based design algorithms, investigation of the energy penalty associated with drying of the flue gas upstream of the MBTSA unit and studying the effect of non-binary flue gas compositions on the process behavior. However, the recommendations for future work given below are limited to topics relevant for the continuation of the work carried out in this Ph.D project.

The results presented in Publication II showed that measurement delays have a significant effect on the closed-loop behavior of the MBTSA process. This motivates a more detailed evaluation of the effect of delays in future work. A weakness of the scenarios considered in this project is the assumption that a change in the sorbent flow rate is instantly implemented in all sections of the MBTSA unit. Introducing delays for the sorbent flow rate and other manipulated variables would make the system more representative of real-life operation. Considering the effect of signal noise would also be an improvement. In practice, signal noise can originate from sensor inaccuracies or estimation errors for variables that are not possible to measure directly.

Another key topic for future work will be the investigation of new control structures that can further improve the closed-loop behavior of the MBTSA process. For decentralized control, implementing decoupling approaches for the higher-level control layer could be beneficial. Centralized control approaches such as model predictive control will also be relevant to consider. Model predictive control has the potential for improving the control performance due to the inherent handling of coupled variables, the ability to handle constraints and the possibility of including cost or energy-related aspects in the control algorithm.

The work in Publication III demonstrated that thermal energy storage could provide flexibility to the power plant – carbon capture system. However, there are several topics that could be investigated to build on these results. Firstly, a techno-economic evaluation of the concept would give more knowledge on its viability and could be used to determine the cost-optimal capacity and operation strategy. The steam accumulator could also be compared to other thermal energy storage technologies, and alternative integration options could be investigated. Studying how the thermal energy storage can contribute to other flexibility modes such as rapid load ramps, startups and shutdowns would provide a more complete understanding of its potential. To study such scenarios, a dynamic power plant model would be required.

Finally, a central topic for future work should be the validation of the MBTSA process model with experimental data. Initially, the steady-state predictions of the model at nominal load should be validated. At a later stage, validation off the off-design and transient predictions of the model can be performed. This would give more confidence in the results provided by the model and the competitiveness of the MBTSA technology compared to other post-combustion capture technologies.

References

Abdilahi, A.M., Mustafa, M.W., Abujarad, S.Y., Mustapha, M., 2018. Harnessing flexibility potential of flexible carbon capture power plants for future low carbon power systems: Review. Renewable and Sustainable Energy Reviews 81, 3101–3110. doi:https://doi.org/10.1016/j.rser.2017.08.085.

Akinola, T.E., Oko, E., Wu, X., Ma, K., Wang, M., 2020. Nonlinear model predictive control (NMPC) of the solvent-based post-combustion CO_2 capture process. Energy 213, 118840. doi:https://doi.org/10.1016/j.energy.2020.118840.

Akram, M., Milkowski, K., Gibbins, J., Pourkashanian, M., 2021. Controlling capture plants to avoid CO_2 emissions penalties during peak load demand. International Journal of Greenhouse Gas Control 106, 103285. doi:https://doi.org/10.1016/j.ijggc.2021.103285.

Avagianos, I., Rakopoulos, D., Karellas, S., Kakaras, E., 2020. Review of process modeling of solid-fuel thermal power plants for flexible and off-design operation. Energies 13. doi:10.3390/en13246587.

Beck, A., Sevault, A., Drexler-Schmid, G., Schöny, M., Kauko, H., 2021. Optimal selection of thermal energy storage technology for fossil-free steam production in the processing industry. Applied Sciences 11. doi:10.3390/app11031063.

Cao, R., Lu, Y., Yu, D., Guo, Y., Bao, W., Zhang, Z., Yang, C., 2020. A novel approach to improving load flexibility of coal-fired power plant by integrating high temperature thermal energy storage through additional thermodynamic cycle. Applied Thermal Engineering 173, 115225. doi:https://doi.org/10.1016/j.applthermaleng.2020.115225.

Chalmers, H., Lucquiaud, M., Gibbins, J., Leach, M., 2009. Flexible operation of coal fired power plants with postcombustion capture of carbon dioxide. Journal of Environmental Engineering 135, 449–458. doi:10.1061/(ASCE)EE.1943-7870.0000007.

Chan, L.L.T., Chen, J., 2018. Improving the energy cost of an absorber-stripper CO_2 capture process through economic model predictive control. International Journal of Greenhouse Gas Control 76, 158–166. doi:https://doi.org/10.1016/j.ijggc.2018.05.018.

Chen, X., Qiu, R., Wu, X., 2023. Multi-timescale capacity configuration optimization of energy storage equipment in power plant-carbon capture system. Applied Thermal Engineering 227, 120371. doi:https://doi.org/10.1016/j.applthermaleng.2023.120371.

Cheng, F., Patankar, N., Chakrabarti, S., Jenkins, J.D., 2022. Modeling the operational flexibility of natural gas combined cycle power plants coupled with flexible carbon capture and storage via solvent storage and flexible regeneration. International Journal of Greenhouse Gas Control 118, 103686. doi:https://doi.org/10.1016/j.ijggc.2022.103686.

Cohen, S.M., Webber, M.E., Rochelle, G.T., 2010. Utilizing Solar Thermal Energy for Post-Combustion CO_2 Capture, in: 4th International Conference on Energy Sustainability. ASME. volume 1 of *Energy Sustainability*, pp. 663–672. doi:10.1115/ES2010-90147.

Cormos, A.M., Vasile, M., Cristea, M.V., 2015. Flexible operation of CO_2 capture processes integrated with power plant using advanced control techniques. Computer Aided Chemical Engineering 37, 1547–1552. doi:https://doi.org/10.1016/B978-0-444-63577-8.50103-0.

Cristea, V.M., Burca, M.I., Ilea, F.M., Cormos, A.M., 2020. Efficient decentralized control of the post combustion CO_2 capture plant for flexible operation against influent flue gas disturbances. Energy 205, 117960. doi:https://doi.org/10.1016/j.energy.2020.117960.

Dhoke, C., Zaabout, A., Cloete, S., Amini, S., 2021. Review on reactor configurations for adsorption-based CO_2 capture. Industrial & Engineering Chemistry Research 60, 3779–3798. doi:10.1021/acs.iecr.0c04547.

Dziejarski, B., Krzyżyńska, R., Andersson, K., 2023. Current status of carbon capture, utilization, and storage technologies in the global economy: A survey of technical assessment. Fuel 342, 127776. doi:https://doi.org/10.1016/j.fuel.2023.127776.

European Commission, 2019. Communication From The Commission To The European Parliament. The European Council, Brussels. The Council, THE EUROPEAN ECONOMIC AND SOCIAL COMMITTEE AND THE COMMITTEE OF THE REGIONS: The European Green Deal.

Garbrecht, O., Bieber, M., Kneer, R., 2017. Increasing fossil power plant flexibility by integrating molten-salt thermal storage. Energy 118, 876–883. doi:https://doi.org/10.1016/j.energy.2016.10.108.

Gardarsdottir, S.O., Montañés, R.M., Normann, F., Nord, L.O., Johnsson, F., 2017. Effects of CO_2-absorption control strategies on the dynamic performance of a supercritical pulverized-coal-fired power plant. Industrial & Engineering Chemistry Research 56, 4415–4430. doi:10.1021/acs.iecr.6b04928.

Gardarsdottir, S.O., Normann, F., Andersson, K., Prölß, K., Emilsdóttir, S., Johnsson, F., 2015. Post-combustion CO_2 capture applied to a state-of-the-art coal-fired power plant—the influence of dynamic process conditions. International Journal of Greenhouse Gas Control 33, 51–62. doi:https://doi.org/10.1016/j.ijggc.2014.12.001.

Gaspar, J., Ricardez-Sandoval, L., Jørgensen, J.B., Fosbøl, P.L., 2016. Controllability and flexibility analysis of CO_2 post-combustion capture using piperazine and MEA. International Journal of Greenhouse Gas Control 51, 276–289. doi:https://doi.org/10.1016/j.ijggc.2016.06.003.

Global CCS Institute, 2022. Global Status of CCS 2022. Technical Report. Global CCS Institute.

Gonzalez-Salazar, M.A., Kirsten, T., Prchlik, L., 2018. Review of the operational flexibility and emissions of gas- and coal-fired power plants in a future with growing renewables. Renewable and Sustainable Energy Reviews 82, 1497–1513. doi:https://doi.org/10.1016/j.rser.2017.05.278.

Haider, M., Werner, A., 2013. An overview of state of the art and research in the fields of sensible, latent and thermo-chemical thermal energy storage. e & i Elektrotechnik und Informationstechnik 130, 248–259. doi:10.1007/s00502-013-0151-3.

Hasan, M.F., Zantye, M.S., Kazi, M.K., 2022. Challenges and opportunities in carbon capture, utilization and storage: A process systems engineering perspective. Computers & Chemical Engineering 166, 107925. doi:https://doi.org/10.1016/j.compchemeng.2022.107925.

Huber, M., Dimkova, D., Hamacher, T., 2014. Integration of wind and solar power in Europe: Assessment of flexibility requirements. Energy 69, 236–246. doi:https://doi.org/10.1016/j.energy.2014.02.109.

Huber, M.L., Lemmon, E.W., Bell, I.H., McLinden, M.O., 2022. The NIST REFPROP database for highly accurate properties of industrially important fluids. Industrial & Engineering Chemistry Research 61, 15449–15472. doi:10.1021/acs.iecr.2c01427.

IEA, 2015. Energy technology perspectives (ETP). Harnessing electricity's potential. Technical Report. International Energy Agency.

IEA, 2022. World Energy Outlook 2022. Technical Report. International Energy Agency.

IEA, 2023. CO_2 Emissions in 2022. Technical Report. International Energy Agency.

IEA-ECES, 2018. Applications of thermal energy storage in the energy transition - benchmarks and developments. Technical Report. IEA technology collaboration programme on energy conservation through energy storage.

IPCC, 2018. Global Warming of 1.5 °C. An IPCC Special Report on the impacts of global warming of 1.5 °C above pre-industrial levels and related global greenhouse gas emission pathways, in the context of strengthening the global response to the threat of climate change. Technical Report. Intergovernmental Panel on Climate Change.

IPCC, 2023. Climate Change 2023: Synthesis Report. Technical Report. Intergovernmental Panel on Climate Change.

Jung, H., Heo, S., Lee, J.H., 2021. Model predictive control for amine-based CO_2 capture process with advanced flash stripper. Control Engineering Practice 114, 104885. doi:https://doi.org/10.1016/j.conengprac.2021.104885.

Jung, H., Im, D., Heo, S., Kim, B., Lee, J.H., 2020. Dynamic analysis and linear model predictive control for operational flexibility of post-combustion CO_2 capture processes. Computers & Chemical Engineering 140, 106968. doi:https://doi.org/10.1016/j.compchemeng.2020.106968.

Jung, W., Lee, J., 2022. Economic evaluation for four different solid sorbent processes with heat integration for energy-efficient CO_2 capture based on PEI-silica sorbent. Energy 238, 121864. doi:https://doi.org/10.1016/j.energy.2021.121864.

Kazemifar, F., 2022. A review of technologies for carbon capture, sequestration, and utilization: Cost, capacity, and technology readiness. Greenhouse Gases: Science and Technology 12, 200–230. doi:https://doi.org/10.1002/ghg.2131.

Kebede, A.A., Kalogiannis, T., Van Mierlo, J., Berecibar, M., 2022. A comprehensive review of stationary energy storage devices for large scale renewable energy sources grid integration. Renewable and Sustainable Energy Reviews 159, 112213. doi:https://doi.org/10.1016/j.rser.2022.112213.

Kim, H., Miller, D.C., Modekurti, S., Omell, B., Bhattacharyya, D., Zitney, S.E., 2016. Mathematical modeling of a moving bed reactor for post-combustion CO_2 capture. AIChE Journal 62, 3899–3914. doi:https://doi.org/10.1002/aic.15289.

Kim, K., Son, Y., Lee, W.B., Lee, K.S., 2013. Moving bed adsorption process with internal heat integration for carbon dioxide capture. International Journal of Greenhouse Gas Control 17, 13–24. doi:https://doi.org/10.1016/j.ijggc.2013.04.005.

Kosman, W., Rusin, A., 2020. The application of molten salt energy storage to advance the transition from coal to green energy power systems. Energies 13. doi:10.3390/en13092222.

Krüger, M., Muslubas, S., Loeper, T., Klasing, F., Knödler, P., Mielke, C., 2020. Potentials of thermal energy storage integrated into steam power plants. Energies 13. doi:10.3390/en13092226.

Kvamsdal, H., Jakobsen, J., Hoff, K., 2009. Dynamic modeling and simulation of a CO_2 absorber column for post-combustion CO_2 capture. Chemical Engineering and Processing: Process Intensification 48, 135–144. doi:https://doi.org/10.1016/j.cep.2008.03.002.

Lawal, A., Wang, M., Stephenson, P., Koumpouras, G., Yeung, H., 2010. Dynamic modelling and analysis of post-combustion CO_2 chemical absorption process for coal-fired power plants. Fuel 89, 2791–2801. doi:https://doi.org/10.1016/j.fuel.2010.05.030.

Lawal, A., Wang, M., Stephenson, P., Obi, O., 2012. Demonstrating full-scale post-combustion CO_2 capture for coal-fired power plants through dynamic modelling and simulation. Fuel 101, 115–128. doi:https://doi.org/10.1016/j.fuel.2010.10.056.

Lawal, A., Wang, M., Stephenson, P., Yeung, H., 2009. Dynamic modelling of CO_2 absorption for post combustion capture in coal-fired power plants. Fuel 88, 2455–2462. doi:https://doi.org/10.1016/j.fuel.2008.11.009.

Li, D., Wang, J., 2018. Study of supercritical power plant integration with high temperature thermal energy storage for flexible operation. Journal of Energy Storage 20, 140–152. doi:https://doi.org/10.1016/j.est.2018.09.008.

Li, H., Yan, J., Campana, P.E., 2012. Feasibility of integrating solar energy into a power plant with amine-based chemical absorption for CO_2 capture. International Journal of Greenhouse Gas Control 9, 272–280. doi:https://doi.org/10.1016/j.ijggc.2012.04.005.

Li, Q., Zhang, W., Qin, Y., An, A., 2021. Model predictive control for the process of MEA absorption of CO_2 based on the data identification model. Processes 9. doi:10.3390/pr9010183.

Liao, P., Li, Y., Wu, X., Wang, M., Oko, E., 2020. Flexible operation of large-scale coal-fired power plant integrated with solvent-based post-combustion CO_2 capture based on neural network inverse control. International Journal of Greenhouse Gas Control 95, 102985. doi:https://doi.org/10.1016/j.ijggc.2020.102985.

Liao, P., Wu, X., Wang, M., Li, Z., Qian, F., 2023. Robust control and flexible operation for commercial-scale coal-fired power plant with solvent-based post-combustion carbon capture. International Journal of Greenhouse Gas Control 123, 103831. doi:https://doi.org/10.1016/j.ijggc.2023.103831.

Lin, Y.J., Pan, T.H., Wong, D.S.H., Jang, S.S., Chi, Y.W., Yeh, C.H., 2011. Plantwide control of CO_2 capture by absorption and stripping using monoethanolamine solution. Industrial & Engineering Chemistry Research 50, 1338–1345. doi:10.1021/ie100771x.

Lund, P.D., Lindgren, J., Mikkola, J., Salpakari, J., 2015. Review of energy system flexibility measures to enable high levels of variable renewable electricity. Renewable and Sustainable Energy Reviews 45, 785–807. doi:https://doi.org/10.1016/j.rser.2015.01.057.

Ma, C., Zhang, W., Zheng, Y., An, A., 2021. Economic model predictive control for post-combustion CO_2 capture system based on MEA. Energies 14. doi:10.3390/en14238160.

Mechleri, E., Lawal, A., Ramos, A., Davison, J., Dowell, N.M., 2017. Process control strategies for flexible operation of post-combustion CO_2 capture plants. International Journal of Greenhouse Gas Control 57, 14–25. doi:https://doi.org/10.1016/j.ijggc.2016.12.017.

Mechleri, E.D., Biliyok, C., Thornhill, N.F., 2014. Dynamic simulation and control of post-combustion CO_2 capture with MEA in a gas fired power plant. Computer Aided Chemical Engineering 33, 619–624. doi:https://doi.org/10.1016/B978-0-444-63456-6.50104-6.

Mejdell, T., Kvamsdal, H., Hauger, S., Gjertsen, F., Tobiesen, F., Hillestad, M., 2022. Demonstration of non-linear model predictive control for optimal flexible operation of a CO_2 capture plant. International Journal of Greenhouse Gas Control 117, 103645. doi:https://doi.org/10.1016/j.ijggc.2022.103645.

Merel, J., Clausse, M., Meunier, F., 2008. Experimental investigation on CO_2 post-combustion capture by indirect thermal swing adsorption using 13X and 5A zeolites. Industrial & Engineering Chemistry Research 47, 209–215. doi:10.1021/ie071012x.

Moioli, S., Pellegrini, L.A., 2019. Operating the CO_2 absorption plant in a post-combustion unit in flexible mode for cost reduction. Chemical Engineering Research and Design 147, 604–614. doi:https://doi.org/10.1016/j.cherd.2019.03.027.

Moioli, S., Pellegrini, L.A., 2020. Fixed and capture level reduction operating modes for carbon dioxide removal in a natural gas combined cycle power plant. Journal of Cleaner Production 254, 120016. doi:https://doi.org/10.1016/j.jclepro.2020.120016.

Mokhtar, M., Ali, M.T., Khalilpour, R., Abbas, A., Shah, N., Hajaj, A.A., Armstrong, P., Chiesa, M., Sgouridis, S., 2012. Solar-assisted post-combustion carbon capture feasibility study. Applied Energy 92, 668–676. doi:https://doi.org/10.1016/j.apenergy.2011.07.032.

Mondino, G., 2022. Assessment of Moving Bed Temperature Swing Adsorption Process for Post-Combustion CO_2 Capture. Ph.D. thesis. Norwegian University of Science and Technology.

Mondino, G., Grande, C.A., Blom, R., 2017. Effect of gas recycling on the performance of a moving bed temperature-swing (MBTSA) process for CO_2 capture in a coal fired power plant context. Energies 10. doi:10.3390/en10060745.

Mondino, G., Grande, C.A., Blom, R., Nord, L.O., 2019. Moving bed temperature swing adsorption for CO_2 capture from a natural gas combined cycle power plant. International Journal of Greenhouse Gas Control 85, 58–70. doi:https://doi.org/10.1016/j.ijggc.2019.03.021.

Mondino, G., Grande, C.A., Blom, R., Nord, L.O., 2022. Evaluation of MBTSA technology for CO_2 capture from waste-to-energy plants. International Journal of Greenhouse Gas Control 118, 103685. doi:https://doi.org/10.1016/j.ijggc.2022.103685.

Montañés, R.M., Flø, N.E., Nord, L.O., 2018. Experimental results of transient testing at the amine plant at Technology Centre Mongstad: Open-loop responses and performance of decentralized control structures for load changes. International Journal of Greenhouse Gas Control 73, 42–59. doi:https://doi.org/10.1016/j.ijggc.2018.04.001.

Montañés, R.M., Gardarsdottir, S.O., Normann, F., Johnsson, F., Nord, L.O., 2017. Demonstrating load-change transient performance of a commercial-scale natural gas combined cycle power plant with post-combustion CO_2 capture. International Journal of Greenhouse Gas Control 63, 158–174. doi:https://doi.org/10.1016/j.ijggc.2017.05.011.

Morales-Ospino, R., Santos, V.N., Lima, A.R.A.J., Torres, A.E.B., Vilarrasa-García, E., Bastos-Neto, M., Cavalcante, C.L.J., Azevedo, D.C.S., Marques, C.R.M., de Aquino, T.F., Vasconcelos, L.B., Knaebel, K.S., 2021. Parametric analysis of a moving bed temperature swing adsorption (MBTSA) process for postcombustion CO_2 capture. Industrial & Engineering Chemistry Research 60, 10736–10752. doi:10.1021/acs.iecr.0c05067.

NETL, 2019. Cost and performance baseline for fossil energy plants volume 1: bituminous coal and natural gas to electricity. Technical Report. National Energy Technology Laboratory.

Nie, L., Mu, Y., Jin, J., Chen, J., Mi, J., 2018. Recent developments and consideration issues in solid adsorbents for CO_2 capture from flue gas. Chinese Journal of Chemical Engineering 26, 2303–2317. doi:https://doi.org/10.1016/j.cjche.2018.07.012.

Nittaya, T., Douglas, P.L., Croiset, E., Ricardez-Sandoval, L.A., 2014. Dynamic modelling and control of MEA absorption processes for CO_2 capture from power plants. Fuel 116, 672–691. doi:https://doi.org/10.1016/j.fuel.2013.08.031.

Nord, L.O., Bolland, O., 2022. Carbon Dioxide Emission Management in Power Generation. 1 ed., John Wiley & Sons.

Okumura, T., Yoshizawa, K., Nishibe, S., Iwasaki, H., Kazari, M., Hori, T., 2017. Parametric testing of a pilot-scale design for a moving-bed CO_2 capture system using low-temperature steam. Energy Procedia 114, 2322–2329. doi:https://doi.org/10.1016/j.egypro.2017.03.1369. 13th International Conference on Greenhouse Gas Control Technologies, GHGT-13, 14-18 November 2016, Lausanne, Switzerland.

Okumura, T., Yoshizawa, K., Numaguchi, R., Nishibe, S., Kanou, A., Hasegawa, Y., Inoue, S., Tsuji, K., Fujita, S., Nabeshima, M., Yamada, H., Yamamoto, S., Takayama, N., Yogo, K., 2018. Demonstration plant of the Kawasaki CO_2 capture (KCC) system with solid sorbent for coal-fired power station. SSRN Electronic Journal doi:https://doi.org/10.2139/ssrn.3365953. 14th Greenhouse Gas Control Technologies Conference, GHGT-14, 21-26 October 2018, Melbourne, Australia.

Ordorica-Garcia, G., Delgado, A.V., Garcia, A.F., 2011. Novel integration options of concentrating solar thermal technology with fossil-fuelled and CO_2 capture processes. Energy Procedia 4, 809–816. doi:https://doi.org/10.1016/j.egypro.2011.01.123. 10th International Conference on Greenhouse Gas Control Technologies.

Palizban, O., Kauhaniemi, K., 2016. Energy storage systems in modern grids—matrix of technologies and applications. Journal of Energy Storage 6, 248–259. doi:https://doi.org/10.1016/j.est.2016.02.001.

Panahi, M., Skogestad, S., 2012. Economically efficient operation of CO_2 capturing process. part ii. design of control layer. Chemical Engineering and Processing: Process Intensification 52, 112–124. doi:https://doi.org/10.1016/j.cep.2011.11.004.

Park, Y.J., Lee, S.J., Moon, J.H., Choi, D.K., Lee, C.H., 2006. Adsorption equilibria of O_2, N_2, and Ar on carbon molecular sieve and zeolites 10X, 13X, and LiX. Journal of Chemical & Engineering Data 51, 1001–1008. doi:10.1021/je050507v.

Parvareh, F., Sharma, M., Qadir, A., Milani, D., Khalilpour, R., Chiesa, M., Abbas, A., 2014. Integration of solar energy in coal-fired power plants retrofitted with carbon capture: A review. Renewable and Sustainable Energy Reviews 38, 1029–1044. doi:https://doi.org/10.1016/j.rser.2014.07.032.

Patron, G.D., Ricardez-Sandoval, L., 2020. A robust nonlinear model predictive controller for a post-combustion CO_2 capture absorber unit. Fuel 265, 116932. doi:https://doi.org/10.1016/j.fuel.2019.116932.

Patrón, G.D., Ricardez-Sandoval, L., 2022. An integrated real-time optimization, control, and estimation scheme for post-combustion CO_2 capture. Applied Energy 308, 118302. doi:https://doi.org/10.1016/j.apenergy.2021.118302.

Posch, S., Haider, M., 2013. Dynamic modeling of CO_2 absorption from coal-fired power plants into an aqueous monoethanolamine solution. Chemical Engineering Research and Design 91, 977–987. doi:https://doi.org/10.1016/j.cherd.2012.09.016.

Raganati, F., Miccio, F., Ammendola, P., 2021. Adsorption of carbon dioxide for post-combustion capture: A review. Energy & Fuels 35, 12845–12868. doi:10.1021/acs.energyfuels.1c01618.

Richter, M., Möllenbruck, F., Starinsk, A., Oeljeklaus, G., Görner, K., 2015. Flexibilization of coal-fired power plants by dynamic simulation. doi:http://dx.doi.org/10.3384/ecp15118715. Proceedings of the 11th International Modelica Conference, Versailles, France, Sept. 21-23 2015.

Richter, M., Oeljeklaus, G., Görner, K., 2019. Improving the load flexibility of coal-fired power plants by the integration of a thermal energy storage. Applied Energy 236, 607–621. doi:https://doi.org/10.1016/j.apenergy.2018.11.099.

Ritchie, H., Rosado, P., 2023. Our world in data - electricity mix. https://ourworldindata.org/electricity-mix. Accessed: 2023-10-17.

Rúa, J., Hillestad, M., Nord, L.O., 2021. Model predictive control for combined cycles integrated with CO_2 capture plants. Computers & Chemical Engineering 146, 107217. doi:https://doi.org/10.1016/j.compchemeng.2020.107217.

Saghafifar, M., Gabra, S., 2020. A critical overview of solar assisted carbon capture systems: Is solar always the solution? International Journal of Greenhouse Gas Control 92, 102852. doi:https://doi.org/10.1016/j.ijggc.2019.102852.

Samanta, A., Zhao, A., Shimizu, G.K.H., Sarkar, P., Gupta, R., 2012. Post-combustion CO_2 capture using solid sorbents: A review. Industrial & Engineering Chemistry Research 51, 1438–1463. doi:10.1021/ie200686q.

Sayed, E.T., Olabi, A.G., Alami, A.H., Radwan, A., Mdallal, A., Rezk, A., Abdelkareem, M.A., 2023. Renewable energy and energy storage systems. Energies 16. doi:10.3390/en16031415.

Seborg, D.E., Edgar, T.F., Mellichamp, D.A., Doyle, F.J., 2016. Process Dynamics and Control. John Wiley & Sons, Hoboken, New Jersey.

Seo, K., Retnanto, A.P., Martorell, J.L., Edgar, T.F., Stadtherr, M.A., Baldea, M., 2023. Simultaneous design and operational optimization for flexible carbon capture process using ionic liquids. Computers & Chemical Engineering 178, 108344. doi:https://doi.org/10.1016/j.compchemeng.2023.108344.

Shamsuzzoha, M., Skogestad, S., 2010. The setpoint overshoot method: A simple and fast closed-loop approach for PID tuning. Journal of Process Control 20, 1220–1234. doi:https://doi.org/10.1016/j.jprocont.2010.08.003.

Sharifzadeh, M., Shah, N., 2019. MEA-based CO_2 capture integrated with natural gas combined cycle or pulverized coal power plants: Operability and controllability through integrated design and control. Journal of Cleaner Production 207, 271–283. doi:https://doi.org/10.1016/j.jclepro.2018.09.115.

Skogestad, S., 2003. Simple analytic rules for model reduction and PID controller tuning. Journal of Process Control 13, 291–309. doi:https://doi.org/10.1016/S0959-1524(02)00062-8.

Steinmann, W.D., Eck, M., 2006. Buffer storage for direct steam generation. Solar Energy 80, 1277–1282. doi:https://doi.org/10.1016/j.solener.2005.05.013.

Stevanovic, V.D., Maslovaric, B., Prica, S., 2012. Dynamics of steam accumulation. Applied Thermal Engineering 37, 73–79. doi:https://doi.org/10.1016/j.applthermaleng.2012.01.007.

Stevanovic, V.D., Petrovic, M.M., Milivojevic, S., Ilic, M., 2020. Upgrade of the thermal power plant flexibility by the steam accumulator. Energy Conversion and Management 223, 113271. doi:https://doi.org/10.1016/j.enconman.2020.113271.

Sultan, T., Zabiri, H., Shahbaz, M., Maulud, A.S., 2022. Performance evaluation of the fast model predictive control scheme on a CO_2 capture plant through absorption/stripping system. Process Safety and Environmental Protection 157, 218–236. doi:https://doi.org/10.1016/j.psep.2021.11.018.

Tait, P., Buschle, B., Milkowski, K., Akram, M., Pourkashanian, M., Lucquiaud, M., 2018. Flexible operation of post-combustion CO_2 capture at pilot scale with demonstration of capture-efficiency control using online solvent measurements. International Journal of Greenhouse Gas Control 71, 253–277. doi:https://doi.org/10.1016/j.ijggc.2018.02.023.

Tang, Z., Wu, X., 2023. Distributed predictive control guided by intelligent reboiler steam feedforward for the coordinated operation of power plant-carbon capture system. Energy 267, 126568. doi:https://doi.org/10.1016/j.energy.2022.126568.

Thermoflow, 2023. STEAM PRO and STEAM MASTER. https://www.thermoflow.com/products_conventionalsteam.html. Accessed: 2023-12-06.

Tregambi, C., Montagnaro, F., Salatino, P., Solimene, R., 2015. A model of integrated calcium looping for CO_2 capture and concentrated solar power. Solar Energy 120, 208–220. doi:https://doi.org/10.1016/j.solener.2015.07.017.

Trojan, M., Taler, D., Dzierwa, P., Taler, J., Kaczmarski, K., Wrona, J., 2019. The use of pressure hot water storage tanks to improve the energy flexibility of the steam power unit. Energy 173, 926–936. doi:https://doi.org/10.1016/j.energy.2019.02.059.

Wagner, W., Pruß, A., 2002. The IAPWS Formulation 1995 for the Thermodynamic Properties of Ordinary Water Substance for General and Scientific Use. Journal of Physical and Chemical Reference Data 31, 387–535. doi:10.1063/1.1461829.

Wang, J., Liu, L., Zeng, X., Li, K., 2021. Solar-assisted CO_2 capture with amine and ammonia-based chemical absorption: A comparative study. Thermal Science 25, 717–732. doi:https://doi.org/10.2298/TSCI191222149W.

Wellner, K., Marx-Schubach, T., Schmitz, G., 2016. Dynamic behavior of coal-fired power plants with postcombustion CO_2 capture. Industrial & Engineering Chemistry Research 55, 12038–12045. doi:10.1021/acs.iecr.6b02752.

Wibberley, L., 2007. CO_2 capture using solar thermal energy. Patent WO2008009049A1.

Wu, X., Shen, J., Wang, M., Lee, K.Y., 2020a. Intelligent predictive control of large-scale solvent-based CO_2 capture plant using artificial neural network and particle swarm optimization. Energy 196, 117070. doi:https://doi.org/10.1016/j.energy.2020.117070.

Wu, X., Wang, M., Lee, K.Y., 2020b. Flexible operation of supercritical coal-fired power plant integrated with solvent-based CO_2 capture through collaborative predictive control. Energy 206, 118105. doi:https://doi.org/10.1016/j.energy.2020.118105.

Wu, X., Wang, M., Liao, P., Shen, J., Li, Y., 2020c. Solvent-based post-combustion CO_2 capture for power plants: A critical review and perspective on dynamic modelling, system identification, process control and flexible operation. Applied Energy 257, 113941. doi:https://doi.org/10.1016/j.apenergy.2019.113941.

Wu, X., Wang, M., Shen, J., Li, Y., Lawal, A., Lee, K.Y., 2019. Flexible operation of coal fired power plant integrated with post combustion CO_2 capture using model predictive control. International Journal of Greenhouse Gas Control 82, 138–151. doi:https://doi.org/10.1016/j.ijggc.2018.12.004.

Yu, M., Biegler, L.T., 2018. Economic NMPC strategies for solid sorbent-based CO_2 capture. IFAC-PapersOnLine 51, 103–108. doi:https://doi.org/10.1016/j.ifacol.2018.09.283. 10th IFAC Symposium on Advanced Control of Chemical Processes ADCHEM 2018.

Zaman, M., Lee, J.H., 2015. Optimization of the various modes of flexible operation for post-combustion CO_2 capture plant. Computers & Chemical Engineering 75, 14–27. doi:https://doi.org/10.1016/j.compchemeng.2014.12.017.

Zhang, K., Liu, M., Zhao, Y., Yan, H., Yan, J., 2022. Design and performance evaluation of a new thermal energy storage system integrated within a coal-fired power plant. Journal of Energy Storage 50, 104335. doi:https://doi.org/10.1016/j.est.2022.104335.

Zhao, R., Liu, L., Zhao, L., Deng, S., Li, S., Zhang, Y., 2019. A comprehensive performance evaluation of temperature swing adsorption for post-combustion carbon dioxide capture. Renewable and Sustainable Energy Reviews 114, 109285. doi:https://doi.org/10.1016/j.rser.2019.109285.

Zhu, Q., Lu, P., Yang, Z., Ji, X., Han, Y., 2019. Multi-parameter optimization for the wet steam accumulator of a steam-powered catapult. Energies 12. doi:10.3390/en12020234.

Ziaii, S., Rochelle, G.T., Edgar, T.F., 2009. Dynamic modeling to minimize energy use for CO_2 capture in power plants by aqueous monoethanolamine. Industrial & Engineering Chemistry Research 48, 6105–6111. doi:10.1021/ie801385q.

Zima, W., Gradziel, S., Cebula, A., Rerak, M., Kozak-Jagiela, E., Pilarczyk, M., 2023. Mathematical model of a power boiler operation under rapid thermal load changes. Energy 263, 125836. doi:https://doi.org/10.1016/j.energy.2022.125836.

Appendix A

Publications

Publication I
V.T. Skjervold, G. Mondino, L. Riboldi and L.O. Nord (2023). Investigation of control strategies for adsorption-based CO_2 capture from a thermal power plant under variable load operation. *Energy*, 268, 126728.

Publication II
V.T. Skjervold and L.O. Nord (2023). Enhanced single-loop control of a moving bed temperature swing adsorption CO_2 capture process. *Computers & Chemical Engineering*, 178, 108387.

Publication III
V.T. Skjervold and L.O. Nord (2024). Thermal energy storage integration for increased flexibility of a power plant with post-combustion CO_2 capture. *Applied Thermal Engineering*, 246, 122907.

Energy 268 (2023) 126728

Contents lists available at ScienceDirect

Energy

journal homepage: www.elsevier.com/locate/energy

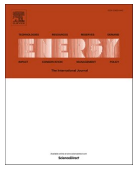

Investigation of control strategies for adsorption-based CO_2 capture from a thermal power plant under variable load operation

Vidar T. Skjervold [a,*], Giorgia Mondino [b], Luca Riboldi [c], Lars O. Nord [a]

[a] NTNU - Norwegian University of Science and Technology, Department of Energy and Process Engineering, Trondheim, Norway
[b] SINTEF Industry, P.O. Box 124, Blindern, N0314, Oslo, Norway
[c] SINTEF Energy Research, Sem Sælands vei 11, 7034, Trondheim, Norway

ARTICLE INFO

Handling Editor: Petar Sabev Varbanov

Keywords:
CO_2 capture
Temperature-swing adsorption
Moving bed
Variable load
Process control
Dynamic simulations

ABSTRACT

This work considers the closed-loop behavior of a moving bed temperature swing adsorption process designed to capture CO_2 from a coal-fired power plant. Four decentralized control strategies were studied based on step changes and ramps of flue gas feed flow rate and controller setpoint changes. A proportional-integral (PI) control configuration, where CO_2 purity was controlled by hot fluid velocity to the desorption section and CO_2 recovery was controlled by the sorbent flow rate, demonstrated the overall best performance. The 99% settling time for higher-level control variables varied from 0 to 13 min for most control configurations and the settling time for CO_2 purity was generally longer than for CO_2 recovery. The simulations show that using ratio controllers lead to larger offsets but can give around 10 times faster purity response compared to PI-control. All investigated control combinations were able to keep the controlled variables relatively close to the setpoints and the largest relative steady state setpoint offset was 2%.

1. Introduction

1.1. Background and motivation

To mitigate the effects of global warming, CO_2 emissions need to be significantly reduced over the coming decades. The transition to a low-carbon energy system will impact the operation of thermal power plants in several ways. Firstly, it is expected that variable renewable energy sources will stand for an increasing share of electricity production. Based on announced policies and targets, the International Energy Agency recently estimated that renewables will make up 80% of the growth in global electricity demand in the next decade [1]. Furthermore, they expect nearly 40% of the global electricity demand in 2030 to be covered by the combination of hydro, wind, solar, bioenergy, geothermal and marine power. The intermittency of such electricity sources represents a challenge for the electrical grid since supply and demand must balance. The residual load can be met by fossil power plants [2], which need to operate at varying loads due to the lack of large-scale energy storage solutions [3]. Ensuring reliability of supply will be important to achieve a fair energy transition, which is a key aspect of the United Nations Sustainable Development Goal 7 on affordable and clean energy [4].

It is likely that the deployment of CO_2 capture on thermal power plants will be necessary to meet our climate targets. As an example, a recent IPCC report shows a wide range of carbon capture and storage deployed on both natural gas and coal-fired power plants across pathways compatible with the 1.5 °C global warming scenario [5]. Post-combustion capture technologies are suitable for retrofit to existing plants, and the most mature technology is absorption-based CO_2 capture with chemical solvents [6]. However, due to the absence of large amounts of water, adsorption-based capture technologies could have lower regeneration duties [7], which would reduce the penalty on the power plant efficiency caused by integration with the CO_2 capture process.

This work considers post-combustion CO_2 capture by the moving bed temperature swing adsorption (MBTSA) technology. One of the main features distinguishing the moving bed configuration from the conventional fixed bed systems is that the former can be operated continuously. This is beneficial because it renders complex cycle schedules unnecessary and eliminates the parasitic energy losses associated with intermittent heating/cooling of the heat exchanger walls. The possibility to operate continuously is also an advantage in terms of internal heat recovery, process integration with the power plant, and process control. However, in the context of CO_2 capture from a load-following power

* Corresponding author.
E-mail address: vidar.t.skjervold@ntnu.no (V.T. Skjervold).

https://doi.org/10.1016/j.energy.2023.126728
Received 28 February 2022; Received in revised form 3 November 2022; Accepted 14 January 2023
Available online 17 January 2023

plant, the MBTSA process will frequently deviate from nominal operation due to disturbances from the power plant. In the work presented by Kim et al. a one-dimensional, non-isothermal model was used to study the response of the MBTSA process regeneration step to disturbances typical for power plants [8]. Since only a part of the process was studied, a complete picture of the dynamic behavior of the system is not obtained. The complete MBTSA process including adsorption, desorption and cooling is studied in a paper by Morales-Ospino et al. [9]. A parametric analysis was used to investigate the effect of several variables on the key performance parameters of the process. Using a similar modelling approach, the MBTSA process was studied in a coal-fired power plant context [10] and for a natural gas combined cycle power plant [11]. These studies do not consider the operation of the CO_2 capture system away from the steady state.

A control system is required to keep the operation of the MBTSA process stable during variations in power plant operation. As evidenced by the review of Wu et al. [12], both conventional, decentralized feedback controllers and advanced model predictive control approaches have been widely studied for post-combustion CO_2 capture. A summary of relevant literature is given in the following sections.

1.2. Decentralized control of post-combustion CO_2 capture

The control system is often divided into two main parts: a regulatory control layer aiming at stabilizing operation and a higher-level control layer aiming at maintaining performance. The regulatory layer includes sump levels, column pressures, reboiler, condenser and lean solvent temperatures, makeup water and solvent flows [12]. A decentralized control approach is based on single input – single output loops, where one manipulated variable (MV) is needed for each controlled variable (CV). The regulatory layer therefore leaves only a few degrees of freedom to be used as MVs in the higher-level control layer. The most common approach is to use the solvent circulation rate and flow rate of steam as MVs and CO_2 capture rate and a temperature somewhere in the process (e.g. the reboiler) as CVs for higher-level control [13].

Most of the studies in the literature focus on modelling and control of only the post-combustion capture process, meaning that variations in power plant operation are treated as external disturbances to the system. Cormos and her group carried out a comparison of proportional-integral (PI) control with model predictive control (MPC) based on step changes in inlet flue gas flow rate [14]. The solvent flow rate was used to control the sweet gas CO_2 concentration, which is closely linked to the CO_2 capture rate. No significant difference in performance between the feedback control and MPC scheme was observed. A similar conclusion was found by Panahi and Skogestad, who recommended a simple control structure over MPC due to similar performance and easier implementation [15]. Gaspar and coworkers presented a comparison of control of piperazine-based and monoethanolamine (MEA) based capture systems under varying power plant load, valve disturbance in the lean solvent stream and reduced heat delivery [16]. The CO_2 capture rate was controlled by manipulating the solvent flow rate. Similar control pairings are used in other research studies that analyzed MEA-based capture processes under various disturbances [17–19]. In these studies, the reboiler temperature is also included in the control scheme, paired with the reboiler duty. Lawal et al. considered switching off water balance control, increased flue gas flow, reduced reboiler duty and increased flue gas CO_2 concentration [17]. Lin et al. studied changes in water makeup flow, flue gas flow rate and CO_2 capture rate setpoint [18]. Mechleri and coworkers considered positive and negative changes in flue gas flow rate [19]. In the work presented by Nittaya et al. the reverse pairing is also considered, i.e. using reboiler duty to control CO_2 capture rate and solvent flow (both lean and rich) to control reboiler temperature [20]. A heuristic pairing philosophy was found to give the best controller performance. Cristea et al. presented an augmented CO_2 capture process with an additional solvent buffer tank and auxiliary heat exchanger to reduce interactions within the system [21]. A decentralized control system was investigated and shown to be reliable for disturbances in flue gas flow rate and inlet CO_2 concentration as well as CV setpoint changes.

In a few articles, coupled models of the power plant and post-combustion CO_2 capture system are used to study the integrated system under dynamic conditions [13,22–24]. In addition to the flue gas flowing from the power plant to the capture process, these models consider the extraction of steam from the power plant (typically in the cross-over between the intermediate and low-pressure turbines) and the return of condensate to the boiler feedwater line. Mechleri et al. investigated coupled models of both a supercritical, pulverized coal power plant and a natural gas combined cycle power plant with the capture process [22]. In addition, the CO_2 compression is included in the model. Feedback control strategies similar to the ones reported by Nittaya et al. (i.e., capture rate controlled by the reboiler duty and reboiler temperature by solvent flow) [20] are employed, in addition to a case with dynamic switching between modes. A supercritical coal-fired power plant with MEA-based capture is also considered by Gardarsdottir et al. [13]. In addition to the standard MV-CV pairings, the authors include a control strategy that replaces the CO_2 capture rate with the liquid to gas ratio as control objective and a case where the solvent flow is kept constant. These control alternatives are also studied for a natural gas combined cycle (NGCC)-MEA system, in addition to feedforward (ratio) controllers for the solvent and reboiler steam flow [23]. A subcritical coal-fired power plant coupled to an amine solvent CO_2 capture process is studied by Lawal et al. [24], using the same control system as in their previous work, i.e., by manipulating the solvent flow rate [17].

1.3. Model predictive control of post-combustion CO_2 capture

In model predictive control, a centralized approach is applied at every time step to determine the optimal control action for a given predictive horizon [12]. As the name suggests, MPC requires a predictive dynamic model of the post-combustion CO_2 capture system, providing the future values of CVs based on the current state and future values of the MVs. If a linear predictive model is used, the control method is referred to as linear model predictive control (LMPC). Similarly, in non-linear model predictive control (NMPC) a non-linear process model is applied. The best control inputs at a given time step are determined by solving a dynamic optimization problem consisting of an objective function and constraints on the input and output variables. The objective function usually reflects the control performance [25], containing terms penalizing deviations from the controller setpoints and large changes in the manipulated variables (aggressive controller action) [26]. Several recent studies have considered MPC for post-combustion CO_2 capture.

In the case of LMPC, a quadratic programming optimization solver can often be used to determine the control action, since the predictive model is linear and the objective function is often quadratic. This reduces the computational demand of the controller [27] compared to NMPC. Li and coworkers found LMPC to give better setpoint tracking and less aggressive input usage compared to traditional PID control for an MEA-based capture process with the CO_2 capture rate as the only control objective [28]. Based on a first-principle model validated with pilot-scale experimental data, Jung et al. applied gap metric analysis and developed a linear predictive model around the optimal reference point for linearization [27]. Three LMPC controller options were studied for set point changes and flue gas flow disturbances. The same group used a state-space predictive model to study LMPC for an amine-based capture process with an advanced flash stripper [29]. The model predictive controller was found to outperform decentralized control structures. LMPC for an entire NGCC plant with integrated post-combustion capture was studied by Rua et al. [26]. The predictive model consisted of several linear autoregressive with exogeneous input (ARX) models that were combined in a local model network using a Gaussian validity function to weigh the individual contributions. The MPC was found to outperform the PID control approach from a previous study [23]. Sultan and coworkers increased the computational efficiency of an LMPC by solving

the quadratic programming problem in smaller fragments [30]. They compared the "fast model predictive controller" to a conventional approach and reported shorter settling times and smaller setpoint deviations.

In cases where the controller should be applicable to a wide range of operation, NMPC might be necessary in order to capture the non-linear dynamics of the post-combustion CO_2 capture process [12]. Wu et al. developed a first-principle model of a solvent-based capture process in gPROMS and identified a non-linear artificial neural network prediction model via a feed-forward back propagation method [25]. Particle swarm optimization was applied to determine controller settings. The NMPC was tested for disturbances in flue gas flow rate and compared to LMPC based on a state-space model. In another study, a nonlinear autoregressive with exogeneous input (NARX) model was used for prediction [31]. NMPC was compared to LMPC for variations in flue gas flow rate and CV setpoints and found to give better performance. Patron and Ricardez-Sandoval considered the absorber unit of a post-combustion CO_2 capture system and applied a multi-scenario NMPC where uncertainties were taken into account in the optimization step of the control algorithm [32]. Mejdell and coworkers tested the commercial NMPC software CENIT at the Tiller pilot plant in Norway, concluding that the control system was able to handle both setpoint changes and disturbance rejection [33].

The optimization problem used to determine controller action can contain terms related to the economics of the process, giving economic model predictive control (EMPC). Chan and Chen investigated EMPC for an absorber-stripper system by including the cost of solvent and utilities in the objective function [34]. In addition to the solvent cost, Ma et al. considered the cost of carbon emissions in their EMPC [35]. Yu and Biegler applied a regularization approach to give EMPC with stability guarantees [36]. The control framework was demonstrated for a bubbling fluidized-bed solid-sorbent CO_2 capture process and considered operational costs related to cooling water and purge gas in the economic term of the optimization problem. A comprehensive economic objective function was used by Patron and Ricardez-Sandoval for an MEA-based absorber connected to a fuel-fired power plant [37]. Energy, chemical and utility costs as well as the cost of emitting CO_2, income from selling captured CO_2 and non-market related negative effects of carbon emissions were considered. A real-time optimization routine solved a steady-state economic optimization problem to provide regular updates of the setpoints for the NMPC.

1.4. Knowledge gaps and scope of paper

The literature review shows that both decentralized and model predictive control approaches for post-combustion CO_2 capture have been extensively studied. However, previous studies are mostly limited to solvent-based systems, and to our knowledge process control of an MBTSA process for post-combustion CO_2 capture has not been considered. In addition, the dynamic behavior of a complete MBTSA system under typical disturbances from a power plant has not been reported in the literature. These two knowledge gaps will be addressed in this work.

The research objective of this work is to investigate control structures for the MBTSA process for post-combustion CO_2 capture. The focus is on simple, decentralized control structures. They have shown to be viable for control of post-combustion CO_2 capture and are easy to implement since no additional models or optimization routines are required to determine the control action. Furthermore, it is useful to establish a baseline for control of the MBTSA process that more advanced control approaches can be compared to in the future. We consider an activated carbon-based MBTSA process designed to capture CO_2 from a coal-fired power plant. The closed-loop behavior of different control combinations is studied based on step changes and ramps of flue gas flow as well as controller setpoint changes. Controller performance is quantified by settling times and steady-state deviation from the control targets. The analysis is based on a dynamic model of the moving bed system developed in gPROMS.

The article is structured as follows. In Section 2 the overall method and design basis is explained, before the principle, modelling and design of the moving bed temperature swing adsorption system are described. In Section 3, the choice of control combinations, tuning of controllers and controller test cases are described. Results are presented and discussed in Section 4. Conclusions and recommendations for further work are given in Section 5.

2. Moving bed temperature swing adsorption

2.1. Method

This work considers the application of the MBTSA process for capturing CO_2 from a coal-fired power plant. The flue gas specifications at nominal conditions, as reported in Table 1, were taken as reference for the design. It has been assumed that the flue gas is cooled and dried before entering the CO_2 capture unit, which increases the energy use of the system. However, since the energy performance is not used as a performance indicator in this work, this effect has been neglected. In addition, the flue gas is taken as a binary mixture of CO_2 and N_2, where it has been assumed that O_2 and Ar exhibit similar behavior as N_2 [11]. This assumption reduces the computational time of the MBTSA simulations and is not expected to significantly affect the behavior of the CO_2 capture process.

After designing the MBTSA process model (described in Section 2.3) for the nominal operating point, the dynamic behavior of the system at off-design conditions was studied through a series of simulations. The current study only considers the effect of variations in flue gas flow on the CO_2 capture system, neglecting the integration with the steam/water cycle of the power plant. No power plant model has been developed, and load variations are assumed to be represented by changes in the flue gas feed flow to the MBTSA process. The composition, temperature and pressure of the flue gas is kept constant in all scenarios. Four different control configurations are investigated. An overview of the methodology is given in Fig. 1.

2.2. Process description

The moving bed temperature swing adsorption process makes use of a solid adsorbent with the ability of: (i) removing the CO_2 from the flue gas by selectively adsorbing the CO_2 onto its surface, (ii) releasing the adsorbed CO_2 when heated to a certain temperature. The first of the two properties is what allows the separation of the CO_2 from the rest of the flue gas components, while the second is responsible for allowing extraction of a high purity CO_2 stream and the regeneration of the adsorbent.

The process, shown schematically in Fig. 2, is continuous and operated in a cyclic manner by circulating the adsorbent through different sections. In the adsorption section the sorbent particles fall downwards counter-currently to the flue gas so that the CO_2 is retained by the adsorbent while the rest of the flue gas is released to the atmosphere. When leaving the adsorption section, the adsorbent is loaded with CO_2 and is sent to the desorption section for regeneration. The desorption section is essentially an indirect-contact heat exchanger where heat is

Table 1
Nominal flue gas specifications.

Quantity	Value	Unit
Temperature	25	°C
Pressure	1.05	bar
Flowrate	57.68	kg/s
Composition:		
CO_2	14.82	vol%
N_2	85.18	vol%

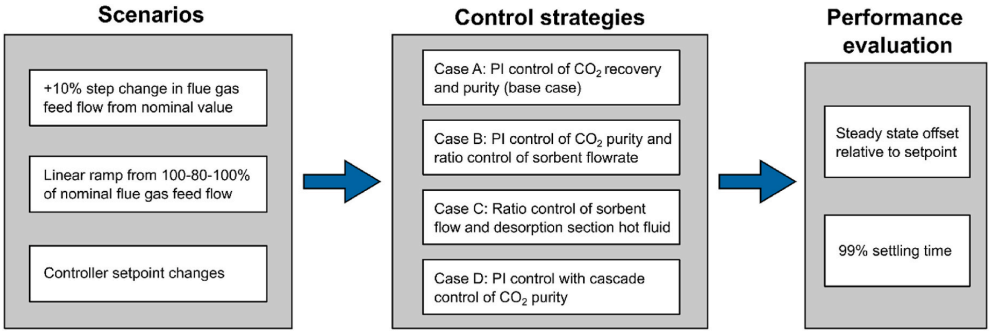

Fig. 1. Overview of methodology, including investigated scenarios, control strategies and controller performance evaluation.

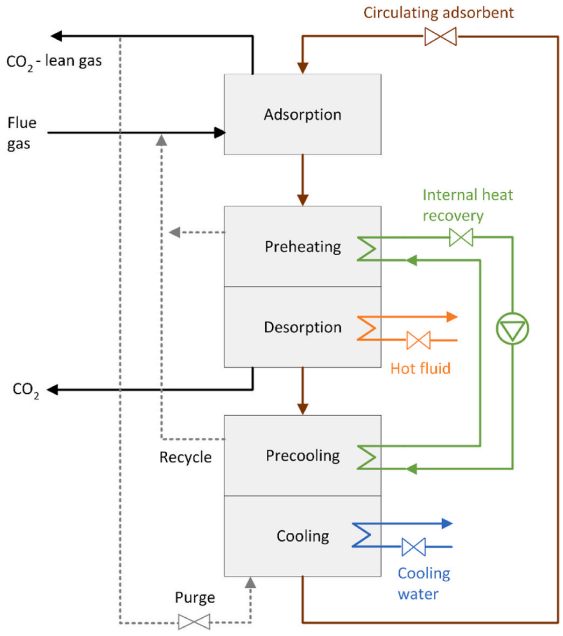

Fig. 2. Schematic diagram of the moving bed temperature swing adsorption (MBTSA) process. The manipulated variables to be used by the control system are indicated by valves.

provided to the adsorbent for promoting desorption of CO_2. As the temperature increases, the CO_2 is released by the adsorbent and can be withdrawn in a high purity stream. From the desorption section the unloaded adsorbent proceeds to the cooling section, which is again an indirect contact heat exchanger using cold water as media, where the temperature levels suitable for adsorption are restored. A fraction of the CO_2-lean gas leaving the adsorption section is recycled to the cooling section as a purge stream. After leaving the precooling section it is mixed with the flue gas feed to the adsorption section. The cooled adsorbent is finally collected and lifted back to the adsorption section with a conveyor belt system, so that the cycle is closed, and continuous system operation is maintained.

2.3. Mathematical model of MBTSA process

The MBTSA process was simulated with a previously developed model in gPROMS ModelBuilder version 6.0.4 [38]. Although it is dynamic, the model has previously only been used in steady-state design simulations. Therefore, the transient simulations from this work represent a novel application of the gPROMS model. A complete description of the model implementation and previous simulations can be found elsewhere [11], but for clarity the main characteristics of the model are described below. In addition, supplementary information is given in Appendix A.

The model makes use of the composite model capabilities of gPROMS to link the individual sections (adsorption, preheating, desorption, precooling and cooling section) via gas, solid and control signal ports. Each individual section is described by a set of partial differential equations (unsteady and one-dimensional) including mass, energy and momentum balances. In Table 2, a summary of the main model equations is given. Although the numerical value of certain design parameters (e.g., void fraction and section height) and operating conditions differ from section to section, the model equations and the underlying

Table 2
Summary of model equations used in gPROMS model of MBTSA process.

Mass balance in gas phase	$\varepsilon_c\frac{\partial C_i}{\partial t}+\frac{\partial(uC_i)}{\partial z}=\varepsilon_c\frac{\partial}{\partial z}\left(D_{z,i}C_T\frac{\partial Y_i}{\partial z}\right)-\frac{(1-\varepsilon_c-\xi)a'k_{T,i}}{\mathrm{Bi}_i/5+1}(C_i-C_{p,i})$	(1)
Mass balance in macropores	$\varepsilon_p\frac{\partial C_{p,i}}{\partial t}+v_s\frac{\partial C_{p,i}}{\partial z}=\varepsilon_p\frac{15D_{p,i}}{{r_p}^2}\frac{\mathrm{Bi}_i}{5+\mathrm{Bi}_i}(C_i-C_{p,i})-\rho_p\frac{15D_{c,i}}{r_c^2}(q_i^*-q_i)$	(2)
Mass balance in solid phase	$\frac{\partial q_i}{\partial t}+v_s\frac{\partial q_i}{\partial z}=\frac{15D_{c,i}}{r_c^2}(q_i^*-q_i)$	(3)
Momentum bal. (adsorption section)	$-\frac{\partial P}{\partial z}=(1-\varepsilon_c-\xi)a(\rho_p-\rho_g)$	(4)
Momentum bal. (other sections)	$-\frac{\partial P}{\partial z}=\frac{150\mu(1-\varepsilon_c)^2}{\varepsilon_c^3d_p^2}u+\frac{1.75(1-\varepsilon_c)\rho_g}{\varepsilon_c^3d_p}\lvert u\rvert u$	(5)
Energy balance in gas phase	$\varepsilon_cC_T\widehat{c}_v\frac{\partial T}{\partial t}+uC_T\widehat{c}_p\frac{\partial T}{\partial z}=\frac{\partial}{\partial z}\left(\lambda_g\frac{\partial T}{\partial z}\right)+\varepsilon_cRT\sum_i\frac{\partial C_i}{\partial t}-(1-\varepsilon_c-\xi)\,a'h_{gs}(T-T_s)-\alpha_{gt}h_{gw}(T-T_w)$	(6)
Energy balance in solid phase	$[(1-\varepsilon_c-\xi)\rho_pc_{p,s}+\xi\rho_{pk}c_{p,pk}]\left(\frac{\partial T_s}{\partial t}+v_s\frac{\partial T_s}{\partial z}\right)=(1-\varepsilon_c-\xi)\varepsilon_pRT_s\sum_i\left[\frac{\partial C_{p,i}}{\partial t}+v_s\frac{\partial C_{p,i}}{\partial z}\right]++\xi\frac{\partial}{\partial z}\left(\lambda_{pk}\frac{\partial T_s}{\partial z}\right)+(1-\varepsilon_c-\xi)a'h_{gs}(T-T_s)+(1-\varepsilon_c-\xi)\rho_p\sum_i\left(-\Delta H_i\left[\frac{\partial q_i}{\partial t}+v_s\frac{\partial q_i}{\partial z}\right]\right)$	(7)
Energy balance in the HX-wall	$\rho_wc_{p,w}\frac{\partial T_w}{\partial t}=\alpha_{w,ext}h_{gw}(T-T_w)-\alpha_{w,int}h_{fw}(T_w-T_f)$	(8)
Energy balance in the HX-fluid	$\rho_fc_{p,f}\frac{\partial T_f}{\partial t}=-u_f\rho_fc_{p,f}\frac{L_z}{L_x}\frac{\partial T_f}{\partial z}-\alpha_{w,in}h_{fw}(T_f-T_w)$	(9)
Adsorption equilibrium	$P_i=\frac{q_i^*}{K_i}\exp[\sum_{j=1}^N A_{ij}q_j^*+\sum_{j=1}^N\sum_{k=1}^N B_{ijk}q_j^*q_k^*]$	(10)
	$A_{ij}=\frac{A_i+A_j}{2};\ B_{ijk}=\frac{B_i+B_j+B_k}{3}$	(11)

assumptions are the same for each section. These include negligible gradients in the radial direction, constant cross-sectional area, constant sorbent velocity, uniform and constant void fraction, and ideal gas behaviour in the bulk phase. The mass transfer rate from the bulk gas to the adsorbent pores and from the pores to the adsorbed phase is modelled using linear driving force (LDF) approximations. With regards to the energy balances, the gas in the pores is assumed to be in thermal equilibrium with the adsorbent temperature, while the convective heat transfer between the bulk gas and the adsorbent is modelled with a heat transfer coefficient estimated with a common Nusselt correlation for flow around a sphere. In addition to the energy balance of the gas phase and the solid phase, two equations are included to describe the temperature of the heating/cooling fluid and the temperature of heat exchanger wall, respectively. This only applies to the sections that are operated as heat exchangers (preheating, desorption, precooling and cooling). The equation of the heat exchanger wall was derived by assuming that the thermal conduction resistance of the heat exchanger walls is negligible, while taking into account the effect of their thermal capacity. This approach is based on the consideration that the limiting thermal resistance of the system is found in the sorbent-gas side of the heat exchangers. The convection from the heating/cooling fluid to the wall is modelled with a constant heat transfer coefficient, representative of water flowing in tubes (5000 W/(m^2K)). Lastly, the convection from the wall to the gas is also modelled with a heat transfer coefficient. A value of 150 W/(m^2K) is assumed in this case.

2.4. Bead-shaped activated carbon adsorbent

The adsorbent material considered in the present study is a commercial bead-shaped activated carbon (BAC) supplied by Kurhea (Japan). It is well-suited for moving bed applications due to its particle size (0.7 mm average particle diameter) and highly spherical shape, which gives good flow properties. To provide necessary data for the MBTSA model, the adsorbent was characterized in terms of adsorption equilibrium by measuring pure component isotherms of CO_2 and N_2 at different temperatures between 10 and 150 °C. Prior the measurements the sample was pre-treated by applying vacuum for 10 h at a temperature of 150 °C. The collected data are shown in Fig. 2. As expected, the adsorbent presents higher affinity towards CO_2 compared to that of N_2, i.e., for a given temperature the adsorption capacity for CO_2 is higher than that of N_2 in the whole pressure range. However, at relevant temperature and pressure conditions, i.e., 25 °C, partial pressure of 15 kPa for CO_2, 85 kPa for N_2, the adsorption selectivity is relatively low due to the limited amount of CO_2 adsorbed (only about 0.5 mol/kg), and the significant amount of N_2 adsorbed (almost half of that of CO_2).

As shown in Fig. 3, the set of experimental data were fitted with a Virial isotherm model, of which parameters were then used as input to the gPROMS program.

The Virial model for pure component isotherms is given by:

$$P_i = \frac{q_i^*}{K_i}\exp\left(A_i q_i^* + B_i q_i^{*2}\right) \tag{12}$$

where P is the pressure, q is the amount of gas adsorbed, and K is the Henry constant. The latter was calculated with the Van't Hoff equation

$$K_i = K_i^{\infty}\left(\frac{-\Delta H_i}{RT_s}\right) \tag{13}$$

while the temperature dependence of the Virial coefficients A and B was expressed by

$$A_i = A_{0,i} + \frac{A_{1,i}}{T_s},\ B_i = B_{0,i} + \frac{B_{1,i}}{T_s}. \tag{14}$$

Fitting of the pure component adsorption data was carried out taking the data at all temperatures simultaneously. The resulting model parameters are listed in Table 3. The pure component parameters were used to simulate the multi-component separation by using the Virial model extension for multi-component gas mixtures.

2.5. Design and nominal performance

In Table 4, the design of the MBTSA system as well as the nominal operating conditions in the different sections are summarized. In the design, a cooling water inlet temperature of 10 °C and a heating fluid inlet temperature to the desorption section of 203 °C were assumed. The latter corresponds to a saturated steam pressure of around 16.5 bar. In Table 5, the overall process performance and additional operating conditions are given. Due to the somewhat low adsorption capacity of the adsorbent, a high amount of material (730 kg/s) was required to process the flue gas while capturing a large share of the incoming CO_2. In addition, the process was operated using a quite high regeneration temperature (above 180 °C), and a certain degree of vacuum (80 kPa) to extract the CO_2. The system delivers CO_2 with a purity of 95.4% with a CO_2 recovery rate of 81.7%. The CO_2 recovery is defined as:

$$\eta_{CO_2} = \frac{\dot{m}_{CO_2,out}}{\dot{m}_{CO_2,in}}. \tag{15}$$

Table 3
Virial isotherm model parameters for CO_2 and N_2 on the BAC adsorbent.

	K^{∞} x 10^6 mol/(kg kPa)	− ΔH kJ/mol	A_0 kg/mol	A_1 kg K/mol	B_0 (kg/mol)^2	B_1 kg^{2}K/mol^2
CO_2	1.8510	25.241	−0.294	243.088	0.035	−29.710
N_2	3.3827	17.185	−3.7245	1198.9	0	0

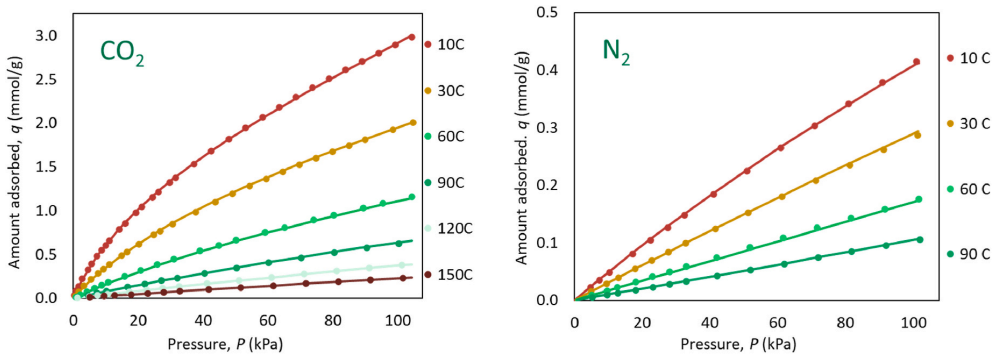

Fig. 3. Adsorption isotherms of CO_2 and N_2: measured data (dots) and Virial model fitting (continuous lines).

Table 4
Design parameters and nominal operating conditions in sections of the MBTSA.

		Adsorption	Preheating	Desorption	Precooling	Cooling
Section height	m	1.6	1.4	2.1	1.4	2.5
Section footprint (horizontal cross-sec.)	m^2	113	55	55	55	55
Sorbent residence time	s	33.6	30.3	45.5	30.3	54.2
Heating/cooling fluid inlet temperature	°C	–	149	203	64	10
Heating/cooling fluid outlet temperature	°C	–	64	135	149	75
Sorbent inlet temperature	°C	–	53	109	184	101
Sorbent outlet temperature	°C	–	109	184	101	24

Table 5
Overall process performance and main operating conditions.

Amount of circulating sorbent	730	kg/s
Sorbent regeneration temperature	184	°C
CO_2 extraction pressure	80	kPa
CO_2 purity	95.4	%
CO_2 recovery	81.7	%
CO_2 captured	10.2	kg/s
External heat duty (sorbent regeneration)	56.8	MW
Fraction of total heat recovered by inner loop	49.1	%
External cooling duty	53.8	MW_{th}
Specific heat duty	5.56	MJ_{th}/kg CO_2

Where $\dot{m}_{CO_2,in}$ is the mass flow of CO_2 entering the system via the flue gas feed and $\dot{m}_{CO_2,out}$ is the mass flow of CO_2 in the CO_2-rich stream leaving the desorption section.

3. Process control

In the MBTSA process considered in this work, there are five degrees of freedom that can be used as manipulated variables for process control. As shown in Fig. 1, these are the sorbent flow rate, flow rates of each of the three heat exchanger fluids (external heat, internal heat recovery loop and cooling water) and the flow rate of CO_2-lean gas used as purge in the cooling/precooling sections. Within the MBTSA model, the flow rates of the heat exchanger fluids are represented by their velocities.

3.1. Open-loop step responses

In order to choose CV-MV pairings and carry out controller tuning, it is necessary to investigate the open-loop behavior of the system. The control system was divided into a regulatory and a higher level. Simulations were performed by inactivating the higher-level controllers and introducing step changes in the main disturbance (flue gas feed flow) and manipulated variables. The regulatory layer remained active to ensure process stability. Due to the nonlinearity of the moving bed adsorption system, step changes of the same magnitude in opposite directions do not give opposite dynamic responses.

In Fig. 4, the response of CO_2 purity and recovery to a positive and negative 10% step in flue gas feed flow is shown. A reduction in the flue gas flow rate increases the sorbent to gas ratio in the adsorption section. As shown in the isotherms in Section 2.4, the activated carbon adsorbent is selective to CO_2 but also has considerable affinity for N_2. When the sorbent to gas ratio increases, an increase in the loading of N_2 and decrease in loading of CO_2 on the sorbent particles leaving the adsorption section is observed. The relative loading of CO_2 and N_2 on the sorbent influences the purity of the CO_2-rich gas leaving the desorption section. Therefore, a negative step change in the flue gas flow rate leads to a reduction in the CO_2 purity. The initial increase in the CO_2 recovery is caused by the sudden reduction of the denominator in Eq. (15). After approximately one cycle of the moving bed (3.2 min), the CO_2 recovery has stabilized at a 0.3% higher value than before the step change. This is due to the decrease in CO_2 loading on the particles leaving the adsorption section, which balances out the reduction in flue gas flow rate, thus ultimately leading to an almost unchanged CO_2 recovery.

When increasing the flue gas flow rate, the CO_2 recovery decreases due to a partial breakthrough of the moving bed. This means that at the bottom part of the adsorption section, the sorbent particles are saturated, and more CO_2 will pass through the column without being adsorbed. Since the relative loading of the adsorbed species is not significantly affected by the breakthrough, the CO_2 purity remains almost constant. The small change in purity can be explained by minor variations in adsorption section sorbent inlet temperature due to regulatory control and a slight decrease in inlet CO_2 concentration to the adsorption section caused by more flue gas being added relative to the recycled stream from the precooling section.

In Fig. 5, the open-loop responses of CO_2 purity to step changes in HX fluid velocity in the desorption section and CO_2 recovery to step changes in the sorbent flow rate are shown. Increasing or reducing the amount of heat supplied to the desorption section by 10% leads to a change in desorption section outlet sorbent temperature of ±3 °C. A higher desorption temperature leads to lower CO_2 loading on the sorbent entering the adsorption section, which will lead to a higher CO_2/N_2 ratio on the particles leaving this section. This will increase the CO_2 purity.

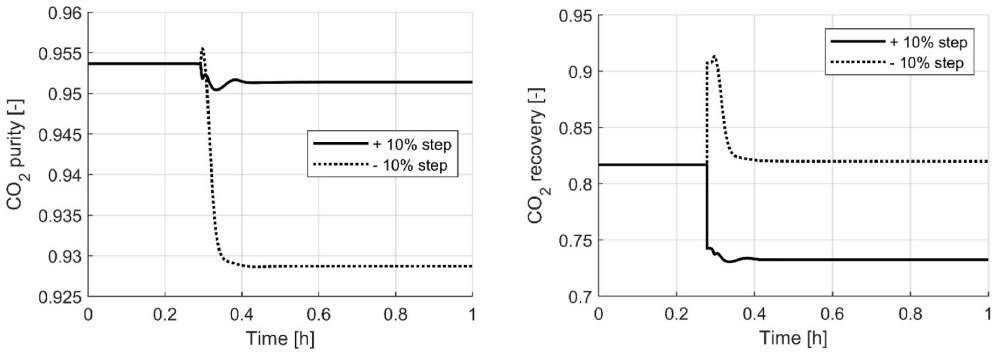

Fig. 4. Open-loop response of CO_2 purity (left) and recovery (right) to a positive and negative 10% step in flue gas flow.

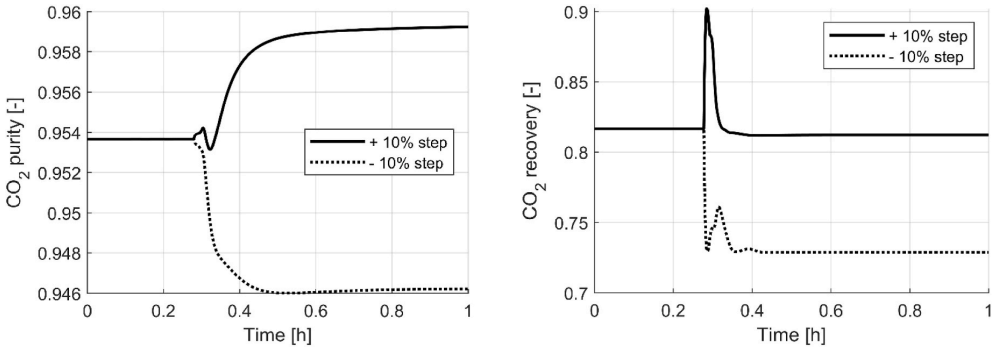

Fig. 5. Open-loop response of CO_2 purity (left) to a positive and negative 10% step in HX fluid velocity in the desorption section and open-loop response of CO_2 recovery (right) to a positive and negative 10% step in sorbent flow rate.

Reducing the HX fluid velocity has the opposite effect on the purity.

The effect of increasing the sorbent flow rate on CO_2 recovery is similar to the trend seen in Fig. 4 for a reduction in flue gas flow. After an initial increase, the system settles at a similar recovery rate as before the step change. In the adsorption section, an increase in sorbent inlet CO_2 loading and decrease in outlet CO_2 loading is observed, meaning that the working capacity of the adsorbent is reduced. The increase in inlet sorbent loading is caused by a reduction of the desorption temperature, since the heating of the desorption section remains unchanged. Reducing the sorbent flow rate leads to a partial breakthrough of the moving bed, leading to more CO_2 passing through the top of the adsorption section. This gives a reduction in CO_2 recovery of slightly below 9%.

3.2. Control combinations

The variable pairings were chosen based on heuristics and CV-MV step responses. Pairings for the regulatory layer, which in this case consists of three controllers, were chosen first. For the internal heat recovery loop, the velocity of working fluid was adjusted to maintain a constant ratio with the sorbent flow rate, to keep the fraction of heating/cooling delivered by the internal loop constant throughout operation. The temperature of the sorbent leaving the cooling section was controlled by adjusting the velocity of the cooling water flow. Finally, purge gas flow was adjusted to control the gas velocity at the top of the precooling section and prevent flow reversal. This phenomenon can occur as the adsorbent cools down and the CO_2 that is present in the pores is re-adsorbed, causing a local pressure reduction. Another phenomenon that should be avoided in the moving bed system is the fluidization of adsorbent particles. However, due to the large sorbent flow rates and particle size considered in this work, this is not expected to be an issue and fluidization has not been included in the regulatory control layer.

The regulatory layer leaves two degrees of freedom to be used for higher-level control. In this work, the CO_2 purity and recovery were chosen as control variables in this layer. The open-loop simulations in Section 3.1 show that varying the velocity of heating fluid to the desorption section influences the CO_2 purity and varying the sorbent flow rate affects the CO_2 recovery. These combinations were therefore chosen as CV-MV pairings in the higher-level control layer. As described in Section 1.2, this pairing follows the most common approach for control of post-combustion CO_2 capture processes.

Four control combinations are considered, namely Cases A, B, C and D. In Case A, PI-control is used for both higher-level control variables. The controllers were implemented using the PID controller block available in gPROMS ModelBuilder. The calculated value of the manipulated variable, u_{calc}, is given by the following equation:

$$u_{calc} = K_c(P + I)(u_{max} - u_{min}) + B \tag{16}$$

Where B is the controller bias, P is the contribution from the proportional term, I is the contribution from the integral term, u_{max} is the maximum allowable value of the manipulated variable and u_{min} is the minimum allowable value of the manipulated variable. The controller error, e, is defined as:

$$e = \frac{y_{SP} - y}{y_{max} - y_{min}} \tag{17}$$

Where y is the value of the controlled variable, and SP, max and min represent its setpoint, maximum and minimum allowable value. The proportional and integral terms are calculated based on the error:

$$P = e \tag{18}$$

$$\tau_I \frac{dI}{dt} = e \tag{19}$$

The MBTSA process is a cyclic process, meaning that there is significant delay between a control action is taken and its effect on the higher-level variables is seen. Such delays have a negative impact on the performance of feedback controllers. By adjusting the manipulated variables directly based on the disturbances, i.e. using feedforward control, this delay can be avoided. In this work, two feedforward control cases based on ratio control were investigated. The equation for such a controller is:

$$u_{calc} = \left(\frac{u}{d}\right)_{SP} d \tag{20}$$

Where d is the disturbance. In Case B, the sorbent flowrate is manipulated to maintain a given ratio between the sorbent flow rate and feed flue gas flow rate. The control of CO_2 purity is equal to Case A. Since a ratio controller has no feedback loop to gradually reduce the offset between the controlled variable and the setpoint, it is important to determine a correct ratio to avoid large steady-state offsets. It is likely that the optimal ratio will vary with operation. Steady-state simulations maintaining the desired purity and recovery at various loads were carried out to study the behavior of the ratio at off-design. The results are given in Fig. 6, and a linear trendline was used to adjust the ratio for the sorbent flow rate controller with the load.

In Case C, feedback control is given up entirely, and both higher-level controllers are ratio controllers. Since the sorbent flow rate is scaled adaptively based on the disturbance, a fixed ratio is used in the second controller, which adjusts the velocity of heating fluid to the desorption section based on the sorbent flow rate.

In Case D, we investigate a cascade controller for control of CO_2 purity. For CO_2 recovery, the same PI-controller as in Case A is used. A

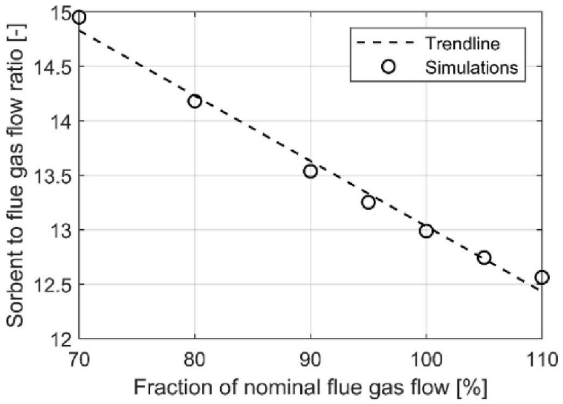

Fig. 6. Sorbent to flue gas feed flow ratio vs. fraction of nominal flue gas flow.

cascade control configuration makes use of an additional, fast measurement which is related to the controlled variable (in this case the sorbent temperature leaving the desorption section) with the aim of achieving faster control. An outer loop compares the CO_2 purity to the higher-level setpoint. Instead of adjusting the manipulated variable directly (as in Case A), the outer loop controller provides the setpoint to the inner loop, which adjusts the hot fluid velocity to the desorption section to control the outlet sorbent temperature. This configuration is shown in Fig. 7. The closed-loop time constant of the inner loop should be significantly smaller than the outer loop to avoid conflict between the two controllers. In this case the closed-loop time constant ratio of the two controllers is around 11.

The investigated control combinations with tuning parameters and setpoints are given in Table 6.

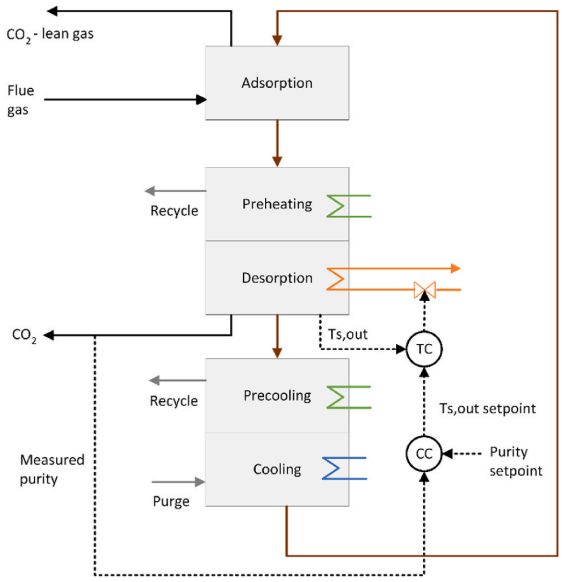

Fig. 7. CO_2 purity cascade control configuration studied in Case D. Dotted lines are signals, TC stands for temperature controller and CC stands for composition controller.

3.3. Tuning of PI-controllers

The tuning of the PI-controllers was based on the simplified internal model control (SIMC) rules developed by Skogestad [39]. For a PI-controller, a first-order transfer function between the MV and CV with effective delay is needed for the tuning:

$$g(s) = \frac{ke^{-\theta s}}{\tau s + 1} \tag{21}$$

Where k is the gain, θ is the effective delay and τ is the time constant of the transfer function $g(s)$ in the Laplace domain. The SIMC-rules give the controller gain K_c and the integral time constant τ_I using information from the transfer function and the adjustable closed-loop time constant τ_c:

$$K_c = \frac{1}{k}\frac{\tau}{\tau_c + \theta} \tag{22}$$

$$\tau_I = \min\lfloor \tau, 4(\tau_c + \theta)\rfloor. \tag{23}$$

Two different methods were used to obtain the transfer function. For simple responses that follow first-order behavior, the values were obtained graphically by inspection of the open-loop step response. The gain was taken as the difference between the initial and final value of the CV. The delay θ was taken as the time it took after the step in the MV before a continuous evolution of the CV in the same direction as the gain was observed. This means that any inverse responses are included in the effective delay. The time constant τ was taken as the time it took for the CV to reach 63% of its final value. When the open loop step response did not exhibit first-order behavior, the setpoint overshoot method using P-control [40] was applied. An example of the type of response used for tuning with this method is shown graphically in Fig. 8.

3.4. Controller testing and performance evaluation

Three types of simulations were performed to test the control combinations.

1) A positive 10% step change in flue gas feed flow from the nominal value
2) Linear ramps from 100 to 80 to 100% of nominal flue gas feed flow with slopes of 4% of nominal load per minute
3) Controller setpoint changes (for feedback controllers only)

The controller performance was quantified by the steady state offset relative to the setpoint and the 99% settling time, defined as the time it takes for the controlled variable to reach and stay within ±1% of the final steady-state value [23]. In all simulations, the time domain resolution was 5 s.

4. Results and discussion

4.1. Step on flue gas feed

In Fig. 9, the closed-loop responses of CO_2 purity and recovery as well as their corresponding manipulated variables to a +10% step on flue gas feed flow rate introduced at t = 0 are shown. An initial decrease in the CO_2 recovery rate is observed, since a larger fraction of the incoming CO_2 will leave at the top of the adsorption section before the sorbent flow rate is increased by the controller. The purity of the captured CO_2 is determined by the relative amounts of adsorbed CO_2 and N_2 on the adsorbent at the bottom of the desorption section, which is influenced by the adsorbent loadings out of the adsorption section and the heat provided to the preheating and desorption sections. The increased flue gas feed flow rate leads to a lower CO_2/N_2 ratio on the adsorbent, which gives the initial decrease in CO_2 purity.

Table 6
Summary of investigated cases for higher-level control and regulatory controllers with tuning parameters and setpoints.

Case	Description	CV	MV	τ_c (s)	K_c	τ_I (s)	Setpoint
A	PI control of both CO_2 purity and recovery (base case)	CO_2 purity	u_f desorption section	205	13.8	227	0.95
		CO_2 recovery	Sorbent flow	3.12	2.00	4.83	0.82
B	Ratio control of sorbent flowrate	CO_2 purity	u_f desorption section	205	13.8	227	0.95
		Sorbent/flue gas feed flow ratio	Sorbent flow	–	–	–	Adaptive
C	Ratio control of sorbent flowrate and hot fluid to desorption section	u_f/sorbent flow ratio desorption section	u_f desorption section	–	–	–	0.0023
		Sorbent/flue gas feed flow ratio	Sorbent flow	–	–	–	Adaptive
D	PI with cascade control of CO_2 purity	CO_2 purity (outer loop)	Setpoint for T_s, out desorption section	205	13.8	227	0.95
		T_s, out desorption section (inner loop)	u_f desorption section	18.5	0.34	74	From outer loop
		CO_2 recovery	Sorbent flow	3.12	2.00	4.83	0.82
	Regulatory control of cooling section sorbent outlet temperature	T_s, out cooling section	u_f cooling section	15.4	−0.57	62	298 K
	Regulatory control of internal heat recovery loop	u_f/sorbent flow ratio in precooling and preheating sections	u_f internal heat recovery loop	–	–	–	0.0015
	Regulatory control of gas outlet velocity in pre-cooling section	u_{out} precooling section	Purge gas flowrate	2.2	13.6	2.2	0.078 m/s

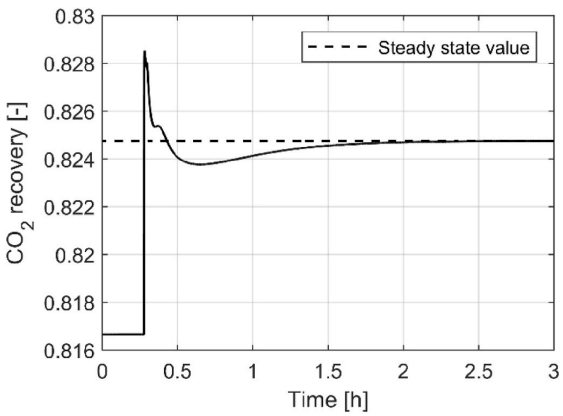

Fig. 8. Response of P-controlled CO_2 recovery with sorbent flow as MV to setpoint step from 0.82 to 0.83.

For purity control, Case C shows the quickest response, followed by Case A and B. The cascade controller in Case D reaches the desired setpoint but is not able to give a faster purity response than the standard PI configuration. The pure ratio control scheme in Case C is not able to precisely meet either the purity or recovery setpoint, but the final values are not far from the PI-controller setpoints. The sorbent flow ratio controller from Case B gives an absolute deviation of around 1% compared to the recovery setpoint. The overall best performance to the flue gas feed flow step change is achieved by Case A.

4.2. Flue gas flow ramps

The flue gas feed flow rate profile used in the simulations is showed in Fig. 10. The flow rate is first changed from 100 to 80% of nominal flow with a slope of 4% nominal flow per minute, before it is kept constant for several hours. After the controllers have stabilized, it is increased from 80 to 100% of nominal flow, keeping the same slope as for the ramp-down.

In Fig. 11, the response of both CVs and MVs in Case A-D from the ramp simulations are shown. The PI regulatory controllers are also included. Due to differences in the initialization of the model, the ratio control cases (Case B and C) start from slightly different values than Case A and D. This is, however, not expected to significantly influence the results. The reduction in flue gas flow rate leads to an increase of the CO_2 purity. As explained in section 4.1, the purity is governed by the ratio between adsorbed CO_2 and N_2 on the particles leaving the desorption section. Since the purity initially is higher than the setpoint, the heat supply to the desorption section is reduced. The adsorbed CO_2/N_2 ratio also depends on the temperature of the sorbent entering the adsorption section. Since the process is cyclic, this is equivalent to the temperature at the bottom outlet of the cooling section, which is controlled in the regulatory layer. For the negative flue gas flow ramp, this temperature is initially lower than the setpoint, and the flow of coolant in the cooling section is therefore reduced. The CO_2 recovery rate increases significantly when the flue gas feed flow is reduced, due to the sudden increase in solid to gas ratio in the adsorption section. The sorbent flow rate decreases by approximately 100 kg/s in order to bring the recovery rate to its setpoint. There is no delay between a change in the purge gas flow rate and the gas velocity in the pre-cooling section, which leads to only small variations in the value of this variable during the simulations. For all variables, the observed trends for the positive flue gas feed ramp are opposite of those described above for the negative ramp.

Regarding the controller performance, it is firstly seen that the regulatory control of both desorption section sorbent outlet temperature and precooling outlet gas velocity quickly stabilizes at the setpoint for both positive and negative ramps. The cascade controller in Case D generally uses a wider range of the manipulated variables than the other controllers but does not give improved performance. The response of sorbent temperature in Case A oscillates in the initial part of the response. Similar behavior is seen in the CO_2 purity profile, where the response in Case A oscillates initially. The use of ratio control (Case B) for sorbent flow rate shows no oscillations. As for the flue gas step, the purity controller in Case D exhibits the slowest response. The ratio controllers in Case C give a significantly larger steady-state offset for the ramp-down than the ramp-up case. In the latter case they are able to reach the setpoints for purity and recovery with similar accuracy as the feedback controllers. It is expected that the offsets of Case C could be significantly reduced by using an adaptive ratio also for the purity controller and by considering more accurate regression profiles than the linear trendline shown in Fig. 6. This would make it a more attractive option.

In the ramp simulations, Case A and B show the overall best performance. The oscillations seen in Case A could be caused by the PI controller tuning, which was carried out based on a positive step change from the nominal point. Since the behavior of the MBTSA process varies with load, these tunings might be too aggressive for the system at 80%,

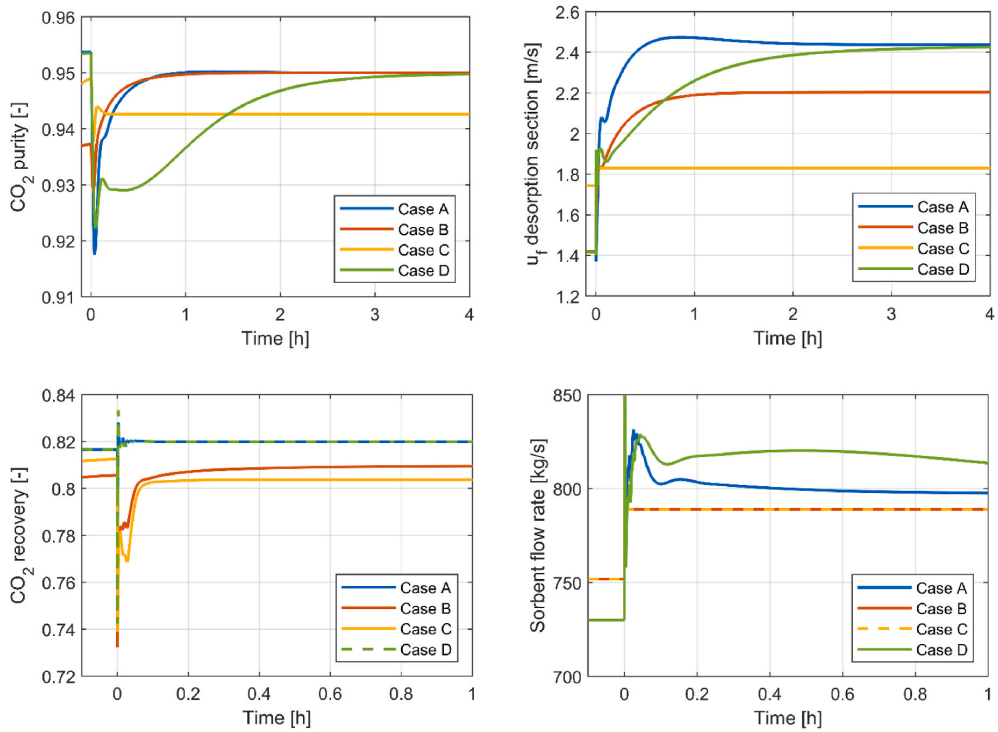

Fig. 9. Response of higher-level CVs (left) and MVs (right) to a 10% step on flue gas feed flow at t = 0.

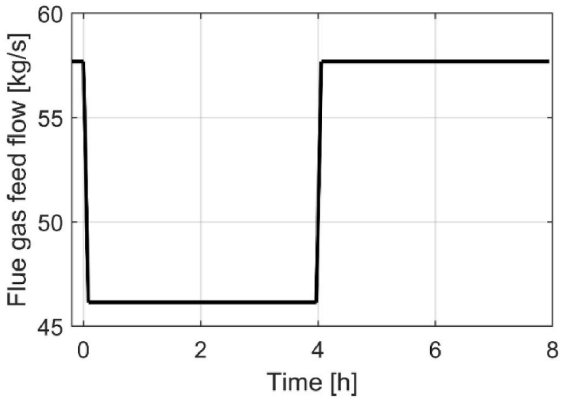

Fig. 10. Flue gas feed flow profile from the 100-80-100% ramp simulations.

giving an oscillatory response. For operation at loads below 80%, adaptive controller tuning might be necessary.

A simulation with one third of the original purity controller gain (K_c = 4.6) for Case A was carried out to demonstrate the effect of reduced gain on the oscillations. The results are shown in Fig. 12. It is seen that reducing the controller gain removes most of the oscillations but leads to larger over- and undershoot and slower regulation speed, especially for the ramp-up scenario. However, the purity control with reduced gain is still faster than Case D.

4.3. Step on controller setpoints

In Figs. 13 and 14, the higher-level controlled and manipulated variable responses to setpoint changes for purity (from 0.95 to 0.96) and recovery (from 0.82 to 0.83) introduced at t = 0 are shown. Only the PI-controllers are included in these graphs since the ratio controllers do not use the value of higher-level control variables as a setpoint. Case A shows the most efficient response to the purity setpoint change, followed by case B. The cascade controller in case D is not able to reach the new setpoint of 0.96 within the period of approximately 4 h used in the simulation, and in addition shows larger variations in sorbent flow rate than the standard PI-controller. Case A and D show similar responses to the recovery setpoint change, quickly adjusting to the new setpoint. These two cases have the same PI-controller for recovery control, and the similar response is therefore expected. The ratio used in the recovery controller of case B is not adaptively adjusted in the case of a purity setpoint change, since the flue gas feed flow remains constant. It is therefore not able to keep the recovery at the desired value of 0.82.

4.4. Summary of performance

In Table 7 and Table 8, the 99% settling time and steady state offset are given for the different cases for purity and recovery, respectively. For the flue gas flow step change, the settling time for CO_2 recovery is significantly shorter than for CO_2 purity in all cases except for the ratio control in Case C. Purity control is also significantly slower in the ramp simulations for Case A and D, which use PI control for the CO_2 recovery. The results show that ratio control can give around 10 times quicker purity control response and could therefore be a relevant option if response times are critical. The 99% settling time is in the order of minutes in all considered cases, apart from Case D. For this cascade

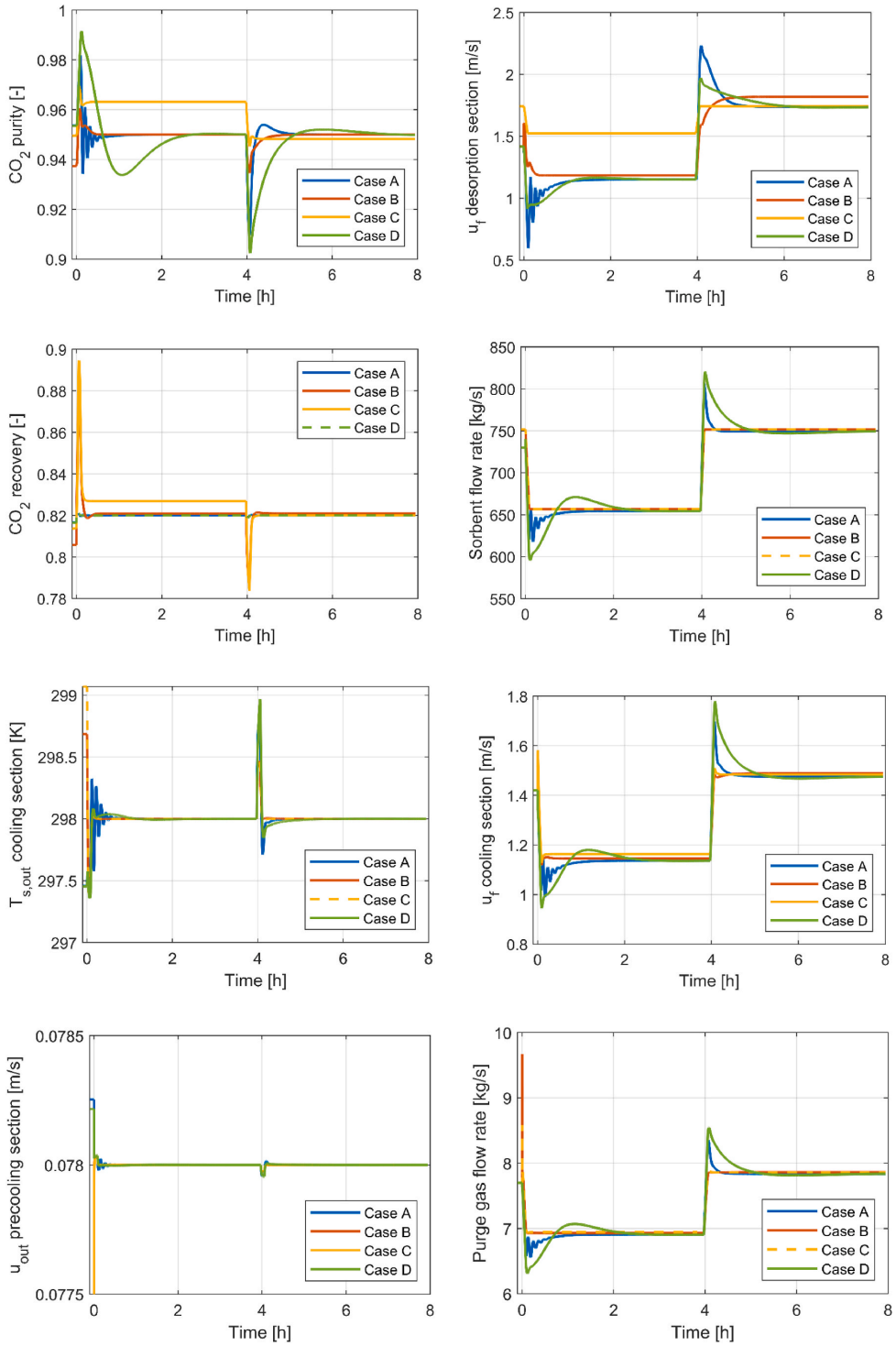

Fig. 11. Response of CVs (left) and MVs (right) to 100-80-100% flue gas feed flow ramps starting at t = 0.

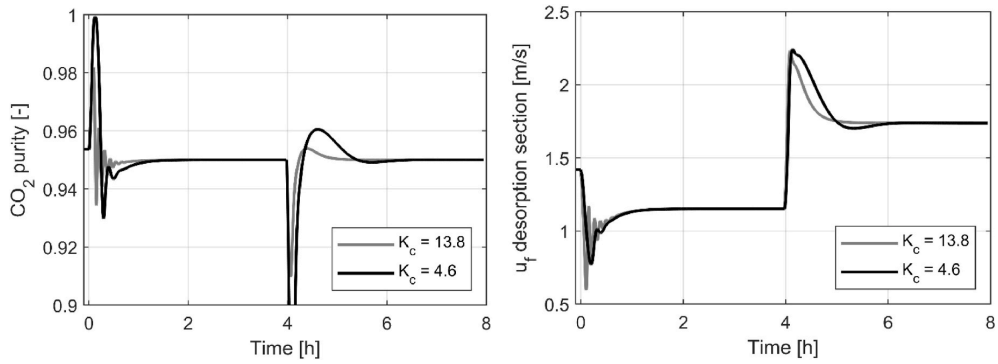

Fig. 12. Case A response of CO_2 purity and corresponding MV to 100-80-100% flue gas feed flow ramps starting at t = 0 with original (K_c = 13.8, grey line) and reduced (Kc = 4.6, black line) purity controller gain.

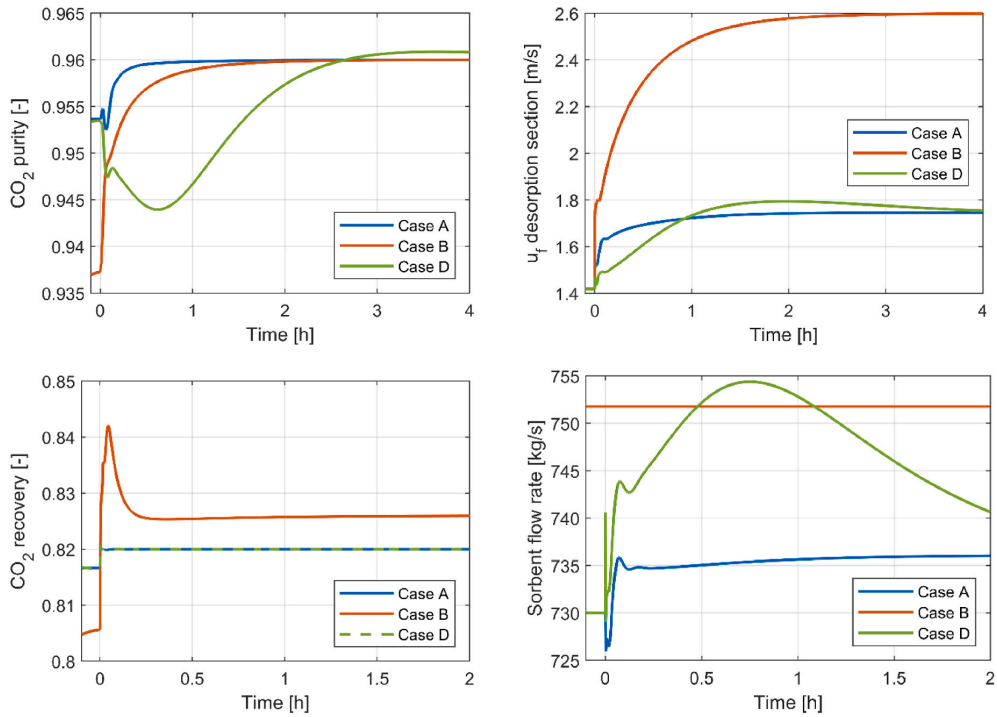

Fig. 13. Response of higher-level CVs (left) and MVs (right) to purity setpoint change from 0.95 to 0.96 at t = 0.

controller, the purity takes between 37 and 96 min to settle. In general, the controllers keep the controlled variables relatively close to the setpoints. The largest steady state offset is 1.98% on CO_2 recovery from Case C in the flue gas step simulation.

CO_2 recovery settling times for solvent-based post-combustion CO_2 capture processes with similar control structures as in this work have been reported in many studies. Some values from the literature are mentioned below to put the results from this work into context. Montanes et al. reported 99.9% settling times between 45 and 400 min for a gas turbine ramp of 100–75-100% [23]. Gardardsdottir et al. observed 99% settling times around 100 min for 90-70-90% ramps on a coal-fired power plant [13]. Graphical estimation based on the results from Lin et al. shows a settling time of around 1 h for a 10% increase in flue gas flow rate [18]. In the work of Nittaya et al. [20], settling times from 7.5 to over 10 h for a 10% increase in flue gas flow rate were reported. The variations in settling times between studies are large, due to e.g. differences in system scales, modelling approach, underlying assumptions, ways of calculating settling time and scenarios used for controller testing. The settling times for CO_2 recovery found in this work are significantly shorter than values from the literature, indicating that the MBTSA process can be controlled efficiently. However, due to the reasons above, the values are not directly comparable, and a conclusion should not be made solely based on this work.

In this work, it has been assumed that all variables are available for

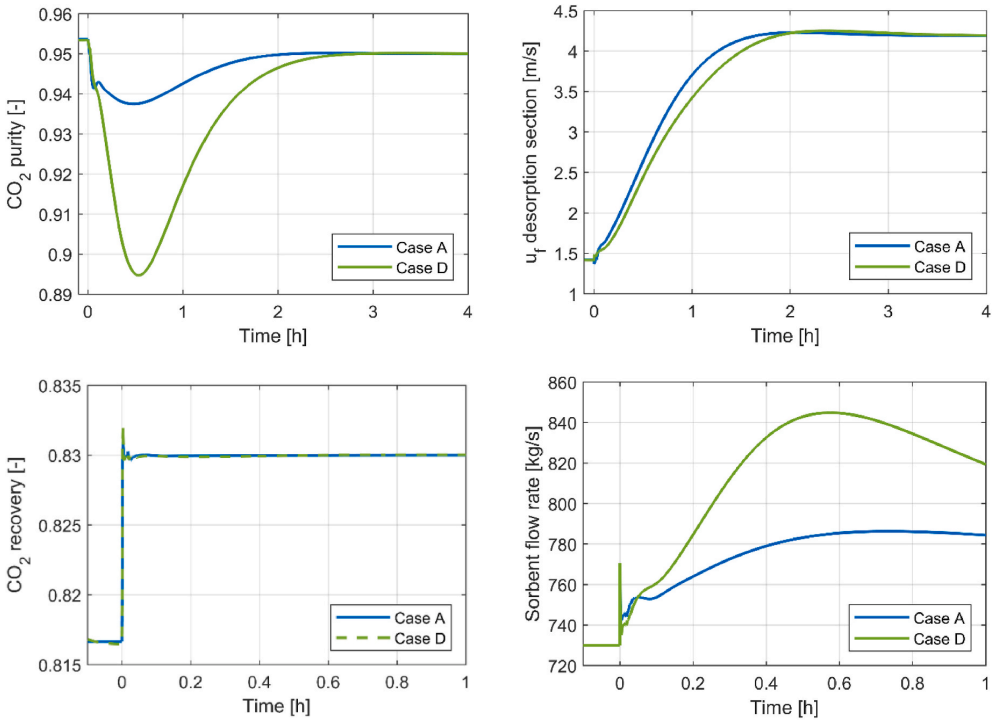

Fig. 14. Response of higher-level CVs (left) and MVs (right) to recovery setpoint from 0.82 to 0.83 at t = 0.

Table 7
CO_2 purity settling time and steady state offset for step change and ramps of flue gas feed flow. In cases with no reported settling time, the controlled variable did not move outside the ±1% range of the final value.

	+10% step on flue gas flow		Linear ramp 100-80%		Linear ramp 80–100%	
	99% settling time [min]	Steady-state offset (%)	99% settling time [min]	Steady-state offset (%)	99% settling time [min]	Steady-state offset (%)
Case A	11.3	0.00	12.8	0.00	10.3	0.00
Case B	6.00	0.00	5.42	0.00	7.50	0.00
Case C	–	0.78	1.33	1.38	1.58	0.18
Case D	75.3	0.02	95.5	0.01	37.1	0.01

Table 8
CO_2 recovery settling time and steady state offset for step change and ramps of flue gas feed flow. In cases with no reported settling time, the controlled variable did not move outside the ±1% range of the final value.

	+10% step on flue gas flow		Linear ramp 100-80%		Linear ramp 80–100%	
	99% settling time [min]	Steady-state offset (%)	99% settling time [min]	Steady-state offset (%)	99% settling time [min]	Steady-state offset (%)
Case A	0.17	0.00	–	0.00	–	0
Case B	3.42	1.26	8.00	0.12	7.50	0.12
Case C	2.67	1.98	7.42	0.85	7.58	0.01
Case D	0.25	0.00	–	0.00	–	0.00

measurement and that the measurements are without error and delay. In addition, no valve dynamics are considered when adjusting the manipulated variables. It is expected that this idealized approach will somewhat overestimate the performance of the controllers investigated. However, the model used in this work does consider important delays such as the transience of heating the walls of the different sections in the process, heating of gas and adsorbent and the cycling time of the adsorbent through the system. Another limitation of the proposed method is the fixed tuning parameters for the feedback controllers. In a practical application, the plant characteristics could change over time due to e.g. fouling, corrosion and particle degradation. In such cases, the controller tuning should be updated on-line.

5. Conclusions

In this work, four decentralized control strategies were investigated for an activated carbon-based MBTSA process designed to capture CO_2 from a coal-fired power plant. Through dynamic simulations with a composite model built in gPROMS, the closed-loop behavior of the control combinations was studied based on a step change and ramps of flue gas feed flow as well as controller setpoint changes.

The control system was divided into a regulatory and higher-level layer. The regulatory layer controls the internal heat recovery loop, sorbent outlet temperature of desorption section and outlet gas velocity of precooling section. It demonstrated fast response to both positive and negative ramps in flue gas feed flow and was able to keep the control

variables at their specified setpoint.

For the higher-level control layer, the standard PI configuration (Case A) generally showed the best response for both feed flow disturbances and setpoint changes. In this configuration, the CO_2 purity was controlled by the velocity of hot fluid to the desorption section and the sorbent flow rate was used to control the CO_2 recovery. The cascade controller (Case D) investigated for control of CO_2 purity was not able to give a faster purity response than the standard PI-configuration, and in addition showed wider input usage than the other controllers.

The two control configurations involving ratio control (Case B and C) in general gave larger steady-state offsets than the feedback controllers. However, in the case of ramp-up from 80 to 100% of nominal flue gas feed flow rate, these configurations yielded steady-state offsets in the same range as the PI-controllers. It is expected that the offset for other scenarios can be reduced by including an adaptive ratio also for purity control and by considering more accurate regression profiles. Due to their short stabilization time, ratio controllers might therefore be a viable control option for the MBTSA system.

In general, the settling time for CO_2 purity was longer than for CO_2 recovery. The 99% settling time for purity varied from 0 to 13 min in Cases A-C. Significantly slower responses were seen in Case D, with settling times for CO_2 purity ranging from 37 to 96 min approximately. For CO_2 recovery, the settling time varied from 0 to 8 min. The simulations show that using ratio controllers can give around 10 times quicker purity response compared to PI-control. All investigated control configurations were able to keep the controlled variables relatively close to the setpoints. The largest steady-state setpoint offset was 2.0%.

For ramp-down of flue gas feed flow from 100 to 80% of the nominal value, an oscillatory response was observed for Case A. This indicates that the controller tuning, which was based on +10% step responses from the nominal point, might not be suitable for lower loads. In this operation regime, adaptive PI-controller tunings might be necessary to avoid oscillations. This should be investigated in future work. In addition, simulations outside the 100-80% load range considered in this work will be necessary to test the effectiveness of the controllers in the case of wide operating changes. The current analysis does not consider measurement delays, assumes that all control variables are measurable and assumes that all manipulated variables can be adjusted instantaneously. This is expected to overestimate controller performance, and future investigations should therefore aim at including these additional delays and limitations in the modelling. In future work, it is also relevant to include additional performance indicators such as specific energy consumption in the evaluation of control configurations.

Credit author statement

V.T. Skjervold: Conceptualization, Formal analysis, Investigation, Methodology, Software, Visualization, Writing – original draft, G. Mondino: Conceptualization, Formal analysis, Funding acquisition, Investigation, Methodology, Software, Writing – review & editing, L. Riboldi: Methodology, Supervision, Writing – review & editing, L.O. Nord: Conceptualization, Funding acquisition, Methodology, Project administration, Supervision, Writing – review & editing.

Declaration of competing interest

The authors declare that they have no known competing financial interests or personal relationships that could have appeared to influence the work reported in this paper.

Data availability

Data will be made available on request.

Acknowledgements

We acknowledge financial support from the Polish-Norwegian Research Program for funding the InnCapPlant project (Grant NOR/POLNORCCS/0015/2019-00).

Nomenclature

ABBREVIATIONS

ARX	Autoregressive with exogeneous input
BAC	Bead-shaped activated carbon
CV	Controlled variable
EMPC	Economic model predictive control
LMPC	Linear model predictive control
MBTSA	Moving bed temperature-swing adsorption
MEA	Monoethanolamine
MPC	Model predictive control
MV	Manipulated variable
NARX	Non-linear autoregressive with exogeneous input
NGCC	Natural gas combined cycle
NMPC	Non-linear model predictive control
PI	Proportional-integral
SIMC	Simplified internal model control

LATIN SYMBOLS

a'	Particle specific area, $m^2\ m^{-3}$
A_i	First single-component Virial coefficient, kg mol^{-1}
A_{ij}	First multi-component Virial coefficient, kg mol^{-1}
B	Controller bias
B_i	Second single-component Virial coefficients of component i, $kg^2\ mol^{-2}$
B_{ij}	Second multi-component Virial coefficient, $kg^2\ mol^{-2}$
Bi_i	Biot number of component i
$c_{p,f}$	Specific heat of the heating/cooling fluid, J $kg^{-1}K^{-1}$
$c_{p,g}$	Specific heat of the gas mixture, J $kg^{-1}K^{-1}$

$c_{p,\mathrm{pk}}$	Specific heat of the packing material, J $kg^{-1}K^{-1}$
$c_{p,\mathrm{s}}$	Specific heat of the adsorbent, J $kg^{-1}K^{-1}$
$c_{p,\mathrm{w}}$	Specific heat of the heat exchanger tubes wall, J $kg^{-1}K^{-1}$
$\widehat{c}_p$	Molar heat of gas mixture at constant pressure, J mol^{-1} K^{-1}
$\widehat{c}_v$	Molar heat of gas mixture at constant volume, J mol^{-1} K^{-1}
C_i	concentration of component *i* in bulk gas phase, mol m^{-3}
$C_{\mathrm{p},i}$	concentration of component *i* in the macropores, mol m^{-3}
C_{T}	Total molar gas concentration in bulk phase, mol m^{-3}
d	Disturbance
$D_{\mathrm{c},i}$	Micropores/crystals diffusivity of component *i*, m^2 s^{-1}
$D_{\mathrm{p},i}$	Macropore diffusivity of component *i*, m^2 s^{-1}
$D_{\mathrm{z},i}$	Axial dispersion coefficient of component *i*, m^2 s^{-1}
e	Controller error, -
g	Transfer function
I	Controller integral term
k	Process gain
K_{c}	Controller gain
$k_{f,i}$	Film mass transfer coefficient of component *i*, m s^{-1}
K_i	Equilibrium constant of component *i*, mol kg^{-1} kPa^{-1}
K^{∞}	Equilibrium constant at infinite temperature, mol kg^{-1} kPa^{-1}
L_x	Tubes length along the flow direction, m
L_z	Tubes length along vertical axis, m
$\dot{m}$	Mass flow rate, kg s^{-1}
h_{gs}	Heat transfer coefficient between the gas and the solid, J $s^{-1}m^{-2}$ K^{-1}
h_{fw}	Heat transfer coefficient between the fluid and the tubes wall, J s^{-1} m^{-2} K^{-1}
h_{gw}	Heat transfer coefficient between the gas and the tubes wall, J $s^{-1}m^{-2}$ K^{-1}
P	Total pressure of the gas mixture, Pa
p	Controller proportional term
P_i	Partial pressure of component *i*, bar
q_i	Adsorbed phase concentration of component *i*, mol kg^{-1}
q_i^*	Adsorbed concentration of component *i* at equilibrium, mol kg^{-1}
R	Ideal gas constant, J $K^{-1}mol^{-1}$
r_{c}	Crystals/micropore radius, m
r_{p}	Particle radius, m
s	Laplace variable, s^{-1}
t	Time, s
T	Temperature of the gas phase, K
T_{f}	Temperature of the heating/cooling fluid, K
T_{s}	Temperature of the solid phase, K
T_{w}	Temperature of the heat exchanger tubes wall, K
u	Superficial gas velocity, m s^{-1}
u	Manipulated variable
v_s	Velocity of the solid phase, m s^{-1}
y	Controlled variable
Y_i	Molar fraction of component *i*
z	Axial coordinate along the section height, m

GREEK SYMBOLS

α_{gt}	Ratio of external surface area of tubes to gas-solid volume, m^2m^{-3}
$\alpha_{\mathrm{w,ext}}$	Ratio of external surface area of tubes to gas-solid volume, m^2m^{-3}
$\alpha_{\mathrm{w,int}}$	Ratio of internal surface area of tubes to gas-solid volume, m^2m^{-3}
ΔH_i	Heat of adsorption of component *i*, J mol^{-1}
ε_{c}	Column void fraction, -
ε_{p}	Particle porosity, -
η_{CO_2}	CO_2 capture (recovery) rate , -
θ	Effective delay, s
λ_{g}	Axial heat dispersion coefficient of the gas mixture, W m^{-1} K^{-1}
λ_{pk}	Axial heat dispersion coefficient of the structured packing, W m^{-1} K^{-1}
ξ	Volumetric fraction of the structured packing, -
ρ_{f}	Density of heating/cooling fluid, kg m^{-3}
ρ_{g}	Density of the gas mixture, kg m^{-3}
ρ_{p}	Density of adsorbent particles, kg m^{-3}
ρ_{pk}	Density of the structured packing, kg m^{-3}
ρ_{w}	Density of heat exchanger tubes wall, kg m^{-3}

τ_c Closed-loop time constant, s
τ_I Controller integral time, s

Appendix A. Supplementary information on gPROMS model

In Table A1 and Table A2, supplementary information on the gPROMS model is given.

Table A1
Values of fixed parameters and solver-related information from gPROMS model.

Parameter	Value	Unit	Parameter	Value	Unit
ρ_f	1000	kgm^{-3}	$c_{p,f}$	4200	J kg^{-1} K^{-1}
ρ_p	904	kgm^{-3}	$c_{p,pk}$	500	J kg^{-1} K^{-1}
ρ_{pk}	1000	kgm^{-3}	$c_{p,s}$	880	J kg^{-1} K^{-1}
ρ_w	4420	kgm^{-3}	$c_{p,w}$	526	J kg^{-1} K^{-1}
ε_c (ads sec.)	0.8	–	h_{fw}	5000	W m^{-2} K^{-1}
ε_c (other sec.)	0.5	–	h_{gw}	150	W m^{-2} K^{-1}
ε_p	0.5	–	L_x	52.8	m
ξ	0.05	–	L_z	1	m
λ_{pk}	0.001	W m^{-1} K^{-1}			
Number of discretization points					
Precooling	200	–			
Cooling	100	–			
Preheating	100	–			
Desorption	100	–			
Adsorption	200	–			
Discretization method		Central finite difference			
Differential-algebraic solver		SRADAU			
Linear algebra solver		MA28			
Absolute tolerance		1E-8			
Relative tolerance		1E-8			

Table A2
Correlations used in gPROMS model, from Ref. [11].

Binary diffusivity	$D_{ij} = \frac{0.01883T^{3/2}}{P\sigma_{ij}^2\Omega_{D_{ij}}}\sqrt{\frac{1}{M_{w,i}}+\frac{1}{M_{w,j}}}$
Molecular diffusivity	$D_m = \frac{1-y_i}{\sum_{j\neq i}^{n}\frac{y_j}{D_{ij}}}$
Knudsen diffusivity	$D_k = 97r_p\sqrt{\frac{T}{M_w}}$
Macropore diffusivity	$\frac{1}{D_p} = \tau_p\left(\frac{1}{D_k}+\frac{1}{D_m}\right)$
Axial dispersion coefficient	$D_z = \frac{D_m}{\varepsilon_c}(20 + 0.5\,\mathrm{Sc}\,\mathrm{Re})$
Adsorption rate in micropores	$\frac{D_c}{r_c^2} = \frac{D_c^0}{r_c^2}\exp\left(-\frac{E_a}{RT}\right)$
Axial thermal conductivity of gas	$\lambda_g = k_g(7 + 0.5\,\mathrm{Pr}\,\mathrm{Re})$
Sherwood number correlation	$\mathrm{Sh} = 2.0 + 1.1\mathrm{Re}^{0.6}\mathrm{Sc}^{1/3}$
Nusselt number correlation	$\mathrm{Nu} = 2.0 + 1.1\mathrm{Re}^{0.6}\mathrm{Pr}^{1/3}$

References

[1] IEA. World energy outlook 2020. 2020 [Online]. Available: https://www.iea.org/reports/world-energy-outlook-2020. Paris.
[2] Richter M, Möllenbruck F, Starinsk A, Oeljeklaus G, Görner K. Flexibilization of coal-fired power plants by dynamic simulation. Proceedings of the 11th International Modelica Conference, Versailles, France, Sept. 21-23 2015;118:715–23. https://doi.org/10.3384/ecp15118715. 2015.
[3] Gonzalez-Salazar MA, Kirsten T, Prchlik L. Review of the operational flexibility and emissions of gas- and coal-fired power plants in a future with growing renewables. Renew Sustain Energy Rev 2018;82(July 2017):1497–513. https://doi.org/10.1016/j.rser.2017.05.278.
[4] United Nations Department of Economic and Social Affairs. Sustain Dev Goal 2022;7. accessed Feb. 16, 2022), https://sdgs.un.org/goals/goal7.
[5] IPCC, "Global Warming of 1.5°C. An IPCC Special Report on the impacts of global warming of 1.5°C above pre-industrial levels and related global greenhouse gas emission pathways. In: The context of strengthening the global response to the threat of climate change; 2018.
[6] Feron PHM, Cousins A, Jiang K, Zhai R, Garcia M. An update of the benchmark post-combustion CO_2-capture technology. Fuel 2020;273(February):117776. https://doi.org/10.1016/j.fuel.2020.117776.
[7] Samanta A, Zhao A, Shimizu GKH, Sarkar P, Gupta R. Post-combustion CO_2 capture using solid sorbents: a review. Ind Eng Chem Res 2012;51(4):1438–63. https://doi.org/10.1021/ie200686q.
[8] Kim H, Miller D, Modekurti S, Omell B, Bhattacharyya D, Zitney S. Mathematical modeling of a moving bed reactor for post-combustion CO_2 capture. AIChE J 2016;62(11):3899–914.
[9] Morales-Ospino R, et al. Parametric analysis of a moving bed temperature swing adsorption (MBTSA) process for postcombustion CO_2 capture. Ind Eng Chem Res 2021. https://doi.org/10.1021/acs.iecr.0c05067.
[10] Mondino G, Grande CA, Blom R. Effect of gas recycling on the performance of a moving bed temperature-swing (MBTSA) process for CO_2 capture in a coal fired power plant context. Energies 2017;10(6). https://doi.org/10.3390/en10060745.
[11] Mondino G, Grande CA, Blom R, Nord LO. Moving bed temperature swing adsorption for CO_2 capture from a natural gas combined cycle power plant. Int J Greenh Gas Control 2019;85(October 2018):58–70. https://doi.org/10.1016/j.ijggc.2019.03.021.

[12] Wu X, Wang M, Liao P, Shen J, Li Y. Solvent-based post-combustion CO_2 capture for power plants: a critical review and perspective on dynamic modelling, system identification, process control and flexible operation. Appl Energy 2020;257 (October 2019):113941. https://doi.org/10.1016/j.apenergy.2019.113941.
[13] Gardarsdóttir S, Montañés RM, Normann F, Nord LO, Johnsson F. Effects of CO_2-absorption control strategies on the dynamic performance of a supercritical pulverized-coal-fired power plant. Ind Eng Chem Res 2017;56(15):4415–30. https://doi.org/10.1021/acs.iecr.6b04928.
[14] Cormos AM, Vasile M, Cristea MV. Flexible operation of CO_2 capture processes integrated with power plant using advanced control techniques. Comput Aided Chem Eng 2015;37(June):1547–52. https://doi.org/10.1016/B978-0-444-63577-8.50103-0.
[15] Panahi M, Skogestad S. Economically efficient operation of CO_2 capturing process. Part II. Design of control layer. Chem Eng Process: Process Intensif 2012;52: 112–24. https://doi.org/10.1016/j.cep.2011.11.004.
[16] Gaspar J, Ricardez-Sandoval L, Jørgensen JB, Fosbøl PL. Controllability and flexibility analysis of CO_2 post-combustion capture using piperazine and MEA. Int J Greenh Gas Control 2016;51:276–89. https://doi.org/10.1016/j.ijggc.2016.06.003.
[17] Lawal A, Wang M, Stephenson P, Koumpouras G, Yeung H. Dynamic modelling and analysis of post-combustion CO_2 chemical absorption process for coal-fired power plants. Fuel 2010;89(10):2791–801. https://doi.org/10.1016/j.fuel.2010.05.030.
[18] Lin YJ, Pan TH, Wong DSH, Jang SS. Plantwide control of CO_2 capture by absorption and stripping using monoethanolamine solution. Ind Eng Chem Res 2011;50(3):1388. 1345.
[19] Mechleri ED, Biliyok C, Thornhill NF. Dynamic simulation and control of post-combustion CO_2 capture with MEA in a gas fired power plant. In: Proceedings of the 24th European symposium on computer aided process engineering - ESCAPE 24; 2014. Budapest, Hungary, June 15-18.
[20] Nittaya T, Douglas PL, Croiset E, Ricardez-Sandoval LA. Dynamic modelling and control of MEA absorption processes for CO_2 capture from power plants. Fuel 2014; 116:672–91. https://doi.org/10.1016/j.fuel.2013.08.031.
[21] Cristea VM, Burca MI, Ilea FM, Cormos AM. Efficient decentralized control of the post combustion CO_2 capture plant for flexible operation against influent flue gas disturbances. Energy 2020;205:117960. https://doi.org/10.1016/j.energy.2020.117960.
[22] Mechleri E, Lawal A, Ramos A, Davison J, Mac Dowell N. Process control strategies for flexible operation of post-combustion CO_2 capture plants. Int J Greenh Gas Control 2017;57:14–25. https://doi.org/10.1016/j.ijggc.2016.12.017.
[23] Montañés RM, GarÐarsdóttir S, Normann F, Johnsson F, Nord LO. Demonstrating load-change transient performance of a commercial-scale natural gas combined cycle power plant with post-combustion CO_2 capture. Int J Greenh Gas Control 2017;63(April):158–74. https://doi.org/10.1016/j.ijggc.2017.05.011.
[24] Lawal A, Wang M, Stephenson P, Obi O. Demonstrating full-scale post-combustion CO_2 capture for coal-fired power plants through dynamic modelling and simulation. Fuel 2012;101:115–28. https://doi.org/10.1016/j.fuel.2010.10.056.
[25] Wu X, Shen J, Wang M, Lee KY. Intelligent predictive control of large-scale solvent-based CO_2 capture plant using artificial neural network and particle swarm optimization. Energy 2020;196:117070. https://doi.org/10.1016/j.energy.2020.117070.
[26] Rúa J, Hillestad M, Nord LO. Model predictive control for combined cycles integrated with CO_2 capture plants. Comput Chem Eng 2021;146. https://doi.org/10.1016/j.compchemeng.2020.107217.
[27] Jung H, Im D, Heo S, Kim B, Lee JH. Dynamic analysis and linear model predictive control for operational flexibility of post-combustion CO_2 capture processes. Comput Chem Eng 2020;140. https://doi.org/10.1016/j.compchemeng.2020.106968.
[28] Li Q, Zhang W, Qin Y, An A. Model predictive control for the process of mea absorption of CO_2 based on the data identification model. Processes 2021;9(1): 1–16. https://doi.org/10.3390/pr9010183.
[29] Jung H, Heo S, Lee JH. Model predictive control for amine-based CO_2 capture process with advanced flash stripper. Control Eng Pract 2021;114(June):104885. https://doi.org/10.1016/j.conengprac.2021.104885.
[30] Sultan T, Zabiri H, Shahbaz M, Maulud AS. Performance evaluation of the fast model predictive control scheme on a CO_2 capture plant through absorption/stripping system. Process Saf Environ Protect 2022;157:218–36. https://doi.org/10.1016/j.psep.2021.11.018.
[31] Akinola TE, Oko E, Wu X, Ma K, Wang M. Nonlinear model predictive control (NMPC) of the solvent-based post-combustion CO_2 capture process. Energy 2020; 213:118840. https://doi.org/10.1016/j.energy.2020.118840.
[32] Patron GD, Ricardez-Sandoval L. A robust nonlinear model predictive controller for a post-combustion CO_2 capture absorber unit. Fuel 2020;265(December 2019): 116932. https://doi.org/10.1016/j.fuel.2019.116932.
[33] Mejdell T, Kvamsdal HM, Hauger SO, Gjertsen F, Tobiesen FA, Hillestad M. Demonstration of non-linear model predictive control for optimal flexible operation of a CO_2 capture plant. Int J Greenh Gas Control 2022;117(September 2021):103645. https://doi.org/10.1016/j.ijggc.2022.103645.
[34] Chan LLT, Chen J. Improving the energy cost of an absorber-stripper CO_2 capture process through economic model predictive control. Int J Greenh Gas Control 2018;76(July):158–66. https://doi.org/10.1016/j.ijggc.2018.05.018.
[35] Ma C, Zhang W, Zheng Y, An A. Economic model predictive control for post-combustion CO_2 capture system based on MEA. Energies 2021;14(23):1–15. https://doi.org/10.3390/en14238160.
[36] Yu M, Biegler LT. Economic NMPC strategies for solid sorbent-based CO_2 capture. IFAC-PapersOnLine 2018;51(18):103–8. https://doi.org/10.1016/j.ifacol.2018.09.283.
[37] Patrón GD, Ricardez-Sandoval L. An integrated real-time optimization, control, and estimation scheme for post-combustion CO_2 capture. Appl Energy September 2021; 308:2022. https://doi.org/10.1016/j.apenergy.2021.118302.
[38] PSE. gPROMS ModelBuilder 2022. https://www.psenterprise.com/products/gproms/modelbuilder. [Accessed 19 February 2022]. accessed.
[39] Skogestad S. Simple analytic rules for model reduction and PID controller tuning. J Process Control 2003;13:291–309. https://doi.org/10.4173/mic.2004.2.2.
[40] Shamsuzzoha M, Skogestad S. The setpoint overshoot method: a simple and fast closed-loop approach for PID tuning. J Process Control 2010;20(10):1220–34. https://doi.org/10.1016/j.jprocont.2010.08.003.

Computers and Chemical Engineering 178 (2023) 108387

Contents lists available at ScienceDirect

Computers and Chemical Engineering

journal homepage: www.elsevier.com/locate/compchemeng

Enhanced single-loop control of a moving bed temperature swing adsorption CO_2 capture process

Vidar T. Skjervold *, Lars O. Nord

Department of Energy and Process Engineering, NTNU - Norwegian University of Science and Technology, Trondheim, Norway

ARTICLE INFO

Keywords:
MBTSA
Post-combustion CO_2 capture
Process modeling
Process control
Adaptive tuning
Dynamic simulations

ABSTRACT

Using a model in gPROMS, we study a Zeolite 13X-based moving bed temperature swing adsorption (MBTSA) process designed to capture CO_2 from a coal-fired power plant. Two enhanced single-loop control strategies were compared to a proportional-integral configuration for variations in power plant load, control variable setpoints, flue gas CO_2 concentration and external heat source temperature. Measurement delays were also investigated. Adaptive adjustment of controller parameters with system load gave smoother and narrower manipulated variable profiles and efficient CO_2 recovery setpoint tracking. The controller gain is the most important parameter for adaptive tuning. A combined feedback and feedforward scheme showed improved control of the regenerated sorbent temperature, possibly due to better decoupling of the higher-level control loops. When delays were considered, the investigated strategies significantly outperformed the reference case for CO_2 recovery control. The results demonstrate that the MBTSA process can be efficiently controlled for several disturbances and changes in operation.

1. Introduction

1.1. Background and motivation

In 2022, global energy-related CO_2 emissions reached a previously unprecedented level of 36.8 Gt, an increase of 0.9% compared to 2021 (IEA, 2023). To mitigate the effects of global warming and reach the goals of the Paris Agreement, these emissions must be significantly reduced in the coming years. The European Union aims at an economy with net zero greenhouse gas emissions by 2050, as outlined in the European Green Deal (European Commission, 2019). Fossil fuel-based power plants stand for almost two thirds of electricity generation, leading to approximately 40% of global energy-related emissions (IEA, 2020). In the transition to an energy system based on renewable energy sources, it is likely that CO_2 capture from thermal power plants will be necessary to reduce emissions while ensuring security of energy supply. The Intergovernmental Panel on Climate Change estimates wide deployment of carbon capture and storage on both natural gas and coal-fired power plants in pathways limiting the global temperature increase to 1.5 °C above pre-industrial levels (IPCC, 2018).

Post-combustion CO_2 capture is suitable for existing power plants, since it can be retrofitted without requiring major changes to the combustion process (Kazemifar, 2022). The state-of-the-art technology for post-combustion CO_2 capture is chemical absorption, which has been proven at commercial scale. However, other technologies such as membrane separation, cryogenic distillation, adsorption and hybrid processes have reached high technology readiness levels and could be viable alternatives (Dziejarski et al., 2023). Adsorption-based processes are considered promising because they have the potential for reduced energy requirements compared to standard amine-based absorption (Raganati et al., 2021). These processes can vary greatly, depending on the choice of reactor configuration, regeneration mode and adsorbent material. In this work, a moving bed temperature swing adsorption (MBTSA) process with a Zeolite 13X adsorbent is considered. The primary advantage of moving beds compared to the fixed bed configuration is the possibility of continuous operation, which avoids the complex operation cycles associated with switching between operation modes (Dhoke et al., 2021). Temperature swings are suitable for CO_2 capture from power plants due to the potential availability of low-grade thermal energy for desorption and the significant electrical power requirements associated with vacuum or pressure swings of the near-atmospheric flue gas discharged from the power plant (Zhao et al., 2019). Zeolite-based adsorbents have fast adsorption kinetics and low regeneration duties, making them attractive for post-combustion CO_2 capture (Samanta et al., 2012). Potential drawbacks of zeolites are their

* Corresponding author.
E-mail address: vidar.t.skjervold@ntnu.no (V.T. Skjervold).

https://doi.org/10.1016/j.compchemeng.2023.108387
Received 15 May 2023; Received in revised form 5 July 2023; Accepted 7 August 2023
Available online 9 August 2023

Nomenclature

Acronyms

CV	controlled variable
FF	feedforward
IAE	integral absolute error
MBTSA	moving bed temperature-swing adsorption
MEA	monoethanolamine
MPC	model predictive control
MV	manipulated variable
PI	proportional-integral
PID	proportional-integral-derivative
RGA	relative gain array
SIMC	simplified internal model control
SRD	specific regeneration duty

Latin symbols

$a^{'}$	particle specific area, $m^2\ m^{-3}$
A_i	first single-component Virial coefficient, kg mol^{-1}
A_{ij}	first multi-component Virial coefficient, kg mol^{-1}
B	controller bias
B_i	second single-component Virial coefficients of component i, $kg^2\ mol^{-2}$
B_{ijk}	second multi-component Virial coefficient, $kg^2\ mol^{-2}$
Bi_i	biot number of component i
c	controller transfer function
$c_{p,f}$	specific heat of the heating/cooling fluid, J $kg^{-1}K^{-1}$
$c_{p,pk}$	specific heat of the packing material, J $kg^{-1}K^{-1}$
$c_{p,s}$	specific heat of the adsorbent, J $kg^{-1}K^{-1}$
$c_{p,w}$	specific heat of the heat exchanger tubes wall, J $kg^{-1}K^{-1}$
$\widehat{c}_p$	molar heat of gas mixture at constant pressure, J $mol^{-1}\ K^{-1}$
$\widehat{c}_v$	molar heat of gas mixture at constant volume, J $mol^{-1}\ K^{-1}$
C_i	concentration of component i in bulk gas phase, mol m^{-3}
$C_{p,i}$	concentration of component i in the macropores, mol m^{-3}
C_T	total molar gas concentration in bulk phase, mol m^{-3}
d	disturbance
d_p	particle diameter, m
$D_{c,i}$	micropores/crystals diffusivity of component i, $m^2\ s^{-1}$
$D_{p,i}$	macropore diffusivity of component i, $m^2\ s^{-1}$
$D_{z,i}$	axial dispersion coefficient of component i, $m^2\ s^{-1}$
e	controller error, -
g	transfer function
I	controller integral term
k	process gain
K_c	controller gain
$k_{f,i}$	film mass transfer coefficient of component i, m s^{-1}
K_i	equilibrium constant of component i, mol $kg^{-1}\ kPa^{-1}$
K^{∞}	equilibrium constant at infinite temperature, mol $kg^{-1}\ kPa^{-1}$
L_x	tubes length along the flow direction, m
L_z	tubes length along vertical axis, m
$\dot{m}$	mass flow rate, kg s^{-1}
h_{gs}	heat transfer coefficient between the gas and the solid, J $s^{-1}m^{-2}\ K^{-1}$
h_{fw}	heat transfer coefficient between the fluid and the tubes wall, J $s^{-1}\ m^{-2}\ K^{-1}$
h_{gw}	heat transfer coefficient between the gas and the tubes wall, J $s^{-1}m^{-2}\ K^{-1}$
P	total pressure of the gas mixture, Pa
P	controller proportional term
P_i	partial pressure of component i, bar
q_i	adsorbed phase concentration of component i, mol kg^{-1}
q_i^*	adsorbed concentration of component i at equilibrium, mol kg^{-1}
R	ideal gas constant, J $K^{-1}mol^{-1}$
r_c	crystals/micropore radius, m
r_p	particle radius, m
s	Laplace variable, s^{-1}
t	time, s
T	temperature of the gas phase, K
T_f	temperature of the heating/cooling fluid, K
T_s	temperature of the solid phase, K
T_w	temperature of the heat exchanger tubes wall, K
u	superficial gas velocity, m s^{-1}
u	manipulated variable
$u^{'}$	ratio calculated by outer feedback loop
v_s	velocity of the solid phase, m s^{-1}
y	controlled variable
y_{SP}	controlled variable setpoint
Y_i	molar fraction of component i
z	axial coordinate along the section height, m

Greek symbols

α_{gt}	ratio of external surface area of tubes to gas-solid volume, m^2m^{-3}
$\alpha_{w,ext}$	ratio of external surface area of tubes to gas-solid volume, m^2m^{-3}
$\alpha_{w,int}$	ratio of internal surface area of tubes to gas-solid volume, m^2m^{-3}
ΔH_i	heat of adsorption of component i, J mol^{-1}
ε_c	column void fraction, -
ε_p	particle porosity, -
η_{CO_2}	CO_2 capture (recovery) rate, -
θ	effective delay, s
λ_g	axial heat dispersion coefficient of the gas mixture, W $m^{-1}\ K^{-1}$
λ_{pk}	axial heat dispersion coefficient of the structured packing, W $m^{-1}\ K^{-1}$
μ	gas dynamic viscosity, kg $m^{-1}\ s^{-1}$
ξ	volumetric fraction of the structured packing, -
ρ_f	density of heating/cooling fluid, kg m^{-3}
ρ_g	density of the gas mixture, kg m^{-3}
ρ_p	density of adsorbent particles, kg m^{-3}
ρ_{pk}	density of the structured packing, kg m^{-3}
ρ_w	density of heat exchanger tube wall, kg m^{-3}
τ	time constant of open-loop response, s
τ_c	closed-loop time constant, s
τ_I	controller integral time, s
φ	flue gas feed flow rate divided by nominal value, -

temperature-sensitive adsorption capacity, high regeneration temperature requirement and the negative impact of moisture on their CO_2 capture capacity (Nie et al., 2018).

In the work of Mondino et al., a dynamic, first-principle model was used to evaluate the MBTSA process for post-combustion CO_2 capture from a natural gas combined cycle power plant (Mondino et al., 2019), coal-fired power plant (Mondino et al., 2017) and waste-to-energy plant (Mondino et al., 2022). Simulation results indicate that the MBTSA process can achieve high CO_2 recovery rates and purity of the captured CO_2 for all three applications. In a paper by Morales-Ospino et al., a similar mathematical model was applied in a parametric analysis to investigate how various process variables affected the MBTSA

performance (Morales-Ospino et al., 2021). The specific energy consumption of the process was found to be competitive against commercial amine absorption processes, and up to 99 mol% CO_2 recovery and 91 mol% purity could be achieved. Jung and Lee performed a techno-economic evaluation of CO_2 capture with an amine-functionalized solid sorbent from a coal-fired power plant, reporting that the CO_2 capture cost of a moving bed process was lower than the reference amine-based absorption process (Jung and Lee, 2022). MBTSA has also been demonstrated experimentally at large scale. The KCC process developed by Kawasaki Heavy Industries, which uses an amine-impregnated adsorbent, has been tested at 5 (Okumura et al., 2017) and 40 (Okumura et al., 2018) tons of captured CO_2 per day. This process uses low-grade steam at 60 °C in a direct-contact configuration for regeneration of the adsorbent material. Also, CO_2 capture systems based on fluidized beds with temperature-swing adsorption have been demonstrated at pilot scale. ADA tested an amine functionalized ion-exchange resin sorbent on a 1 MW_e flue gas stream from a coal-fired power plant (Sjostrom and Senior, 2020). KEPCO tested an Na/K carbonate-based capture process on 10 MW_e scale at a coal-fired power plant in Korea, showing that over 80% CO_2 recovery and 95% purity could be achieved (Park et al., 2014).

Most of the studies on MBTSA focus on steady-state operation, but CO_2 capture from thermal power plants will likely need to deviate from steady-state due to expected changes in the energy system. Based on stated policies, the International Energy Agency estimates that renewable energy sources will stand for 43% of global electricity generation in 2030 and 65% in 2050 (IEA, 2022). The intermittent nature of such energy sources represents a challenge since there must always be a balance between supply and demand. Alongside energy storage and demand response measures, the residual load not covered by renewables is expected to be met by flexible operation of fossil-fueled power plants, particularly in the short to medium term (Gonzalez-Salazar et al., 2018). In the case of post-combustion CO_2 capture, variations in the power plant load will require flexible operation of the capture plant. A recent study by Singh et al. concluded that profitable operation of CCS deployed on flexibly operating power plants could be achieved in the future through a combination of market incentives, cost reductions and the use of depreciated assets (Singh et al., 2022). This would further increase the probability of CO_2 capture deployment on thermal power plants. For flexible operation, well-designed process control systems must be developed for the CO_2 capture process to ensure safety and robustness under various uncertainties and disturbances (Hasan et al., 2022). Thus, the main motivation for studying process control in this work is to ensure that the MBTSA process can reliably capture CO_2 from a power plant even under varying operating conditions.

1.2. Process control of post-combustion CO_2 capture

Both decentralized and centralized control structures have been extensively studied in the literature for solvent-based post-combustion CO_2 capture from coal-fired power plants. Most studies consider the CO_2 recovery rate and reboiler temperature as higher-level control variables, using the lean solvent flow rate and reboiler heat duty (or flow rate of extracted steam from the power plant) as manipulated variables (Wu et al., 2020b). In the following paragraphs, a summary of relevant articles within this topic is provided.

Decentralized control structures are based on single input – single output loops, pairing one manipulated variable (MV) with each control variable (CV). They are easy to implement and widely studied in the literature. Lawal et al. (2010) studied a chemical absorption process based on monoethanolamine (MEA) under several dynamic scenarios, using the solvent flow rate to control CO_2 recovery and the reboiler duty to control the reboiler temperature. Based on a relative gain array (RGA) analysis, Gaspar et al. arrived at the same pairing for piperazine and MEA-based processes (Gaspar et al., 2016). Nittaya et al. (2014) studied the reverse pairing (i.e., using the reboiler duty to control CO_2 recovery and solvent flow to control reboiler temperature) and found a heuristic approach to give better performance than RGA analysis. Mechleri et al. used the same MV-CV coupling as Mechleri et al. (2017) to investigate control of a coupled supercritical coal-fired power plant – CO_2 capture process. Using the same control structure as their previous work, Lawal et al. (2012) studied the dynamic behavior of a supercritical power plant integrated with an MEA-based capture process. Gardarsdóttir et al. (2017) compared a range of decentralized control structures using a coupled power plant – CO_2 capture model implemented in Dymola.

In recent years, emphasis has shifted towards centralized control approaches such as model predictive control (MPC). Compared to classical structures, such controllers have the benefit of better handling of coupled control loops and the ability to handle constraints (Akinola et al., 2020). The simplest form of MPC uses linear predictive models in the optimization problem used to determine the control action. An example is the work of Jung et al., which used gap metric analysis to determine the optimal reference point for linear controller design (Jung et al., 2020). The control structure was tested for dynamic simulations of CO_2 recovery setpoint changes and flue gas flow rate variations for a stand-alone capture plant. Rúa et al. used several linear models combined in a local model network for MPC of natural gas combined cycle power plant with solvent-based CO_2 capture (Rúa et al., 2021). A nonlinear artificial neural network predictive model with online updating of weights was studied by Wu et al., combined with particle swarm optimization to solve the optimal control problem (Wu et al., 2020a). The same group studied a supercritical power plant with post-combustion CO_2 capture, using MPC based on state-space models for both sub-processes and considering operation modes prioritizing either the power plant or CO_2 capture (Wu et al., 2019). For similar systems, other recent articles have investigated distributed MPC based on dynamic matrix controllers (Tang and Wu, 2023), linear MPC with state-space models and an extended state observer (Liao et al., 2023) and inverse control using a neural network to predict MV values from CV setpoints instead of the process state (Liao et al., 2020).

As shown above, most studies on control of post-combustion CO_2 capture from thermal power plants have either focused on simple feedback or feedforward controllers or advanced model predictive configurations. Although MPC generally gives improved performance over single-loop control, it is not always recommended. Panahi and Skogestad (2012) and Cormos et al. (2015) both recommended simple control structures over MPC, due to comparable performance and easier implementation.

Enhanced single-loop control is a collective term for advanced control strategies that aim at improving performance beyond what is achievable with single-loop proportional-integral-derivative (PID) controllers without the complexity of MPC (Seborg et al., 2016). Examples of such strategies are time-delay compensation, inferential control, selective and override control, input or output variable transformations, fuzzy logic control and adaptive control. The most commonly applied enhanced single-loop strategy is updating PID controller gains based on operating conditions, a strategy known as gain scheduling (Wei et al., 2014). A few examples from the literature from thermo-mechanical applications are provided here. Modekurti et al. (2017) applied a control structure involving gain scheduling to avoid surge during operation of a multistage CO_2 compression train. Hernandez et al. (2017) demonstrated that a gain-scheduled PID controller showed comparable performance with MPC for a small-scale waste heat recovery system. Cui et al. (2022) adaptively adjusted the controller integral time (keeping the gain constant) for control of superheated steam temperature in a thermal power plant.

Enhanced single-loop control strategies are not widely studied in the literature for post-combustion CO_2 capture but could improve the decentralized control performance of such processes. In this work we focus on two strategies that have been suggested by previous studies but have not yet been evaluated in detail. The strategies are explained in Section 3.1. Firstly, we consider adaptive controller tuning, which

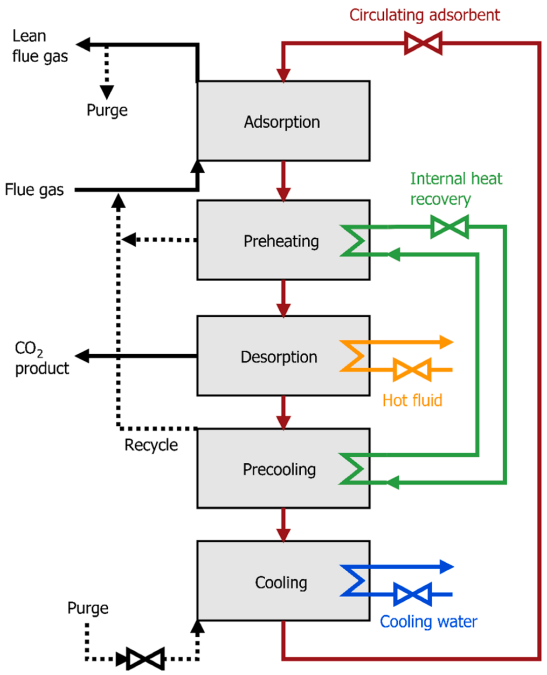

Fig. 1. The moving bed temperature swing adsorption post-combustion CO_2 capture process. The manipulated variables are indicated by valves.

means that a model is used to automatically adjust the tuning parameters based on system conditions. In our previous work (Skjervold et al., 2023), simulations for an activated carbon-based MBTSA process indicated that adaptive tuning could improve the performance and robustness of the controllers. This was especially relevant at lower power plant loads. As shown by the above literature review, adjusting both the controller gain and integral time can be advantageous.

Another recommendation from Skjervold et al. (2023) was that more sophisticated modification of the ratio used in feedforward control of CO_2 recovery is required to avoid steady-state setpoint offsets. Similar suggestions were made by other studies (Gardarsdóttir et al., 2017; Montañés et al., 2017; Posch and Haider, 2013). Based on testing of different control structures at Technology centre Mongstad in Norway, Montañés et al. (2018) suggested that a combined feedforward and feedback structure could lead to fast and stable disturbance rejection. Following these suggestions, the second enhanced single-loop control strategy studied in this work is the application of an outer feedback controller to adjust the ratio used in a feedforward controller for CO_2 recovery. Compared to standalone feedforward control, this combined approach has the advantage of eliminating steady-state setpoint offsets if integral action is included.

In this work, the MBTSA post-combustion capture process is studied as a standalone system, i.e., without a detailed model of the coal-fired power plant. In this approach, variations in power plant operation are treated as external disturbances to the capture plant. The disturbances should therefore be representative of real-life power plant operation. In the CO_2 capture-related studies described above, the control structures are commonly tested for variations in the flue gas flow rate (using ramps or step changes) as well as setpoint changes for higher-level control variables. However, there are other disturbances relevant for power plant operation that could be considered. Variations in flue gas CO_2 concentration can occur due to e.g., changes in boiler operation, leakages in the flue gas ducts and changes in coal composition and quality. A few studies have included such disturbances for solvent-based processes in the form of periodic variations in CO_2 concentration (Cristea et al., 2020), increased CO_2 concentration due to partial oxy-combustion of the coal (Lawal et al., 2010) and a step change in the carbon content of the coal feed (Liao et al., 2023). However, such disturbances have not been considered for an MBTSA-based capture process. Another possible disturbance is variations in the amount and state of extracted steam for regeneration due to changes in power plant operation. Several articles have considered reductions in the steam flow rate due to peaks in electricity demand (Gardarsdóttir et al., 2015; Gaspar et al., 2016; Lawal et al., 2010). To our knowledge, disturbances in the temperature or pressure of the extracted steam have not been considered in the literature.

1.3. Knowledge gaps and scope of paper

From the literature review it is evident that although process control of solvent-based post-combustion CO_2 capture has been widely studied, the MBTSA process has received little attention in this context. This work addresses several knowledge gaps in the literature and the main novel contributions are summarized below:

1) We study a zeolite-based MBTSA process designed for post-combustion CO_2 capture from a large-scale coal-fired power plant. Process control of such a system has not previously been investigated.
2) We investigate two strategies for enhanced single-loop control, namely adaptive controller tuning based on system load and a combined feedback and ratio feedforward controller. Such control strategies have not previously been studied for post-combustion CO_2 capture.
3) We consider disturbances in the flue gas CO_2 concentration and external heat source temperature. These disturbances have not previously been studied for MBTSA-based CO_2 capture.

The research objective of this work is to perform a model-based comparison of the two enhanced single-loop control strategies with a proportional-integral (PI) controller for several types of dynamic scenarios. Controller performance is evaluated both based on graphical comparison and a quantitative metric.

1.4. Article structure

The article is structured as follows. In Section 2 the main principles of the MBTSA process along with the modeling approach and open-loop behavior of key variables are explained. In Section 3 the investigated control structures, applied tuning methods and scenarios for controller testing are described. Results from the dynamic controller testing simulations are presented in Section 4 and discussed in Section 5. The work is concluded in Section 6.

2. Moving bed temperature swing adsorption CO_2 capture process

In this section, the main principles of the MBTSA process are explained, along with a description of the dynamic first-principle model built in gPROMS and the open-loop dynamic behavior of key control variables.

2.1. Process description

The MBTSA process considered in this work is shown in Fig. 1. The process consists of five main stages, through which the moving bed of adsorbent particles passes from top to bottom due to gravity. Flue gas from the power plant is fed at the bottom of the adsorption section, moving in the opposite direction of the moving bed. This counter-

Table 1
System characteristics and nominal boundary conditions for the MBTSA process.

Variable	Value	Unit
Power plant net power output (without CO_2 capture)	642	MW
Total flue gas mass flow rate	804	kg/s
Number of parallel CO_2 capture units	2	–
Hot fluid inlet temperature	2 40	°C
Cooling water inlet temperature	2 0	°C
Flue gas temperature	3 0	°C
Flue gas pressure	1.02	bar
Flue gas mass flow rate per unit	402	kg/s
Flue gas composition:		
CO_2	14.6	mol%
N_2	85.4	mol%

Table 2
Nominal operating conditions and performance of the MBTSA process.

Variable	Value	Unit
Circulating sorbent mass flow rate	1313	kg/s
Sorbent residence time	322.7	s
Lean sorbent CO_2 loading	0.69	mol CO_2/kg
Rich sorbent CO_2 loading	2.12	mol CO_2/kg
Sorbent cyclic CO_2 working capacity	1.43	mol CO_2/kg
CO_2 purity	96.5	mol%
CO_2 recovery	90.0	%
Lean sorbent temperature	3 0	°C
Regenerated sorbent temperature	2 02	°C
External regeneration heat duty	133	MW
Fraction of total heat recovered by inner loop	37.7	%
External cooling duty	110	MW

current configuration gives even distribution of the driving forces for adsorption because CO_2-depleted flue gas at the top of the adsorption section meets CO_2-lean adsorbent material. The adsorption section is operated adiabatically. After leaving the adsorption section, the circulating adsorbent is heated in the preheating section via an internal heat recovery loop and desorption section using an external heat source. Due to a reduction in the CO_2 adsorption capacity at higher temperatures, CO_2 is desorbed from the adsorbent particles and extracted in a high-purity CO_2 stream. An indirect heat transfer configuration is used, meaning the heat source is not directly in contact with the adsorbent material (Knaebel, 2009). Before being transported back to the top of the adsorption section, the circulating adsorbent is brought back to its original temperature by passing through the precooling and cooling section. There are five manipulated variables used for process control: the circulating adsorbent mass flow rate, flow rate of purge gas used in the cooling/precooling section, as well as the flow rate of internal heat recovery fluid, hot fluid and cooling water.

The CO_2 capture process is designed for the flue gas of a supercritical coal-fired power plant with a net power output of 642 MW. The nominal boundary conditions are given in Table 1. Due to the large amount of flue gas, two parallel CO_2 capture units are considered, each handling 50% of the incoming flue gas. It has been assumed that the flue gas consists of a binary mixture of carbon dioxide and nitrogen that has been dried and cooled to 30 °C upstream of the MBTSA unit. Since nitrogen has a stronger affinity towards Zeolite 13X than oxygen and argon (Park et al., 2006), dry flue gas is well approximated by this binary mixture (Merel et al., 2008).

A summary of the nominal operating conditions and performance of the MBTSA process is given in Table 2. At full load, the process delivers CO_2 at a purity of 96.5% with a CO_2 recovery rate of 90.0%. The CO_2 recovery definition used in this work is:

$$\eta_{CO_2} = \frac{\dot{m}_{CO_2,\text{out}}}{\dot{m}_{CO_2,\text{in}}}. \tag{1}$$

Where $\dot{m}_{CO_2,\text{in}}$ is the mass flow of CO_2 in the flue gas feed and $\dot{m}_{CO_2,\text{out}}$ is the mass flow of CO_2 in the stream extracted from the desorption section.

2.2. Dynamic process model

The MBTSA process model applied in this work is a modified version of the gPROMS program described in a previous article from our group (Mondino et al., 2019). It was built in gPROMS ModelBuilder version 7.1.1 (PSE, 2023). The model was scaled to match the nominal flue gas mass flow rate of 402 kg/s per unit and necessary model modifications were made to prepare for the implementation and comparison of different control structures. The design parameters were adjusted to give the desired CO_2 product purity and recovery.

For each individual section of the model (i.e., the adsorption, preheating, desorption, precooling and cooling section) a set of partial differential equations are implemented. The model equations and underlying assumptions are identical for each sub-domain, but design parameter values and operating conditions vary between sections. The equations describe the mass, energy and momentum balances and are dynamic and one-dimensional in the spatial domain. Three separate phases are considered, namely the bulk gas phase, solid phase and gas within the macropores of the adsorbent material. The different sections of the model are connected by using the composite modeling capabilities in gPROMS. For completeness, the set of equations, correlations and supplementary information on the model are given in Appendix A.

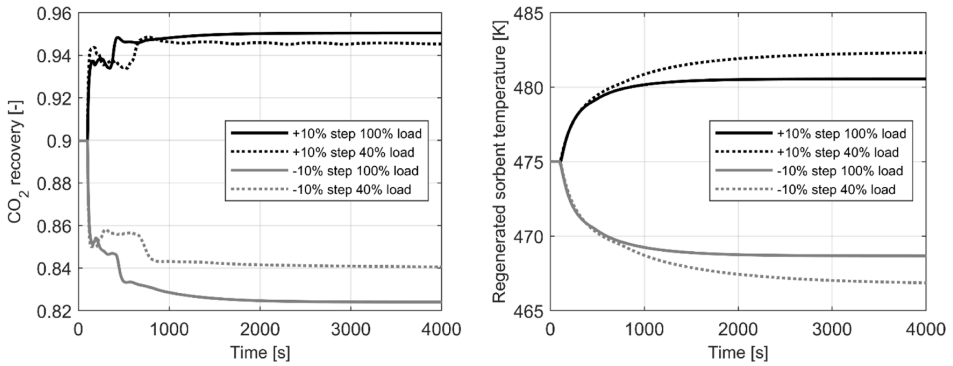

Fig. 2. Open-loop response of CO_2 recovery to step changes in circulating sorbent flow rate (left) and regenerated sorbent temperature to step changes in the flow rate of hot fluid in the desorption section (right). Steps are introduced at $t = 100$ s.

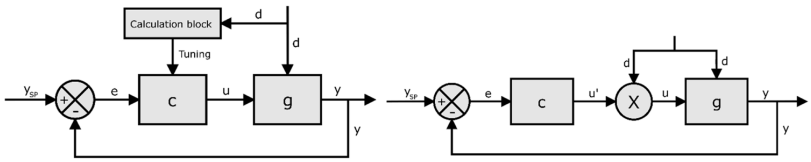

Fig. 3. Enhanced single-loop control strategies investigated in this work. Left: adaptive adjustment of feedback controller tuning based on measured disturbance. Right: combined feedforward and feedback control.

Table 3
Summary of controller tuning parameters and setpoints.

Scheme	CV	MV	τ_c (s)	K_c	τ_I (s)	Setpoint
Std PI	CO_2 recovery	Sorbent mass flow	5.0	99.6	20.0	0.90
	Regenerated sorbent temp	u_f desorption section	16.3	1.65	65.0	475 K
FF + PI	CO_2 recovery (outer loop)	Sorbent / flue gas feed flow ratio	30.6	54.1	115	0.90
	Regenerated sorbent temp	u_f desorption section	16.3	1.65	65.0	475 K
Adaptive *Kc*	CO_2 recovery	Sorbent mass flow	$\tau/32$	$0.674\varphi + 16.8$	30.6	0.90
	Regenerated sorbent temp	u_f desorption section	$\tau/16$	$0.026\varphi - 0.946$	80.0	475 K
Adaptive $Kc + \tau_I$	CO_2 recovery	Sorbent mass flow	$\tau/32$	$0.674\varphi + 16.8$	$-0.575\varphi + 79$	0.90
	Regenerated sorbent temp	u_f desorption section	$\tau/16$	$0.026\varphi - 0.946$	$-1.36\varphi + 196$	475 K
Regulatory layer	T_s, *out* cooling section	u_f cooling section	38.1	−0.925	153	303 K
	u_f/sorbent flow ratio in precooling and preheating sections	u_f internal heat recovery loop	–	–	–	0.00019
	u_{out} precooling section	Purge gas mass flow	80.0	1.82	160	0.08 m/s

2.3. Open-loop simulations

Due to a lack of available data in the open literature, it is not possible to validate the complete MBTSA model with experimental results. Therefore, open-loop simulations are necessary to demonstrate that the mathematical model predicts reasonable responses to various changes in operation. Furthermore, the open-loop behavior of the process is the basis for the choice of CV-MV pairings and calculation of controller tuning parameters. Step response simulations were carried out by setting all controllers in manual mode and introducing positive and negative steps of 10% on selected manipulated variables. Simulations at both 100% and 40% power plant load were carried out, to demonstrate the effect of power plant load changes on the open-loop MBTSA process behavior.

In Fig. 2, the responses of CO_2 recovery to sorbent mass flow step changes and regenerated sorbent temperature to desorption section hot fluid flow rate step changes are shown. Previous studies (Morales-Ospino et al., 2021) show that increasing the solid/gas flow rate ratio leads to increased CO_2 recovery and that reduced sorbent flow rates will have a negative effect. Similarly, an increase in the hot fluid flow rate to the desorption section will increase the regenerated sorbent temperature. The figure shows that the model predictions agree with the trends from previous work. The process takes time to settle after a step change has been introduced, since several cycles are required before a new steady-state is reached. The open-loop behavior varies with load, indicating that adaptive adjustment of the controller tuning parameters can be beneficial.

3. Process control

In this section, the process control strategies and controller tuning methods applied in this work are described. The scenarios used to test the investigated control structures are also described.

3.1. Higher-level control structures

As mentioned in Section 1.2, the most common choice of CV-MV pairings for post-combustion CO_2 capture is using the solvent flow rate to control CO_2 recovery and the steam flow rate extracted from the power plant to control the reboiler temperature. In this work, we have followed this pairing strategy for the higher-level control layer. The circulating sorbent mass flow rate is used to control CO_2 recovery and the flow rate of hot fluid in the desorption section is used to control the regenerated sorbent temperature. In the gPROMS model, heat transfer fluid flow rates are represented by their velocity. The regenerated sorbent temperature is closely linked to the CO_2 product purity. As shown in Fig. 2, the input variables have a significant steady-state effect on their respective outputs and short delays, indicating that the chosen pairings are suitable.

Two different types of enhanced single-loop control strategies are investigated in this work, as illustrated in Fig. 3. The first configuration consists of PI controllers with adaptive adjustment of the tuning parameters based on a measured disturbance d (in this case the flue gas feed mass flow rate). The control action is determined by the following equation:

$$u = K_c(\varphi)[P + I(\varphi)](u_{max} - u_{min}) + B. \tag{2}$$

Where u is the calculated value of the manipulated variable, K_c is the controller gain, P is the proportional term, I is the integral term, u_{max} is the upper limit of the manipulated variable, u_{min} is the lower limit of the manipulated variable and B is the controller bias. The flue gas feed mass flow rate normalized by its nominal value, φ, is used in the adaptive tuning relations, as shown in Table 3. The proportional and integral terms are given by:

$$P = e \tag{3}$$

$$\tau_I(\varphi)\frac{dI}{dt} = e \tag{4}$$

Where τ_I is the integral time and e is the controller error. The error is defined as:

$$e = \frac{y_{SP} - y}{y_{max} - y_{min}} \tag{5}$$

Where the subscripts max and min represent the maximum and minimum allowable value of the CV.

In the second configuration, a combination of feedforward and feedback control is used. This configuration is essentially a special type

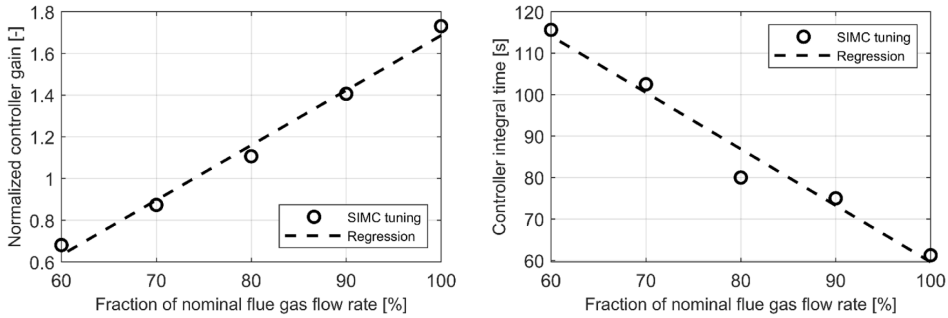

Fig. 4. SIMC tuning parameters for the regenerated sorbent temperature controller vs. fraction of nominal flue gas mass flow rate. The reported values are the average of calculations for positive and negative step responses at each operating point, with $\tau_c = \tau/16$.

of cascade control, where the inner loop is a ratio-type feedforward controller. The control action in such a controller is given by:

$$u = u^{'}d \tag{6}$$

Where the ratio $u^{'}$ is the calculated MV value from the outer feedback loop, given by Eq. (6) with fixed tuning parameters. The integral action included in the outer feedback loop will remove the steady-state setpoint offset typically associated with pure feedforward control.

The enhanced single-loop configurations are compared with a reference case consisting of standard PI controllers with constant tuning. The short name and main characteristics of the control structures studied in this work are summarized below:

1) Std PI: PI controllers with fixed tuning parameters are used to control both the CO_2 recovery and regenerated sorbent temperature (base case).
2) FF + PI: Combined feedforward and feedback control structure for CO_2 recovery, where the ratio used in the feedforward controller is calculated by an outer feedback loop with fixed tuning parameters. The regenerated sorbent temperature controller is identical to the standard PI case.
3) Adaptive K_c: PI control of CO_2 recovery and regenerated sorbent temperature with online adjustment of controller gains based on the system load. The integral times are kept constant.
4) Adaptive $K_c + \tau_I$: PI control of CO_2 recovery and regenerated sorbent temperature with online adjustment of controller gains and integral times based on the system load.

3.2. Regulatory layer

In addition to the higher-level control loops, a regulatory layer is needed to control additional variables needed for stable operation of the process under varying operation. As shown in Fig. 1, three manipulated variables are available for regulatory control after the control loops for CO_2 recovery and regenerated sorbent temperature have been specified. The pairing philosophy and controller configurations for the regulatory layer follow the approach in our previous work (Skjervold et al., 2023), and they are therefore only briefly explained here.

Firstly, the velocity of the working fluid in the internal heat recovery loop is adjusted to maintain a constant ratio with the sorbent mass flow rate. The aim of this controller is to keep the fraction of heat transfer delivered by the internal loop constant throughout varying operation. To maintain the sorbent adsorption capacity during cyclic operation, the particles are cooled to a given temperature before entering the adsorption section. This is achieved by manipulating the velocity of the cooling water flow to the cooling section in a PI controller. Finally, the mass flow rate of purge gas is adjusted in a PI controller with the gas velocity at the top of the precooling section as the controlled variable. The regulatory control structures are identical in all the cases considered in this work.

3.3. Controller tuning

Feedback controller tuning was based on the simplified internal model control (SIMC) rules (Skogestad, 2003). For a PI-controller, a first-order transfer function $g(s)$ describing the open-loop relation between the manipulated and controlled variable is used to calculate the controller tuning parameters:

$$g(s) = \frac{ke^{-\theta s}}{\tau s + 1} \tag{7}$$

Where k is the gain, θ is the effective delay and τ is the time constant of the response. For each CV-MV pairing and considered system load, the parameters of the transfer function were determined from MV step response simulations. The SIMC rules give the controller gain and integral time based on the user-defined closed-loop time constant τ_c:

$$K_c = \frac{1}{k}\frac{\tau}{\tau_c + \theta} \tag{8}$$

$$\tau_I = \min\lfloor \tau, 4(\tau_c + \theta)\rfloor. \tag{9}$$

Since no significant observable delay is seen in the open-loop simulations, the choice of closed-loop time constant is not evident. For each control loop, different values of τ_c were tested before arriving at the controller tuning parameters summarized in Table 3. For the combined feedforward and feedback control structure, a more robust tuning (i.e., larger closed-loop time constant) was chosen, since the gain from MV to CV will vary due to multiplication with the measured disturbance.

In order to determine parametrized tuning relations for the adaptive PI controllers, tuning at several system loads was necessary. For φ-values of 60, 70, 80, 90 and 100%, open-loop simulations with ± 10% MV steps followed by SIMC-based tuning were performed. At each point, the average tuning parameter values from the positive and negative steps were calculated. In Fig. 4, the results for the regenerated sorbent temperature controller are shown as an example. The figure shows that the SIMC controller gain increases and the integral time decreases with increasing φ, indicating that more robust tuning is necessary at lower loads. Linear regression was used to parametrize the variation of K_c and τ_I with φ.

In Table 3, a summary of the tuning parameters and setpoints for the control structures investigated in this work is given.

3.4. Investigated scenarios and quantitative performance metric

A range of scenarios are considered to test the investigated control

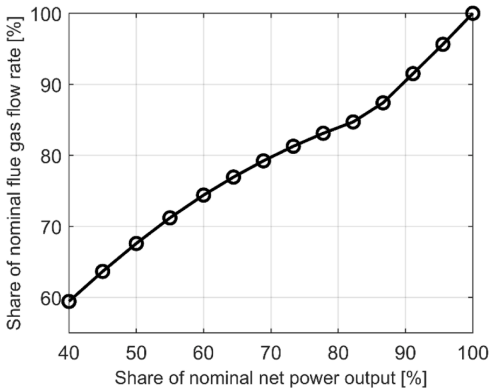

Fig. 5. Relationship between flue gas mass flow rate and nominal net power output, based on part-load simulations (steady-state off-design) in the STEAM MASTER program (Thermoflow Inc, 2023).

structures with cases representative of real-life power plant operation and disturbances. They are listed below:

1) Ramps in power plant load in the 100–40% range.
2) Setpoint changes for CO_2 recovery.
3) Setpoint changes for the regenerated sorbent temperature.
4) Variations in the flue gas feed CO_2 concentration.
5) Variations in the temperature of the external heat source.
6) Delays in the measurement of CO_2 recovery and regenerated sorbent temperature.

No dynamic power plant model has been included, meaning that the scenarios used for controller testing are implemented in the form of variations in the boundary conditions to the MBTSA process. The integral absolute error (IAE) was used to quantify the controller performance. It is defined as:

$$\mathrm{IAE} = \int_0^t |y_{SP}(t) - y(t)|dt \tag{10}$$

Where y_{SP} is the setpoint for a given CV and y is its actual value. A steady-state power plant model in version 30 of the STEAM MASTER program (Thermoflow Inc, 2023) was used to determine the relationship between flue gas mass flow rate and net power output at part-load conditions. The simulation results are shown in Fig. 5 and were used to convert the power plant net power output to a flue gas mass flow rate, which was used as input to the gPROMS model. Ramps in power plant load follow a rate of change of 5% nominal load over a period of 30 s, following the requirement for newly built power units in Poland (Zima et al., 2023).

4. Results from controller test scenarios

In this section, the simulation results are presented and explained. The purpose of these simulations was to test the different control configurations with various dynamic scenarios that could be relevant for a power plant with post-combustion CO_2 capture.

4.1. Power plant load ramps

In Fig. 6, CV and MV responses to ramps in power plant load in the 40–100% load range are shown. To emulate a power plant varying its operation between different loads, ramps from 40 to 60%, 60–80% and 80–100% load were simulated, allowing the controllers to settle over a period of 20 min between each ramp. Only positive ramps were included since ramp-down simulations showed similar relative behavior of the different control configurations. The feedback controllers for adsorbent cooling and precooling gas velocity are included in the results, to show the performance of both control layers over a wide operating range.

Increasing the flue gas feed mass flow rate to the MBTSA process leads to a reduction in CO_2 recovery before the controllers compensate by increasing the circulating sorbent flow rate. The increased sorbent flow causes a reduction in the regenerated sorbent temperature, which is eventually counteracted by an increase in the heating fluid flow to the desorption section. Similarly, the flow of cooling water must be increased to cover the higher cooling duty requirement associated with a larger sorbent flow rate. The main purpose of the purge flow in the cooling and precooling sections is to facilitate transport of gaseous CO_2 from the macropores in the adsorbent to the bulk phase, to avoid re-adsorption of CO_2 as the particles are cooled. When the sorbent flow rate is increased, the gas velocity at the top of the precooling section is reduced due to more CO_2 being re-adsorbed on the particles. This is counteracted by an increase in the purge flow rate. Due to the identical tuning, the regulatory controllers show similar behavior for all configurations.

Since they are more robustly tuned, the adaptive controllers give a slower CO_2 recovery and regenerated sorbent temperature response than the Std PI configuration. As expected, the difference is most evident at lower loads. The MV usage of the adaptive controllers is marginally smoother than the other control schemes. For all CVs, no steady state setpoint offsets are observed in any of the control configurations.

As shown in Table 3, the outer loop in the FF + PI configuration is less aggressively tuned than the other CO_2 recovery controllers. Since the optimal sorbent to flue gas flow ratio varies with load, the FF + PI scheme is dependent on the outer loop to adjust the ratio before the setpoint is reached, leading to a slower CO_2 recovery response. The regenerated sorbent temperature response of the FF + PI configuration is similar to the Std PI case.

4.2. Setpoint changes for CO_2 recovery

In Fig. 7, the response of the higher-level CVs and MVs to CO_2 recovery setpoint changes at 40% power plant load is shown. The recovery setpoint changes from 0.9 to 0.95 and the controllers are allowed to settle before the setpoint is reduced to its original value.

Increasing the CO_2 recovery setpoint requires an increase in the sorbent flow rate, which is followed by an increase in the heating fluid flow to maintain the desired regenerated sorbent temperature. In this case, the adaptively tuned PI controllers show the most efficient CO_2 recovery setpoint tracking, particularly for the positive setpoint change from 0.9 to 0.95. No significant differences between the adaptive K_c and adaptive $K_c + \tau_I$ configurations are observed. The Std PI and FF + PI schemes demonstrate tighter control of the regenerated sorbent temperature.

4.3. Varying flue gas feed CO_2 concentration

In Fig. 8, the closed-loop responses to variations in the flue gas feed CO_2 concentration at 60% load are shown. Firstly, the mol fraction of CO_2 in the flue gas is reduced from 0.146 to 0.135 and the controllers are given time to settle. Subsequently, the CO_2 mol fraction is increased back to its nominal value of 0.146. It is seen from the definition in Eq. (1) that reducing the concentration of CO_2 in the flue gas will give an immediate increase in the CO_2 recovery, which is counteracted by a reduction in the sorbent flow rate. However, a lower CO_2 feed concentration gives less favorable conditions for adsorption, which is expected to lead to a higher sorbent/flue gas ratio than in the nominal case. Ultimately, decreasing the CO_2 feed concentration leads to a reduction in the steady state value of the sorbent mass flow rate.

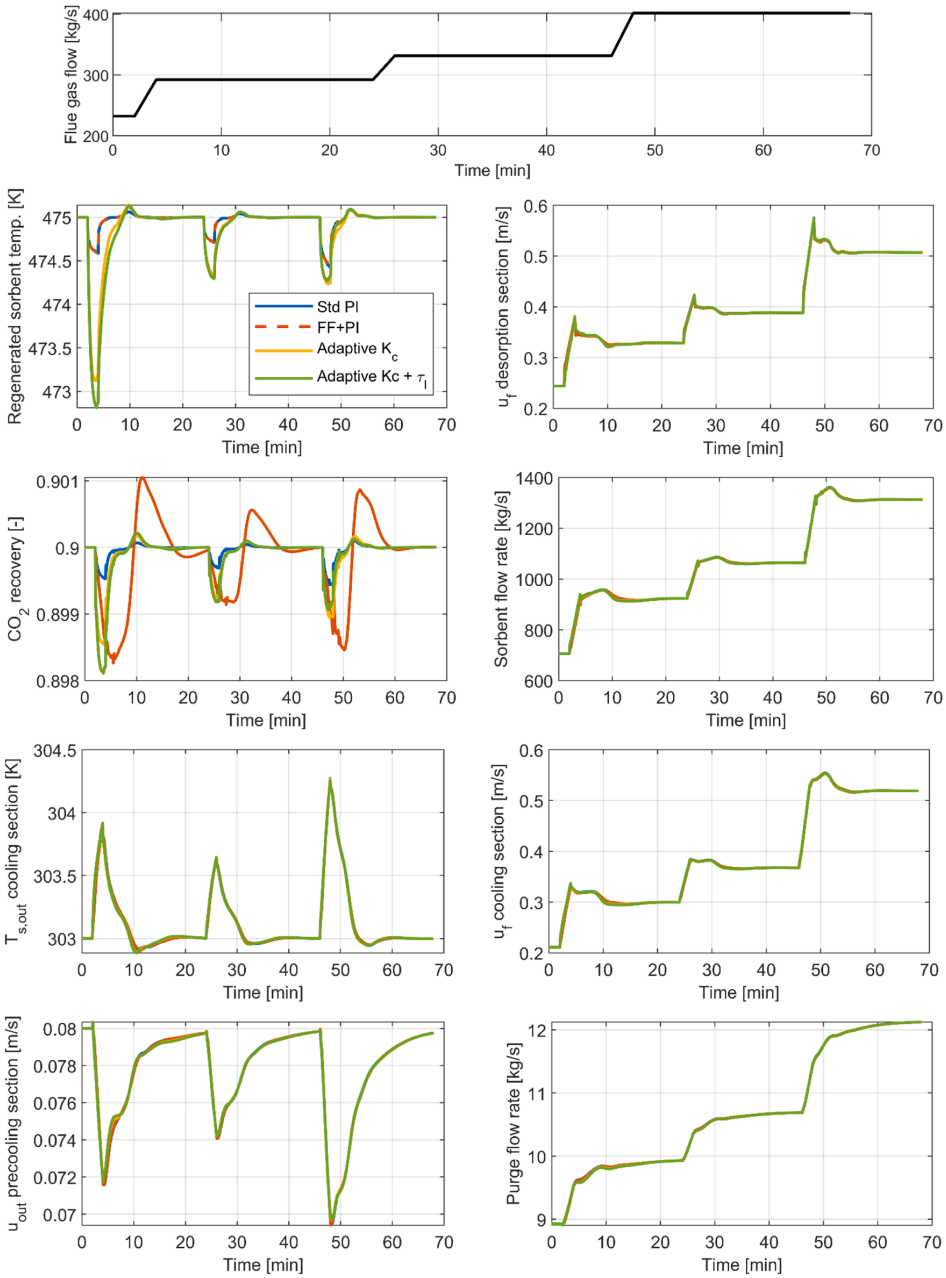

Fig. 6. Response of CVs (left) and MVs (right) to power plant load ramps between 40 and 100%. The top graph shows the variation in flue gas mass flow rate during the simulation.

In this scenario, the FF + PI scheme keeps the CO_2 recovery quite close to the setpoint for both positive and negative CO_2 concentration step changes, but it requires more time to settle due to the more robust tuning. The adaptively tuned controllers and the Std PI configuration show similar disturbance rejection profiles for CO_2 recovery. As in the previous scenarios, the FF + PI and Std PI configurations control the regenerated sorbent temperature most efficiently.

4.4. Varying external heat source temperature

In Fig. 9, the responses of higher-level CVs and MVs to a 20 K reduction in the hot fluid inlet temperature at full load are shown. This scenario emulates a change in power plant operation that leads to reduced temperature of the extracted steam to the CO_2 capture process. To maintain similar driving forces for heat transfer as in the nominal

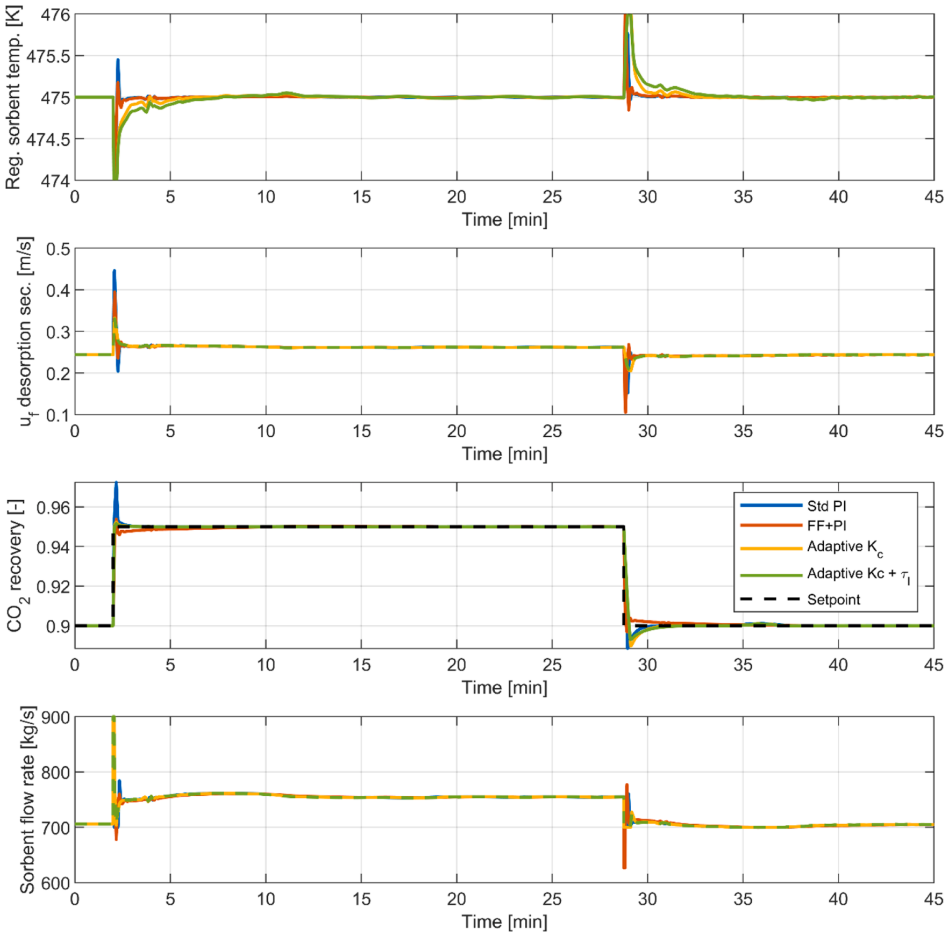

Fig. 7. Response of higher-level CVs and MVs to CO_2 recovery setpoint changes at 40% load.

case, the setpoint for the regenerated sorbent temperature is simultaneously reduced to 455 K. The adaptive cases are not included since they will give almost identical results as the Std PI configuration at full load.

A lower regenerated sorbent temperature increases the lean CO_2 loading of the adsorbent particles entering the adsorption section, leading to a reduction in the cyclic working capacity. To maintain the CO_2 recovery requirement of 90%, a significant increase in the sorbent mass flow rate is observed.

4.5. Effect of measurement delays

When generating the results presented in Sections 4.1–4.4, it was assumed that all measurements and control actions take place without delay. This is not achievable in practice. In this section, the effect of delays on the closed-loop behavior is studied by introducing measurement delays of 15 s for the CO_2 recovery and 5 s for the regenerated sorbent temperature. Compared to the previously presented scenarios, controllers with larger delay margins were required in this case to avoid instabilities. Therefore, the closed-loop time constant was increased to $\tau_c = \tau$ for the Std PI and FF + PI CO_2 recovery controllers and $\tau_c = \tau/4$ for all regenerated sorbent temperature controllers. Since the adaptive controllers are made less aggressive at lower loads, a closed-loop time constant of $\tau_c = \tau/2$ for CO_2 recovery could be applied without causing unstable behavior.

In Fig. 10, the responses of higher-level CVs and MVs to a ramp from 60 to 80% power plant load when considering measurement delays are shown. In the feedforward part of the FF + PI controller, the sorbent flow rate during the ramp is increased independently of the CO_2 recovery measurement. This keeps the CO_2 recovery closer to its setpoint than the other configurations at the start of the simulation. In this scenario, the adaptive control schemes demonstrate tighter control of the CO_2 recovery than the Std PI configuration since they can handle more aggressive tuning. For the regenerated sorbent temperature, a smaller initial reduction is seen for the Std PI case since the sorbent flow rate changes more slowly in this configuration. The shortest regenerated sorbent temperature settling time is observed for the FF + PI controller. In general, the settling times observed in this scenario are longer than in the previous cases, showing that delays have a significant effect on the controllers.

4.6. Summary of quantified controller performance

In Table 4, the IAE values for CO_2 recovery and regenerated sorbent temperature for ramps from 40 to 100% load, recovery setpoint changes

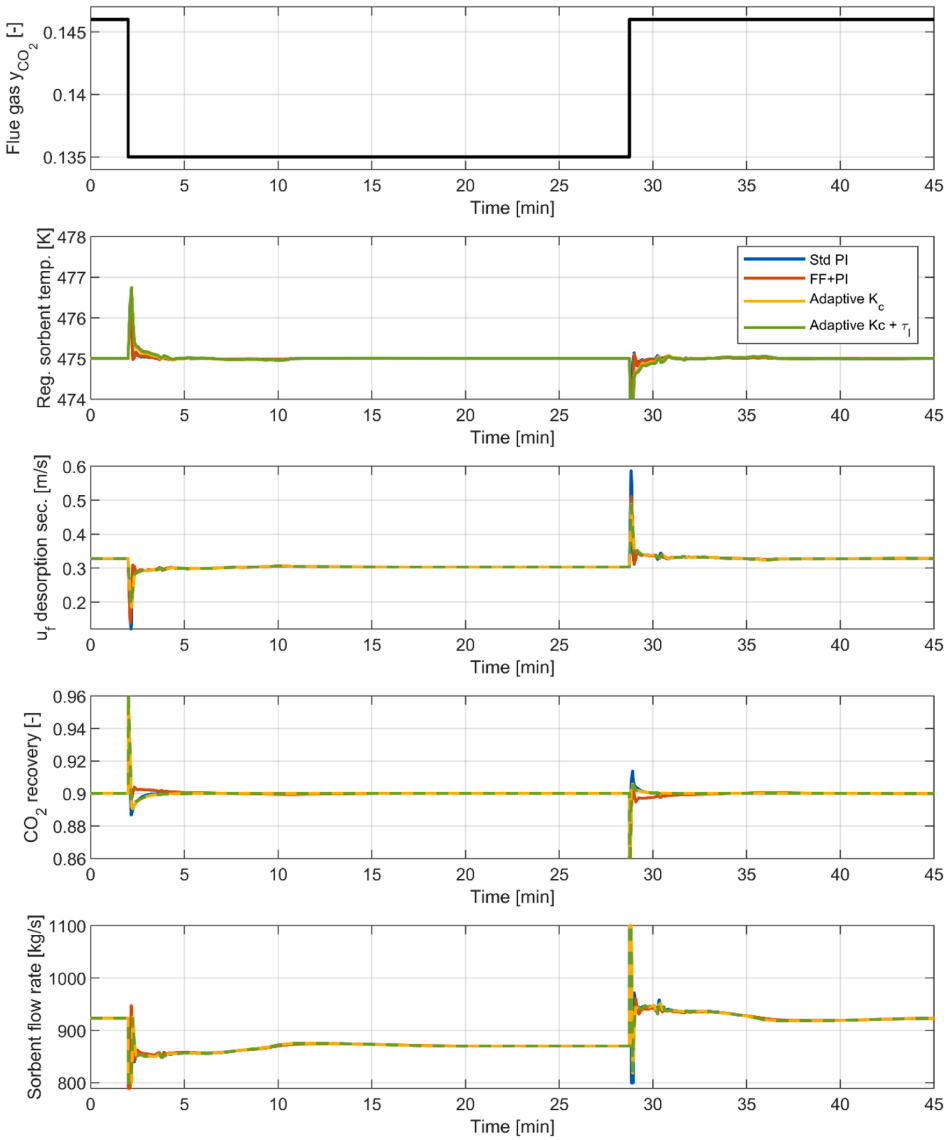

Fig. 8. Response of higher-level CVs and MVs to step changes in flue gas feed CO_2 concentration at 60% load.

at 40% load and flue gas feed CO_2 concentration at 60% load are reported. The selected cases are expected to be representative examples of the relative controller performance without measurement delays.

The Std PI configuration achieved the lowest CO_2 recovery IAE values in all three scenarios. However, similar values are observed for the adaptively tuned PI controllers. Slightly lower IAE values are obtained by adjusting both the integral time and controller gain. For regenerated sorbent temperature, the FF + PI configuration has the lowest IAE values. For this CV, the adaptive $K_c + \tau_I$ configuration has higher IAE values than the adaptive K_c case in all scenarios.

In Table 5, the IAE values for CO_2 recovery and regenerated sorbent temperature for the 60–80% power plant load ramp with measurement delays are given. Since the controllers are slower in this scenario, significantly larger values than in Table 4 are obtained.

5. Discussion

The dynamic scenarios investigated in this work demonstrate the benefits and drawbacks of the enhanced single-loop configurations compared to the standard PI reference case. For the results presented in Sections 4.1–4.4, it was assumed that all variables needed in the control system are measurable without delay and that control actions can be implemented instantaneously. This is not achievable in practice, and these results should therefore be seen as optimistic predictions of controller performance. In these scenarios, the adaptively tuned controllers give smoother and narrower MV profiles than the other configurations, which is important in a real-life installation due to less wear on valves and other process equipment. These controllers also showed the best CO_2 recovery setpoint tracking performance. Modifying both the

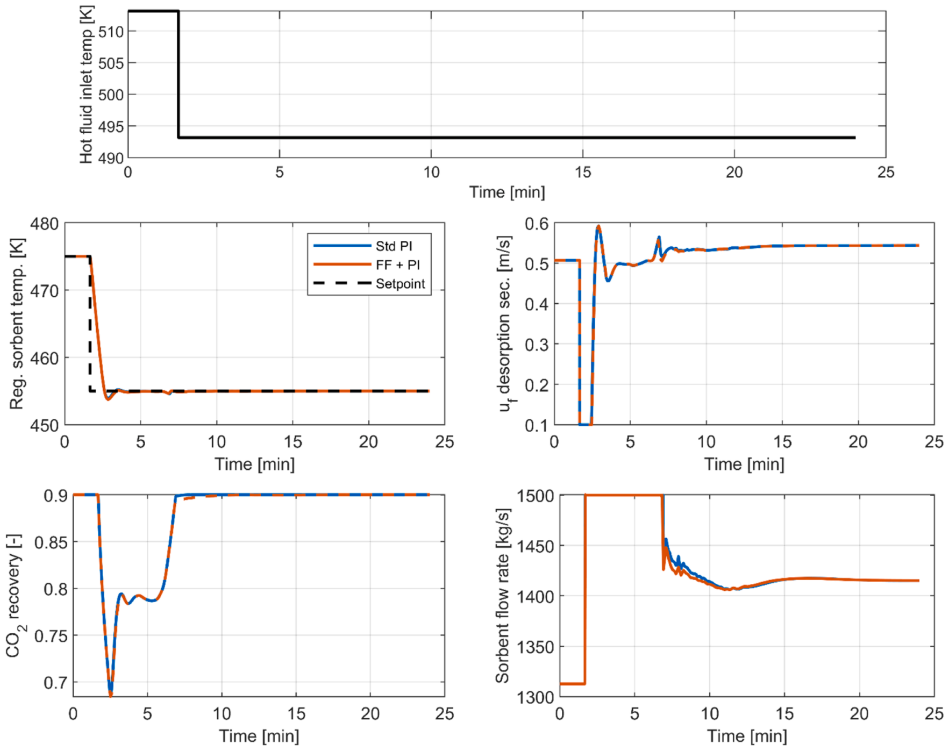

Fig. 9. Response of higher-level CVs and MVs to a simultaneous change in hot fluid inlet temperature and regenerated sorbent temperature setpoint at 100% load. The top graph shows the step change in hot fluid inlet temperature at $t = 1.67$ min.

integral time and controller gain does not significantly improve the controller performance compared to only adjusting the controller gain. This indicates that K_c is the most important parameter for adaptive tuning.

Except for CO_2 feed concentration disturbance rejection, the FF + PI configuration did not improve the control of CO_2 recovery compared to the reference case when no measurement delays were considered. The main benefit of this configuration was better control of the regenerated sorbent temperature. A possible explanation of this improvement is that the combined feedback and feedforward structure contributes to a better decoupling of the recovery and sorbent temperature control loops. This suggests that implementing decoupling approaches such as the one proposed by Shinskey (1977) or the use of model predictive control methods with inherent handling of coupled variables could improve the control of the MBTSA process. More detailed evaluation of this topic and testing of such approaches is left for future work.

In Sections 4.1–4.4, no significant differences between the performance of the different control configurations are observed. Since no delays or noise is considered in these scenarios, the controllers can be tuned with small closed-loop time constants, prioritizing controller speed over robustness. As a result, the settling time is short for all four control schemes and the Std PI configuration would be recommended due to its lower complexity. Another factor contributing to short settling times is the assumption that any change in the sorbent flow rate is instantly introduced in all sections of the MBTSA process.

When measurement delays are considered, the advantages of the enhanced single-loop control schemes compared to the standard PI configuration become more evident. A faster CO_2 recovery response is achieved by the adaptive controllers since they can handle more aggressive controller tuning. The feedforward part of the FF + PI configuration leads to closer CO_2 recovery tracking during changes in power plant load. A more detailed investigation of the effect of delays is suggested for future work. This could include studying delays in the manipulated variable control action, which would be more realistic than the assumption of instantaneous action applied in this work. In practice, measurements can be noisy, for example due to sensor inaccuracies or estimation errors for variables that are not possible to measure directly. To account for this, the effect of signal noise could be considered. This would require even more emphasis on controller robustness. Furthermore, the effect of delays in other types of dynamic scenarios could be studied.

The results from Section 4.4 show that the MBTSA process can maintain the desired CO_2 recovery under disturbances in the external heat source temperature. However, we do not consider the effect of such changes in operation on the specific regeneration duty (SRD) of the process. Since the SRD is an important part of the operating costs of the CO_2 capture plant, it would be interesting to include in future work. The control strategies considered in this work are not able to handle constraints, but using an MPC-based control strategy would allow the consideration of additional variables such as the SRD in the control problem.

6. Conclusion

In the coming years, it is likely that flexible operation of post-combustion CO_2 capture from thermal power plants will be necessary to reduce greenhouse gas emissions in an energy system with increasing shares of variable renewable energy sources. In this context, efficient process control systems for the capture plant are needed to ensure safe and robust operation. This work considers a Zeolite 13X-based moving

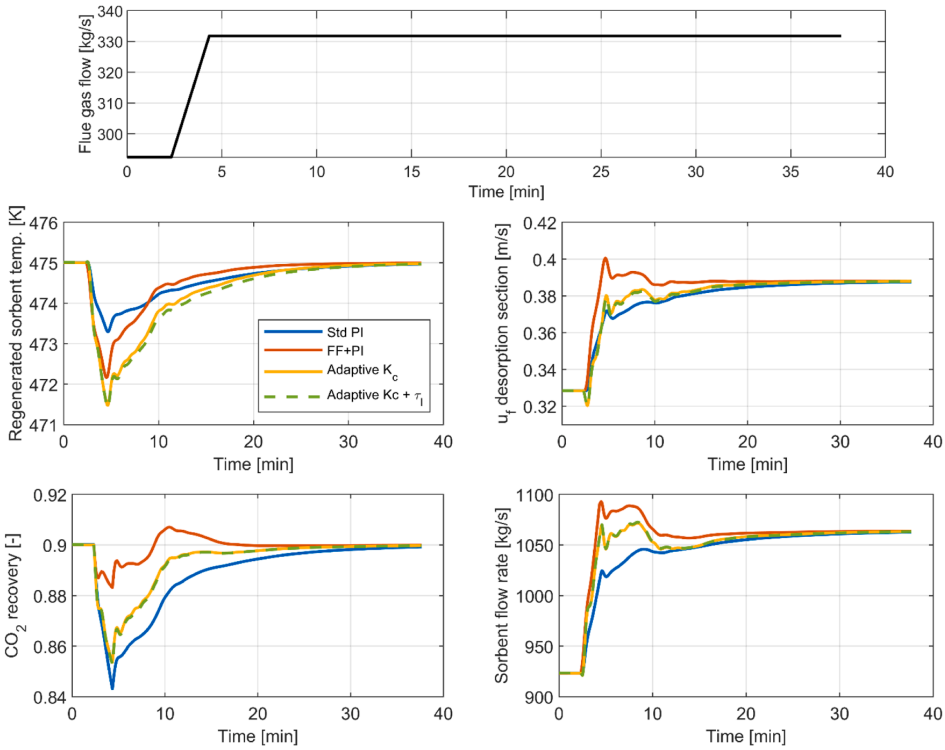

Fig. 10. Response of higher-level CVs and MVs to a ramp from 60 to 80% power plant load with a 15 s delay in the CO_2 recovery measurement and 5 s delay in the regenerated sorbent temperature measurement. The top graph shows the flue gas mass flow rate ramp starting at $t = 1.67$ min.

Table 4
IAE values for CO_2 recovery and regenerated sorbent temperature for selected controller test simulations without measurement delays. The lowest IAE value from each scenario is shown in bold.

	Ramps from 40 to 100% load		Recovery SP changes at 40% load		Flue gas y_{CO_2} steps at 60% load	
Control scheme	IAE CO_2 recovery	IAE reg. sorbent temp.	IAE CO_2 recovery	IAE reg. sorbent temp.	IAE CO_2 recovery	IAE reg. sorbent temp.
Std PI	**0.213**	185.4	**0.925**	37.53	**0.914**	45.64
FF + PI	1.801	**181.0**	1.518	**34.68**	1.477	**42.94**
Adaptive *Kc*	0.534	530.3	0.971	109.2	0.952	83.90
Adaptive $Kc + \tau_I$	0.578	593.4	0.946	142.6	0.941	92.14

Table 5
IAE values for CO_2 recovery and regenerated sorbent temperature for a 60–80% power plant load ramp with measurement delays. The lowest IAE value from each scenario is shown in bold.

Control scheme	IAE CO_2 recovery	IAE reg. sorbent temp.
Std PI	25.17	**911.52**
FF + PI	**5.41**	928.13
Adaptive *Kc*	14.63	1491.22
Adaptive $Kc + \tau_I$	15.07	1645.80

bed temperature swing adsorption process designed to capture CO_2 from a large-scale coal-fired power plant. The analysis was based on dynamic simulations using a first principle-model built in gPROMS.

Two enhanced single-loop control strategies were implemented and compared with a standard PI configuration. Firstly, adaptive adjustment of the controller gains and integral times based on system load was studied for the CO_2 recovery and the regenerated sorbent temperature. In the second strategy, a cascade approach consisting of a combined feedback and ratio feedforward controller was used to control the CO_2 recovery. In addition to the higher-level control strategies, an identical regulatory control layer was included in all configurations. The different control configurations were tested with several dynamic scenarios that could be relevant for operation of a power plant with post-combustion CO_2 capture. This included power plant load ramps, setpoint changes for CO_2 recovery and regenerated sorbent temperature, variations in flue gas feed CO_2 concentration, changes in the external heat source temperature and the effect of measurement delays. Controller performance was evaluated both based on graphical comparison and using the integral absolute error as a quantitative metric.

All investigated control schemes provided satisfactory performance without steady state offsets, showing that the MBTSA process can be efficiently controlled for different types of scenarios. Nevertheless, the dynamic simulation results revealed benefits and drawbacks of the different approaches. The adaptively tuned controllers gave smoother and narrower manipulated variable profiles than the other configurations and showed the best performance for step changes in the CO_2 recovery setpoint. When measurement delays were included, the adaptive controllers achieved faster CO_2 recovery response for a power plant load

ramp than the reference case. However, these controllers showed less efficient control of the regenerated sorbent temperature. The results indicated that the controller gain is the most important parameter for adaptive tuning. The main benefit of the combined feedback and feed-forward structure in the case of no measurement delays was improved control of the regenerated sorbent temperature. This improvement is possibly caused by better decoupling of the higher-level control loops. When measurement delays were included, this control scheme showed a significant improvement in CO_2 recovery tracking compared to the standard PI configuration.

Several topics can be considered for future work. These include investigation of decoupling approaches for the higher-level control loops and making the mathematical model more representative of real-life operation by including additional delays and signal noise. Furthermore, model predictive control of the MBTSA process could give better handling of coupled variables and allow the inclusion of additional variables such as the specific regeneration duty in the control problem. An MBTSA test stand capturing CO_2 from a coal-fired power plant is currently under construction in Poland as part of the InnCapPlant project (Cracow University of Technology, 2023). Experimental campaigns at this facility will provide valuable information on operation of the process and necessary data for validation of the mathematical model.

CRediT authorship contribution statement

Vidar T. Skjervold: Conceptualization, Formal analysis, Investigation, Methodology, Software, Visualization, Writing – original draft. **Lars O. Nord:** Conceptualization, Funding acquisition, Methodology, Project administration, Supervision, Writing – review & editing.

Declaration of Competing Interest

The authors declare that they have no known competing financial interests or personal relationships that could have appeared to influence the work reported in this paper.

Data availability

Data will be made available on request.

Acknowledgements

We acknowledge financial support from the Polish-Norwegian Research Program for funding the InnCapPlant project (Grant NOR/POLNORCCS/0015/2019-00).

Appendix A Model equations and supplementary information on gPROMS model

The model equations in the gPROMS model are given in Table A.1.

As shown in Table A.1, the Virial model extension for multi-component gas mixtures was applied in this work. It uses the pure component isotherm parameters as input. The Virial model for pure component isotherms is given by:

$$P_i = \frac{q_i^*}{K_i} e^{\left(A_i q_i^* + B_i q_i^{*2}\right)} \tag{A.1}$$

where P is the pressure, q is the amount of gas adsorbed, and K is the Henry constant. This parameter was calculated with the Van't Hoff equation

$$K_i = K_i^{\infty}\left(\frac{-\Delta H_i}{RT_s}\right) \tag{A.2}$$

and the dependence of the Virial coefficients A and B with temperature was expressed by

$$A_i = A_{0,i} + \frac{A_{1,i}}{T_s} B_i = B_{0,i} + \frac{B_{1,i}}{T_s}. \tag{A.3}$$

Table A1
Model equations.

Mass balance in gas phase	$\varepsilon_c \frac{\partial C_i}{\partial t} + \frac{\partial (u C_i)}{\partial z} = \varepsilon_c \frac{\partial}{\partial z}\left(D_{z,i} C_T \frac{\partial Y_i}{\partial z}\right) - \frac{(1-\varepsilon_c-\xi) a' k_{f,i}}{\mathrm{Bi}_i/5+1}(C_i - C_{p,i})$
Mass balance in macropores	$\varepsilon_p \frac{\partial C_{p,i}}{\partial t} + v_s \frac{\partial C_{p,i}}{\partial z} = \varepsilon_p \frac{15 D_{p,i}}{r_p^2} \frac{\mathrm{Bi}_i}{5+\mathrm{Bi}_i}(C_i - C_{p,i}) - \rho_p\left(\frac{\partial q_i}{\partial t} + v_s \frac{\partial q_i}{\partial z}\right)$
Mass balance in solid phase	$\frac{\partial q_i}{\partial t} + v_s \frac{\partial q_i}{\partial z} = \frac{15 D_{c,i}}{r_c^2}(q_i^* - q_i)$
Momentum bal. (adsorption section)	$-\frac{\partial \boldsymbol{P}}{\partial z} = 2\boldsymbol{u}(1-\boldsymbol{\varepsilon_c}-\boldsymbol{\xi})(\boldsymbol{\rho_p}-\boldsymbol{\rho_g})$
Momentum bal. (other sections)	$-\frac{\partial \boldsymbol{P}}{\partial z} = \frac{150\boldsymbol{\mu}(1-\boldsymbol{\varepsilon_c})^2}{\boldsymbol{\varepsilon_c^3 d_p^2}}\boldsymbol{u} + \frac{1.75(1-\boldsymbol{\varepsilon_c})\boldsymbol{\rho_g}}{\boldsymbol{\varepsilon_c^3 d_p}}\lvert\boldsymbol{u}\rvert\boldsymbol{u}$
Energy balance in gas phase	$\varepsilon_c C_T \hat{c}_v \frac{\partial T}{\partial t} + u C_T \hat{c}_p \frac{\partial T}{\partial z} = \frac{\partial}{\partial z}\left(\lambda_g \frac{\partial T}{\partial z}\right) - (1-\varepsilon_c-\xi)\, a' h_{gs}(T - T_s) - \alpha_{gt} h_{gw}(T - T_w)$
Energy balance in solid phase	$\left[(1-\varepsilon_c-\xi)\left(\rho_p c_{p,s} + \varepsilon_p \sum_i C_{p,i}\hat{c}_{v,i} + \rho_p \sum_i q_i \hat{c}_{v,i}\right) + \xi \rho_{pk} c_{p,pk}\right]\left(\frac{\partial T_s}{\partial t} + v_s \frac{\partial T_s}{\partial z}\right) = (1-\varepsilon_c-\xi)\varepsilon_p R T_s \sum_i \left[\frac{\partial C_{p,i}}{\partial t} + v_s \frac{\partial C_{p,i}}{\partial z}\right] + \xi \frac{\partial}{\partial z}\left(\lambda_{pk} \frac{\partial T_s}{\partial z}\right) + (1-\varepsilon_c-\xi) a' h_{gs}(T - T_s) + (1-\varepsilon_c-\xi)\rho_p \sum_i \left(-\Delta H_i \left[\frac{\partial q_i}{\partial t} + v_s \frac{\partial q_i}{\partial z}\right]\right)$
Energy balance in the HX-wall	$\rho_w c_{p,w} \frac{\partial T_w}{\partial t} = \alpha_{w,ext} h_{gw}(T - T_w) - \alpha_{w,int} h_{fw}(T_w - T_f)$
Energy balance in the HX-fluid	$\rho_f c_{p,f} \frac{\partial T_f}{\partial t} = -\, u_f \rho_f c_{p,f} \frac{L_z}{L_x} \frac{\partial T_f}{\partial z} - \alpha_{w,int} h_{fw}(T_f - T_w)$
Adsorption equilibrium	$P_i = \frac{q_i^*}{K_i} \exp\left[\sum_{j=1}^{N} A_{ij} q_j^* + \sum_{j=1}^{N}\sum_{k=1}^{N} B_{ijk} q_j^* q_k^*\right]$
	$A_{ij} = \frac{A_i + A_j}{2};\ B_{ijk} = \frac{B_i + B_j + B_k}{3}$

The pure component parameters used in this work are shown in Table A.2.
In Table A.3, the correlations used in the gPROMS model are shown.
In Table A.4, values of fixed parameters used in the model are provided.

Table A2
Pure component virial isotherm parameters for CO_2 and N_2 on Zeolite 13X (Mondino et al., 2019).

	K^{∞} x 10^7 mol/(kg kPa)	− ΔH kJ/mol	A_0 kg/mol	A_1 kg K/mol	B_0 (kg/mol)^2	B_1 kg^{2}K/mol^2
CO_2	1.61935	44.7838	0.4220	7.8371	−0.0485	34.8669
N_2	5.48207	22.6591	−13.037	3889.5	24.961	−7213.8

Table A3
Correlations used in gPROMS model.

Binary diffusivity	$D_{ij} = \frac{0.01883T^{3/2}}{P\sigma_{ij}^2\Omega_{D_{ij}}}\sqrt{\frac{1}{M_{w,i}}+\frac{1}{M_{w,j}}}$
Molecular diffusivity	$D_m = \frac{1-y_i}{\sum_{j\neq i}^{n}\frac{y_j}{D_{ij}}}$
Knudsen diffusivity	$D_k = 97r_p\sqrt{\frac{T}{M_w}}$
Macropore diffusivity	$\frac{1}{D_p} = \tau_p\left(\frac{1}{D_k}+\frac{1}{D_m}\right)$
Axial dispersion coefficient	$D_z = \frac{D_m}{\epsilon_c}(20 + 0.5\,Sc\,Re)$
Adsorption rate in micropores	$\frac{D_c}{r_c^2} = \frac{D_c^0}{r_c^2}\exp\left(-\frac{E_a}{RT}\right)$
Axial thermal conductivity of gas	$\lambda_g = k_g(7 + 0.5\,\mathrm{Pr}\,Re)$
Sherwood number correlation	$\mathrm{Sh} = 2.0 + 1.1\mathrm{Re}^{0.6}\mathrm{Sc}^{1/3}$
Nusselt number correlation	$\mathrm{Nu} = 2.0 + 1.1\mathrm{Re}^{0.6}\mathrm{Pr}^{1/3}$

Table A4
Values of fixed parameters used in the gPROMS model.

Parameter	Value	Unit	Parameter	Value	Unit
ρ_f	1000	kgm^{-3}	λ_{pk}	0.001	W m^{-1} K^{-1}
ρ_p	924	kgm^{-3}	$c_{p,f}$	4200	J kg^{-1} K^{-1}
ρ_{pk}	1000	kgm^{-3}	$c_{p,pk}$	500	J kg^{-1} K^{-1}
ρ_w	4420	kgm^{-3}	$c_{p,s}$	880	J kg^{-1} K^{-1}
r_p	0.35	mm	$c_{p,w}$	526	J kg^{-1} K^{-1}
ϵ_c (ads *sec.*)	0.8	–	h_{fw}	5000	W m^{-2} K^{-1}
ϵ_c (other *sec.*)	0.6	–	h_{gw}	150	W m^{-2} K^{-1}
ϵ_p	0.34	–	L_x	47.5	m
ξ	0.05	–	L_z	1	m

References

Akinola, T.E., Oko, E., Wu, X., Ma, K., Wang, M., 2020. Nonlinear model predictive control (NMPC) of the solvent-based post-combustion CO_2 capture process. Energy 213, 118840. https://doi.org/10.1016/j.energy.2020.118840.

Cormos, A.M., Vasile, M., Cristea, M.V., 2015. Flexible operation of CO_2 capture processes integrated with power plant using advanced control techniques. Comput. Aided Chem. Eng. 37, 1547–1552. https://doi.org/10.1016/B978-0-444-63577-8.50103-0.

Cracow University of Technology, 2023. InnCapPlant project [WWW Document]. URL https://ke.pk.edu.pl/en/inncapplant-project/ (accessed 5.11.23).

Cristea, V.M., Burca, M.I., Ilea, F.M., Cormos, A.M., 2020. Efficient decentralized control of the post combustion CO_2 capture plant for flexible operation against influent flue gas disturbances. Energy 205, 117960. https://doi.org/10.1016/j.energy.2020.117960.

Cui, X., Xu, P., Song, G., Gu, H., Gu, H., Wang, L., Zhu, H., 2022. PID control of a superheated steam temperature system based on integral gain scheduling. Energies 15, 1–16. https://doi.org/10.3390/en15238978.

Dhoke, C., Zaabout, A., Cloete, S., Amini, S., 2021. Review on reactor configurations for adsorption-based CO_2 capture. Ind. Eng. Chem. Res. 60, 3779–3798. https://doi.org/10.1021/acs.iecr.0c04547.

Dziejarski, B., Krzyżyńska, R., Andersson, K., 2023. Current status of carbon capture, utilization, and storage technologies in the global economy: a survey of technical assessment. Fuel 342. https://doi.org/10.1016/j.fuel.2023.127776.

European Commission, 2019. Communication From The Commission To The European Parliament. The European Council, Brussels. The Council, THE EUROPEAN ECONOMIC AND SOCIAL COMMITTEE AND THE COMMITTEE OF THE REGIONS: The European Green Deal.

Gardarsdóttir, S., Montañés, R.M., Normann, F., Nord, L.O., Johnsson, F., 2017. Effects of CO_2-absorption control strategies on the dynamic performance of a supercritical pulverized-coal-fired power plant. Ind. Eng. Chem. Res. 56, 4415–4430. https://doi.org/10.1021/acs.iecr.6b04928.

Gardarsdóttir, S.Ó., Normann, F., Andersson, K., Prölß, K., Emilsdóttir, S., Johnsson, F., 2015. Post-combustion CO_2 capture applied to a state-of-the-art coal-fired power plant-The influence of dynamic process conditions. Int. J. Greenh. Gas Control 33, 51–62. https://doi.org/10.1016/j.ijggc.2014.12.001.

Gaspar, J., Ricardez-Sandoval, L., Jørgensen, J.B., Fosbøl, P.L., 2016. Controllability and flexibility analysis of CO_2 post-combustion capture using piperazine and MEA. Int. J. Greenh. Gas Control 51, 276–289. https://doi.org/10.1016/j.ijggc.2016.06.003.

Gonzalez-Salazar, M.A., Kirsten, T., Prchlik, L., 2018. Review of the operational flexibility and emissions of gas- and coal-fired power plants in a future with growing renewables. Renew. Sustain. Energy Rev. 82, 1497–1513. https://doi.org/10.1016/j.rser.2017.05.278.

Hasan, M.M.F., Zantye, M.S., Kazi, M.K., 2022. Challenges and opportunities in carbon capture, utilization and storage: a process systems engineering perspective. Comput. Chem. Eng. 166, 107925 https://doi.org/10.1016/j.compchemeng.2022.107925.

Hernandez, A., Desideri, A., Gusev, S., Ionescu, C.M., Van Den Broek, M., Quoilin, S., Lemort, V., De Keyser, R., 2017. Design and experimental validation of an adaptive control law to maximize the power generation of a small-scale waste heat recovery system. Appl. Energy 203, 549–559. https://doi.org/10.1016/j.apenergy.2017.06.069.

IEA, 2023. CO2 Emissions in 2022. Paris.

IEA, 2022. World Energy Outlook 2022. Paris.

IEA, 2020. The role of CCUS in low-carbon power systems. Paris.

IPCC, 2018. Global Warming of 1.5°C. An IPCC Special Report on the impacts of global warming of 1.5°C above pre-industrial levels and related global greenhouse gas emission pathways, in the context of strengthening the global response to the threat of climate change.

Jung, H., Im, D., Heo, S., Kim, B., Lee, J.H., 2020. Dynamic analysis and linear model predictive control for operational flexibility of post-combustion CO_2 capture processes. Comput. Chem. Eng. 140 https://doi.org/10.1016/j.compchemeng.2020.106968.

Jung, W., Lee, J., 2022. Economic evaluation for four different solid sorbent processes with heat integration for energy-efficient CO_2 capture based on PEI-silica sorbent. Energy 238, 121864. https://doi.org/10.1016/j.energy.2021.121864.

Kazemifar, F., 2022. A review of technologies for carbon capture, sequestration, and utilization: cost, capacity, and technology readiness. Greenh. Gases Sci. Technol. 12, 200–230. https://doi.org/10.1002/ghg.2131.

Knaebel, K.S., 2009. Temperature swing adsorption system. US8353978B2.

Lawal, A., Wang, M., Stephenson, P., Koumpouras, G., Yeung, H., 2010. Dynamic modelling and analysis of post-combustion CO_2 chemical absorption process for coal-fired power plants. Fuel 89, 2791–2801. https://doi.org/10.1016/j.fuel.2010.05.030.

Lawal, A., Wang, M., Stephenson, P., Obi, O., 2012. Demonstrating full-scale post-combustion CO_2 capture for coal-fired power plants through dynamic modelling and simulation. Fuel 101, 115–128. https://doi.org/10.1016/j.fuel.2010.10.056.

Liao, P., Li, Y., Wu, X., Wang, M., Oko, E., 2020. Flexible operation of large-scale coal-fired power plant integrated with solvent-based post-combustion CO_2 capture based on neural network inverse control. Int. J. Greenh. Gas Control 95, 102985. https://doi.org/10.1016/j.ijggc.2020.102985.

Liao, P., Wu, X., Wang, M., Li, Z., Qian, F., 2023. Robust control and flexible operation for commercial-scale coal-fired power plant with solvent-based post-combustion carbon capture. Int. J. Greenh. Gas Control 123, 103831. https://doi.org/10.1016/j.ijggc.2023.103831.

Montañés, R.M., GarÞarsdóttir, S.O., Normann, F., Johnsson, F., Nord, L.O., 2017. Demonstrating load-change transient performance of a commercial-scale natural gas combined cycle power plant with post-combustion CO_2 capture. Int. J. Greenh. Gas Control 63, 158–174. https://doi.org/10.1016/j.ijggc.2017.05.011.

Mechleri, E., Lawal, A., Ramos, A., Davison, J., Mac Dowell, N., 2017. Process control strategies for flexible operation of post-combustion CO_2 capture plants. Int. J. Greenh. Gas Control 57, 14–25. https://doi.org/10.1016/j.ijggc.2016.12.017.

Merel, J., Clausse, M., Meunier, F., 2008. Experimental investigation on CO_2 post-combustion capture by indirect thermal swing adsorption using 13X and 5A zeolites. Ind. Eng. Chem. Res. 47, 209–215. https://doi.org/10.1021/ie071012x.

Modekurti, S., Eslick, J., Omell, B., Bhattacharyya, D., Miller, D.C., Zitney, S.E., 2017. Design, dynamic modeling, and control of a multistage CO_2 compression system. Int. J. Greenh. Gas Control 62, 31–45. https://doi.org/10.1016/j.ijggc.2017.03.009.

Mondino, G., Grande, C.A., Blom, R., 2017. Effect of gas recycling on the performance of a moving bed temperature-swing (MBTSA) process for CO_2 capture in a coal fired power plant context. Energies 10. https://doi.org/10.3390/en10060745.

Mondino, G., Grande, C.A., Blom, R., Nord, L.O., 2022. Evaluation of MBTSA technology for CO_2 capture from waste-to-energy plants. Int. J. Greenh. Gas Control 118, 103685. https://doi.org/10.1016/j.ijggc.2022.103685.

Mondino, G., Grande, C.A., Blom, R., Nord, L.O., 2019. Moving bed temperature swing adsorption for CO_2 capture from a natural gas combined cycle power plant. Int. J. Greenh. Gas Control 85, 58–70. https://doi.org/10.1016/j.ijggc.2019.03.021.

Montañés, R.M., Flø, N.E., Nord, L.O., 2018. Experimental results of transient testing at the amine plant at Technology Centre Mongstad: open-loop responses and performance of decentralized control structures for load changes. Int. J. Greenh. Gas Control 73, 42–59. https://doi.org/10.1016/j.ijggc.2018.04.001.

Morales-Ospino, R., Santos, V.N., Lima, A.R.A., Torres, A.E.B., Vilarrasa-García, E., Bastos-Neto, M., Cavalcante, C.L., Azevedo, D.C.S., Marques, C.R.M., De Aquino, T. F., Vasconcelos, L.B., Knaebel, K.S., 2021. Parametric analysis of a moving bed temperature swing adsorption (MBTSA) process for postcombustion CO_2 capture. Ind. Eng. Chem. Res. https://doi.org/10.1021/acs.iecr.0c05067.

Nie, L., Mu, Y., Jin, J., Chen, J., Mi, J., 2018. Recent developments and consideration issues in solid adsorbents for CO_2 capture from flue gas. Chin. J. Chem. Eng. 26, 2303–2317. https://doi.org/10.1016/j.cjche.2018.07.012.

Nittaya, T., Douglas, P.L., Croiset, E., Ricardez-Sandoval, L.A., 2014. Dynamic modelling and control of MEA absorption processes for CO_2 capture from power plants. Fuel 116, 672–691. https://doi.org/10.1016/j.fuel.2013.08.031.

Okumura, T., Yoshizawa, K., Nishibe, S., Iwasaki, H., Kazari, M., Hori, T., 2017. Parametric testing of a pilot-scale design for a moving-bed CO_2 capture system using low-temperature steam. Energy Procedia 114, 2322–2329. https://doi.org/10.1016/j.egypro.2017.03.1369.

Okumura, T., Yoshizawa, K., Numaguchi, R., Nishibe, S., Kanou, A., Hasegawa, Y., Inoue, S., Tsuji, K., Fujita, S., Nabeshima, M., Yamada, H., Yamamoto, S., Takayama, N., Yogo, K., 2018. Demonstration plant of the kawasaki CO_2 capture (KCC) system with solid sorbent for coal-fired power station. SSRN Electron. J. https://doi.org/10.2139/ssrn.3365953.

Panahi, M., Skogestad, S., 2012. Economically efficient operation of CO_2 capturing process. Part II. Design of control layer. Chem. Eng. Process. Process Intensif. 52, 112–124. https://doi.org/10.1016/j.cep.2011.11.004.

Park, Y.C., Jo, S.H., Kyung, D.H., Kim, J.Y., Yi, C.K., Ryu, C.K., Shin, M.S., 2014. Test operation results of the 10 MWe-scale dry-sorbent CO_2 capture process integrated with a real coal-fired power plant in Korea. Energy Procedia 63, 2261–2265. https://doi.org/10.1016/j.egypro.2014.11.245.

Park, Y.J., Lee, S.J., Moon, J.H., Choi, D.K., Lee, C.H., 2006. Adsorption equilibria of O_2, N_2, and Ar on carbon molecular sieve and zeolites 10X, 13X, and LiX. J. Chem. Eng. Data 51, 1001–1008. https://doi.org/10.1086/505023.

Posch, S., Haider, M., 2013. Dynamic modeling of CO2 absorption from coal-fired power plants into an aqueous monoethanolamine solution. Chem. Eng. Res. Des. 91, 977–987. https://doi.org/10.1016/j.cherd.2012.09.016.

PSE, 2023. gPROMS ModelBuilder [WWW Document]. URL https://www.psenterprise.com/products/gproms/modelbuilder (accessed 3.29.23).

Raganati, F., Miccio, F., Ammendola, P., 2021. Adsorption of carbon dioxide for post-combustion capture: a review. Energy Fuels 35, 12845–12868. https://doi.org/10.1021/acs.energyfuels.1c01618.

Rúa, J., Hillestad, M., Nord, L.O., 2021. Model predictive control for combined cycles integrated with CO_2 capture plants. Comput. Chem. Eng. 146 https://doi.org/10.1016/j.compchemeng.2020.107217.

Samanta, A., Zhao, A., Shimizu, G.K.H., Sarkar, P., Gupta, R., 2012. Post-combustion CO_2 capture using solid sorbents: a review. Ind. Eng. Chem. Res. 51, 1438–1463. https://doi.org/10.1021/ie200686q.

Seborg, D., Edgard, T., Mellichamp, D., Doyle, F., 2016. Process Dynamics and Control, 4th ed. John Wiley & Sons, Hoboken, NJ.

Shinskey, F.G., 1977. The stability of interacting control loops with and without decoupling. IFAC Proc. 10, 21–30. https://doi.org/10.1016/B978-0-08-022010-9.50008-6. Vol.

Singh, S.P., Ku, A.Y., Macdowell, N., Cao, C., 2022. Profitability and the use of flexible CO_2 capture and storage (CCS) in the transition to decarbonized electricity systems. Int. J. Greenh. Gas Control 120. https://doi.org/10.1016/j.ijggc.2022.103767.

Sjostrom, S., Senior, C., 2020. Pilot testing of CO_2 capture from a coal-fired power plant - Part 2: results from 1-MWe pilot tests. Clean Energy 4, 12–25. https://doi.org/10.1093/ce/zkz034.

Skjervold, V.T., Mondino, G., Riboldi, L., Nord, L.O., 2023. Investigation of control strategies for adsorption-based CO_2 capture from a thermal power plant under variable load operation. Energy 268, 126728. https://doi.org/10.1016/j.energy.2023.126728.

Skogestad, S., 2003. Simple analytic rules for model reduction and PID controller tuning. J. Process Control 13, 291–309. https://doi.org/10.4173/mic.2004.2.2.

Tang, Z., Wu, X., 2023. Distributed predictive control guided by intelligent reboiler steam feedforward for the coordinated operation of power plant-carbon capture system. Energy 267, 126568. https://doi.org/10.1016/j.energy.2022.126568.

Thermoflow Inc, 2023. STEAM PRO and STEAM MASTER [WWW Document]. URL https://www.thermoflow.com/products_conventionalsteam.html (accessed 3.30.23).

Wei, G., Wang, Z., Li, W., Ma, L., 2014. A survey on gain-scheduled control and filtering for parameter-varying systems. Discret. Dyn. Nat. Soc. https://doi.org/10.1155/2014/105815.

Wu, X., Shen, J., Wang, M., Lee, K.Y., 2020a. Intelligent predictive control of large-scale solvent-based CO_2 capture plant using artificial neural network and particle swarm optimization. Energy 196, 117070. https://doi.org/10.1016/j.energy.2020.117070.

Wu, X., Wang, M., Liao, P., Shen, J., Li, Y., 2020b. Solvent-based post-combustion CO_2 capture for power plants: a critical review and perspective on dynamic modelling, system identification, process control and flexible operation. Appl. Energy 257, 113941. https://doi.org/10.1016/j.apenergy.2019.113941.

Wu, X., Wang, M., Shen, J., Li, Y., Lawal, A., Lee, K.Y., 2019. Flexible operation of coal fired power plant integrated with post combustion CO_2 capture using model predictive control. Int. J. Greenh. Gas Control 82, 138–151. https://doi.org/10.1016/j.ijggc.2018.12.004.

Zhao, R., Liu, L., Zhao, L., Deng, S., Li, S., Zhang, Y., 2019. A comprehensive performance evaluation of temperature swing adsorption for post-combustion carbon dioxide capture. Renew. Sustain. Energy Rev. 114, 109285 https://doi.org/10.1016/j.rser.2019.109285.

Zima, W., Grądziel, S., Cebula, A., Rerak, M., Kozak-Jagieła, E., Pilarczyk, M., 2023. Mathematical model of a power boiler operation under rapid thermal load changes. Energy 263. https://doi.org/10.1016/j.energy.2022.125836.

Applied Thermal Engineering 246 (2024) 122907

Contents lists available at ScienceDirect

Applied Thermal Engineering

journal homepage: www.elsevier.com/locate/apthermeng

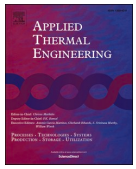

Research Paper

Thermal energy storage integration for increased flexibility of a power plant with post-combustion CO_2 capture

Vidar T. Skjervold *, Lars O. Nord

NTNU - Norwegian University of Science and Technology, Department of Energy and Process Engineering, Trondheim, Norway

ARTICLE INFO

Keywords:
Steam accumulator
Moving bed temperature-swing adsorption
Flexible operation
Primary reserve
Widened operating range
Coal-fired power plant

ABSTRACT

Flexible operation of thermal power plants will become increasingly relevant in the coming years. This work evaluates the effect of integrating a steam accumulator into a 598 MW supercritical coal-fired power plant with moving bed temperature-swing adsorption CO_2 capture. Charging the accumulator with reheat steam from the turbine train can reduce the net power output by up to 1.4 % (8.2 MW) for around 200 min. Small charging flow rates are recommended to maximize the final pressure of the accumulator. Covering the sorbent regeneration duty and meeting the demand of two feedwater heaters were considered as alternatives for discharging of the accumulator. Thermal storage discharging was found to give relative power plant load increases between 1.7 and 11.2 % (10.2–66.9 MW) for up to 37.5 min, which exceeds the requirement for primary reserve. Increases in the electrical energy output of 10.5–11 MWh were achieved. The flexibility modes studied in this work are compatible with high CO_2 recovery rates.

1. Introduction

1.1. Background and motivation

Global CO_2 emissions related to energy and industrial processes increased by 321 Mt from 2021 to 2022, reaching an all-time high of 36.8 Gt [1]. To meet the target of net zero greenhouse gas emissions by 2050 [2], this trend must be reversed and then upheld to significantly reduce emissions in the coming years. The power sector stands for approximately 42 % of global CO_2 emissions [1] and will be central in the transition to a low-carbon society. In 2022, 61 % of global electricity generation came from fossil fuel-based thermal power plants. The dominant sources in the electricity mix were gas and coal, standing for respectively 22 % and 36 % of the total electricity production [3].

The operation of thermal power plants is likely to be affected in several ways by the foreseen changes in the energy system. The International Energy Agency estimates that 65 % of global electricity generation in 2050 will be met by renewables [4]. The intermittency of these energy sources represents a challenge since other means of electricity supply must be used to balance the demand. In addition to grid-scale energy storage solutions and demand response measures, flexible operation of thermal power plants is expected to be necessary to meet the residual load not covered by renewables, especially in the short to medium term [5]. Several flexibility modes will be relevant, including rapid power plant load changes, more frequent start-ups and shutdowns, reduced minimum loads and increased maximum electricity output [6]. Furthermore, it is likely that CO_2 capture from thermal power plants will be required during the transition to a renewable-based energy system to reduce emissions while maintaining energy supply security. In its pathways limiting the global temperature increase to 1.5 °C above pre-industrial levels, the Intergovernmental Panel on Climate Change includes significant deployment of carbon capture and storage on both natural gas and coal-fired units [7].

For power plants already in operation, post-combustion CO_2 capture is suitable due to the possibility of retrofit without requiring large modifications of the existing equipment [8]. Although chemical absorption has been demonstrated at full scale and is the state-of-the-art post-combustion capture technology [9], adsorption-based processes are interesting alternatives due to their potential for reduced energy requirements [10]. The CO_2 capture technology considered in this work is a moving bed temperature swing adsorption (MBTSA) process. The main advantage of the moving bed configuration compared to the conventional fixed bed system is the possibility of continuous operation [11], which avoids complex operation schedules, enables easier integration with the power plant and is beneficial for process control [12]. Previous modelling work has shown that this process can achieve high CO_2 recovery rates and CO_2 purity for a natural gas combined cycle

* Corresponding author.
E-mail address: vidar.t.skjervold@ntnu.no (V.T. Skjervold).

https://doi.org/10.1016/j.applthermaleng.2024.122907
Received 7 November 2023; Received in revised form 23 January 2024; Accepted 7 March 2024
Available online 9 March 2024

Nomenclature

ACRONYMS AND ABBREVIATIONS

FWH	Feedwater heater
G	Generator
HP	High-pressure
IP	Intermediate-pressure
LHV	Lower heating value
LP	Low-pressure
MBTSA	Moving bed temperature-swing adsorption
PCM	Phase change material
SRD	Specific regeneration duty

LATIN SYMBOLS

c_p	Specific heat capacity, J kg^{-1} K^{-1}
h	Specific enthalpy, J kg^{-1}
h'	Saturated water specific enthalpy, J kg^{-1}
h''	Saturated steam specific enthalpy, J kg^{-1}
ha	Heat transfer parameter, J K^{-1} s^{-1} m^{-3}
M	Mass inventory, kg
$\dot{m}$	Mass flow rate, kg s^{-1}
p	Pressure, Pa
$\dot{Q}$	Heat transfer rate, J/s
r	Latent heat of vaporization, J kg^{-1}
t	Time, s
T	Temperature, K
v	Specific volume, m^3 kg^{-1}
V	Volume, m^3

GREEK SYMBOLS

α	Isobaric expansivity, K^{-1}
κ	Isothermal compressibility, Pa^{-1}
ρ	Density, kg m^{-3}
τ	Relaxation time, s

SUBSCRIPTS

1	Water
2	Steam
21	Superheated steam – water interface
c	Condensation
e	Evaporation
i	Discharge location
in	Incoming flow
out	Outgoing flow
tank	Steam accumulator

power plant [13], coal-fired power plant [14] and waste-to-energy plant [15]. MBTSA has also been demonstrated experimentally at a scale of 40 tons of captured CO_2 per day [16].

1.2. Flexible operation of power plants with post-combustion CO_2 capture

Several strategies for flexible operation of power plants with post-combustion CO_2 capture have been investigated in the literature. A popular topic has been the development of control structures for the capture process with the aim of maintaining its performance under variable power plant operation. In this approach, the goal is to ensure that the capture process does not negatively influence the load-following capabilities of the power plant. For solvent-based CO_2 capture, both conventional and model predictive control approaches have been investigated, as summarized in the review of Wu et al. [17]. In our previous work we have developed control strategies for the MBTSA process for activated carbon [12] and Zeolite 13X [18] as the adsorbent material, showing that a high CO_2 recovery rate and CO_2 product purity can be achieved for various flexible power plant scenarios. The main drawback of this approach is that all changes in power plant load are driven by changes in the boiler firing rate, meaning that the rate of change is limited by thermal inertia in the steam generators. Furthermore, repeated load changes can impose large stresses on the process equipment. It is therefore of interest to study methods for achieving power plant flexibility without modifying the boiler operation.

CO_2 capture processes that utilize temperature swings for regeneration of the solvent or adsorbent require large amounts of thermal energy, which leads to a power plant efficiency penalty through extraction of additional steam from its steam cycle. However, this coupling also represents an additional mode of flexibility that can be used to rapidly change the power plant electricity output. Based on testing at the PACT pilot plant in the United Kingdom, Tait et al. showed that reducing or closing the flow of hot fluid to the reboiler can be used for grid balancing operations or maximizing electrical power output during periods of high electricity prices [19]. Zaman and Lee investigated a flexible mode where the CO_2 recovery rate setpoint was modified in response to variations in electricity demand and price [20]. The simultaneous deployment of a regenerated solvent storage was also considered. The strategy of reducing the steam flow rate to the reboiler has also been studied as a part of advanced control strategies for the combined power plant – carbon capture system. Wu et al. employed a collaborative control strategy where the extracted steam flow rate was temporarily reduced to achieve faster power plant load ramps [21]. Tang and Wu developed a neural network-based feedforward controller to determine the reboiler steam flow rate considering the trade-off between power output tracking and CO_2 capture performance [22]. The main disadvantage of these strategies is that the power plant flexibility improvements come at the expense of reduced CO_2 recovery rates. In a future situation where CO_2 emissions are penalized more strictly, it will be an advantage to utilize flexibilization strategies that are able to maintain high CO_2 recovery rates.

It was recently shown by Chen et al. that integration of energy storage into the power plant – carbon capture system can improve the plant economics by enabling rapid adjustment of the power output while keeping the CO_2 recovery rate at a high level [23]. A molten salt thermal storage, battery energy storage system and lean/rich solvent storage system were compared, and it was concluded that the battery system provided the best operating benefits with the drawback of large investment costs. Thermal energy storage technologies typically have a longer lifetime and lower levelized cost of electricity than battery-based systems [24] and could be preferable for storage with more than a few MW capacity [25]. Furthermore, thermal energy storage has the potential of utilizing existing infrastructure and equipment in the power plant, reducing the need for new investments. An energy storage unit contributes to boiler-turbine decoupling since it can be charged during periods of low demand and discharged when the demand is high, for example during a grid event or periods of high electricity prices [26]. In this work, we investigate how a thermal energy storage can be integrated into a coal-fired power plant with MBTSA-based CO_2 capture to provide flexibility.

1.3. Previous work on thermal energy storage

Using thermal energy storage to provide a stable supply of solar-based heat for solvent regeneration in CO_2 capture processes has received much attention in the literature [27]. Examples of considered combinations are thermochemical energy storage with calcium looping-based carbon capture [28], molten salt thermal storage with amine

solvent CO_2 capture from coal-fired [29] and natural gas-fired power plants [30] and phase change material thermal storage integrated with ammonia-based CO_2 capture for a coal-fired power plant [31]. In these studies, the main purpose of the thermal storage is to ensure continuous heat supply for the capture process, not to provide power plant flexibility. For coal-fired power plants without CO_2 capture, thermal storage integration as a flexibilization measure has been widely studied. A summary of energy storage technologies and integration options that have been investigated in this context is given in the next three paragraphs.

Kosman et al. studied a solar salt thermal energy storage system acting as a buffer between a supercritical and subcritical steam turbine [32]. The thermal storage is charged either via electrical heaters or excess steam from the supercritical turbine, which is fed by a coal-fired boiler always operating at full load to maximize efficiency. During periods of high demand, the hot molten salt is used to generate additional steam that is fed to the subcritical turbine. Zhang et al. investigated a similar energy storage system, where a combination of flue gas and superheated steam from the coal-fired boiler was used to heat up the molten salt [26]. Discharging of the energy storage is used to provide heat to feedwater heaters, which reduces the flow rate of extracted high and intermediate pressure steam and increases the electrical power output of the plant. A system consisting of two separate molten salt loops at different temperature levels was presented by Garbrecht et al. [33], where charging of the energy storage takes place by extracting additional steam from the turbine train. To provide positive reserve, the high-pressure steam turbine extraction is closed, and the high-temperature molten salt is used to cover additional reheat demand while the low-temperature loop is used for high-pressure feedwater heating. A disadvantage with molten salt-based energy storage systems is the requirement of several additional heat exchangers and significant modifications to the steam cycle, which increases complexity and investment costs.

In the work of Li and Wang, a high temperature storage system consisting of five phase change materials (PCM) in series was applied to provide grid frequency control and power plant load balancing [34]. Several charging strategies based on steam extraction from either the intermediate or low-pressure turbine inlet were studied. Heat from discharging of the thermal storage was used either to generate additional steam for the low-pressure turbine or to cover parts of the feedwater heating demand. Kruger et al. performed an evaluation of several storage technology - power plant integration combinations based on economic and technical requirements, concluding that a combined PCM – steam accumulator concept was promising [35]. Molten salt thermal storage and solid media heat storage were also identified as lead concepts by the study. In the case of solid media thermal storage, charging takes place by redirecting parts of the flue gas flow from the evaporator section of the boiler to heat up a solid material. The hot solid can then be used to preheat an additional air mass flow that is fed to the boiler, leading to higher live steam mass flow rates and increased electrical power production. Cao et al. presented an alternative concept where an additional supercritical Rankine cycle is retrofitted to a coal-fired power plant for peak electrical power production [36]. A high temperature thermal storage system is charged by an electric boiler during periods of low demand and used to generate steam for the additional Rankine cycle during periods of high electricity demand.

Using water or steam as the thermal energy storage medium avoids exergy losses associated with intermediate heat transfer loops, since the thermal storage can interact directly with the water/steam cycle of the power plant [26]. Trojan et al. evaluated the use of pressurized hot water tanks for widening of the load range and shortening start-up times of a 200 MW power unit [37]. The concept was found to be profitable unless the difference between high and low demand electricity prices is small. Richter et al. investigated the integration of a steam accumulator thermal storage into the power plant, reporting a minimum load reduction of up to 7.0 % and an additional net power supply of 4.3 % [38]. The accumulator is charged with superheated steam from the cold reheat at full load and live steam from the boiler at low loads. Discharged steam is used to cover the heating demand of one of the high-pressure feedwater heaters. A similar concept is studied by Stevanovic et al. [39], where an increase in the power plant load is achieved by sending discharged steam to two of the low pressure condensate heaters. In this case, a net power increase of 4.2 % of the nominal load is reported. An advantage of using steam as the thermal storage medium is the more efficient heat transfer compared to sensible heat sources [40]. Furthermore, it provides additional flexibility since the storage medium can also be fed directly to the steam turbines.

1.4. Knowledge gaps and scope of paper

The literature review shows that even though thermal energy storage integration is a promising method for enabling flexible operation of power plants with CO_2 capture, this topic has not received much attention in the literature. This work bridges several knowledge gaps and the main novel contributions are listed below:

1) The integration of a thermal energy storage system into a power plant with MBTSA post-combustion CO_2 capture has not previously been studied in the literature.
2) We compare two options for discharging of the thermal energy storage: regeneration of the CO_2 capture process and the use in feedwater heaters. A comparison of these two alternatives has not previously been made in the literature.
3) We perform a quantitative evaluation of the power plant flexibility increase achieved by thermal storage integration.

The research objective of this work is to carry out a model-based evaluation of how a steam accumulator can contribute to increased operational flexibility of a supercritical coal-fired power plant with MBTSA post-combustion CO_2 capture. The flexibility mode of interest is the net power output increase capability of the power plant, which can be employed both in the case of grid events or during periods of high electricity prices. Furthermore, we limit the scope of the paper to methods that are compatible with maintaining a high CO_2 recovery rate and do not significantly influence boiler operation.

The article is structured as follows. In Section 2, a description of the coal-fired power with integrated MBTSA and thermal storage is given. The modelling approach is explained in Section 3. Results are presented and discussed in Section 4 before the work is concluded in Section 5.

2. Coal-fired power plant with MBTSA and steam accumulator

2.1. Process description

The system considered in this work consists of three main sections: a supercritical coal-fired power plant, an MBTSA CO_2 capture process and a steam accumulator thermal energy storage. A flow diagram of the process is shown in Fig. 1. The design of the power plant is based on the supercritical pulverized coal-fired reference plant from NETL [41] and has a gross power output of 642 MW after CO_2 capture integration. The net power output after subtracting transformer losses and the electrical power requirement of fans, pumps, fuel delivery, flue gas treatment, ash handling and additional minor auxiliaries is 598 MW. The boiler delivers steam at 244 bar and 595 °C to the turbine train, which consists of one high pressure turbine, two intermediate pressure turbines and two low pressure turbines. A single reheat stage between the high pressure and intermediate pressure turbine is included. After leaving the condenser, boiler feedwater is heated by steam extracted from various ports along the steam turbine train. The feedwater heating train consists of seven heaters and a deaerator.

The flue gas generated from combustion of coal passes through an electrostatic precipitator, a wet flue gas desulfurization unit and a

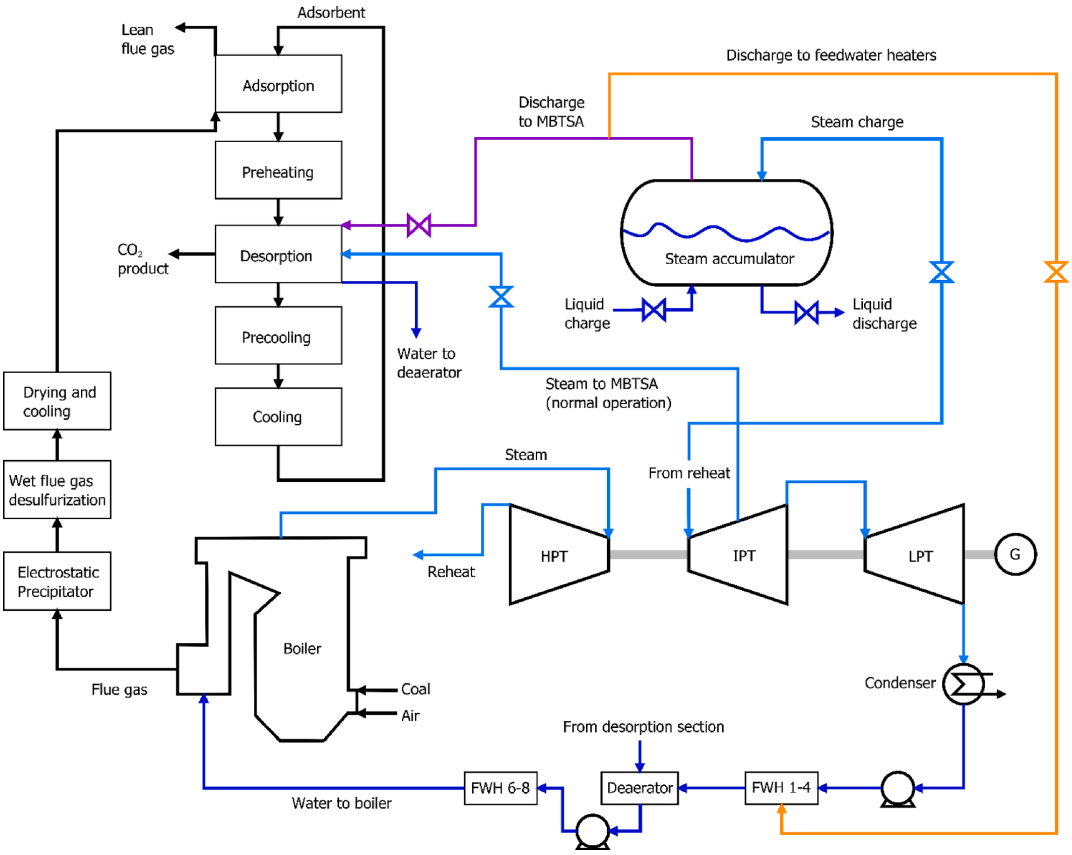

Fig. 1. Simplified flowsheet of supercritical coal-fired power plant with integrated MBTSA post-combustion CO_2 capture and steam accumulator thermal energy storage. HPT stands for high-pressure turbine, IPT stands for intermediate-pressure turbine, LPT stands for low-pressure turbine, G stands for generator and FWH stands for feedwater heater.

cooling and drying step after leaving the boiler. When leaving the desulfurization unit, the flue gas temperature is approximately 66 °C. It is cooled to 30 °C, which requires around 29 MW of cooling duty. Multiple options for flue gas dehydration exist, including refrigeration, compression and cooling, membranes and triethylene glycol absorption [42]. Adsorbents such as alumina or silica-based materials can also be applied [43]. The cooled and dried gas is sent to the adsorption section of the MBTSA process, where it moves counter-currently to the Zeolite 13X adsorbent, transferring CO_2 to the solid phase. The CO_2-lean flue gas leaves the top of the adsorption section and the CO_2-loaded adsorbent leaves at the bottom. The adsorbent is heated up in the preheating and desorption sections to a final temperature of 202 °C, releasing CO_2 that is collected in a high purity stream. During normal operation, steam is extracted from a port in the intermediate pressure turbine to provide heat to the desorption section. At full load, the extracted steam for sorbent regeneration is at 28.1 bar and 508 °C. The saturated water that leaves the desorption section is fed to the shell of the deaerator. Before entering the adsorption section, the adsorbent is cooled in the precooling and cooling sections to complete the cycle. Due to the large flow of flue gas, two parallel carbon capture units are employed, each processing 402 kg/s of flue gas. At nominal conditions, the MBTSA process captures 90.0 % of the CO_2 in the flue gas and delivers CO_2 with a purity of 96.1 %. The key characteristics of the power plant – carbon capture system at nominal load are summarized in Table 1.

During periods of low electricity prices or demand from the market, the power plant electrical output can be reduced by charging the steam accumulator. This involves sending a fraction of the reheated steam flow at the intermediate pressure turbine inlet to the thermal storage unit. At nominal load, the reheated steam has a temperature of 591 °C and a pressure of 47.1 bar. Later, the steam accumulator can be discharged to increase the power output of the system. Two discharging alternatives

Table 1
Key characteristics of power plant – carbon capture system at nominal load.

Variable	Value	Unit
Power plant with steam extraction for CO_2 capture		
HP turbine inlet pressure	244	bar
HP turbine inlet temperature	595	°C
HP turbine inlet steam mass flow rate	574	kg/s
Gross electric power output	642	MW_{el}
Net electric power output	598	MW_{el}
Power plant LHV efficiency	35.6	%
MBTSA process		
Flue gas inlet temperature	30	°C
Flue gas inlet pressure	1.018	bar
Flue gas mass flow rate (per unit)	402	kg/s
Flue gas inlet CO_2 concentration	13.7	mol%
Circulating sorbent mass flow rate	1255	kg/s
Sorbent regeneration duty	250	MW_{th}
CO_2 recovery	90.0	%
CO_2 purity	96.1	mol%

are considered in this work. In the first option, steam from the thermal storage is initially sent to the MBTSA process to cover the sorbent regeneration heat duty. When the steam quality is too low to be used in the MBTSA unit, the thermal storage is discharged to feedwater heater (FWH) 3 and 4, replacing the extracted steam from the turbine train. At nominal load, FWH3 requires 21.7 kg/s of steam at 4.95 bar and 278.2 °C and FWH4 requires 17.3 kg/s of steam at 9.82 bar and 363.6 °C. In the second option, the thermal storage is only used to cover the feedwater heating demand. In both discharging alternatives, the steam flow rates in the intermediate and low-pressure turbines are increased, which gives a temporary increase in power production. Since no adjustment of the boiler load is needed, the load increase takes place quickly. The pressure within the accumulator will decrease during the discharging process. The flow of steam to a given discharge point is stopped when the accumulator pressure equals its nominal steam side pressure. Between cycles, it is assumed that liquid water is added to restore the tank to its initial liquid volume fraction of 55 %.

2.2. Steam accumulator capacity

The capacity of the steam accumulator depends on its size and the pressure limits it operates within. In this work, the minimum pressure of the accumulator is set to 5 bar. This value is slightly higher than the steam side pressure of FWH3, which is the discharged steam destination with the lowest quality requirement in the system. The maximum operating pressure of the accumulator is set to 47 bar, which is slightly lower than the reheated steam pressure at full load.

When the pressure range is fixed, the tank capacity will be determined by the choice of tank volume. In this work we have chosen a tank size that enables the thermal storage system to contribute to primary reserve frequency control. Based on the classification from Palizban and Kauhaniemi, primary reserve should be available instantaneously and have a duration between 15 and 30 min [44]. To obtain an initial estimate of the tank volume, we followed the method presented by Richter et al. [38] with the requirement that the steam accumulator should be able to cover the 101 kg/s of steam (see section 4.1) needed for MBTSA regeneration for a period of 20 min. This gave a tank size estimate of 562 m^3. This estimate is expected to be conservative regarding the primary reserve time requirement due to the very large steam flow rate needed by the CO_2 capture unit. In Stevanovic et al. [39] a tank volume of 600 m^3 was used. Since this is close to our estimated value, a tank size of 600 m^3 was also chosen in this work to make direct comparison of results easier. The key design data for the steam accumulator is provided in Table 2.

Table 2
Key design data for the steam accumulator.

Parameter	Value	Unit
Internal volume	600	m^3
Minimum pressure	5	bar
Maximum pressure	47	bar
Initial volume fraction	55	%
Thermal energy storage capacity	62	MWh_{th}

3. Modelling approach

To simulate the integrated system, individual models of the three sub-domains of the process were coupled via a soft-linking approach. This means that the models are not collected in a single modelling environment, and a manual approach was applied to transfer data between entities. In this section, the modelling approach for each individual model is described.

3.1. Supercritical coal-fired power plant

The power plant model was built in version 30 of the STEAM PRO and STEAM MASTER programs delivered by Thermoflow [45]. The design of the power plant was carried out in STEAM PRO. After fixing the design, STEAM MASTER was used to perform steady-state off-design simulations. To estimate the effect of thermal storage discharging to the feedwater heaters, external steam flows matching the flow rate and conditions of the steam required by these heaters were added to the off-design model. The effect of discharging to the MBTSA process and accumulator charging was estimated directly by closing/opening valves in the off-design model.

We are only considering load variations at constant boiler firing rates introduced by the opening and closing of valves in the water/steam cycle of the power plant. Since such manipulations will affect the power plant power production without significant delays, a steady-state power plant model is assumed to be sufficient for the scope of this work. A limitation of this approach is that the model is unsuitable for other flexibility modes, such as ramps in power plant load, startups and shutdowns. The power plant load is here defined as the fraction of the nominal net power output, and a minimum load value of 40 % has been chosen. This is similar to the value chosen by Hanak et al. for a coal-fired power plant with post-combustion CO_2 capture [46].

3.2. MBTSA CO_2 capture process

The MBTSA process model was built in gPROMS ModelBuilder version 7.1.1 [47]. It is based on the model used in our previous work to study process control of the MBTSA process [18], and the reader is referred to this article for a complete description. Small modifications of the model have been made to match the flue gas conditions predicted by STEAM PRO/MASTER. As shown in Fig. 1, the MBTSA process consists of five separate sections. Each section is described by a set of dynamic, one-dimensional partial differential equations accounting for the mass, energy and momentum balance in the bulk gas phase, solid phase and macropores of the adsorbent material. The model equations and underlying assumptions are the same for each sub-domain, but the value of design parameters and the operating conditions vary between sections. The different sub-models are connected using the composite modeling capabilities of gPROMS to give a modelling tool for the entire moving bed. The equations were discretized using a central finite difference method, the SRADAU solver was used for differential–algebraic equations and the MA28 solver was used for linear algebra.

In this work, the gPROMS model is used to predict the steady-state behavior of the MBTSA process. The implemented control structure, which includes both a regulatory and performance layer, is used to adjust the manipulated variables of the process so that the targets for CO_2 recovery and purity are met in all scenarios. A limitation of the modelling approach used in this work is the assumption of no attrition of the circulating adsorbent material. Zeolites can be brittle, which represents a challenge for practical operation of the moving bed system. However, recent work has shown that new preparation methods can produce Zeolite 13X particles with high mechanical strength and specific surface area without reducing the CO_2 uptake capacity [48]. The results in this work can therefore be viewed as representative of a future adsorbent material with such properties.

3.3. Steam accumulator

A dynamic non-equilibrium mathematical model based on the approach presented by Stevanovic et al. [49] is used to simulate the steam accumulator. A complete description of the model is given below, but the reader is referred to the original article for the derivation of the equations. As indicated in Fig. 2, the model has separate mass and energy balances for the liquid water (phase 1) and steam (phase 2). The pressure of the two phases is equal. The model was implemented in MATLAB version R2022b.

The mass distribution of water and steam inside the tank depends on

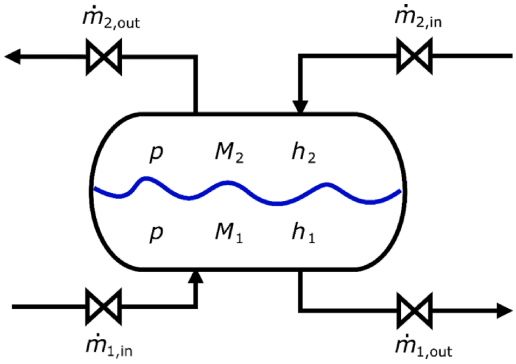

Fig. 2. Simplified layout of the steam accumulator.

the inlet and outlet flows and the internal mass transfer between the phases via evaporation or condensation. The liquid and steam mass balances are given by:

$$\frac{dM_1}{dt} = \dot{m}_{1,\text{in}} - \dot{m}_{1,\text{out}} + \dot{m}_c - \dot{m}_e \tag{1}$$

$$\frac{dM_2}{dt} = \dot{m}_{2,\text{in}} - \dot{m}_{2,\text{out}} + \dot{m}_e - \dot{m}_c \tag{2}$$

The condensation rate, $\dot{m}_c$, and evaporation rate, $\dot{m}_e$, is calculated based on the difference between the liquid enthalpy h_1 and the saturated liquid enthalpy h'. If the water is superheated ($h_1 > h'$), evaporation takes place, and the rate is calculated as:

$$\dot{m}_e = \frac{\rho_1 V_1 (h_1 - h')}{\tau_e r} \tag{3}$$

Where r is the latent heat of vaporization. In the case of evaporation, $\dot{m}_c$ is set to zero. If the water is subcooled ($h_1 < h'$), condensation will occur and $\dot{m}_e = 0$. The condensation rate is then calculated as:

$$\dot{m}_c = \frac{\rho_1 V_1 (h' - h_1)}{\tau_c r} \tag{4}$$

In this work, the relaxation time for evaporation (τ_e) and condensation (τ_c) are treated as constant parameters specified as inputs to the model. The liquid and steam enthalpy balances are given by:

$$\frac{dh_1}{dt} = \frac{1}{M_1}\left[(\dot{m}h)_{1B} + (\dot{m}_c - \dot{m}_e)h'' + \dot{Q}_{21} + M_1 v_1 \frac{dp}{dt} - h_1 \frac{dM_1}{dt}\right] \tag{5}$$

$$\frac{dh_2}{dt} = \frac{1}{M_2}\left[(\dot{m}h)_{2B} + \left(\dot{m}_e - \dot{m}_c\right)h'' - \dot{Q}_{21} + M_2 v_2 \frac{dp}{dt} - h_2 \frac{dM_2}{dt}\right] \tag{6}$$

Here, $(\dot{m}h)_{1B} = \dot{m}_{1,\text{in}}h_{1,\text{in}} - \dot{m}_{1,\text{out}}h_1$ and $(\dot{m}h)_{2B} = \dot{m}_{2,\text{in}}h_{2,\text{in}} - \dot{m}_{2,\text{out}}h_2$ account for the enthalpy flows of incoming and outgoing liquid and steam. The heat transfer rate from the steam to the liquid water is calculated as:

$$\dot{Q}_{21} = (ha)_{21}(T_2 - T_1)V_1 \tag{7}$$

If the water is superheated, which will be the case for example during tank discharging, $\dot{Q}_{21} = 0$. The parameter $(ha)_{21}$ represents the product of the heat transfer coefficient between superheated steam and liquid and the steam-water interface area concentration. It is specified as a constant input parameter to the model. The tank is assumed to be perfectly insulated, meaning no heat is lost to the surroundings. Such heat losses have been shown to have a negligible effect on the tank pressure for storage periods relevant for this work [38].

All thermodynamic properties needed in the model are calculated using version 10 of the REFPROP software [50], which was linked to MATLAB via a Python interface. REFPROP uses the IAPWS-95 equation of state for water and steam [51]. Calls with specific enthalpy and pressure as the input variables were used to calculate the density and temperature of each phase. Saturated enthalpies and the latent heat of vaporization were calculated with pressure as the only input variable.

To calculate the accumulator pressure, different modelling approaches were applied in the case of tank charging and discharging. For discharging, the differential equation for the tank pressure from Stevanovic et al. is used. It is derived from the volume balance $V_{\text{tank}} = V_1 + V_2$ and given by:

$$\frac{dp}{dt} = \frac{\left(h_1 \frac{\partial v_1}{\partial h}\Big|_p - v_1\right)\frac{dM_1}{dt} + \left(h_2 \frac{\partial v_2}{\partial h}\Big|_p - v_2\right)\frac{dM_2}{dt} - (\dot{m}_c - \dot{m}_e)h'' \frac{\partial v_1}{\partial h}\Big|_p - \left[-\dot{m}_{2,out}h_2 + (\dot{m}_e - \dot{m}_c)h''\right]\frac{\partial v_2}{\partial h}\Big|_p}{\left(\frac{\partial v_1}{\partial p}\Big|_h + v_1 \frac{\partial v_1}{\partial h}\Big|_p\right)M_1 + \left(\frac{\partial v_2}{\partial p}\Big|_h + v_2 \frac{\partial v_2}{\partial h}\Big|_p\right)M_2} \tag{8}$$

The partial derivatives of specific volume with regard to enthalpy and steam specific volume with regard to pressure were calculated using the following relations from Zhu et al. [52]:

$$\frac{\partial v_1}{\partial h}\Big|_p = \frac{v_1 \alpha_1}{c_{p,1}} \tag{9}$$

$$\frac{\partial v_2}{\partial h}\Big|_p = \frac{v_2 \alpha_2}{c_{p,2}} \tag{10}$$

$$\frac{\partial v_2}{\partial p}\Big|_h = -v_2 \kappa_2 - \frac{v_2^2 \alpha_2}{c_{p,2}}(1 - T_2 \alpha_2) \tag{11}$$

The isobaric expansivities, specific heat capacities and isothermal compressibility needed in these equations were calculated using REFPROP. The partial derivative of water specific volume with regard to pressure was approximated numerically based on REFPROP calculations for saturated water. The system of equations for tank discharging were solved using the stiff differential equation solver ode15s [53].

In the case of tank charging, using Eq. (8) caused volume conservation errors. An alternative method for calculating the tank pressure was therefore applied to maintain model accuracy. To force volume conservation, the specific volume of steam was calculated as $v_2 = (V_{\text{tank}} - V_1)/M_2$. The tank pressure was calculated from a REFPROP call based on the properties of the steam phase: $p = p(v_2, h_2)$. This means that for charging simulations, a differential–algebraic equation system was solved. The implicit solver ode15i [54] was used for this equation set.

The steam accumulator charging model was validated against experimental data from a charging experiment performed on a 64 m^3 tank [49]. The condensation time τ_c was set to 85 s and the heat transfer parameter $(ha)_{21}$ was set to 2500 W/(m^3 K). The predictions from the charging model, shown in the left part of Fig. 3, agree well with the experimental values. Experimental data for tank discharging is not

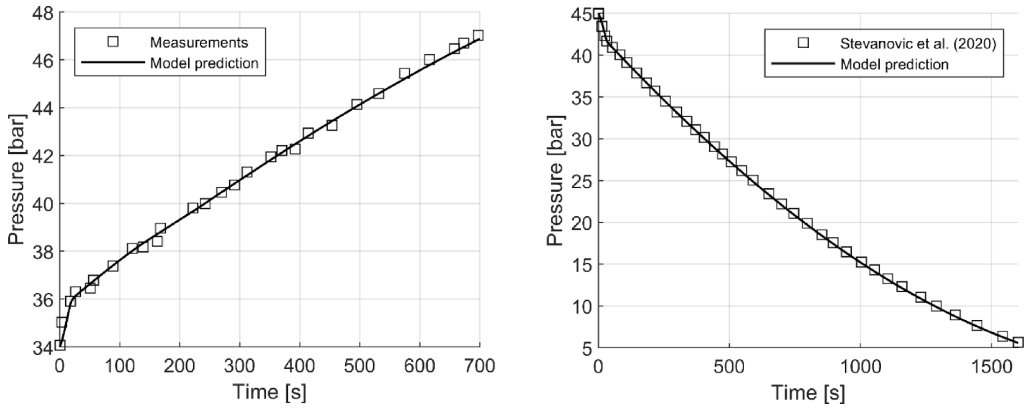

Fig. 3. Steam accumulator model validation results. Left: comparison with experimental data from charging experiment for 64 m^3 tank [49]. Right: comparison with discharging simulation results for 600 m^3 tank [39].

available in the literature, meaning that a complete validation could not be performed for this scenario. However, it was possible to compare our model predictions with simulation results from the validated model of Stevanovic et al. [39] for the same tank size (600 m^3) that is considered in this work. The evaporation time τ_e was set to 85 s. From the right part of Fig. 3, the predictions from the discharging model agree well with the results from the literature. It can therefore be concluded that both the charging and discharging model is suitable for further use. The relaxation times and heat transfer parameter are kept at the same values for all simulations in this work.

4. Results and discussion

In this section, the simulation results are presented and discussed. The main goal of these simulations was to quantify how a steam accumulator charging/discharging cycle affects the net electrical power output of the power plant with CO_2 capture. The integration of the MBTSA unit with the power plant and the dynamic behavior of the steam accumulator are also discussed.

4.1. MBTSA integration at reduced power plant loads

When the power plant load is adjusted by modifying the operation of the coal-fired boiler, conditions that influence the integration of the MBTSA process and the power plant will change. The values of selected key variables at full and minimum load are shown in Table 3. The flue gas conditions, MBTSA specific regeneration duty (SRD) and extracted steam conditions vary significantly with load. Since only one steam extraction location for the CO_2 capture process is considered in this work, it is important to verify that the chosen integration option is sufficient to heat the adsorbent to the desired temperature in the entire load range.

Table 3
Value of key variables related to power plant – MBTSA integration at full and minimum load while maintaining 90% CO_2 recovery.

Power plant load (%)	Flue gas flow rate [kg/s]	Dry flue gas CO_2 concentration [mol%]	MBTSA SRD [MJ/(kg CO_2)]	Steam conditions at extraction port	Extracted steam mass flow rate [kg/s]
100	804	13.7	1.73	508 °C, 28.1 bar	101
40	478	10.2	1.56	447 °C, 11.4 bar	70

TQ-diagrams for the nominal and minimum load cases were made to ensure that temperature crossover in the desorption section of the MBTSA unit is avoided. To generate these diagrams, the gPROMS model was first solved with updated flue gas boundary conditions to determine the required heat duty for regeneration. Subsequently, the off-design power plant model is called iteratively to determine the required steam flow rate. Iterations are needed since changing the extracted steam flow rate influences the conditions at the extraction port. As shown in Fig. 4, the steam can in both cases heat up the adsorbent to the required temperature without crossover. However, at 40 % load the superheating of incoming steam is critical to achieve the desired sorbent temperature increase, since the temperature of saturated steam at this load is lower than 202 °C. The pinch point temperature difference at this load is 3.2 °C.

4.2. Charging of steam accumulator

Charging of the steam accumulator involves extracting additional steam from the power plant and can therefore be used to provide flexibility in the form of negative reserve. This is particularly useful in the case of a reduction of the minimum power plant load, since losses in revenue and additional startups and shutdowns during periods of very low electricity prices can be avoided [6]. However, off-design power plant simulations for the system considered in this work showed that it is not possible to simultaneously charge the steam accumulator and maintain the desired CO_2 recovery rate at 40 % load. When going beyond the already large flow rate of extracted steam for sorbent regeneration, there was not enough steam available to cover the required duty of the feedwater heaters. The lowest possible load where both sorbent regeneration and accumulator charging could take place was around 60 %. Therefore, charging simulations at 60 % load were carried out to show the effect of thermal storage charging at reduced loads. An extracted reheat steam mass flow rate 5 kg/s was used. As shown in Fig. 5, it takes around 139 min before the tank pressure equals the reheat steam pressure and the charging process is stopped. A small pressure relaxation is observed as the water and steam in the tank settle at the equilibrium pressure of 27.7 bar. The tank charging reduces the net power output by 5.6 MW, which is 0.94 % of the nominal net power output. A reduction in electrical energy output of 13.0 MWh is observed.

A disadvantage of charging at reduced loads is that the extracted reheat steam is at a significantly lower quality than at full load, leading to a lower final tank pressure. In Fig. 6, the results from a charging simulation carried out at 100 % power plant load are shown. An extracted steam flow rate of 5 kg/s is used also in this case. Due to the higher quality of reheat steam in this operation regime, the final tank

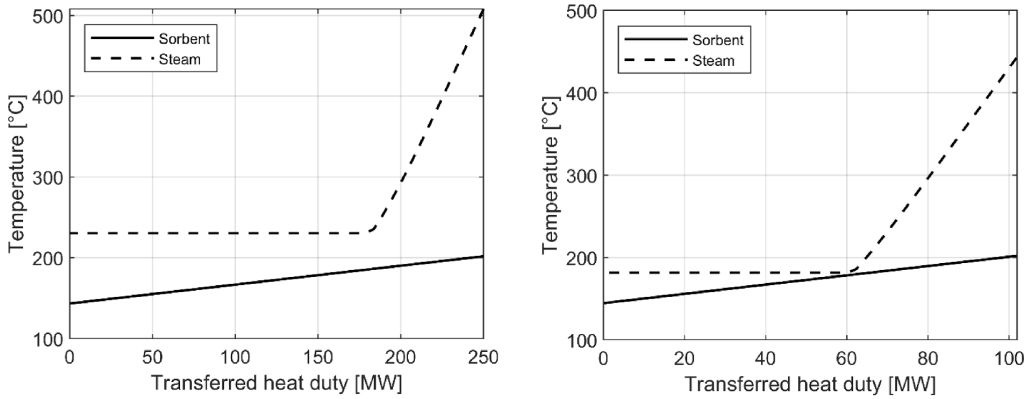

Fig. 4. *TQ*-diagrams for sorbent regeneration with steam from the intermediate pressure turbine inlet at 100% load (left) and 40% load (right).

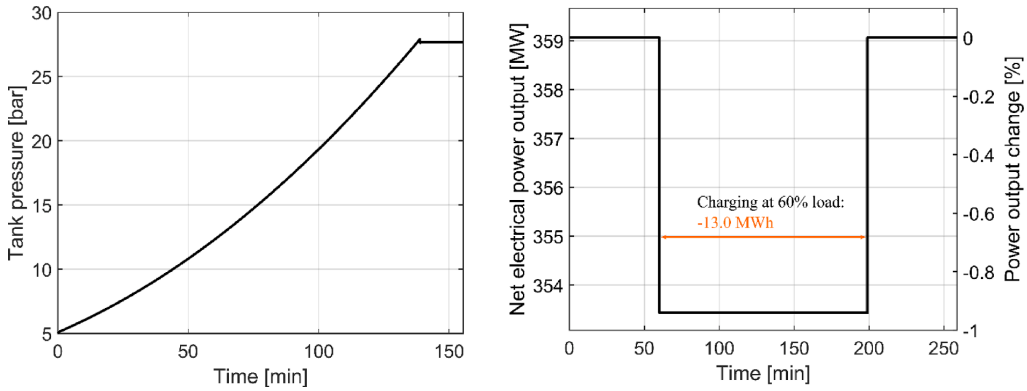

Fig. 5. Steam accumulator charging simulation results at 60 % power plant load with an extracted reheat steam flow rate of 5 kg/s.

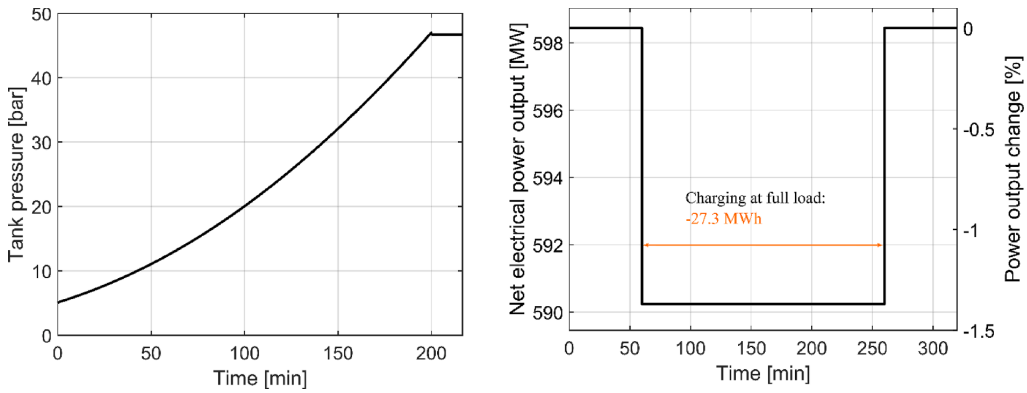

Fig. 6. Steam accumulator charging simulation results at 100 % power plant load with an extracted reheat steam flow rate of 5 kg/s.

pressure is 46.7 bar. This is similar to the pressure of 45 bar reported by Stevanovic et al. [39]. The charging process takes around 200 min. A net power output reduction of 8.2 MW (1.37 % of the nominal net power output) is achieved, reducing the electrical energy output by 27.3 MWh.

In the cases presented above, a relatively small charging steam flow rate is assumed, leading to long charging times. In some cases, long charging times are not acceptable and larger steam flow rates are required. This would be necessary for example if the accumulator needs to be charged during short periods with lower electricity prices during the day. As shown in Fig. 7, the charging flow rate has a significant effect on the final pressure in the accumulator. During charging, the water in the tank becomes sub-cooled. When the charging is stopped, steam

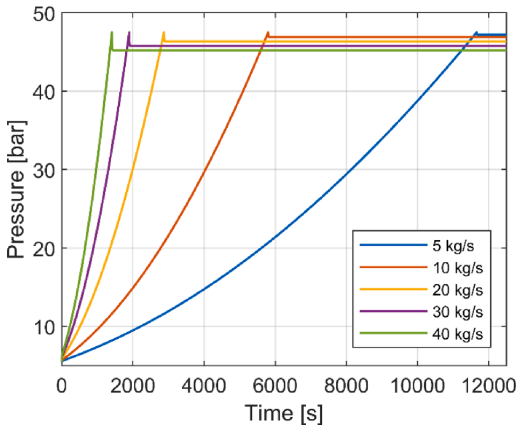

Fig. 7. Steam accumulator pressure vs. time for different reheat steam charging mass flow rates at 100% power plant load.

continues to condense until the water temperature equals the saturation temperature, thus reducing the tank pressure. The degree of sub-cooling increases for larger charging steam flow rates, giving a larger pressure decrease during the relaxation period. A charging flow rate of 40 kg/s reduces the charging time by around 171 min, but leads to around 2 bar lower final tank pressure than a charging flow rate of 5 kg/s. Since a higher tank pressure maximizes the potential for meeting short-term peak demands during discharge, small charging mass flow rates are recommended when possible.

4.3. Discharging of steam accumulator

As described in Section 2.1, covering the heat duty of FWH3 and FWH4 and meeting the regeneration demand of the MBTSA process are considered as the two discharging options in this work. The enthalpy of discharged steam will change over time, but the heat demand of the discharging locations must be continuously fulfilled. Therefore, the mass flow of steam leaving the accumulator will vary throughout the discharging simulation. The following formula is used to calculate the outgoing steam mass flow rate [39]:

$$\dot{m}_{2,\mathrm{out}}(t) = \frac{1}{h_{2,\mathrm{out}}(t)} \sum_i (\dot{m}h)_i \tag{12}$$

Where $(\dot{m}h)_i$ is the enthalpy flow required by a given discharge location. The discharging to the MBTSA process is stopped when the accumulator pressure reaches 24 bar. Similarly, the steam flow to FHW4 and FWH3 is stopped when the tank pressure is 9.82 and 4.95 bar, respectively. In all the cases presented below, it is assumed that the steam accumulator has an initial pressure of 46.7 bar, meaning that it has been charged with a flow rate of 5 kg/s at full load.

In Fig. 8, the discharged steam flow rate and accumulator pressure profile is shown for the case where the thermal storage is used to cover the heat demands of FWH4 and FWH3 at full power plant load. In this case, the steam required for sorbent regeneration is provided in the same way as during normal power plant operation. The required steam flow rate to cover the demand of both feedwater heaters is around 43 kg/s and increases slightly over time to compensate for the decrease in steam enthalpy. After around 23 min, the tank pressure reaches the threshold value of 9.82 bar. After this point, steam is only delivered to FWH3, and the discharged steam flow rate decreases to around 24 kg/s. The discharge to FWH3 continues for around 13 min before the tank pressure equals 4.95 bar.

In Fig. 9, the net electrical power output and relative power output profile for this case is shown. When both FWH4 and FWH3 is replaced by steam from the accumulator, the net electrical power output increases by 20.5 MW (3.43 % of the nominal power output). When only the demand of FWH3 is covered, the increase in net electrical power output is 10.2 MW (1.7 % of the nominal power output).

The discharged steam flow rate and accumulator pressure profile for the second discharging option is shown in Fig. 10. In this case, the thermal storage is first used in the MBTSA process. The required steam mass flow rate is around 126 kg/s, which is significantly larger than for the FWH case. The tank pressure decreases rapidly due to the large flow rate, reaching the threshold value of 24 bar after only 3.2 min. After this point, the thermal storage is discharged to FWH4 and FWH3, and the outgoing steam mass flow rate decreases to around 43 kg/s. A pronounced pressure recovery is seen during this transition, caused by the evaporation of superheated water in the tank. The degree of superheating during discharge to the MBTSA is high due to the large steam mass flow rate. The accumulator can cover the demand of both feedwater heaters for around 15 min before reaching the FWH4 threshold value. The outgoing steam flow rate is again reduced to around 24 kg/s for a period of 13 min, after which the lowest pressure limit is reached.

In Fig. 11, the variation in net and relative electrical power output during the second discharging option is shown. Discharging to the MBTSA process increases the net power output by almost 67 MW (11.2 % of the nominal power output). Discharging to the feedwater heaters

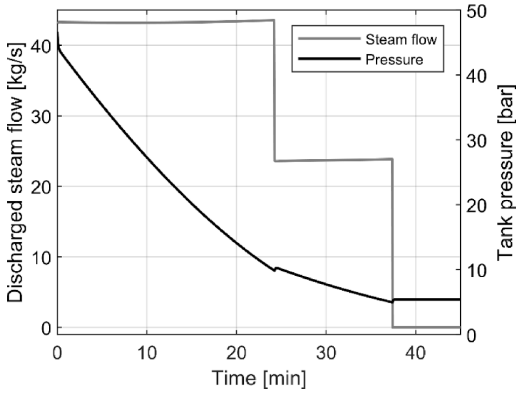

Fig. 8. Discharged steam mass flow rate and steam accumulator pressure profile when thermal storage is used to cover FWH3 and FWH4 heat demands at full power plant load.

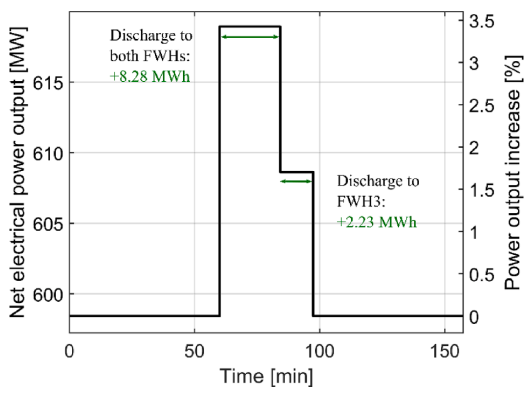

Fig. 9. Net electrical power output profile and relative power output change when thermal storage is used to cover FWH3 and FWH4 heat demand at full power plant load.

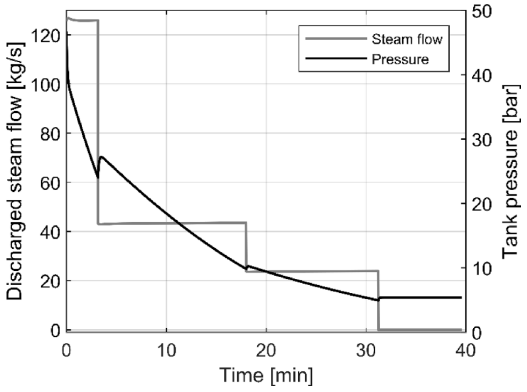

Fig. 10. Discharged steam mass flow rate and steam accumulator pressure profile when thermal storage is used to cover MBTSA regeneration duty and then feedwater heating demand at full power plant load.

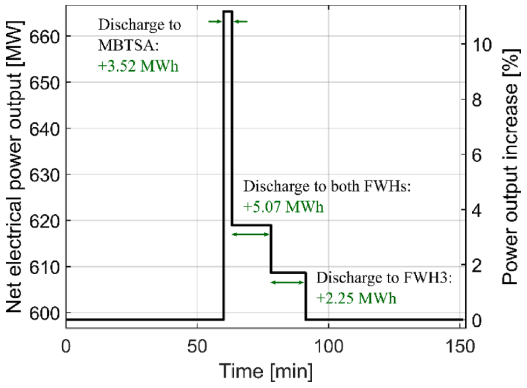

Fig. 11. Net electrical power output profile and relative power output change when thermal storage is used to cover MBTSA regeneration duty and then feedwater heating demand at full power plant load.

has the same effect on the power plant as shown in Fig. 9. As expected, the increase in electrical energy production from covering both FWH4 and FWH3 is smaller than in the first case, since the thermal storage has first been used in the MBTSA process.

A summary of the effect of the two discharging options on the power plant operation is given in Table 4. Both options give an increase in the electrical energy production in the range of 10.5–11 MWh. The FWH discharge case has a total duration of 37.5 min, which is around 6 min longer than the MBTSA + FWH case. Both options exceed the time duration requirement discussed earlier for primary energy reserve. An advantage of discharging to the MBTSA process is the possibility of increasing the net electrical power output by over 11 % of the nominal value, which is useful in the case of large peak demands with a short duration. The relative load increases of 1.7–11.2 % achieved in this work are comparable with values from the literature. For steam accumulator systems, a relative power plant load increase of 4.3 % [38] and 4.2 % [39] has been reported. Kruger et al. reported load increases from 2 to 5 % of the net capacity in their comparison of molten salt, solid media and combined steam accumulator - PCM thermal storage [35].

5. Conclusions

In the future, flexible operation of thermal power plants with carbon capture might be required to reduce emissions while handling increasing shares of variable renewable energy sources in the electricity mix. Thermal energy storage integration is a promising method for enabling flexible operation of such plants without modifying the boiler operation or reducing the CO_2 recovery rate. This work evaluated the impact of integrating a 600 m^3 steam accumulator into a 598 MW supercritical coal-fired power plant with a moving bed temperature-swing adsorption process capturing 90 % of the CO_2 in the flue gas. This combination of technologies had not previously been studied in the literature. A soft-linking approach was applied to couple a power plant model built in ST PRO/MASTER, steam accumulator model in MATLAB and CO_2 capture model in gPROMS.

To charge the steam accumulator, additional reheat steam is extracted from the turbine train. Simulations showed that charging the tank at 60 % load could reduce the net power output by 5.6 MW (0.94 % of nominal net power output) for around 139 min. At full load, the net power output during charging is reduced by 8.2 MW (1.37 % of nominal) for approximately 200 min. The disadvantage of charging at reduced power plant loads is a lower final pressure in the accumulator. Furthermore, it was shown that the choice of tank charging flow rate significantly influences the final pressure of the thermal storage. If possible, small charging flow rates are recommended to maximize the final pressure of the accumulator.

Two alternatives for discharging of the thermal storage were studied, i.e. regeneration of the CO_2 capture process and covering the heat duty of two of the feedwater heaters. In the feedwater heater case, discharging of the steam accumulator was able to cover the demand of both feedwater heaters for 23 min while increasing the net power output by 20.5 MW (3.4 % of nominal). After this period, the thermal storage could cover the demand of the low-pressure feedwater heater for an additional 13 min with a net power output increase of 10.2 MW (1.7 % of nominal). In total, the feedwater heater case gave an electrical energy output increase of 10.5 MWh. In the case where the discharged steam was first used to cover the regeneration duty of the CO_2 capture process, a similar overall increase in the electrical energy output was calculated (10.8 MWh). Since regeneration of the CO_2 capture process requires a large steam flow rate, a net power output increase of almost 67 MW (11.2 % of nominal) for 3.2 min is achieved in this case. After this, the steam tank could cover both feedwater heaters for 15 min and the low-pressure heater for 13 min. The results show that both discharging options exceed the time duration requirement to be suitable for primary reserve. In practice, this type of flexibility would be useful for power plant operation since additional revenue can be earned by adjusting the load based on market conditions and grid requirements.

Table 4
Comparison of the effect of each discharging option on the power plant operation.

	Discharge to MBTSA + feedwater heaters				Discharge to feedwater heaters only			
Discharged steam destination	Time [min]	Load change [% of nominal net power]	Net power output increase [MW_{el}]	Electrical energy output increase [MWh_{el}]	Time [min]	Load change [% of nominal net power]	Net power output increase [MW_{el}]	Electrical energy output increase [MWh_{el}]
MBTSA	3.16	11.2	66.9	3.52	–	–	–	–
Both FWHs	14.9	3.43	20.5	5.07	24.3	3.43	20.5	8.28
FWH3	13.2	1.70	10.2	2.25	13.2	1.70	10.2	2.23
Sum	31.3			10.8	37.5			10.5

Several topics can be considered for future work. Firstly, a techno-economic evaluation of the investigated concept would give more insight into its viability and could be used to determine the cost-optimal capacity and operation of the thermal storage system. Other energy storage technologies such as batteries, molten salt thermal storage and phase change materials could be included for comparison. It is also possible to study alternative integration options, such as sending discharged steam directly from the accumulator to the steam turbines. For a more complete evaluation of the impact on power plant flexibility, other flexibility modes such as rapid load ramps, start-ups and shutdowns could be investigated. Such studies would require a dynamic power plant model and benefit from collecting the different sub-models in a single modelling environment.

CRediT authorship contribution statement

Vidar T. Skjervold: Conceptualization, Formal analysis, Investigation, Methodology, Software, Validation, Visualization, Writing – original draft. **Lars O. Nord:** Conceptualization, Funding acquisition, Methodology, Project administration, Resources, Supervision, Writing – review & editing.

Declaration of competing interest

The authors declare that they have no known competing financial interests or personal relationships that could have appeared to influence the work reported in this paper.

Data availability

Data will be made available on request.

Acknowledgements

We acknowledge financial support from the Polish-Norwegian Research Program for funding the InnCapPlant project (Grant NOR/POLNORCCS/0015/2019-00).

References

[1] IEA, "CO2 Emissions in 2022," Paris, 2023. [Online]. Available: https://www.iea.org/reports/co2-emissions-in-2022.
[2] E. Commission, "COMMUNICATION FROM THE COMMISSION TO THE EUROPEAN PARLIAMENT. The EUROPEAN COUNCIL, THE COUNCIL, THE EUROPEAN ECONOMIC AND SOCIAL COMMITTEE AND THE COMMITTEE OF THE REGIONS, The European Green Deal", Brussels, 2019.
[3] H. Ritchie and P. Rosado, "Our World in Data - Electricity Mix," 2023. https://ourworldindata.org/electricity-mix (accessed Oct. 17, 2023).
[4] IEA, "World Energy Outlook 2022," Paris, 2022. [Online]. Available: https://www.iea.org/reports/world-energy-outlook-2022.
[5] M.A. Gonzalez-Salazar, T. Kirsten, L. Prchlik, Review of the operational flexibility and emissions of gas- and coal-fired power plants in a future with growing renewables, Renew. Sustain. Energy Rev. 82 (2017) (2018) 497–1513, https://doi.org/10.1016/j.rser.2017.05.278.
[6] H. Chalmers, M. Lucquiaud, J. Gibbins, M. Leach, Flexible operation of coal fired power plants with post combustion capture of carbon dioxide, J. Environ. Eng. 135 (6) (2009) 449–458, https://doi.org/10.1061/(ASCE)EE.1943-7870.0000007.
[7] IPCC, "Global Warming of 1.5°C. An IPCC Special Report on the impacts of global warming of 1.5°C above pre-industrial levels and related global greenhouse gas emission pathways, in the context of strengthening the global response to the threat of climate change," 2018.
[8] F. Kazemifar, A review of technologies for carbon capture, sequestration, and utilization: Cost, capacity, and technology readiness, Greenh. Gases Sci. Technol. 12 (1) (2022) 200–230, https://doi.org/10.1002/ghg.2131.
[9] B. Dziejarski, R. Krzyżyńska, K. Andersson, Current status of carbon capture, utilization, and storage technologies in the global economy: A survey of technical assessment, Fuel 342 (2022) 2023, https://doi.org/10.1016/j.fuel.2023.127776.
[10] F. Raganati, F. Miccio, P. Ammendola, Adsorption of carbon dioxide for post-combustion capture: a review, Energy and Fuels 35 (16) (2021) 12845–12868, https://doi.org/10.1021/acs.energyfuels.1c01618.
[11] C. Dhoke, A. Zaabout, S. Cloete, S. Amini, Review on reactor configurations for adsorption-based CO2 capture, Ind. Eng. Chem. Res. 60 (10) (2021) 3779–3798, https://doi.org/10.1021/acs.iecr.0c04547.
[12] V.T. Skjervold, G. Mondino, L. Riboldi, L.O. Nord, Investigation of control strategies for adsorption-based CO2 capture from a thermal power plant under variable load operation, Energy 268 (2023) 126728, https://doi.org/10.1016/j.energy.2023.126728.
[13] G. Mondino, C.A. Grande, R. Blom, L.O. Nord, Moving bed temperature swing adsorption for CO2 capture from a natural gas combined cycle power plant, Int. J. Greenh. Gas Control 85 (2018) (2019) 58–70, https://doi.org/10.1016/j.ijggc.2019.03.021.
[14] G. Mondino, C.A. Grande, R. Blom, Effect of gas recycling on the performance of a moving bed temperature-swing (MBTSA) process for CO2 capture in a coal fired power plant context, Energies 10 (6) (2017) pp, https://doi.org/10.3390/en10060745.
[15] G. Mondino, C.A. Grande, R. Blom, L.O. Nord, Evaluation of MBTSA technology for CO2 capture from waste-to-energy plants, Int. J. Greenh. Gas Control 118 (2021) (2022), https://doi.org/10.1016/j.ijggc.2022.103685.
[16] T. Okumura, et al., Demonstration plant of the kawasaki CO2 capture (KCC) system with solid sorbent for coal-fired power station, SSRN Electron. J. (2018), https://doi.org/10.2139/ssrn.3365953.
[17] X. Wu, M. Wang, P. Liao, J. Shen, Y. Li, Solvent-based post-combustion CO2 capture for power plants: A critical review and perspective on dynamic modelling, system identification, process control and flexible operation, Appl. Energy 257 (2019) (2020), https://doi.org/10.1016/j.apenergy.2019.113941.
[18] V.T. Skjervold, L.O. Nord, Enhanced single-loop control of a moving bed temperature swing adsorption CO2 capture process, Comput. Chem. Eng. 178 (2023) 108387, https://doi.org/10.1016/j.compchemeng.2023.108387.
[19] P. Tait, B. Buschle, K. Milkowski, M. Akram, M. Pourkashanian, M. Lucquiaud, Flexible operation of post-combustion CO2 capture at pilot scale with demonstration of capture-efficiency control using online solvent measurements, Int. J. Greenh. Gas Control 71 (2018) 253–277, https://doi.org/10.1016/j.ijggc.2018.02.023.
[20] M. Zaman, J.H. Lee, Optimization of the various modes of flexible operation for post-combustion CO2 capture plant, Comput. Chem. Eng. 75 (2015) 14–27, https://doi.org/10.1016/j.compchemeng.2014.12.017.
[21] X. Wu, M. Wang, K.Y. Lee, Flexible operation of supercritical coal-fired power plant integrated with solvent-based CO2 capture through collaborative predictive control, Energy 206 (2020) 118105, https://doi.org/10.1016/j.energy.2020.118105.
[22] Z. Tang, X. Wu, Distributed predictive control guided by intelligent reboiler steam feedforward for the coordinated operation of power plant-carbon capture system, Energy 267 (2022) (2023), https://doi.org/10.1016/j.energy.2022.126568.
[23] X. Chen, R. Qiu, X. Wu, Multi-timescale capacity configuration optimization of energy storage equipment in power plant-carbon capture system, Appl. Therm. Eng. 227 (2023) 120371, https://doi.org/10.1016/j.applthermaleng.2023.120371.
[24] E.T. Sayed, et al., Renewable energy and energy storage systems, Energies 16 (3) (2023) pp, https://doi.org/10.3390/en16031415.
[25] A.A. Kebede, T. Kalogiannis, J. Van Mierlo, M. Berecibar, A comprehensive review of stationary energy storage devices for large scale renewable energy sources grid integration, Renew. Sustain. Energy Rev. 159 (2022) 112213, https://doi.org/10.1016/j.rser.2022.112213.
[26] K. Zhang, M. Liu, Y. Zhao, H. Yan, J. Yan, Design and performance evaluation of a new thermal energy storage system integrated within a coal-fired power plant, J. Energy Storage 50 (2022) 104335, https://doi.org/10.1016/j.est.2022.104335.
[27] M. Saghafifar, S. Gabra, A critical overview of solar assisted carbon capture systems: Is solar always the solution? Int. J. Greenh. Gas Control 92 (2020) 102852 https://doi.org/10.1016/j.ijggc.2019.102852.
[28] C. Tregambi, F. Montagnaro, P. Salatino, R. Solimene, A model of integrated calcium looping for CO2 capture and concentrated solar power, Sol. Energy 120 (2015) 208–220, https://doi.org/10.1016/j.solener.2015.07.017.
[29] S. M. Cohen, M. E. Webber, and G. T. Rochelle, "Utilizing solar thermal energy for post-combustion CO2 capture," in *Proceedings of the ASME 2010 4th International Conference on Energy Sustainability*, 2010, 512, 1–10.
[30] G. Ordorica-Garcia, A.V. Delgado, A.F. Garcia, Novel integration options of concentrating solar thermal technology with fossil-fuelled and CO2 capture processes, Energy Procedia 4 (2011) 809–816, https://doi.org/10.1016/j.egypro.2011.01.123.
[31] J. Wang, L. Liu, X. Zeng, K. Li, Solar-assisted CO2 capture with amine and ammonia-based chemical absorption; a comparative study, Therm. Sci. 25 (1) (2021) 717–732, https://doi.org/10.2298/TSCI191222149W.
[32] W. Kosman, A. Rusin, The application of molten salt energy storage to advance the transition from coal to green energy power systems, Energies 13 (2020) 9, https://doi.org/10.3390/en13092222.
[33] O. Garbrecht, M. Bieber, R. Kneer, Increasing fossil power plant flexibility by integrating molten-salt thermal storage, Energy 118 (2017) 876–883, https://doi.org/10.1016/j.energy.2016.10.108.
[34] D. Li, J. Wang, Study of supercritical power plant integration with high temperature thermal energy storage for flexible operation, J. Energy Storage 20 (2018) 140–152, https://doi.org/10.1016/j.est.2018.09.008.
[35] M. Kruger, S. Muslubas, T. Loeper, F. Klasing, P. Knödler, C. Mielke, Potentials of thermal energy storage integrated into steam power plants, energies 13 (2020) 2226.
[36] R. Cao, et al., A novel approach to improving load flexibility of coal-fired power plant by integrating high temperature thermal energy storage through additional thermodynamic cycle, Appl. Therm. Eng. 173 (2020) 115225, https://doi.org/10.1016/j.applthermaleng.2020.115225.

[37] M. Trojan, D. Taler, P. Dzierwa, J. Taler, K. Kaczmarski, J. Wrona, The use of pressure hot water storage tanks to improve the energy flexibility of the steam power unit, Energy 173 (2019) 926–936, https://doi.org/10.1016/j.energy.2019.02.059.
[38] M. Richter, G. Oeljeklaus, K. Görner, Improving the load flexibility of coal-fired power plants by the integration of a thermal energy storage, Appl. Energy 236 (2018) (2019) 607–621, https://doi.org/10.1016/j.apenergy.2018.11.099.
[39] V.D. Stevanovic, M.M. Petrovic, S. Milivojevic, M. Ilic, Upgrade of the thermal power plant flexibility by the steam accumulator, Energy Convers. Manag. 223 (2020) 113271, https://doi.org/10.1016/j.enconman.2020.113271.
[40] R.M. Montañés, S. GarÐarsdóttir, F. Normann, F. Johnsson, L.O. Nord, Demonstrating load-change transient performance of a commercial-scale natural gas combined cycle power plant with post-combustion CO2 capture, Int. J. Greenh. Gas Control 63 (April) (2017) 158–174, https://doi.org/10.1016/j.ijggc.2017.05.011.
[41] NETL, "Cost and performance baseline for fossil energy plants volume 1: bituminous coal and natural gas to electricity," 2019.
[42] M.M.F. Hasan, R.C. Baliban, J.A. Elia, C.A. Floudas, Modeling, simulation, and optimization of postcombustion CO2 capture for variable feed concentration and flow rate. 1. chemical absorption and membrane processes, Ind. Eng. Chem. Res. 51 (48) (2012) 15642–15664, https://doi.org/10.1021/ie301571d.
[43] D. Xu, et al., Effects of water vapour on CO2 capture with vacuum swing adsorption using activated carbon, Chem. Eng. J. 230 (2013) 64–72, https://doi.org/10.1016/j.cej.2013.06.080.
[44] O. Palizban, K. Kauhaniemi, Energy storage systems in modern grids—Matrix of technologies and applications, J. Energy Storage 6 (2016) 248–259, https://doi.org/10.1016/j.est.2016.02.001.
[45] Thermoflow Inc, "STEAM PRO and STEAM MASTER," 2023. https://www.thermoflow.com/products_conventionalsteam.html (accessed Mar. 30, 2023).
[46] D.P. Hanak, C. Biliyok, V. Manovic, Evaluation and modeling of part-load performance of coal-fired power plant with postcombustion CO2 capture, Energy & Fuels 29 (6) (2015) 3833–3844, https://doi.org/10.1021/acs.energyfuels.5b00591.
[47] PSE, "gPROMS ModelBuilder," 2023. https://www.psenterprise.com/products/gproms/modelbuilder (accessed Mar. 29, 2023).
[48] E. Luzzi, P. Aprea, M. de Luna, D. Caputo, G. Filippone, Mechanically coherent zeolite 13X/Chitosan aerogel beads for effective CO2 capture, ACS Appl. Mater. & Interfaces 13 (17) (2021) 20728–20734, https://doi.org/10.1021/acsami.1c04064.
[49] V.D. Stevanovic, B. Maslovaric, S. Prica, Dynamics of steam accumulation, Appl. Therm. Eng. 37 (2012) 73–79, https://doi.org/10.1016/j.applthermaleng.2012.01.007.
[50] NIST, "REFPROP Documentation." 2018, [Online]. Available: https://www.nist.gov/system/files/documents/2018/05/23/refprop10a.pdf.
[51] W. Wagner, A. Pruß, The IAPWS formulation 1995 for the thermodynamic properties of ordinary water substance for general and scientific use, J. Phys. Chem. Ref. Data 31 (2) (2002) 387–535, https://doi.org/10.1063/1.1461829.
[52] Q. Zhu, P. Lu, Z. Yang, X. Ji, Y. Han, Multi-parameter optimization for the wet steam accumulator of a steam-powered catapult, Energies 12 (2019) 2, https://doi.org/10.3390/en12020234.
[53] Mathworks, "MATLAB ode15s solver," 2023. https://se.mathworks.com/help/matlab/ref/ode15s.html (accessed Oct. 27, 2023).
[54] Mathworks, "MATLAB ode15i solver," 2023. https://se.mathworks.com/help/matlab/ref/ode15i.html (accessed Oct. 27, 2023).